APPLICATION OF SYSTEM IDENTIFICATION
TO
SHIP MANEUVERING

by

Wei-Yuan Hwang

B.S., National Taiwan University
(1972)

S.M., Massachusetts Institute of Technology
(1976)
Ocean Engineer, Massachusetts Institute of Technology
(1978)

submitted in
partial fulfillment
of the requirements for the
Degree of Doctor of Philosophy

at the

MASSACHUSETTS INSTITUTE OF TECHNOLOGY
May 1980

© Massachusetts Institute of Technology, 1980

Signature of Author_____
Department of Ocean Engineering
May 2, 1980

Certified by_____
Martin A. Abkowitz
Thesis Supervisor

Accepted by_____
Chairman, Departmental Committee
on Graduate Students

- 1 -

APPLICATION OF SYSTEM IDENTIFICATION TO SHIP MANEUVERING

by

Wei-Yuan Hwang

Submitted to the Department of Ocean Engineering on
May 1980 in partial fulfillment of the requirement
for the degree of Doctor of Philosophy

Abstract

The state augmented extended Kalman filtering technique is applied
to identify the dynamic system of a maneuvering ship in this thesis.
Through the analysis of various hydrodynamic phenomena and the diagnostic
information from parameter estimation, the mathematical model of ship
motion is modified interactively with the processing of sea trial data.
This effort results in a concise and yet more realistic and accurate model.
The identifiability analysis and the sensitivity analysis are explor-
ed to give a proper suggestion of parameterization for parameter estima-
tion.
The cancellation effect among the contributions of hydrodynamic
coefficients is found responsible for the simultaneous drifting phenomena
during the estimation of parameters. The slender body theory is utilized
to explain the intrinsic nature of cancellation effect for the dynamics
of ship motion. "Parallel processing","exaggerated over- and under-
estimated initial guess" and "parameter transformation" are developed to
cure the simultaneous drifting phenomena. "Exaggerated over- and under-
estimated initial guess" is a practical scheme and "parameter transforma-
tion is more rigorous. Both of which have been tested on simulated data
and achieved great success. "Parallel processing" does not cure the
simultaneous drift, but its application to the estimation of ship resis-
tance coefficient is very successful.
The accuracy of estimated hydrodynamic coefficient value for ESSO
OSAKA is checked by comparing the simulated motion and the sea trial
record. The performance of identified system of ESSO OSAKA is very
satisfactory for mild maneuvers. The resulting improvement on the violent
maneuvering simulation is substantial, although further effort can make
the model even better.

Thesis Supervisor: Dr. Martin A. Abkowitz

Title: Professor of Ocean Engineering

- 2 -

ACKNOWLEDGEMENT

To-

My mother and late father

TABLE OF CONTENTS

LIST OF FIGURES

- 9 -

Figure

LIST OF TABLES

NOMENCLATURE

A	Developed area of the propeller
A_R	Rudder area
A_p	Area of the portion of rudder that is in the slip stream
$\underline{B}$	Coefficient matrix of exogeneous input $\underline{u}$
C_D	Drag coefficient of locked propeller
C_L	Lift coefficient of rudder
C_R	Resistance coefficient
c	Mean velocity over the rudder
c_e	Mean velocity over the rudder of equilibrium propeller loading at forward speed u
d	Propeller diameter
e	Effective rudder angle
F_r	Froude number
$\underline{f}$	State function
G	Center of gravity
H	Water depth
$\underline{H}$	Measurement Matrix
$\underline{h}$	Measurement function
$\underline{I}$	Information matrix or Identity matrix
J	Advance ratio or Cost function
K_x	Dimension of the matrix $\underline{x}$
K_t	Thrust coefficient
k	Ratio of u_A to $u_{A\infty}$
L	Characteristic length, length between perpendicular in this study
m	Mass of ship
m_{ij}	Added mass for i,j=1,2,3 and Added moment of inertia for i,j=4,5,6
N	Hydrodynamic moment in z direction or Gaussian distributed random variable

N_0	Asymmetrical yaw moment due to a single propeller
n, n_p	Propeller rotating speed
o	Origin of the coordinate system
$\underline{P}$	Error covariance matrix
$\underline{Q}$	Covariance matrix of process noise
R	Resistance
$\underline{R}$	Covariance of measurement noise
R_n	Reynolds number
r	Yaw speed
$\underline{r}_z$	Normalized residuals
S	Wetted surface area
T	Thrust or the draft of ship
t	Time or thrust deduction factor
U	Resultant ship speed
u_0	Surge speed at equilibrium state
u	Surge speed
$\underline{u}$	Exogeneous input matrix
u_A	Propeller induced velocity
$u_{A\infty}$	Propeller induced velocity far down stream
u_c	Current speed
V_a	Speed of advance
v	Sway speed
$\underline{v}$	Measurement noise
w	Wake fraction
$\underline{w}$	Process noise
X	Hydrodynamic force in x-direction
x	Cartesian coordinate fixed on ship
$\underline{x}$	State variable
x_0	Cartesian coordinate fixed on earth
x_G	Position of the center of gravity
x_p	Position of pivot point

Y	Hydrodynamic force in y-direction
Y_0	Asymmetrical sway force due to single propeller
y	Cartesian coordinate fixed on ship
y_0	Cartesian coordinate fixed on earth
z	Cartesian coordinate fixed on ship
z_0	Cartesian coordinate fixed on earth
$\underline{z}$	Measurements
α	Current direction
$\underline{\alpha}$	Unknown parameter to be estimated
δ	Rudder angle
$\underline{\varepsilon}_z$	Residuals
ζ	Sum of squared residuals
n_1, n_2, n_3	Coefficients in the emperical espression of effective thrust behind propeller
λ	Eigen values
μ_Y	Y-force parameter introduced in the "parameter transformation" scheme
μ_N	N-moment parameter introduced in the "parameter transformation" scheme
ξ	Log likelihood
π	3.141592
ρ	Water density
$\underline{\Sigma}$	Covariance matrix
σ	Cavitation number or Standard deviation
$\underline{\Phi}$	Transition matrix
$\underline{\Psi}$	Error covariance of the initial guess $\underline{x}(0)$
ψ	Heading angle

Mathematical Symbol

$\pm$	plus or minus
∂	partial differential
$\equiv$	identical with or defined as
Δ	finite difference

Superscript

'	indicates nondimensionalized quantities
^	indicates optimal quantities
o	degree
.	$\frac{\partial}{\partial t}$
s	indicates quantitied calculated by strip theory
-	mean value
~	indicates estimation error

Subscript

r	indicates speed relative to water
_	represents matrix
o	represents the equilibrium state, unless specified otherwise

1. INTRODUCTION

Traditionally, the maneuverability of the ship has received quite a lot of attention from naval architects. Due to the inherent difficulties to build a perfect simulation model for describing ship motions, the quantitative analysis of ship maneuvering has not reached a satisfactory state.

The problem was not serious before, because the ship was not so big in size and was sufficiently powered to handle a emergency situation. In recent years, giant ships has been put into service responding to the request of economic operating cost. A careless error in operating those high risk ships, such as VLCC(Very Large Crude Carrier) and LNG(Liquified Natural Gas) tanker, can cause very serious accidents.

Besides the safety problem, due to the revolutionary development of computer and electronic equipment, there is an increasing trend of implementing auto pilot, satellite navigator and automatically controlled power plant systems aboard the ship. Therefore, no matter whether a ship is being designed or being operated already, a sufficient understanding of the very ship's behavior during maneuvering becomes more important nowadays.

The study of surface ship maneuverability has been concerned with the dynamic stability, the ship's response to the control surface and its turning capability. In the design stage, if these performances can be accurately predicted through a proper scheme, faulty design can then be corrected and it is more likely to reach optimal solution under all sorts

of constraints. After the ship is built, it is necessary to know the relevant information for establishing a standard procedure to operate the ship, especially in the restricted water or in the course of avoiding a collision. As to the aspect of professional education, we would like to train the ship operators in an efficient and safe way.

To achieve the above goals, the usage of full scale ship is obviously too expensive, ineffective and risky. Consequently, it is more preferable to resort to a model which simulates the behavior of a real ship. In general, there are two kinds of model. The "physical model" is a scaled ship model run in a towing tank and the "mathematical model" is a mathematical representation of the ship behavior by virtue of computer simulation. Since the model has much smaller Reynolds number than that of a full scale ship, it is necessary to increase the size of model in order to reduce the scale effect. Unfortunately, the investment on a large maneuvering tank is quite heavy and the operating cost is not cheap either. Besides, the time is scaled down by the square root of length scale ratio. Since the trainee and the model are in different time scale, the physical model is not suitable for training purposes.

Considering these disadvantages of physical model and the tremendous amout of information generated by computer within a short time, a mathematical model based on a hypothesized structure of the dynamic system and the associated coefficients is prefered in predicting and simulating the ship motion.

However, few coefficients in the model can be accurately estimated by

theoretical approach. Most of the hydrodynamic coefficients have to be estimated by experimental measurement. Unfortunately, it is almost impossible to measure the hydrodynamic force and moment acting on a real ship. We have to resort to the measurement on the scaled model of the ship.

Among the experimental methods, the captive model test is the most popular one, Abkowitz[1969], Smitt & Chislett[1974], Fujino[1976]. The rotating arm test(RAT) measures the hydrodynamic force and moment by stationary motion and the planar mechanism(PMM) measures the hydrodynamic force and moment by designed unsteady motion. Since the model test suffers from scale effect, the measured hydrodynamic coefficient value is not completely reliable. Especially the test of motion in restricted water, e.g., a shallow water or a narrow canal, the boundary layer around the model is thicker than ships due to smaller Reynolds number. Consequently, the effect of restricted water may be exaggerated significantly during the model test.

It is in the 60's, the system identification technique was introduced to resolve the problem due to the inherent difference between the scaled mcdel and the full size ship. System identification is a subcategory of estimation in the system theory, Schweppe[1973]. Based on a hypothesized structure and using the collected observations, the parameters of the system are estimated. If the resulting model passes the validity test, this identified system is an equivalent counter part of the real system. Therefore, when sufficient sea trial data are measured, the optimal

hydrodynamic coefficients for a ship maneuvering model can be estimated. Notice that the optimality is based on a certain criterion. If this criterion is changed, different results will be obtained.

Although scale effect reduces the reliability of those measured hydrodynamic coefficient values, it does not mean that system identification can replace the model test completely. As a matter of fact, model test value is used as the initial guess for parameter estimation and it is also used to eliminate those mathematically possible but physically infeasible values from identification. For ship design purposes, the information from the model test can hardly be furnished by system identification either. A proper application of these two techniques will best serve for the research of ship maneuverability.

At M. I. T., the application of system identification to ship maneuvering dynamics was started by Hayes[1971]. An intensive study was done to show how model reference method(MRM) and extended Kalman filtering(EKF) can be used to identify the hydrodynamic coefficients of a deep submergence rescue vehicle(DSRV) from the simulated noisy data. Using the simulated data of a Mariner ship, Brinati[1973] explored the application of EKF to the surface ship maneuvering problem. Since MRM was found inferior to the EKF, the application of MRM to the ship maneuvering had been dropped from then on. Lundblad[1974] continued to study the proper type of maneuver which gives the better identification result. The ocean current of unknown magnitude but known direction was introduced into the computer program by Szeto[1977]. The parameter estimation from the simulated data of a

supertanker is equally satisfactory as the study of Mariner's by the previous researchers.

However, there is a problem in the previous studies. A satisfactory result is not always guaranteed. The identification can end up with erroneous estimation of hydrodynamic coefficients, while the measurements are filtered very nicely. In using the EKF technique, this problem is manifested in the phenomenon of "simultaneous drift" of estimated coefficients. In other words, the system model has the problem of identifiability.

Outside this school, Kaplan & Sargent[1972] applied the MRM to the identification of a conventional surface ship system and applied the EKF to estimate the dynamics of a hydrofoil craft and a surface effect ship. The results of MRM is very sensitive to the noise, which is a consistent finding with the conclusion of studies conducted at M. I. T..

Sandman & Kelly[1974] also utilized the MRM to identify the linearized dynamic system of an underwater vehicle. Since the problem of parameter identifiability was not resolved, physically unacceptable value, e.g., a positive pitch moment damping coefficient, has been obtained.

A mixture of output error and equation error method is applied by Gill[1975] to identify an incomplete nonlinear model of ESSO BERNICIA. Within which X_{vr}, $X_{\delta\delta}$ and Y_{rvv} are the only nonlinear terms included in the model and the ship forward speed is used as the velocity parameter for the rudder induced forces and moments. Therefore, what he claimed the applicability of his identified model over a wide range of forward speeds

and ahead engine speed is questionable.

When Nomoto[1975] applied the least square error iteration method to estimate the coefficients of ship steering equation, he met a problem of identifiability. Two coefficients can be adjusted simultaneously to give the same minimum error, as long as their ratio is kept to a certain constant. This is essentially the same phenomenon of simultaneous drift that happened to extended Kalman filtering of ship maneuvering data.

The maximum likelihood method was used by Åström & Källström[1973] [1976], Byström & Källström[1978], Norrbin, Byström, Åström & Källström [1977] to study the ship steering dynamics. Sea trial data was utilized in each study. Åström and Källström[1973][1976] attributed the failure of estimating Y_v', $Y_r'-m'$, N_v', $N_r'-m'x_G'$, Y_δ' and N_δ' simultaneously to the non-linear effect. Since the rudder execution is less than 5° in most of the time during the trial, it is hard to justify that linear model can give very bad result. Actually, even when nonlinear model was applied by Byström & Källström[1978], Norrbin, Byström, Åström & Källström[1977], physically unacceptable values were still obtained. We have found that in their results, simultaneous reduction or simultaneous increase from the model testing value had occured to Y_v', $Y_r'-m'$ pair and N_v', $N_r'-m'x_G'$ pair.

The study of M. I. T., Japan and Sweden has independently indicated that the identifiability is a problem for the ship maneuvering dynamic system. Therefore, in this thesis it is intended to give this "simulta-neous drift" an explanation and develop some practical techniques to avoid this problem. The "cancellation effect" is found to be responsible

for this "simultaneous drift" phenomenon. "Parallel processing", "Exaggerated over- and under-estimated initial guess" and "parameter transformation" are developed to cure this sympton.

In July and August, 1977, extensive maneuvering trials of the 278,000 DWT supertanker ESSO OSAKA were conducted in the Gulf of Mexico. The trials were designed such that the essential maneuvers were all included for research on system identification. A total of 35 data files were provided to M. I. T. in January 1978. Since then much effort has been devoted to processing these data files. Because this is the first time that the real data is fed into our system identification program, we found many flaws in our mathematical model. The modification of model has been carried out interactively between processing the real data and comparing the simulations with these data records. In Chap. 2, we will present the modifications that have been made on the original mathematical description of ship motion.

In Chap. 3, the basic idea of system identification is reviewed briefly. Three parameter estimation techniques: the model reference method, the extended Kalman filtering via state variable augmentation and the maximum likelihood method are mentioned in that chapter, although only the extended Kalman filtering is employed in this work.

The details of model structure, when the system identification technique is applied to the ship maneuvering dynamics, is discussed in Chapter 4.

In Chap. 5, several problems of identifiability is explored. The

slender body theory is used to show that cancellation effect is an in-
trinsic nature of ship dynamics. The sensitivity analysis is studied to
give a proper parameterization strategy for a systematic and reliable
search of the optimal coefficient values.

In Chap. 6, the remedies for eliminating the simultaneous drift are
studied. Among which, the "parallel processing" technique is not as
successful as it thought to be. But we found that it can be used together
with the "exaggerated over- and under-estimated initial guess" to accurete-
ly estimate the ship resistance coefficient.

The ideas proposed in Chap. 6 are illustrated in Chap. 7 by process-
ing the simulated data, the effectiveness of each scheme is evaluated by
comparing the estimated coefficient values to the true values. After
sufficient confidence has been gained, the sea trial data of ESSO OSAKA
is also processed, the accuracy of estimation is checked by comparing the
simulation with the sea trial data.

Conclusions of this work are summarized in Chap. 8, and some recoman-
dations for the future work are also suggested.

2. Governing Equations of Ship Maneuvering Motion

In estimation theory, a mathematical expression is needed to describe the dynamics of the system. A deterministic relationship for ship motion is developed in this chapter as a preparation work for Chapter 4. Most of the time, the derivation is based on Abkowitz's [1969] approach, but modifications are introduced in order to make the modelling more flexible and physically more realistic.

2.1 Assumptions and Coordinate System

Although the ship motion can be described by referring to the coordinate system fixed to the ground, in order to make the calculation of hydrodynamic loading easier, we fix the coordinate system onto ship. For ordinary ships, the geometry is symmetrical about the longitudinal center plane. We choose the intersection of this plane and the calm water surface as x axis, with the positive direction pointing toward bow. Following the sign convention of the Principle of Naval Architecture by Mandel [1967], we let the y axis point to starboard. In order to allow for flexibility, it is not necessary to have the origin coincide with the center of gravity, and the origin can be chosen to take advantage of body geometrical symmetry in the calculation of hydrodymanic force and moment. The midship on x-axis is the preference for the origin in this work.

In general, a ship has six degrees of freedom as illustrated in Fig. 2.1 and we need to consider all these modes to give a complete description of ship motion. By examining the order of magnitude of those
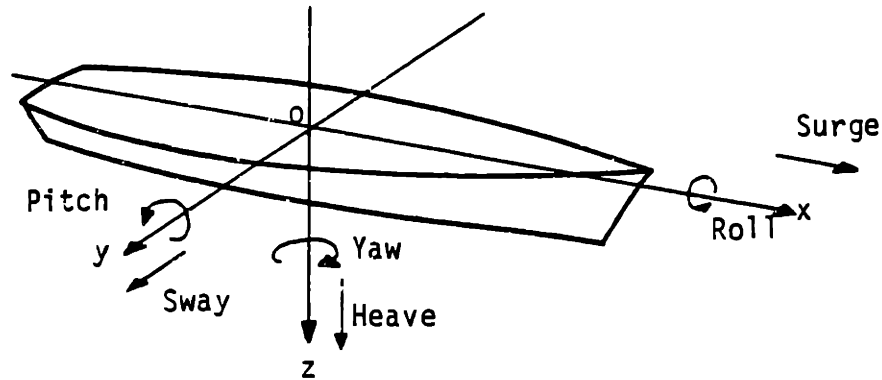
Figure 2.1 Definition of ship motion

cross-coupling hydrodynamic forces and moments between roll and sway
or between roll and yaw, Loukakis and Sclavounous [1979] showed that
roll has minor effect on the sway and the yaw motion, although the
reverse is not true,   the sway and yaw motions do affect the
roll significantly. On the presumption that heave, roll and pitch motion
are not important in the maneuvering problem, the ship is assumed to move
in the horizontal plane only. The coordinate system and the sign
convention for this maneuvering problem is illustrated in Fig. 2.2.
But one must keep it in mind that this statement is not valid when the
ship is

    1. moving at high Froude number;

    2. doing very tight maneuver at high speed,

    3. in restricted water, e.g., canal, channel, harbor...

In this work, merchant ships, such as tankers and cargo ships, are of
main concern. Therefore, the first two situations are most unlikely.

However, open shallow water case will be examined in this work. As long as the rolling, heaving and pitching motion is small and the squat phenomenon is not significant, which is the case during the sea trial of super tanker ESSO OSAKA, surge, sway and yaw are still considered sufficient to describe the ship's maneuvering motion.
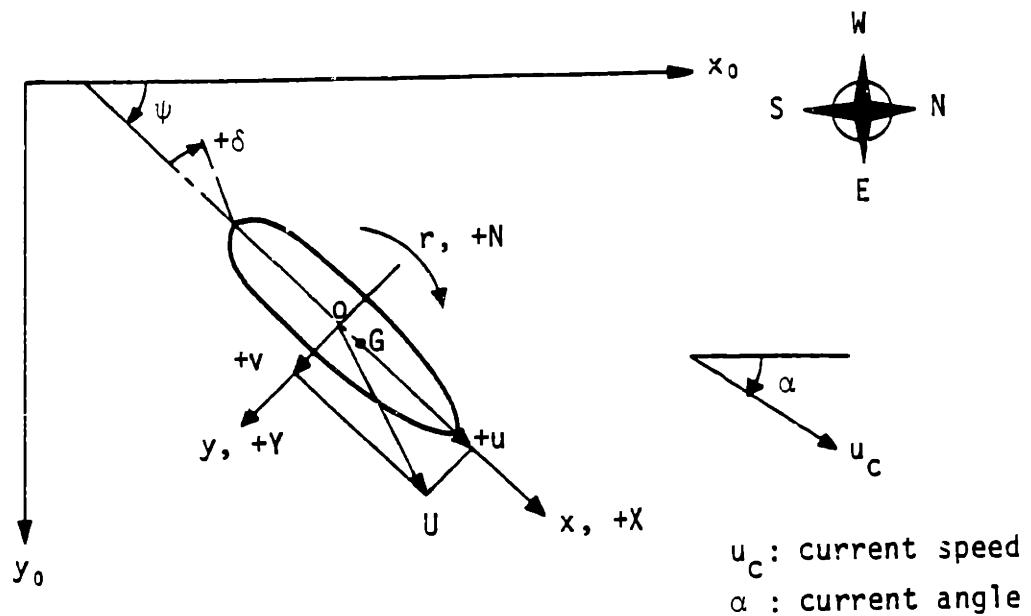
Figure 2.2 Coordinate system and sign conventions

Rigorously speaking, the hydrodynamic force and moment are not only dependent on the instantaneous state of the ship motion but also on the past history of the motion. This is the so-called "memory effect" that is

caused by the vortex shedding and wave generating during the ship maneuvering in that case, the hydrodynamic coefficients are frequency dependent and the exact governing equations of ship motion are integro-differential equations. However, Fujino [1976] found that, within the operating range of merchant ships, these exact equations produced almost the same yaw response to the rudder deflection as that obtained from the quasi-steady state approximation, in which the hydrodynamic force and moment are treated as functions of instantaneous velocities and accelerations only. This observation released the pressure of dealing with a system which is described by a very complicated mathematical relationship. Therefore, the memory effect is neglected in the following part of this thesis.

2.2 Ship Motion in Horizontal Plane

Applying Newton's law of motion, one acquires the following differential equations describing the relationships between the motion variables and the external force and moment:

$$m(\dot{u}-rv-x_G r^2) = X$$

$$m(\dot{v}+ru+x_G \dot{r}) = Y$$

$$I_z \dot{r}+mx_G(\dot{v}+ru) = N \qquad (2.2.1)$$

where X, Y, N are functions of ship properties, fluid properties, motion properties and orientations. If there is a steady current u_c in the direction of α , then the ship velocities relative to water are

$$u_r = u - u_c \cos(\psi - \alpha)$$

$$v_r = v + u_c \sin(\psi - \alpha)$$

$$\dot{u}_r = \dot{u} + u_c r \sin(\psi - \alpha)$$

$$\dot{v}_r = \dot{v} + u_c r \cos(\psi - \alpha) \qquad (2.2.2)$$

Substituting (2.2.2) into (2.2.1), it is found that

$$m[\dot{u}_r - r v_r - x_G r^2] = X(\dot{u}_r, \dot{v}_r, \dot{r}, u_r, v_r, r, \delta, \dots)$$

$$m[\dot{v}_r + r u_r + x_G r] = Y(\dot{u}_r, \dot{v}_r, \dot{r}, u_r, v_r, r, \delta, \dots)$$

$$I_z \dot{r} + m x_G [\dot{v}_r + r u_r] = N(\dot{u}_r, \dot{v}_r, \dot{r}, u_r, v_r, r, \delta, \dots) \qquad (2.2.3)$$

What Eq. (2.2.3) says is that the resulting effect of a steady current on ship motion is just a steady shift of position which can be linearly superimposed on the zero current path as pointed out by Gill [1975]. This finding helps to give a solution of simpler form than that of Szeto [1977]. It is beneficial in reducing the programming difficulty, numerical error, storage memory and computing time.

However, Crane [1979] reported that even   at the same spot but at different depths, the current meters can have 45° difference in direction, 0.3 knots difference in magnitude. Three different methods were employed to estimate the set (direction) and drift (distance) of current; no consistant result was concluded. Among all the maneuvers, the turning circle is probably the only one for which a reasonably good estimation of current is possible, because from the cyclic variation of surge and sway
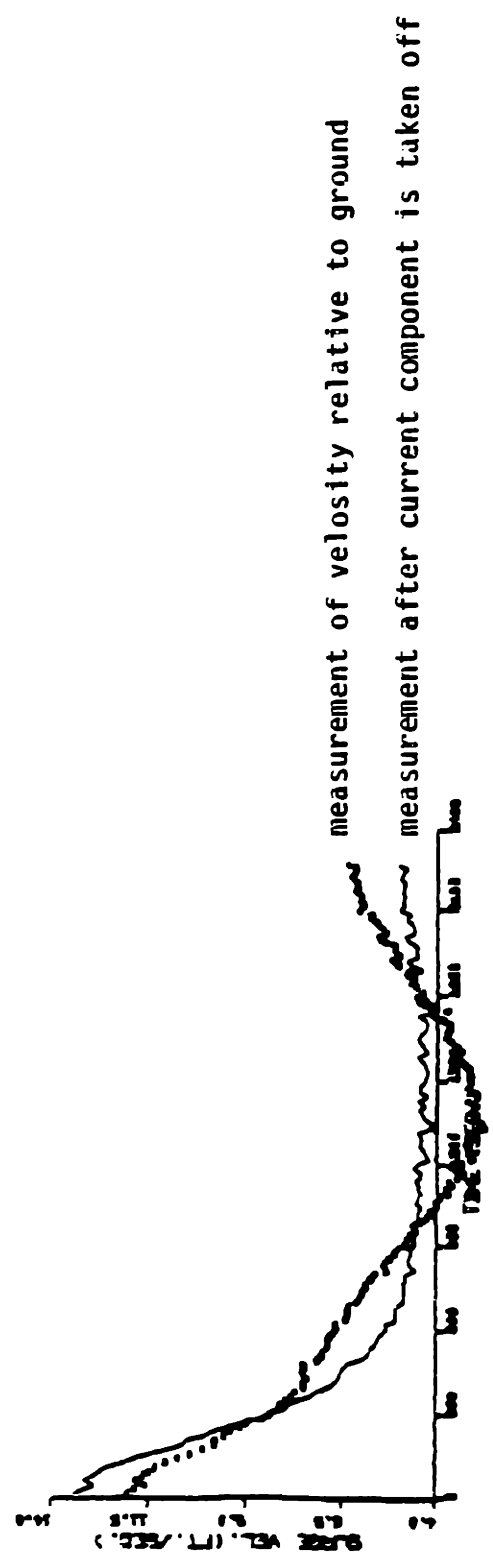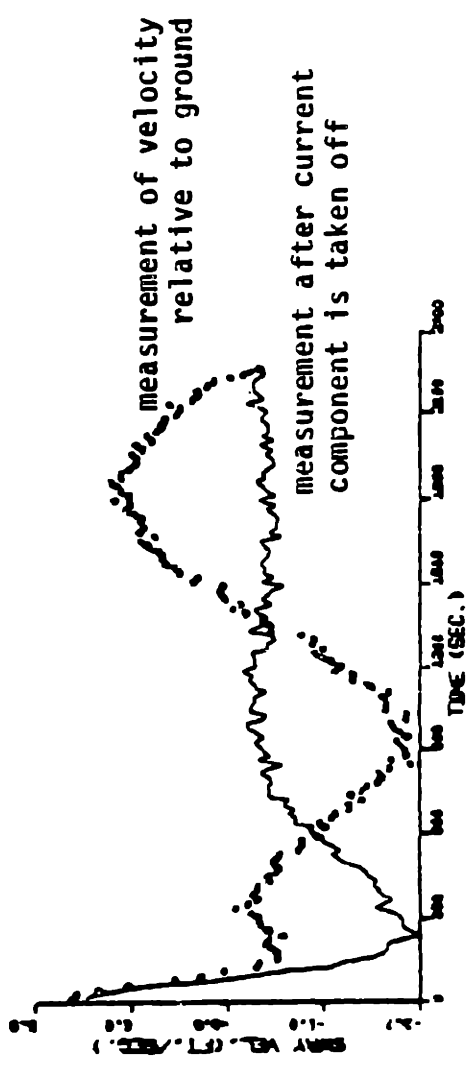
Figure 2.3 Current effect on the measurement of linear velocities

speed in the steady state, the current effect is very obvious. Neverthe-
less, if there is any variation of current during the transient period,
it would be difficult to tell. Figure 2.3 is a comparison between the
absolute ship velocity and the relative velocity to water of ESSO OSAKA's
sea trial data during a turning circle maneuver. Notice that the relative
velocity levels off as it should be, but there may be some error in the
magnitude of peak in the transient period due to a possible changing
current.

These observations raise the question about the validity of constant
current assumption. Indeed, in the latter work, we found that a changing
current can degrade our estimation and we have to avoid this situation by
using the portion of data that current is almost constant. Since a complete
ignorance of current effect would be a disaster for the estimation of hydro-
dynamic coefficients, something awkward is better than nothing, we will
assume a constant current in our model all the time.

2.3 Hydrodynamic Forces and Moments

Due to the complex nature of fluid flow around ship hull, a closed
form expression of the hydrodynamic forces and moments acting on the ship
is almost impossible. Following the conventional approach originated
from Abkowitz [1972], we take the Taylor expansion of these hydrodynamic
force and moment with respect to the motion variables: u_r, v_r, r, $\dot{u}_r$, $\dot{v}_r$, $\dot{r}$
and the deflection of control surface δ about a chosen point at which
$u_r = u_{0_r}$, $v_r = r = \dot{u}_r = \dot{v}_r = \dot{r} = \delta = 0$. Although, the linearized
equation is good enough for studying the stability of ship, it is not

sufficient to simulate the ship motion, Eda [1965]. In order to include the nonlinear effect and yet to keep the number of terms low, the terms of order higher than 3 are considered small and thus neglected. Together with the other assumptions:

. The ship geometry is symmetrical about the center plane.

. The accelerations $\dot{u}_r$, $\dot{v}_r$, $\dot{r}$ are only linearly related to the hydrodynamic force and moment.

There are 60 hydrodynamic coefficients which are retained in the final form. If the factorial coefficient of the Taylor expansions is absorbed into the hydrodynamic coefficient, then

$$X = X_{\dot{u}_r}\dot{u}_r + X_{u_r}\Delta u_r + X_{u_r u_r}(\Delta u_r)^2 + X_{u_r u_r u_r}(\Delta u_r)^3 + X_{v_r v_r}v_r^2 + X_{\delta\delta}\delta^2 + X_{rr}r^2$$

$$+ X_{v_r r}v_r r + X_{v_r\delta}v_r\delta + X_{r\delta}r\delta + X_{\delta\delta u_r}\delta\delta\Delta u_r + X_{rru_r}r^2\Delta u_r + X_{v_r v_r u_r}v_r^2\Delta u_r$$

$$+ X_{v_r ru_r}v_r r\Delta u_r + X_{v_r\delta u_r}v_r\delta\Delta u_r + X_{r\delta u_r}r\delta\Delta u_r \qquad (2.3.1)$$

$$Y = Y_0 + Y_{\dot{v}_r}\dot{v}_r + Y_{\dot{r}}\dot{r} + Y_{v_r}v_r + Y_r r + Y_\delta\delta + Y_{v_r u_r}v_r\Delta u_r + Y_{ru_r}r\Delta u_r + Y_{\delta u_r}\delta\Delta u_r$$

$$+ Y_{v_r v_r v_r}v_r^3 + Y_{rrr}r^3 + Y_{\delta\delta\delta}\delta^3 + Y_{v_r rr}v_r r^2 + Y_{v_r\delta\delta}v_r\delta^2 + Y_{v_r u_r u_r}v_r(\Delta u_r)^2$$

$$+ Y_{rv_r v_r}rv_r^2 + Y_{r\delta\delta}r\delta^2 + Y_{ru_r u_r}r(\Delta u_r)^2 + Y_{\delta v_r v_r}\delta v_r^2 + Y_{\delta rr}\delta r^2 + Y_{\delta u_r u_r}\delta(\Delta u_r)^2$$

$$+ Y_{v_r r\delta}v_r r\delta$$

$$N = N_0 + N_{\dot{v}_r}\dot{v}_r + N_{v_r}v_r + N_r r + N_\delta \delta + N_{v_r u_r}v_r \Delta u_r + N_{ru_r}r\Delta u_r + N_{\delta u_r}\delta \Delta u_r + N_{\dot{r}}\dot{r}$$

$$+ N_{v_r v_r v_r}v_r^3 + N_{rrr}r^3 + N_{\delta\delta\delta}\delta^3 + N_{v_r rr}v_r r^2 + N_{v_r \delta\delta}v_r \delta^2 + N_{v_r u_r u_r}v_r(\Delta u_r)^2$$

$$+ N_{rv_r v_r}r v_r^2 + N_{r\delta\delta}r\delta^2 + N_{ru_r u_r}r(\Delta u_r)^2 + N_{\delta v_r v_r}\delta v_r^2 + N_{\delta rr}\delta r^2 + N_{\delta u_r u_r}\delta(\Delta u_r)^2$$

$$+ N_{v_r r\delta}v_r r\delta$$

Substitute Eq. (2.3.1) into Eq. (2.2.3) and solve for $\dot{u}_r$, $\dot{v}_r$ and $\dot{r}$, we then have

$$\dot{u}_r = \frac{f_1}{m - X_{\dot{u}_r}}$$

$$\dot{v}_r = \frac{(I_z - N_{\dot{r}})f_2 - (mx_G - Y_{\dot{r}})f_3}{f_4} \qquad (2.3.2)$$

$$\dot{r} = \frac{(m - Y_{\dot{v}_r})f_3 - (mx_G - N_{\dot{v}_r})f_2}{f_4}$$

where

$$f_1 = X_{u_r}\Delta u_r + X_{u_r u_r}(\Delta u_r)^2 + X_{u_r u_r u_r}(\Delta u_r)^3 + X_{v_r v_r}v_r^2 + X_{\delta\delta}\delta^2 + (X_{rr} + mx_G)r^2$$

$$+ (X_{v_r r} + m)v_r r + X_{v_r \delta}v_r \delta + X_{r\delta}r\delta + X_{\delta\delta u_r}\delta\delta\Delta u_r + X_{rru_r}r^2 \Delta u_r + X_{v_r v_r u_r}v_r^2 \Delta u_r$$

$$+ X_{v_r ru_r}v_r r\Delta u_r + X_{v_r \delta u_r}v_r \delta \Delta u_r + X_{r\delta u_r}r\delta\Delta u_r$$

$$f_2 = Y_0 + Y_{v_r} v_r + (Y_r - mu_r)r + Y_\delta \delta + Y_{v_r u_r} v_r \Delta u_r + Y_{ru_r} r\Delta u_r + Y_{\delta u_r} \delta \Delta u_r$$

$$+ Y_{v_r v_r v_r} v_r^3 + Y_{rrr} r^3 + Y_{\delta\delta\delta} \delta^3 + Y_{v_r rr} v_r r^2 + Y_{v_r \delta\delta} v_r \delta\delta + Y_{v_r u_r u_r} v_r (\Delta u_r)^2 + Y_{rv_r v_r} rv_r^2$$

$$+ Y_{r\delta\delta} r\delta^2 + Y_{ru_r u_r} r(\Delta u_r)^2 + Y_{\delta v_r v_r} \delta v_r^2 + Y_{\delta rr} \delta r^2 + Y_{\delta u_r u_r} \delta(\Delta u_r)^2 + Y_{v_r r\delta} v_r r\delta$$

$$f_3 = N_0 + N_{v_r} v_r + (N_r - mx_G u_r)r + N_\delta \delta + N_{v_r u_r} v_r \Delta u_r + N_{ru_r} r\Delta u_r + N_{\delta u_r} \delta \Delta u_r$$

$$+ N_{v_r v_r v_r} v_r^3 + N_{rrr} r^3 + N_{\delta\delta\delta} \delta^3 + N_{v_r rr} v_r r^2 + N_{v_r \delta\delta} v_r \delta\delta + N_{v_r u_r u_r} v_r (\Delta u_r)^2 + N_{rv_r v_r} rv_r^2$$

$$+ N_{r\delta\delta} r\delta^2 + N_{ru_r u_r} r(\Delta u_r)^2 + N_{\delta v_r v_r} \delta v_r^2 + N_{\delta rr} \delta r^2 + N_{\delta u_r u_r} \delta(\Delta u_r)^2 + N_{v_r r\delta} v_r r\delta$$

$$f_4 = (m - Y_{\dot v_r})(I_z - N_{\dot r}) - (mx_G - N_{\dot v_r})(mx_G - Y_{\dot r})$$

Having eq. (2.3.2) at hand, it is straightforward to calculate $\dot u$ and $\dot v$ by eq. (2.2.2).

2.4 Non-Dimensionalization of the Hydrodynamic Forces and Moments

Since hydrodynamic force and moment are functions of velocity, those hydrodynamic coefficients in the last section depend on ship's velocity. Experimentally, Eda [1965], Strom-Tejsen & Chislett [1966] have shown that the hydrodynamic force and moment are proportional to the square of velocity and the non-dimensionalized hydrodynamic coefficients are constant in low speed range — the operating range of merchant ships (no Froude number dependency). These observations are very valuable. Otherwise, one will have to store a tremendous amount of information on tnese hydrodynamic coefficients in order to calculate the ship dynamics and the identification

of this system becomes very difficult. In addition, the non-dimensionali-zation of these coefficients allows us to compare the coefficents of different ships and to estimate the dynamics of a full size ship from model test results.

Traditionally, the water density ρ , the ship length L and the ship resultant speed U are employed as the characteristic dimensional parameter. Dividing mass by $\frac{\rho}{2}$ L^3 , length by L and time by $\frac{L}{U}$, one can nondimension-alize all the hydrodynamic coefficients. The list of nondimensionalization factors for major coefficients in Eq. 2.3.2 is shown in Table 2.1.

However, one must notice that it is improper to use only one charac-teristic velocity for all the hydrodynamic coefficients. For instance, due to the wake and race effect, the fluid flow around the rudder has a very different velocity from that around the ship hull. Both Strom-Tejsen & Chislett [1966] and Smitt & Chislett [1974] have shown that if one uses ship velocity to non-dimensionalize the force or moment induced by rudder deflection, the non-dimensionalized curves will not collapse onto one curve. Instead, they are speed dependent. A detail procedure to evaluate the velocity parameter for rudder force and moment will be discussed together with the other modifications of the mathematical model derived in Section 2.5.

2.5 Modification of the Mathematical Model

Until the sea trial data of ESSO OSAKA was provided to M.I.T. in January 1978, the application of system identification to ship maneuvering in this school always worked on the simulated noisy data. The accuracy of

LP	COEFFICIENT	DIMENSIONAL FACTOR
1	$m'-X'_{\dot{u}}$	$0.5\rho L^3$
2	X'_u	$0.5\rho L^2 U$
3	$Y'_{\delta u}$	$0.5\rho L^2 U$
4	$m'-Y'_{\dot{v}}$	$0.5\rho L^3$
5	$m'x'_G-Y'_{\dot{r}}$	$0.5\rho L^4$
6	Y'_v	$0.5\rho L^2 U$
7	Y'_r	$0.5\rho L^3 U$
8	Y'_δ	$0.5\rho L^2 U^2$
9	Y'_0	$0.5\rho L^2 U^2$
10	$m'x'_G-N'_{\dot{v}}$	$0.5\rho L^4$
11	$I'_z-N'_{\dot{r}}$	$0.5\rho L^5$
12	N'_v	$0.5\rho L^3 U$
13	N'_r	$0.5\rho L^4 U$
14	N'_δ	$0.5\rho L^3 U^2$
15	N'_{vrr}	$0.5\rho L^5 U^{-1}$
16	X'_{uu}	$0.5\rho L^2$
17	X'_{uuu}	$0.5\rho L^2 U^{-1}$
18	X'_{vv}	$0.5\rho L^2$
19	$X'_{rr}+m'x'_G$	$0.5\rho L^4$
20	$X'_{\delta\delta}$	$0.5\rho L^2 U^2$
21	$X'_{vr}+m'$	$0.5\rho L^3$
22	$X'_{v\delta}$	$0.5\rho L^2 U$
23	$N'_{\delta u}$	$0.5\rho L^3 U$
24	N'_0	$0.5\rho L^3 U^2$
25	Y'_{vvv}	$0.5\rho L^2 U^{-1}$
26	$Y'_{\delta\delta\delta}$	$0.5\rho L^2 U^2$
27	Y'_{rvv}	$0.5\rho L^3 U^{-1}$
28	$Y'_{\delta vv}$	$0.5\rho L^2$
29	$Y'_{v\delta\delta}$	$0.5\rho L^2 U$
30	N'_{vvv}	$0.5\rho L^3 U^{-1}$
31	$N'_{\delta\delta\delta}$	$0.5\rho L^3 U^2$
32	N'_{rvv}	$0.5\rho L^4 U^{-1}$
33	$N'_{\delta vv}$	$0.5\rho L^3$
34	$N'_{v\delta\delta}$	$0.5\rho L^3 U$
35	Y'_{vrr}	$0.5\rho L^4 U^{-1}$
36	$X'_{u\delta\delta}$	$0.5\rho L^2 U$

Table 2.1 Dimensional factors for nondimensionalizing the hydrodynamic coefficients.

the modelling had never been challenged before that time. In the initial

effort of estimating the hydrodynamic coefficient value by processing

the sea trial data, we found that not only the estimation was physically

unacceptable, but also the validity test indicated some sympton of ill

modelling. There are many possibilities; the deterministic description

of ship motion is the first thing to check. In this section, the author

will present several modifications of the model based on the feedback of

data processing.

2.5.1 Force and Moment Derivatives with Respect to Rudder Deflection

In the discussion of Strom & Chislett's paper [1974], Thulin has

pointed out that it is the flow velocity over rudder that one should use

to nondimensionalize the force and moment induced by rudder deflection.

The entire fluid region around the rudder is highly complicated, not only

because the rudder is behind the ship's wake and propeller's race but

also because the flow is not uniformly distributed over the span. A simple

and yet effective approximation was introduced by Thulin. Let the

geometrical relationship between the propeller and the rudder be illustrated

in Fig. 2.4. Assume the flow far upstream the propeller and the flow over

the portion of rudder which is outside the race have a velocity (1-w)u. The

velocity within the "slipstream" can be calculated by the momentum theory.

Far behind the propeller disk, the induced axial velocity u_{A_∞} is

$$u_{A_\infty} = -(1-w)u + \sqrt{(1-w)^2 u^2 + \frac{8}{\pi} K_T (nd)^2} \qquad (2.5.1)$$

At a general position x , the induced mean axial velocity u_A is acquired

- 46 -
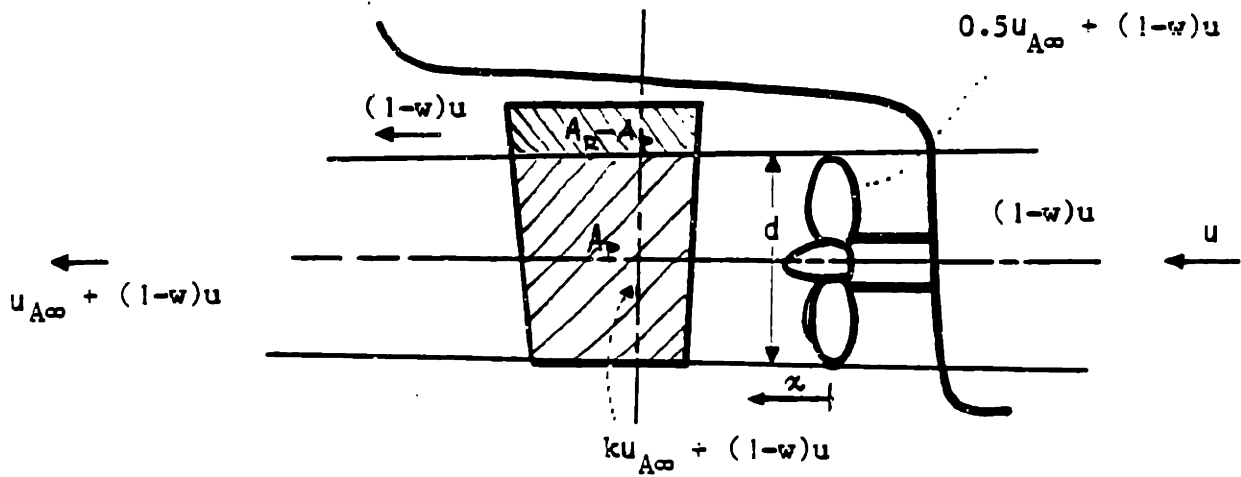
Figure 2.4 Geometrical relationship between the
           propeller and the rudder. Propeller race
           according to momentum theory.
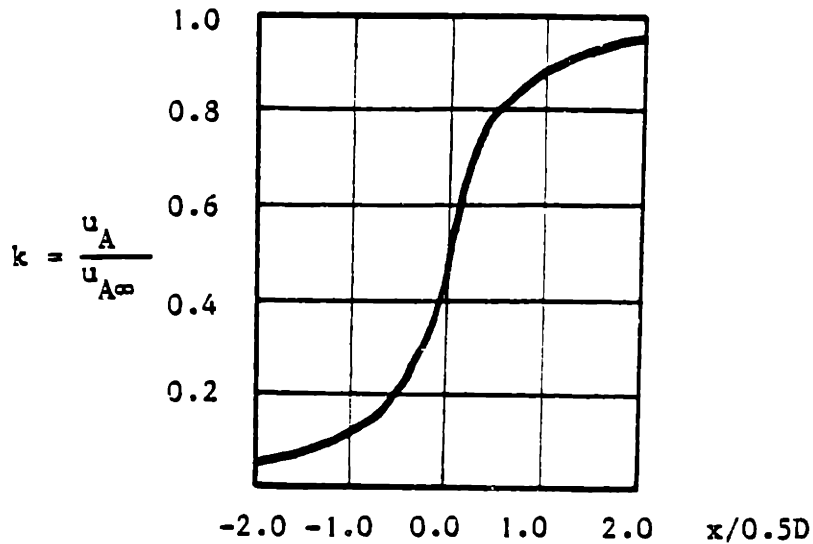
Figure 2.5 The mean axial velocity induced by a
           semi-infinite tube of ring vortices
           determined by the Law of Biot-Savart.
           (ref. Smitt & Chislett[1974])

by multiplying u_{A_∞} a factor k , which is a function of the axial distance x from the propeller disk to the point of interest. In this case x is the location of the quarter mean chord of the rudder. An infinite blade propeller was used to find the functional relationship between k and x . See Fig. 2.5. The mean squared velocity c^2 over the rudder is now evaluated as a weighted sum of $(1-w)^2u^2$ and $u_A{}^2$.

$$c^2 = \frac{A_P}{A_R} \left[(1-w)u+ku_{A_\infty}\right]^2 + \frac{A_R-A_P}{A_R} (1-w)^2u^2 \qquad (2.5.2)$$

Since Eq. (2.5.2) requires the information of open water test of propeller, rudder geometry and the record of ship forward speed u and the rpm of propeller during the trial, it is an expression that relates the major factors to the fluid flow over the rudder. Although several assumptions are made to derive (2.5.2), physically it is still more natural and convincing to use this averaged speed c , instead of the resultant speed of ship U , as the dimensioning factor.

Yet, one must remember that switching from U to c as the dimensioning factor for rudder induced force and moment is not the only modification one has to make in order to make the model more appropriate. Since the hull-propeller-rudder interactions and the speed loss effect have been accounted for in Eq. (2.5.2), it is necessary to remove the terms in the original model, Eq. (2.3.2), that represent these effects. The $X_{u_r\delta\delta}$, $X_{v_r\delta u_r}$, $X_{r\delta u_r}$, $Y_{\delta u_r}$, $Y_{\delta u_r u_r}$, and $N_{\delta u_r}$, $N_{\delta u_r u_r}$ are the very terms that should be removed from the expressions.

Despite the merit of this modification, one may argue that if sufficient number of higher order terms are kept in the model and the ship speed is still employed as velocity parameter, an accurate simulation is still possible. It may be difficult to disapprove this statement, but its disadvantage is obvious. First, the expressions become complicated and it increases the computing burden. Second, it is very difficult to interpret the physical meaning of those higher order terms. The worst of all, it is extremely hard to estimate these coefficients by system identification techniques.

To see the improvement after this modification, we simulate the ship motion by "the old" and "the new" model and compare it with the sea trials. The hydrodynamic coefficients values are based on the model testing value for ESSO OSAKA provided by Stevens Institute of Technology and no system identification has been conducted yet. In Figure 2.6 is a comparison of 20°/20° zigzag maneuver. Notice that we did not use the sea trial record of rudder deflection and propeller rpm in the simulation. If it were the case, the simulations would be even better. Nevertheless, the phase shift of v and r are almost eliminated and the speed loss track the sea trial data very well for the new model. The old model is apparently inferior to the new model.

2.5.2 Longitudinal Force derivatiives on a Straight Course

In eq. (2.3.1), $X_u \Delta u + X_{uu}(\Delta u)^2 + X_{uuu}(\Delta u)^3$ represents the effect of speed loss. On a straight course, this is actually the difference between the effective thrust and the ship resistance, (1-t)T-R. At the first
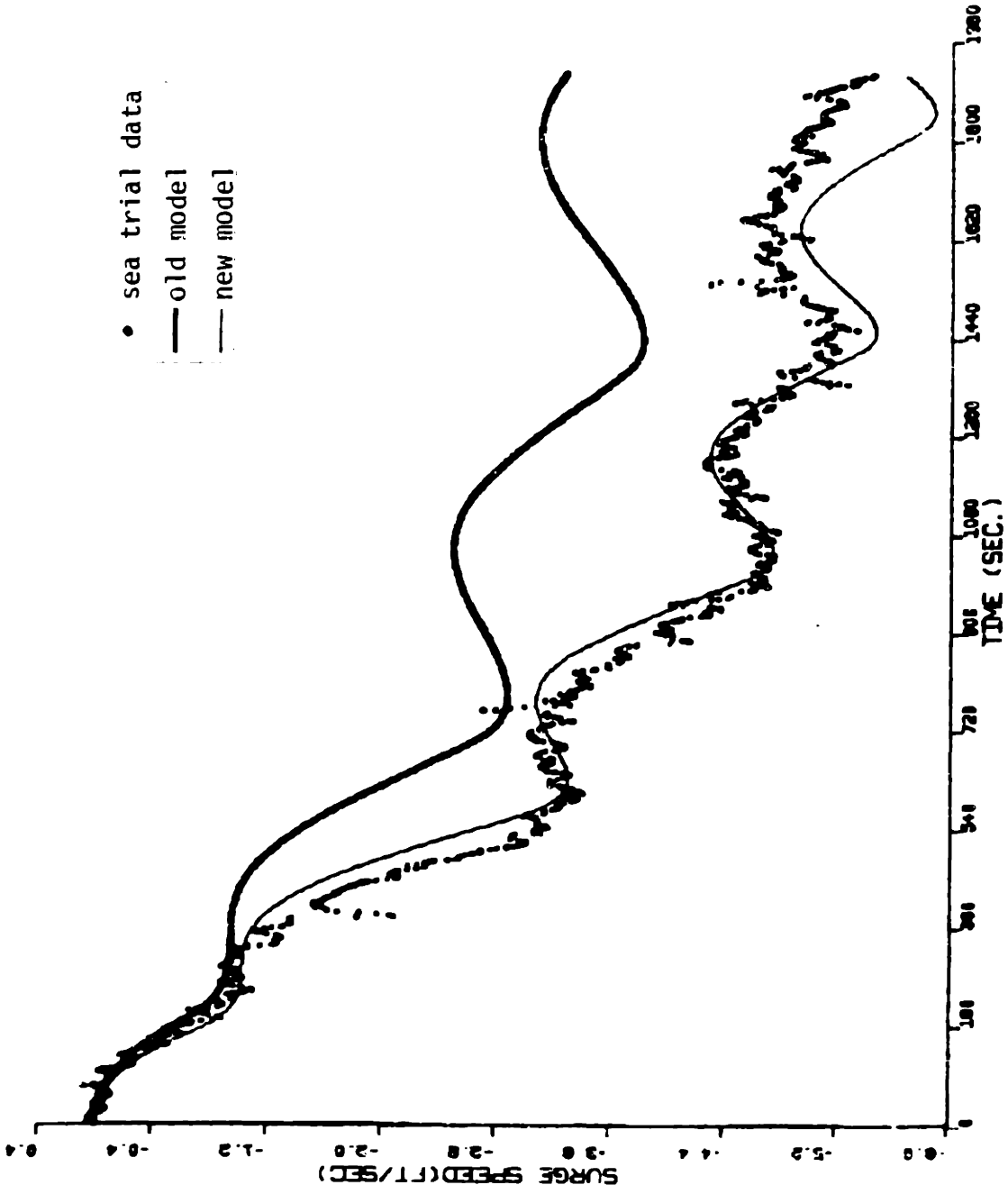
Figure 2.6.a   Improvement on the surge speed simulation of 20°/20° zigzag maneuver
for ESSO OSAKA after the modification of model in Sec. 2.5.1.
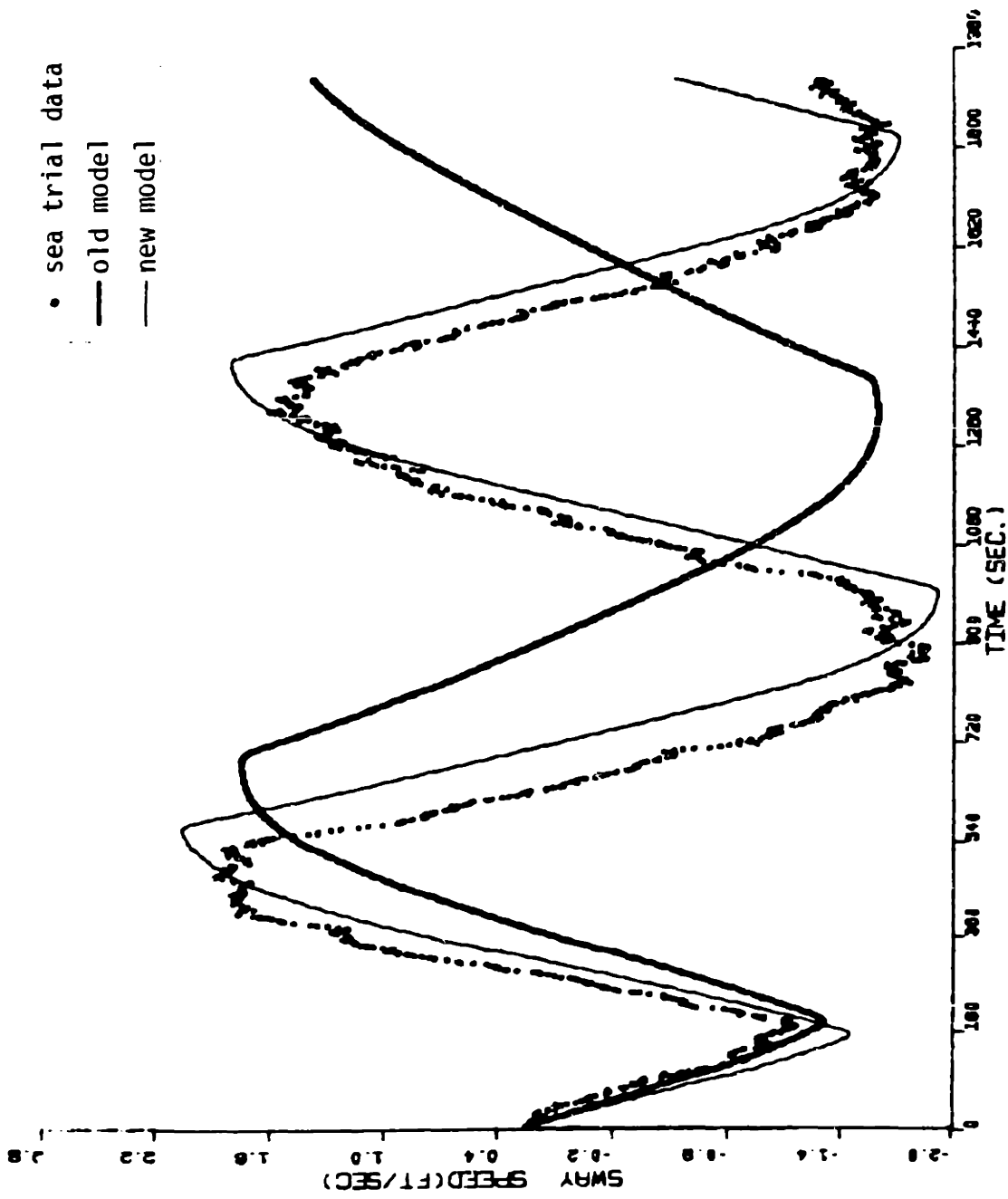
Figure 2.6.b Improvement on the sway speed simulation of 20°/20° zigzag maneuver for ESSO OSAKA after the modification of model in Sec. 2.5.1
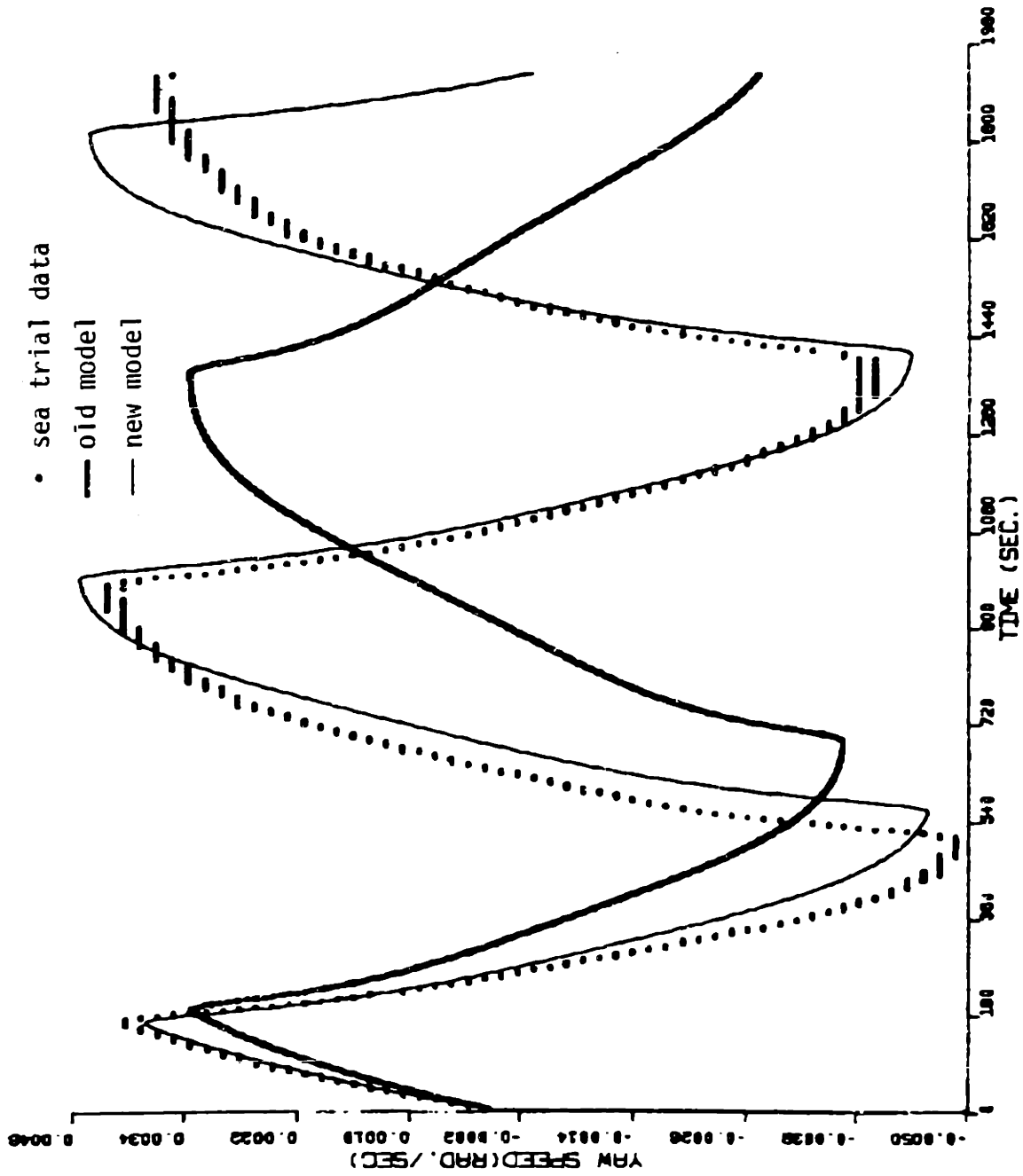
Figure 2.6.c Improvement on the yaw speed simulation of 20°/20° zigzag maneuver for ESSO OSAKA after the modification of model in Sec. 2.5.1.
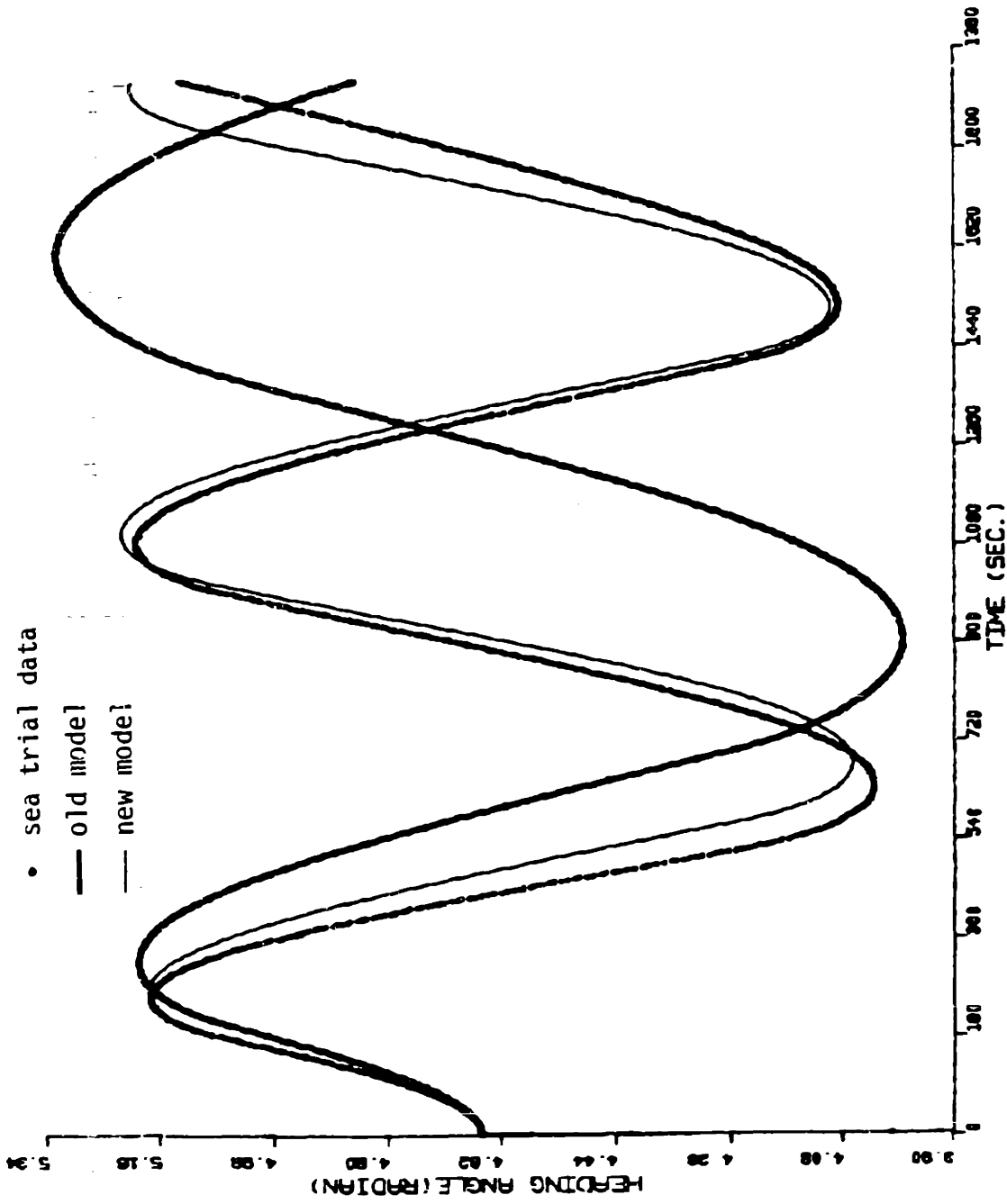
Figure 2.6.d Improvement on the heading simulation of 20°/20° zigzag maneuver for ESSO OSAKA after the modification of model in Sec. 2.5.1.
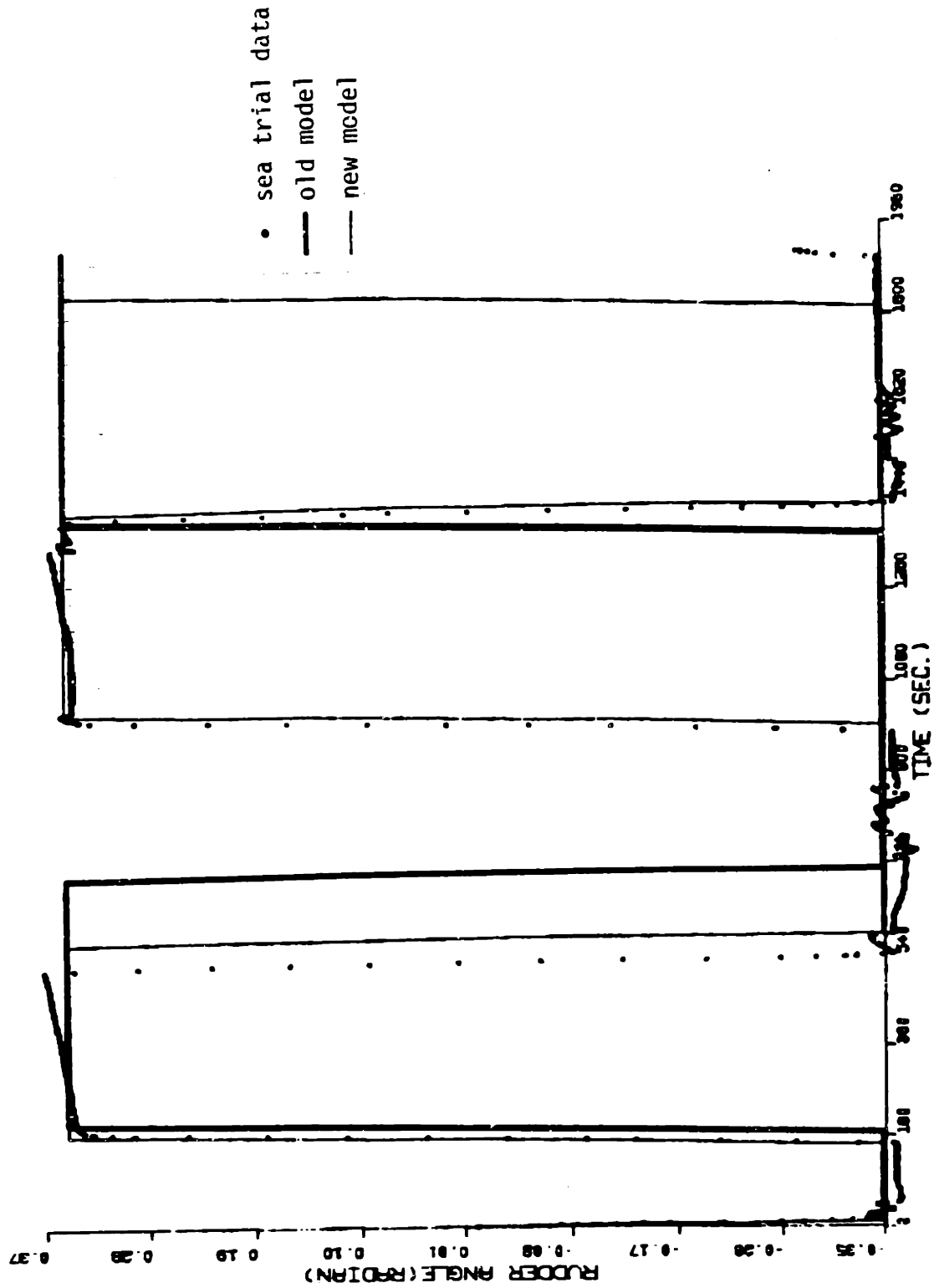
Figure 2.6.e Time histories of rudder execution used in the simulation in Fig. 2.6.a to Fig. 2.6.d and the rudder execution in sea trial.

glance, it is a very neat expression to use. But many questions were raised about the generality of this expression when system identification is applied to estimate the value of X_u', X_{uu}' and X_{uuu}'. For instance, are these values data file independent? can this expression model some special situation like coasting with wind milling propeller or coasting with locked propeller? To understand the problem let us study the expression $(1-t)T-R$ further.

Write $(1-t)T-R$ in the form

$$(1-t)T-R = (1-t)K_t \rho n^2 d^4 - \frac{\rho}{2} C_R S u^2 \qquad (2.5.3)$$

Notice that the calculation of effective thrust force and ship resistance is not so straightforward as it appears to be, because the thrust deduction factor t, the thrust coefficient K_t and the resistance coefficient are not just constant,

1. K_t is a function of advance ratio $J=\frac{u(1-w)}{nd}$ and cavitation number σ, i.e., $K_t=K_t(J,\sigma)$,

2. t varies with the propeller loading K_t, slowly though,

3. A large change in Reynolds number or a change in the ship wave system will cause the change of wake fraction w, Mandel[1967],

4. C_R is a function of R_n and Froude number F_r.

Therefore, if a complete emperical information of K_t, t, w and C_R versus the pertinent parameters is unavailable, we can hardly acquire a good simulation for the ship motion. That is why eq. (2.5.3) is not suitable for the purpose of system identification.

If we assume the propeller operates in the range of no significant change in cavitation number σ and K_t is a linear function of J, then K_t can be approximated by

$$K_t = K_{t_0} + \left(\frac{\partial K_t}{\partial J}\right)_0 \Delta J \tag{2.5.4}$$

Similarly, C_R can be approximated by

$$C_R = C_{R_0} + \left(\frac{\partial C_R}{\partial u}\right)_0 \Delta u \tag{2.5.5}$$

Using the definition of J and the equilibrium condition

$$K_{t_0} \rho n_0^2 d^4 (1-t_0) = C_{R_0} \frac{\rho}{2} S u_0^2 \tag{2.5.6}$$

we can write eq. (2.5.3) as

$$(1-t)T-R = \frac{\rho}{2} S C_{R_0} u_0^2 \left[\left(\frac{n}{n_0}\right)^2 \frac{(1-t)}{(1-t_0)} - \left(\frac{u}{u_0}\right)^2\right] + \left(\frac{\partial K_t}{\partial J}\right)_0 \left[\frac{u(1-w)}{nd}\right.$$
$$\left. - \frac{u_0(1-w_0)}{n_0 d}\right] \cdot \rho n^2 d^4 (1-t) - \frac{\rho}{2}\left(\frac{\partial C_R}{\partial u}\right)_0 S u^2 (u-u_0) \tag{2.5.7}$$

Suppose the change in Reynolds number R_n and in ship wave system is small enough to assume a constant wake fraction w_0 and the change of propeller loading is limited enough to assume a constant thrust deduction coefficient t, then equation (2.5.7) can be simplified to

$$X = \frac{\rho}{2} C_{R_0} S u_0^2 \left[\left(\frac{n}{n_0}\right)^2 - \left(\frac{u}{u_0}\right)^2\right] + \rho n d^3 u_0 \left(\frac{\partial K_t}{\partial J}\right)_0 \left(\frac{u}{u_0} - \frac{n}{n_0}\right)(1-w_0)(1-t_0)$$
$$- \frac{\rho}{2}\left(\frac{\partial C_R}{\partial u}\right)_0 S u^2 (u-u_0) \tag{2.5.8}$$

If the propeller rotating speed can be kept essentially constant, e.g., a ship powered by steam turbine, Abkowitz [1978] showed that

$$X_u = \rho n_0 d^3 \left(\frac{\partial K_t}{\partial J}\right)_0 (1-w_0)(1-t_0) - \rho C_{R_0} S u_0 - \frac{\rho}{2} S u_0^2 \left(\frac{\partial C_R}{\partial u}\right)_0$$

$$X_{uu} = -\frac{\rho S}{2} \left[C_{R_0} + 2 \left(\frac{\partial C_R}{\partial u}\right)_0 u_0 \right] \qquad (2.5.9)$$

$$X_{uuu} = -\frac{\rho S}{2} \left(\frac{\partial C_R}{\partial u}\right)_0$$

Apply the conventional way to nondimensionalize the expressions in equation (2.5.9), one can immediately see the problem of "data-point specific". Unless $\left(\frac{\partial C_R}{\partial u}\right)_0$ is negligibly small, X_u', X_{uu}' and X_{uuu}' are dependent on the equilibrium point. This is probably not a serious problem for commerical ships, because most of them are designed to operate in the flat region of resistance curve. However, one must notice that we made many assumptions to derive equation (2.5.9) from equation (2.5.3), any violation of them will cause the same data specific problem. For the sea trial data of ESSO OSAKA that we have been dealing with, the propeller rotating speed is not essentially constant all the time and the change of thrust coefficient is significant enough to challenge the assumption of constant thrust deduction coefficient t during a tight maneuver.

Therefore, at least for this thesis work, the expressions in equation (2.5.9) are not valid to use. We have to seek for another

model which has less constraints to use and yet is suitable for parameter estimation.

The idea here is to replace the thrust developed behind the ship, $(1-t)T$, by an emperical expression in terms of the propeller rpm and the ship forward speed,

$$(1-t)T \longrightarrow \eta_1 u^2 + \eta_2 nu + \eta_3 n^2 \qquad (2.5.10)$$

When the ship is moving at constant heading, the external force is almost the net effect between the thrust $(1-t)T$ and hull drag $C_R \frac{\rho}{2} Su^2$. In Table 2.2 we list several cases of concern to the naval architect and that can be represented by this new expression without difficulties.

n	u	$(1-t)T - C_R \frac{\rho}{2} Su^2$	Physical Description
0	$\neq 0$	$\eta_1 u^2 - C_R \frac{\rho}{2} Su^2$	Resistance of a locked propeller
$n_{wind\ milling}$	$\neq 0$	$-C_R \frac{\rho}{2} Su^2$ $+\eta_1 u^2 + \eta_2 nu + \eta_3 n^2$	Resistance due to ship hull & appendices + resistance due to windmilling propeller
$\neq 0$	0	$\eta_3 n^2$	Bollard Pull
n_0	u_0	≈ 0	Equilibrium state
n	u	$\eta_1 u^2 + \eta_2 nu + \eta_3 n^2$ $-C_R \frac{\rho}{2} Su^2$	Acceleration

Table 2.2 Cases represented by the emperical expression of effective thrust in (2.5.10) and the resistance in a straight course.

Although we may still have to assume C_R is almost contant in the system identification, it is amazing to see this new expression has more flexibility to model the effective thrust of ship than the other models do. The lack of physical meaning for η_1, η_2 and η_3 does not prevent a good initial guess of their quantities for the identification, because simultaneous equations of η_1, η_2 and η_3 can be solved by using the propeller characteristic curve and one equilibrium operating condition of the ship. A rough calculation showed that the resistance induced by locked propeller is about 15% $\sim$ 20% of the hull drag. This is consistent with the estimation suggested by Mandel[1967], which says that the resistance δR due to a locked propeller is

$$\delta R = C_D \frac{\rho}{2} A V_a^2 \tag{2.5.10}$$

where

A is the developed area of the propeller in square feet

V_a is the speed of advance

C_D is the nondimensional drag coefficient. For the locked propeller, 1.0 is suggested.

2.5.3 <u>Correction of $Y_v^\prime$, $Y_r^\prime$, $N_v^\prime$, $N_r^\prime$ due to the Effect of Propeller</u>
<u>Overloading</u>

In the previous discussion we already pointed out that at each equilibrium state, the non-dimensionalization of Y_v Y_r, N_v and N_r based on the ship resultant speed $\sqrt{u^2+v^2}$ can reduce them to single valued quantities. During the maneuver, if the propeller loading is not

kept constant, we then need a modification to count for the effect of derivation from the equilibrium state.

The component of these forces and moments can be roughly categorized into four parts, if ξ represents v or r ,

$$Y_{\xi_{total}} = Y_{\xi_{hull}} + Y_{\xi_{propeller}} + Y_{\xi_{rudder}} + Y_{\xi_{interactions \; between \; hull, \; propeller \; and \; rudder}}$$

$$N_{\xi_{total}} = N_{\xi_{hull}} + N_{\xi_{propeller}} + N_{\xi_{rudder}} + N_{\xi_{interactions \; between \; hull, propeller \; and \; rudder}}$$

Since the effect of propeller and the interaction between propeller and rudder are implied in the race velocity over rudder and the interactions between hull, propeller and rudder are small, we rewrite Eq. (2.5.11) as

$$Y_{\xi_{total}} = Y_{\xi_{hull}} + Y_{\xi_{propeller+rudder+interactions}}$$

$$(2.5.12)$$

$$N_{\xi_{total}} = N_{\xi_{hull}} + N_{\xi_{propeller+rudder+interactions}}$$

Let us consider the Y_v term first, the rest can be discussed in a similar way. At any maneuvering condition, the Y_v is composed of the Y_v at equilibrium state and the correction of Y_v due to the unequilibrium propeller loading,

2.5.4 Asymmetrical Force Y_0 and Moment N_0 at Zero Rudder for Ships of Single Propeller

For a ship of single propeller there is a hydrodynamic force and moment applied on the ship when the rudder is at the middle position. For example, a ship with a right handed propeller,

1. Due to upward component in the wake field, the propeller blade at starboard side will develop a larger thrust force than that of the blade at port side position. A port moment is thus generated.

2. Due to the higher wake fraction near the 12 o'clock position and the lower wake fraction near the 6 o'clock position in a propeller disk, a net port reaction force and a starboard moment are thus generated.

3. Due to the upward component in the wake field, the propeller blade of starboard side has a heavier loading than that of the blade at port side.

   Therefore, the pressure field around hull at stern is not evenly distributed. A net force to starboard and a net port yawing moment are produced by this pressure difference. However, Shiba [1960] has shown that this effect is not so significant.

4. Due to the higher wake fraction near the 12 o'clock position, the heavier loading of propeller blade causes a greater tangential velocity in the upper part. This effect generates a greater oblique flow impinging on the upper part of the rudder than the similar effect does on the lower part of the rudder. A net starboard force and a net port yawing moment are generated.

$$Y_{v_{total}}\bigg|\begin{matrix}\text{unequilibrium}\\\text{maneuvering}\\\text{state}\end{matrix} = Y_{v_{total}}\bigg|\begin{matrix}\text{equilibrium}\\\text{state at u}\end{matrix}{}^{+\Delta Y_{v_{total}}} \qquad (2.5.13)$$

$$= Y_{v_{total}}\bigg|\begin{matrix}\text{equilibrium}\\\text{state at u}\end{matrix}{}^{+\Delta Y_{v_{hull}}}$$

$$+\Delta Y_{v_{propeller+rudder+interactions}}$$

Since all the interactions are grouped into the third term, the second term thus has a zero value. The unequilibrium propeller loading causes a faster or slower race velocity, thus the third term can be written as:

$$\Delta Y_{v_{propeller+rudder+interaction}}^v$$

$$\approx [\frac{\partial C_L}{\partial \alpha} \tan^{-1} \frac{v}{c} \frac{\rho}{2} A_R(c^2+v^2)] \cos(\tan^{-1} \frac{v}{c}) - [-\frac{\partial C_L}{\partial \alpha} \tan^{-1} \frac{v}{c_e} \frac{\rho}{2} A_R(C_e^2+v^2)]$$

$$\cdot \cos(\tan^{-1} \frac{v}{c_e})$$

$$\approx -\frac{\partial C_L}{\partial \alpha} \frac{\rho}{2} A_R[vc-vc_e] = -\frac{\frac{\partial C_L}{\partial \alpha} \frac{\rho}{2} A_R}{\frac{\rho}{2} L^2} \frac{\rho}{2} L^2[vc-vc_e] \qquad v^2 << c^2$$

$$= -Y_{\delta}' [c-c_e] v \frac{\rho}{2} L^2 \approx 2N_{\delta}'[c-c_e] v \frac{\rho}{2} L^2 \qquad (2.5.14)$$

where

$$\frac{\partial C_L}{\partial \alpha} = \text{slope of rudder lift coefficient}$$

c_e = c of equilibrium propeller loading at forward speed u

A_R = rudder area

By analogy, we have

$$\Delta Y_r \cdot r \Big|_{p+r+i} \approx 0.5\ Y_\delta[c-c_e]r\ \frac{\rho}{2}\ L^3 \approx -N_\delta[c-c_e]\ r\ \frac{\rho}{2}\ L^3 \qquad (2.5.15)$$

$$\Delta N_v \Big|_{p+r+i} \approx -N_\delta\ \frac{\rho}{2}\ L^3\ [c-c_e]v \qquad (2.5.16)$$

$$\Delta N_r r \Big|_{p+r+i} \approx 0.5\ N_\delta\ \frac{\rho}{2}\ L^4[c-c_e]r \qquad (2.5.17)$$

Therefore, the non-dimensionalized Y_v, Y_r, N_v and N_r can be written as:

$$Y_v \Big|_{total}\Big|_{maneuvering\ state} = Y_v \Big|_{equilibrium} - Y_\delta\ \frac{(c-c_e)}{U}$$

$$Y_r \Big|_{total}\Big|_{maneuvering\ state} = Y_r \Big|_{equilibrium} + 0.5\ Y_\delta\frac{(c-c_e)}{U}$$

$$N_v \Big|_{total}\Big|_{maneuvering\ state} = N_v \Big|_{equilibrium} - N_\delta\frac{(c-c_e)}{U}$$

$$N_r \Big|_{total}\Big|_{maneuvering\ state} = N_r \Big|_{equilibrium} + 0.5\ N_\delta\frac{(c-c_e)}{U} \qquad (2.5.18)$$

It is interesting to see that all these modifications are just simple multipliers of Y_δ or N_δ. We thus have the advantage of improving the model accuracy without introducing extra unknown quantities. Actually, these modifications count in $Y_{v_r u_r}$, $Y_{r u_r}$, $Y_{v_r u_r u_r}$, $Y_{r u_r u_r}$ $N_{v_r u_r}$, $N_{r u_r}$, $N_{v_r u_r u_r}$, $N_{r u_r u_r}$ already. Therefore, we should omit them from Eq.(2.3.2). Similarly, $X_{r r u_r}$, $X_{v v u_r}$ account for the effect

- 62 -

of propeller overloading. However, there is no evidence that they are of significant contribution. Therefore, we will omit X_{rru_r} and X_{vvu_r} in X equation of (2.3.2)

A quick estimation of the order of magnitude of these modifications for OSAKA at the end of $20^0/20^0$ zigzag maneuvers shows that

$$\frac{\Delta Y_v'}{Y_v'_{equibrium}} = \frac{-Y_\delta' \frac{(c-c_e)}{U}}{Y_v'_{equilibrium}} = 9.3\%$$

$$\frac{\Delta Y_r'}{Y_r'_{equilibrium}} = \frac{0.5Y_\delta' \frac{c-c_e}{U}}{Y_r'_{equilibrium}} = 33.70\%$$

$$\frac{\Delta N_r'}{N_v'_{equilibrium}} = \frac{-N_\delta' \frac{c-c_e}{U}}{N_v'_{equilibrium}} = -12.08\%$$

$$\frac{\Delta N_r'}{N_r'_{equilibrium}} = \frac{0.5N_\delta' \frac{c-c_e}{U}}{N_r'_{equilibrium}} = 13.17\%$$

Although the coefficients used for this estimation are based on the model testing value, we believe this estimation of order of magnitude is pretty close. Since these modifications due to an unequilibrium propeller loading are very significant, they should be included into the model for an accurate description of the ship motions.

The resultant effect of the above factors usually gives the right handed propeller ship a starboard force and a yawing moment to turn the ship to port.

The observation also tells us that when the ship starts up from zero forward speed, there is a strong tendency to turn to port for a right-handed propeller ship. However, the mechanism is different from the above discussion, because the wake is negligible in this situation. Mandel[1967] pointed out that the water near the surface is easier to set in motion than the deeper water when the propeller is working on them. In addition, if the propeller operates near the surface or breaks the surface, air will be drawn down to the propeller. Therefore, the upper blade suffers a torque loss that gives rise of a starboard force and port moment.

Since the propeller develops a side force and yaw moment even if at zero forward speed, the conventional velocity parameter U for the asymmetrical force Y_0 and N_0 is not a suitable one to use. Otherwise, we will not have any such unbalanced force or moment to account for these phenomena. Also, to meet the condition of (or negligible) zero force and moment of this kind at zero rpm, we think the velocity induced by a rotating propeller at its position, which is $\frac{1}{2}u_{A\infty}$ by the momentum theory, is more appropriate to use. Therefore, the non-dimensionalized force Y_0' and moment N_0' are now defined as

$$Y_0' = \frac{Y_0}{\frac{1}{2}\rho L^2 (\frac{u_{A\infty}}{2})^2} \qquad\qquad (2.5.19)$$

$$N_0' = \frac{N_0'}{\frac{1}{2}\rho L^3 (\frac{u_{A\infty}}{2})^2} \qquad\qquad (2.5.20)$$

where $u_{A\infty}$ is defined by equation (2.5.1).

2.5.5 δ, v, r Cross Correlated Higher Order Force and Moment Derivatives

In equation 2.3.2, $Y_{\delta\delta\delta}\delta\delta$ and $N_{\delta\delta\delta}\delta\delta$ account for the nonlinear effect of rudder force and moment at large rudder deflection in the absence of sway and yaw speed, while $Y_{v\delta\delta}v\delta\delta$, $N_{v\delta\delta}v\delta\delta$ ... represent the correction of these nonlinear effect when the ship is not in straight motion. The main concern here is the difficulty to acquire reliable information of these coefficients. It is not only the problem of time, labor and financial constraints but also a problem of measurement accuracy for the higher order terms. Thus a compact and physically realistic expression is more attractive to use.

In figure 2.7 is an illustration of the fluid flow around a rudder for a maneuvering ship. The effective attack angle e is

$\alpha = \tan^{-1}(\frac{v-0.5rL}{c})$ $\quad$ $v-0.5rL$

$[c^2+(v-0.5rL)^2]^{0.5}$
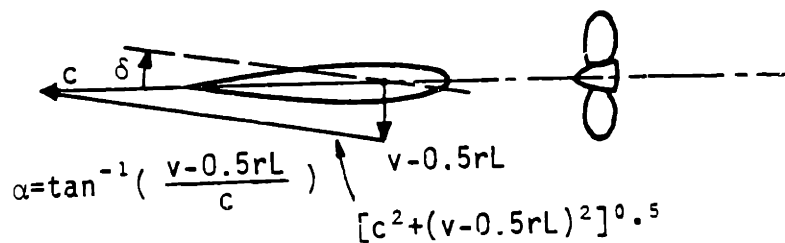
Figure 2.7 Fluid flow around the rudder of a maneuvering ship and effective rudder angle.

the difference between δ and $\alpha=\tan^{-1}(\frac{v-r\frac{L}{2}}{c})$. Since the Y-force is composed of lift force and drag force, we have

$$Y_f = L_f \cos\alpha + D_f \sin\alpha \tag{2.5.21}$$

$$\approx 2\pi\sin[\delta-\tan^{-1}(\frac{v-r\frac{L}{2}}{c})] \frac{\rho}{2}L^2[c^2+(v-r\frac{L}{2})^2] \cos[\tan^{-1}(\frac{v-r\frac{L}{2}}{c})]$$

$$+ \ldots\ldots\ldots$$

$$\approx 2 \sin[\delta-\tan^{-1}(\frac{v-r\frac{L}{2}}{c})] \frac{\rho}{2} L^2[c^2+(v-r\frac{L}{2})^2] [1-\frac{1}{2}(\tan^{-1}\frac{v-r\frac{L}{2}}{c})^2 +\ldots]+\ldots$$

$$\approx 2\pi[\delta-\frac{v-r\frac{L}{2}}{c} + \frac{1}{3}(\frac{v-r\frac{L}{2}}{c})^3 \ldots] \frac{\rho}{2} L^2[c^2+(v-r\frac{L}{2})^2]$$

$$-2\pi\frac{1}{3!}[\delta-\tan^{-1}(\frac{v-r\frac{L}{2}}{c})]^3 \frac{\rho}{2} L^2[c^2+v-r\frac{L}{2})^2]$$

$$+ \ldots$$

Since the first term in the last equation is covered by Y_δ, Y_v , Y_r , Y_{vrr} , Y_{rvv} .....already, our interest is concentrated on the second term. If we expand the second term, they are the contribution from the δ , v, r cross-correlated derivatives, $Y_{\delta vv}$, $Y_{\delta rr}$,... Since the second term covers these components and yet has a much simpler appearance, it is advantageous to use it in this form to replace the lengthy expansion, i.e.

$$Y_{\delta vv} \cdot \delta vv + Y_{v\delta\delta} v\delta\delta + Y_{r\delta\delta} r\delta\delta + Y_{\delta rr} \delta rr + Y_{\delta rv} \delta rv$$

$$\longrightarrow Y_{eee} eee$$

$$N_{\delta vv} \cdot \delta vv + N_{v\delta\delta} v\delta\delta + N_{r\delta\delta} r\delta\delta + N_{\delta rr} \delta rr + N_{\delta rv} \delta rv$$

$$\xrightarrow{\hspace{4cm}} N_{eee} eee$$

(Similarly, $X_{\delta\delta\delta}$, $X_{\delta rr}$, $X_{\delta vv}$....., is replaced by $X_{ee} ee$, and

$$X_{ee} = X_{ee}' \frac{\rho}{2} L^2 c^2)$$

For the study of ESSO OSAKA, this expression has helped us to get around the difficulty of expected inaccuracies in the information on $Y_{\delta vv}'$, $Y_{v\delta\delta}'$, $Y_{r\delta\delta}'$.....

2.5.6 X-Derivatives of Orders Higher Than 2

In the processing of sea trial data, we found that the estimated value of $X_{vr}' + m'$ from $10°/10°$ zigzag maneuver is somewhat different from that of $20°/20°$ zigzag maneuver, not to mention the estimated $X_{vr}'' + m'$ from turning circle maneuver. The problem is that $(X_{vr} + m)vr$ is not a small quantity compared to the drag force $C_R \frac{\rho}{2} \cdot Su^2$. For $10°/10°$ zigzag maneuver, the peak value of $(X_{vr} + m)vr$ could be 1.5 times of the drag force $C_R \frac{\rho}{2} \cdot Su^2$, while for $20°/20°$ maneuver, the ratio of $(X_{vr} + m)vr$ to $C_R \frac{\rho}{2} \cdot Su^2$ could be as high as 3, see figure 5.6 and 5.7. Therefore, a 10% difference in the estimated value of $X_{vr}' + m'$ is equivalent to 15% difference in C_R for $10°/10°$ zigzag maneuver and 30% difference in C_R for $20°/20°$ zigzag maneuver, which explains why the simulation of $20°/20°$ zigzag maneuver based on the estimated parameter value from $10°/10°$ zigzag maneuver would be very different from the simulation based on the estimation from its own.

Since X_{vr}+m has the dimension of mass, the speed loss effect

is not reflected in its contribution. Thus the choice of an

additional term in X equation must meet this requirement. X_{vvrr}

turns out to be the candidate. It has the dimension of

$\frac{\rho}{2} L^4 U^{-2}$. Hence, when speed drops, $X_{vvrr}v^2r^2$ will account for the

further increment of X force due to the cross effect of v and r .

2.6 Summary

The modifications proposed in previous sections are based on the

experience of processing the sea trial data. The model has not been

improved to perfection and probably never will be. However, from the

viewpoint of marginal effectiveness, this modified model in

equation (2.5.22) is already a very good one to cope with the available

ship information and the existing sea trial data for ESSO OSAKA . A

much more sophisticated general model has been proposed by Ogawa and

Kasai [1978] . But that model contains many factors to be determined

by experiments. The feasibility of that model is to be verified by

series of model testing in Japan. In the near future, the author

believes that an expression for ship maneuvering dynamics will remain

the similar form of equation (2.5.22) although a simpler one would be

preferred and sought after.

$$\dot{u} = \dot{u}_r - u_c \cdot r \cdot \sin(\psi - \alpha)$$

$$\dot{u}_r = \frac{f_1}{m - X_{\dot{u}_r}}$$

$$(2.5.22)$$

$$\dot{v} = \dot{v}_r - u_c \cdot r \cdot \cos(\psi - \alpha)$$

$$\dot{v}_r = \frac{1}{f_4} [(I_z - N_{\dot{r}}) f_2 - (m x_G - Y_{\dot{r}}) f_3]$$

$$\dot{r} = \frac{1}{f_4} [(m - Y_{\dot{v}_r}) f_3 - (m x_G - N_{\dot{v}_r}) f_2]$$

where

$$f_1 = \eta_1' [\tfrac{\rho}{2} L^2] u_r^2 + \eta_2' [\tfrac{\rho}{2} L^3] n u_r + \eta_3' [\tfrac{\rho}{2} L^4] n^2 - C_R' [\tfrac{\rho}{2} S u_r^2] + X_{\dot{v}}' {}^2 [\tfrac{\rho}{2} L^2] v_r^2$$

$$+ X_{e^2}' [\tfrac{\rho}{2} L^2 c^2] e^2 + (X_{r^2}' + m' x_G') [\tfrac{\rho}{2} L^4] r^2 + (X_{v_r r}' + m') [\tfrac{\rho}{2} L^3] v_r r$$

$$+ X_{v^2 r^2}' [\tfrac{\rho}{2} L^4 U^{-2}] v_r^2 r^2$$

$$e = \text{effective rudder angle} \simeq \delta - \frac{v}{c} + \frac{rL}{2c}$$

$$c = \text{weighted average flow speed over rudder}$$

$$= \sqrt{\frac{A_p}{A_R} [(1-w)u_r + k u_{A\infty}]^2 + \frac{A_R - A_p}{A_R} (1-w)^2 u_r^2}$$

$$U_r = \sqrt{u_r^2 + v_r^2}$$

$$f_2 = Y_0'[\tfrac{\rho}{2} L^2 (\tfrac{u_{A\infty}}{2})^2] + \{Y_{v_r}'[\tfrac{\rho}{2}L^2 U_r]v_r + Y_\delta'(c-c_0)\tfrac{\rho}{2}L^2 v_r\}$$

$$+\{(Y_r'-m'u_r')\,[\tfrac{\rho}{2}L^3 U_r]r - \tfrac{Y_\delta'}{2}(c-c_0)\tfrac{\rho}{2}L^3 r\} + Y_\delta'[\tfrac{\rho}{2}L^2 c^2]\delta$$

$$+Y_{v_r3}'[\tfrac{\rho}{2}L^2 U_r^{-1}]v_r^3 + Y_{v_r^2 r}'[\tfrac{\rho}{2}L^3 U_r^{-1}]v_r^2 r + Y_{r2v_r}'[\tfrac{\rho}{2}L^4 U_r^{-1}]r^2 v_r$$

$$+Y_{r3}'[\tfrac{\rho}{2}L^5 U_r^{-1}]r^3 + Y_{e3}'[\tfrac{\rho}{2}L^2 c^2]e^3$$

$$f_3 = N_0'[\tfrac{\rho}{2}L^3 (\tfrac{u_{A\infty}}{2})^2] + \{N_{v_r2}'[\tfrac{\rho}{2}L^3 U_r]v_r - N_\delta'(c-c_0)\tfrac{\rho}{2}L^3 v_r\}$$

$$+\{N_r'-m'x_G'u_r')[\tfrac{\rho}{2}L^4 U_r]r + \tfrac{1}{2}N_\delta'(c-c_0)\tfrac{\rho}{2}L^4 r\} + N_\delta'[\tfrac{\rho}{2}L^3 c^2]\delta$$

$$+N_{v_r3}'[\tfrac{\rho}{2}L^3 U_r^{-1}]v_r^3 + N_{v_r^2 r}'[\tfrac{\rho}{2}L^4 U_r^{-1}]v_r^2 r + N_{r2v_r}'[\tfrac{\rho}{2}L^5 U_r^{-1}]r^2 v_r$$

$$+N_{r3}'[\tfrac{\rho}{2}L^6 U_r^{-1}]r^3 + N_{e3}'[\tfrac{\rho}{2}L^3 c^2]e^3$$

$$f_4 = (m'-Y_{v_r}')[\tfrac{\rho}{2}L^3]\,(I_z'-N_r')[\tfrac{\rho}{2}L^5] - (m'x_G'-N_{v_r}')[\tfrac{\rho}{2}L^4](m'x_G'-Y_r')[\tfrac{\rho}{2}L^4]$$

$$u_r = u - u_c \cos(\psi-\alpha)$$

$$v_r = v + u_c \sin(\psi-\alpha)$$

3. SYSTEM IDENTIFICATION

A system consists of collectively functioning components which relates the inputs and outputs to this system. System theory is the kind of technique used to solve the problem of a complicated system such that an optimal design of it can be accomplished. The basic problems of system theory are classified as modeling, analysis, estimation and control. The system identification is a subcategory of estimation theory, within which the observations are used not only to estimate the system states but also to complete the uncertain parts of the model. Since the system is modeled in terms of an a priori structure and some uncertain parameters, Schweppe [1976] suggests that system identification should contain four steps as illustrated in Fig. 3.1.

Each step contains many complicated problems that deserve a seperate treatment, but it is beyond the scope of this thesis to go through them in detail. Only a brief review is covered in the following discussion for the completeness of this thesis. Further information is refered to Schweppe[1973][1976], Gelb[1974], Eykhoff[1974].

3.1 Hypothesize the Model Structure

To simplify the study, the dynamic system is assumed time invariant, a practical approximation for most of the engineering system. A hypothesized model structure contains four components:

a. Input-output classification,

b. Nature of disturbances,

c. Parameterization,
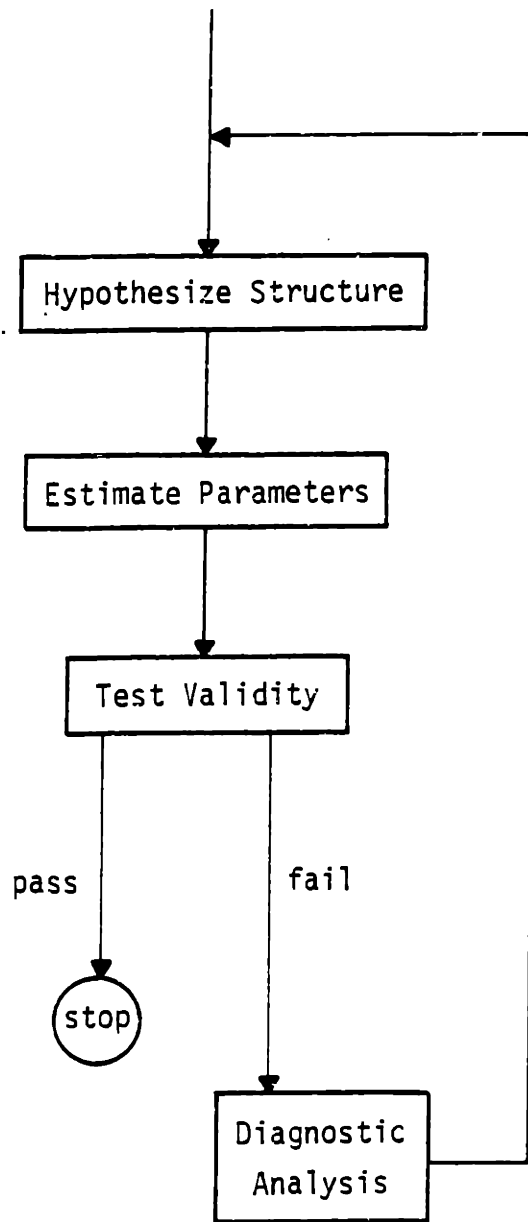
Figure 3.1 Procedure of system identification

d. A priori information.

For clearness, the items considered in each structure component are listed in table 3.1.

3.1.1 Input-output Classification

The "physical input-output" and the "filter input-output" are the two basic types of input-output relationship. As illustrated in Fig. 3.2, the "physical input-output" is a natural way to conceive a system. Whereas the filter input-output is based on an artificial concept, in which the optimal prediction of output at time step N comes from the transformation of past external inputs and the observed outputs.

In this work, the model structure is based on the physical input-output relationship, because the state variables are physical quantities and the unknown parameters correspond to these quantities. The innovation filter structure, diagonal filter structure, elemental filter structure and filter weighting pattern structure are based on "filter input-output" relationship. Although not discussed here, innovations filter structure is an interesting one to notice in the future. Including the gain $\underline{K}$ and measurement error covariance $\underline{\Sigma}_z$ as unknown parameters, it requires no a priori information of the modeling error(process noise) and the measurement error(measurement noise), which are usually not known very well. Similar suggestion on the usage of innovations filter structure was given by Norrbin, et al [1977].

A structure can be expressed in different forms. For instance, the physical system structure of a stochastic model in Fig. 3.3 can have

Input-output Classification	• Specification of type of input-output relationship (physical or filter) • Specification of number of inputs & outputs • Specification of order of the system
Nature of Disturbance	• Specification of type of disturbance
Parameterization	• Specification of parameters whose values are to be estimated • Explicit values for any other parameters
A priori Information	• A priori information for the parameters to be estimated

Table 3.1   Items considered in the hypothesis of model structure
(ref. Schweppe[1976])

white process,
exogeneous input $\underline{u}(n)$

n=1,...,N-1

Dynamic System

observed output
$\underline{z}(N)$

(a)   physical   input-output relationship

white process

exogeneous input $\underline{u}(n)$

observed output $\underline{z}(n)$

n=1,...,N-1

Dynamic System

$\hat{\underline{z}}(N|N-1)$
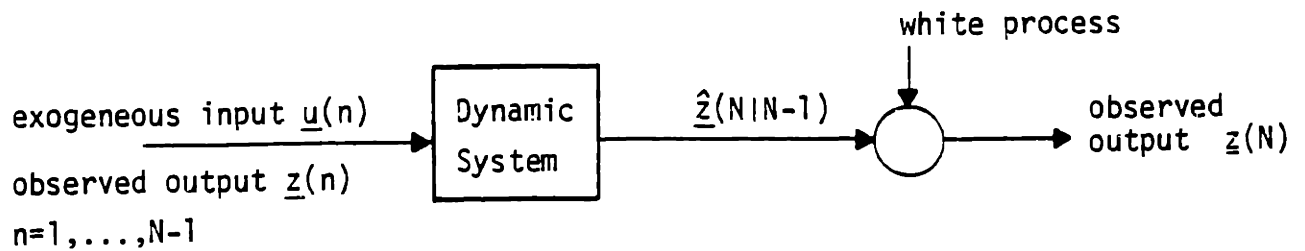
observed
output $\underline{z}(N)$

$\underline{z}(n|n-1)$ is the optimal estimate of $\underline{z}(N)$ from $\underline{z}(n),\underline{u}(n)$, where

n=1,...,N-1

(b)   filter input-output relationship

Figure 3.2   Two types of input-output relationship
(ref. Schweppe[1976])

$$\underline{x}(n+1) = \underline{\Phi}\,\underline{x}(n) + \underline{B}\,\underline{u}(n) + \underline{G}\,\underline{w}(n)$$

$$\underline{z}(n) = \underline{H}\,\underline{x}(n) + \underline{v}(n) \qquad n=1,\ldots,N$$

where

$\underline{x}(n)$: state of dimension K_x

$\underline{z}(n)$: observation of dimension K_z

$\underline{w}(n)$: input white uncertain process of dimension K_w

$\underline{v}(n)$: observation white uncertain process of dimension K_v

$\underline{u}(n)$: known external input of dimension K_u

$\underline{w}(n),\underline{v}(n),\underline{x}(0)$ are zero mean, Gaussian, white, uncorrelated random

process. And

$$E\{\underline{w}(n_1)\underline{w}^T(n_2)\} = \begin{cases} \underline{Q}, & n_1=n_2 \\ \underline{0}, & n_1 \neq n_2 \end{cases}$$

$$E\{\underline{v}(n_1)\underline{v}^T(n_2)\} = \begin{cases} \underline{R}, & n_1=n_2 \\ \underline{0}, & n_1 \neq n_2 \end{cases}$$

$$E\{\underline{x}(0)\underline{x}^T(0)\} = \underline{\Psi}$$

$\underline{\alpha}$: vector containing all the unknown parameters in $\underline{\Phi}$, $\underline{B}$, $\underline{G}$,

$\underline{H}$, $\underline{R}$(including model degree)

Figure 3.3 Physical system structure in the form of a K_x order system

of "State Space-White Process" equations(ref. Schweppe[1976])

$$\underline{x}_\lambda(n+1) = \underline{\Lambda}\,\underline{x}_\lambda(n) + \underline{G}_\lambda w(n) + \underline{B}_\lambda\,\underline{u}(n)$$

$$\underline{z}(n) = \underline{H}_\lambda\,\underline{x}_\lambda(n) + \underline{v}(n)$$

$$\underline{\Lambda} = \begin{bmatrix} \lambda_1 & & & \underline{0} \\ & \ddots & & \\ & & \ddots & \\ \underline{0} & & & \lambda_{K_x} \end{bmatrix} = \underline{C}_\lambda\,\underline{\Phi}\,\underline{C}_\lambda^{-1}$$

$$\underline{x}_\lambda(n) = \underline{C}_\lambda\underline{x}(n)$$

$$\underline{G}_\lambda = \underline{C}_\lambda\underline{G}$$

$$\underline{B}_\lambda = \underline{C}_\lambda\underline{B}$$

$$\underline{H}_\lambda = H_\lambda\underline{C}_\lambda^{-1}$$

$$\left.\begin{array}{l} \underline{w},\ \underline{v} \\[4pt] \underline{u} \\[4pt] \underline{Q},\ \underline{R} \\[4pt] \underline{\alpha} \\[4pt] \text{etc.} \end{array}\right\} \qquad \text{as defined in Fig. 3.2}$$

Figure 3.4 Physical system modal form of the physical system structure

in Fig. 3.3(ref. Schweppe[1976])

another form as in Fig. 3.4. Although the parameterization and a priori information is identical in all different forms of the same structure, the choice of a particular form influences the choice of parameter estimation algorithm and overall computational requirements.

To describe a system, the order is an important parameter. Higher order model represents the system better. The trade-off between the complexity and the modelling error decides the appropriate order. The reduction of system order can be achieved by engineering judgement for some cases. For example:

1. if the state has minor effect on other states, i.e., the state is weakly coupled with others, it can be eliminated.

2. the state variable that has a long time constant compared to the system's can be treated as a constant.

For a complicated system, if the reduction of system order can not be achieved by engineering judgement, a more rigorous treatment on model reduction is refered to Schweppe[1973].

If the necessary order for describing a system is unknown, the models of different hypothesized order are of different structure and the order should be identified as an unknown parameter.

In this study, the known external input u is assumed independent of the disturbances. Therefore, if u is a random process, it is statistically independent of the system, i.e., u is not a feed back from the system itself. Since the results of system identification are affected by the choice of inputs, to design an input which gives good identifica-

tion is desirable. But a general guideline is difficult to lay down, because the design of exogeneous input depends on the input-output structure as discussed in this section and on the true value(may be unknown) of Φ, B, etc. Schweppe[1973] suggests that an input of larger rapid variations should provide a better system identification than a low-amplitude, constant input does. For the estimation of hydrodynamic coefficient of ship motion, this comment is positively confirmed.

3.1.2 Nature of Disturbances

In our stochastic formulation of the problem, two categories of uncertainty are involved, the process noise w and the measurement noise v. See Fig. 3.5.
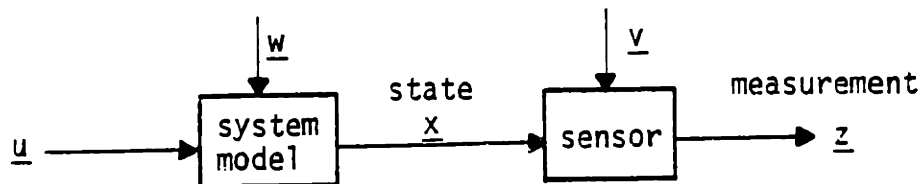
Figure 3.5 Process noise and measurement noise

The model of a physical system usually behaves differently from the real system. The deviation could be attributed to the following reasons:

    a. incomplete knowledge of the system mechanism,

    b. simplified mathematical formulation for a complicated physical law.
The resulting error w is called process noise. Although w is modelled

- 80 -

as zero mean, white, Gaussian distributed, in Fig. 3.2, in general, $\underline{w}$ is not necessarily zero mean or Gaussian.

In case of nonwhite $\underline{w}$, the message says that the order of hypothesized structure is not sufficient. In other words, some dynamics of the system has not been considered, which is usually the case when the time constant of a disturbance is compatible to that of the system dynamics. By augmenting state variables and modifying system dynamics, the time-dependent structure of $\underline{w}$ could be removed.

If the nonzero means of $\underline{w}$ are known, they can be taken care of by the technique of "addition and substraction", Schweppe[1973], under the assumption that $\underline{w}$ is linearly related to the system dynamics. If the mean values of $\underline{w}$ are not known, they can be treated as unknown parameter and estimated.

The assumption of Gaussian is not necessary. But since the random signal generated by linear operation on a Gaussian distributed random signal is still Gaussian, the major advantage of Gaussian assumption is a stronger interpretation of the result(in linear case). Nevertheless, if $\underline{w}$ is composed of independent random variables $\underline{w}_k$,

$$\underline{w} = \sum_{k=1}^{K} \underline{w}_k \qquad (3.1.1)$$

$$E[\underline{w}_k] = \bar{\underline{w}}_k \qquad (3.1.2)$$

$$E[(\underline{w}_k - \bar{\underline{w}}_k)(\underline{w}_k - \bar{\underline{w}}_k)^T] = \underline{Q}_k \qquad (3.1.3)$$

where K is the number of approximations, the central limit theorem says that $\underline{w}$ approaches Gaussian distribution when K approaches infinity. In addition, the noise of the other probability density distribution can be derived by passing the Gaussian random signal through a nonlinear operator. Therefore, the Gaussian distribution is a usual assumption for the study of estimation and control problem.

By the previous discussion, we know that the input uncertainty $\underline{w}$ can be modelled as zero mean, Gaussian distributed noise, when the necessary procedure has been taken, i.e.,

$$\underline{w}(n) = N(\underline{0},\underline{Q}) \hspace{3cm} (3.1.4)$$

Further simplification is possible when we consider the fact that the coupling between the state variables are usually weak. In that case the off-diagonal elements of $\underline{Q}$ are much smaller than those on the diagonal. Thus the elements of the input noise can be assumed uncorrelated and the off-diagonal elements of $\underline{Q}$ are of zero value.

A completely unknown input or bad input data are also possible types of input disturbances. In the presence of completely unknown inputs, the parameter can be estimated by including the entire input process into the unknown parameter vector, refer to Schweppe[1976]. For bad input data, Peterson and Schweppe[   ] suggest that using the normalized updated state residuals (NUSR) to reveal and locate the bad data associated with individual components of state variable vector, which primarily

comes from the exogeneous input data.

The measured data z always contains some noise induced by the environment or by the internal noises of measuring devices. Biases and sensor dynamics can be handled as in the discussion of input uncertainty. The bad measurements can be detected by using normalized updated measurement residuals(NUMR). Since the sources of measurement error are usually many and independent, the uncorrelated zero mean white Gaussian distribution is a reasonably good model for the measurement noise.

3.1.3 Parameterization

In section 3.1.1, we mentioned that different model structures have different parameterization and the choice of a structure's form decides the estimation algorithm and computation requirement. Therefore, the parameterization is a very important step that leads to a successful system identifacation.

In ideal case, all the paremeters of uncertainty can be estimated simultaneously. In reality, there are difficulties that make this wish impractical. First, we have to control the computing time within the affordable range. Second, when one system is excited by exogeneous inputs, the modes are not excited evenly. Therefore, the contribution associated with each parameter differs from file to file of different inputs. A careful study must be carried out in order to find out

1. the parameters that can be measured accurately,

2. which parameters can be accurately identified without knowing the exact value of minor terms for the specific input. The sensitivity of

- 83 -

the ship maneuvering response to the variation of hydrodynamic coeffi-
cient is thus analyzed for different input in chapter 5 for this purpose.

3.1.4 A Priori Information

For the model structure based on physical input-output relationship,
the parameters have physical meanings. A priori information is usually
available to certain extent. It could be a bound or statistical charac-
teristics. The more information we have, the better the chance to have
good identification result, Graupe[1976]. To our disappointment, the a
priori information for those parameters to be estimated is usually in-
sufficient. Engineering experience sometimes is used to estimate this
a priori information. Some of the estimation techniques can include
certain unknown a priori information as parameters to be identified.
For instance, the covariance matrices Q,R in Fig. 3.2 can be estimated by
maximum likelihood method(MLM). For other method that Q,R can not be
estimated directly, e.g., extended Kalman filtering, Q, R can be zeroed
in, based on the information of validity test after each pass of data
processing.

3.2 Parameter Estimation

After the model structure is hypothesized, the next step is to
estimate the unknown parameters through a carefully chosen technique.
The algorithms for estimating parameter values are many. Each one has
its advantages and disadvantages. The choice not only depends on the
hypothesized structure, it is also affected by the special considerations
of each problem. One obvious example is on-line estimation. In that

case the computational speed may be the major factor of decision. In the following, we are going to discuss three popular methods of estimation: the model reference method(MLM), the state augmented extended Kalman filtering(SAEKF) and the maximum likelihood method via extended Kalman filtering(MLM). Both the later two methods use extended Kalman filtering technique. Since EKF is a well developed technique that its derivation can be found from most text of control & estimation, we only quote the concise result in Appendix B.

3.2.1 Model Reference Method

If the hypothesized structure does not involve stochastic process, MRM is a straightforward approach to estimate the unknown parameters. Figure 3.6 illustrates the basic steps of this method for a discrete-time dynamic system. Although MRM is intuitively simple, it has several disadvantages:

1. Since no stochastic process is involved, this method can not estimate the modelling and observation uncertainties. Unfortunately these are very important information to validate the model.

2. This method can not estimate the order of the system as an unknown parameter.

3. The presence of structural error makes the judgement on the goodness of fitting difficult.

4. MRM can generate estimations of large biases which do not decrease even when the number of observation increases.

5. This method is more sensitive to noise than the Kalman filtering.

- 85 -

Initial guess of unknown parameter $\underline{\alpha}$

Generate model output:

$$\underline{x}_{model}(n+1) = \underline{\Phi}\, \underline{x}_{model}(n) + \underline{B}\, \underline{u}_{model}(n)$$

$$\underline{z}_{model}(n) = \underline{H}\, \underline{x}_{model}(n)$$

$\underline{\alpha}$: unknown parameters in $\underline{\Phi}$, $\underline{B}$, $\underline{H}$

Calculate the cost function J,

$$J(\underline{\alpha}:\underline{x}_{model}(0), \underline{w}(n), n=1,\ldots\ldots,N)$$

$$= \sum_{n=1}^{N} [\underline{z}(n) - \underline{H}\, \underline{x}_{model}(n)]^T \underline{R}^{-1} [\underline{z}(n) - \underline{H}\, \underline{x}(n)]$$

$$+ \sum_{n=1}^{N} \underline{w}^T(n) \underline{Q}^{-1} \underline{w}(n) + \underline{x}_{model}^T(0) \underline{\Psi}\, \underline{x}_{model}(0);$$

where $\underline{Q}$, $\underline{R}$, $\underline{\Psi}$ are chosen by engineering

judgement,

$$\underline{w}(n) \equiv \underline{B}(\underline{u}_{model}(n) - \underline{u}(n))$$

Modify the value of $\underline{\alpha}$ by some modification algorithm

No ← Is J minimized?

Yes

Stop

Figure 3.6 Basic steps of model reference method, ref. Schwepp[1973]

- 86 -

6. When contour plot is used to determine the identifiability, only two parameters can be handled at one time. Excessive computer time and costs are required to go through a systematic variation of many parameters.

At M.I.T., MRM was applied to ship maneuvering problem by Hayes[1971] and Brinati[1973]. But since this method is inferior to the extended Kalman filtering, therefore this method was put aside for the above reasons.

3.2.2 State Augmented Extended Kalman Filtering

The Kalman filter is a widely used technique in modern control theory for a linear system. Based on the hypothesized model structure and using the measurement of system up to the present time step, the Kalman filter makes the optimal estimation of the state of system. Although similar in form, thus bearing the name of Kalman, the extended Kalman filter differs from the conventional Kalman filter at many important aspects. Serving to the nonlinear model, the gain $\underline{K}_n$ depends on the optimal state estimate $\underline{\hat{x}}_n(-)$, due to the fact that $\underline{F}_n$ and $\underline{H}_n$ are just approximation of $\underline{f}_n$ and $\underline{h}_n$ evaluated at the point $\underline{\hat{x}}_n(-)$. Similarly, the error covariance matrix $\underline{P}$ is also a random variable, whose value depends on the time history of $\underline{\hat{x}}_n(-)$. Since this error covariance matrix $\underline{P}$ is just an approximation to the true covariance matrix, the resulting estimation is not necessarily truely optimal. The Monte Carlo simulation can be used to verify the filter performance. For several important practical applications, the EKF has yielded accurate estimates.

When it is applied to ship maneuvering problem, Hayes[1971], Reis [1971], Brinati[1973], Lunblad[1974] and Szeto[1977] showed that a

straightforward usage of EKF, the state augmented extended Kalman filtering, is a satisfactory method of system identification. In order to estimate the unknown parameter $\underline{\alpha}$ in the following mathematical formulation of a system

$$\underline{x}(n+1) = \underline{f}(\underline{x}(n),\underline{u}(n),\underline{w}(n))$$

$$\underline{z}(n) = \underline{h}(\underline{x}(n),\underline{v}(n)) \ ,$$

(3.2.1)

the state variable $\underline{x}(n)$ is augmented by the unknown parameter $\underline{\alpha}$. Therefore,

$$\underline{x}'(n+1) = \begin{bmatrix} \underline{x}(n+1) \\ \underline{\alpha} \end{bmatrix} = \underline{f}'(\underline{x}'(n),\underline{u}(n),\underline{w}(n))$$

$$\underline{z}(n) = \underline{h}'(\underline{x}'(n),\underline{v}(n))$$

(3.2.2)

Now, using the measurement of the system, the EKF not only estimates the original state variable, it also estimates the unknown parameter $\underline{\alpha}$. The advantages of this technique are

1. It does not need many passes of data processing. Therefore, it is more suitable for the real time estimation.

2. The statistical validity test not only decides whether the estimation result is acceptable but also helps to diagnose the ill part of model.

3. Since the unknown parameters are assumed constant, the plot of estimation time history provides a lot of information about the model. This unique feature makes SAEKF a very useful technique to diagnose the hypothesized model structure.

straightforward usage of EKF, the state augmented extended Kalman filtering, is a satisfactory method of system identification. In order to estimate the unknown parameter $\underline{\alpha}$ in the following mathematical formulation of a system

$$\underline{x}(n+1) = \underline{f}(\underline{x}(n),\underline{u}(n),\underline{w}(n))$$

$$\underline{z}(n) = \underline{h}(\underline{x}(n),\underline{v}(n)) ,$$

(3.2.1)

the state variable $\underline{x}(n)$ is augmented by the unknown parameter $\underline{\alpha}$. Therefore,

$$\underline{x}'(n+1) = \begin{pmatrix} \underline{x}(n+1) \\ \underline{\alpha} \end{pmatrix} = \underline{f}'(\underline{x}'(n),\underline{u}(n),\underline{w}(n))$$

$$\underline{z}(n) = \underline{h}'(\underline{x}'(n),\underline{v}(n))$$

(3.2.2)

Now, using the measurement of the system, the EKF not only estimates the original state variable, it also estimates the unknown parameter $\underline{\alpha}$. The advantages of this technique are

1. It does not need many passes of data processing. Therefore, it is more suitable for the real time estimation.

2. The statistical validity test not only decides whether the estimation result is acceptable but also helps to diagnose the ill part of model.

3. Since the unknown parameters are assumed constant, the plot of estimation time history provides a lot of information about the model. This unique feature makes SAEKF a very useful technique to diagnose the hypothesized model structure.

4. When the time history of parameter estimation indicates that certain parameter is really not a constant relative to the system dynamics, its variation can be tracked by assuming the dynamics of this parameter is a random process, i.e., $\dot{\alpha}_i = w_i$. The approximation of noise strength and an illustrative working example have been given by Gelb[1974].

Besides the shortcoming of EKF itself, the disadvantages of this technique are that

1. The computation burden increases very quickly as the number of unknown parameters increases. However, fortunately, to calculate the Riccati equation, the computing burden is proportional to the number of measurement only. When $\underline{H}$ can be partitioned into identity matrix and zero matrix, then the computing burden of Ricatti equation is independent of the number of unknown parameter. Nevertheless, the error covariance propagation always requests more computing time when the number of unknown parameter increases.

2. The estimation of $\underline{Q}$ and $\underline{R}$ is not as easy as in the MLM.

3.2.3 Maximum Likelihood Method via Extended Kalman Filtering

For one set of unknown parameter $\underline{\alpha}$, the idea of MLM is to maximize the probability density function $p(\underline{z}_N; \underline{\alpha})$ of the measurement $\underline{z}$ by adjusting the value of $\underline{\alpha}$. Notice that the probability density function $p(\underline{z}_N; \underline{\alpha})$ should not be interpreted as a conditional probability density function. It is just the density function for a given $\underline{\alpha}$. Mathematically, to maximize $p(\underline{z}_N; \underline{\alpha})$ is equivalent to maximizing $\ln\{p(\underline{z}_N; \underline{\alpha})\}$. Define the log likelihood function $\xi(N; \underline{\alpha}) = \ln\{p(\underline{z}_N; \underline{\alpha})\}$ and use the Gaussian assumption,

$\xi(N;\underline{\alpha})$ can be expressed as follows:

$$2\xi(N;\underline{\alpha})=\xi_{bias}(N;\underline{\alpha})+\xi_{observation}(N;\underline{\alpha})$$

$$\xi_{bias}(N;\underline{\alpha})=-NK_z\ln(2\pi)-\sum_{n=1}^{N}\ln|\underline{\Sigma}_z(n|n-1;\underline{\alpha})| \qquad (3.2.3)$$

$$\xi_{observation}(N;\underline{\alpha})=-\sum_{n=1}^{N}\underline{\delta}_z^T(n;\underline{\alpha})\underline{\Sigma}_z^{-1}(n|n-1;\underline{\alpha})\underline{\delta}_z(n;\underline{\alpha})$$

where

K_z is the dimension of measurement $\underline{z}$

N is the number of measurement(observation)

Since the computation of $\xi(N;\underline{\alpha})$ uses the residual $\underline{\delta}_z$ and the predicted measurement covariance $\underline{\Sigma}_z(n|n-1;\underline{\alpha})$ for the Gaussian case, the computation can be done recursively while EKF goes through the measurement data. Figure 3.7 illustrates the procedure searching for the optimal $\hat{\underline{\alpha}}$ to maximize $\xi(N;\underline{\alpha})$. The advantages of this technique are

1. The number of unknown parameters can be increased without increasing the computing burden of matrix multiplication.

2. For a linear system, the estimation of unknown parameter does not convert the system into a nonlinear system. For nonlinear system, the estimation does not increase the nonlinearity.

3. The a priori statistical information of the unknown parameters is not necessary.

In addition to the shortcoming of EKF, the disadvantages of this method are
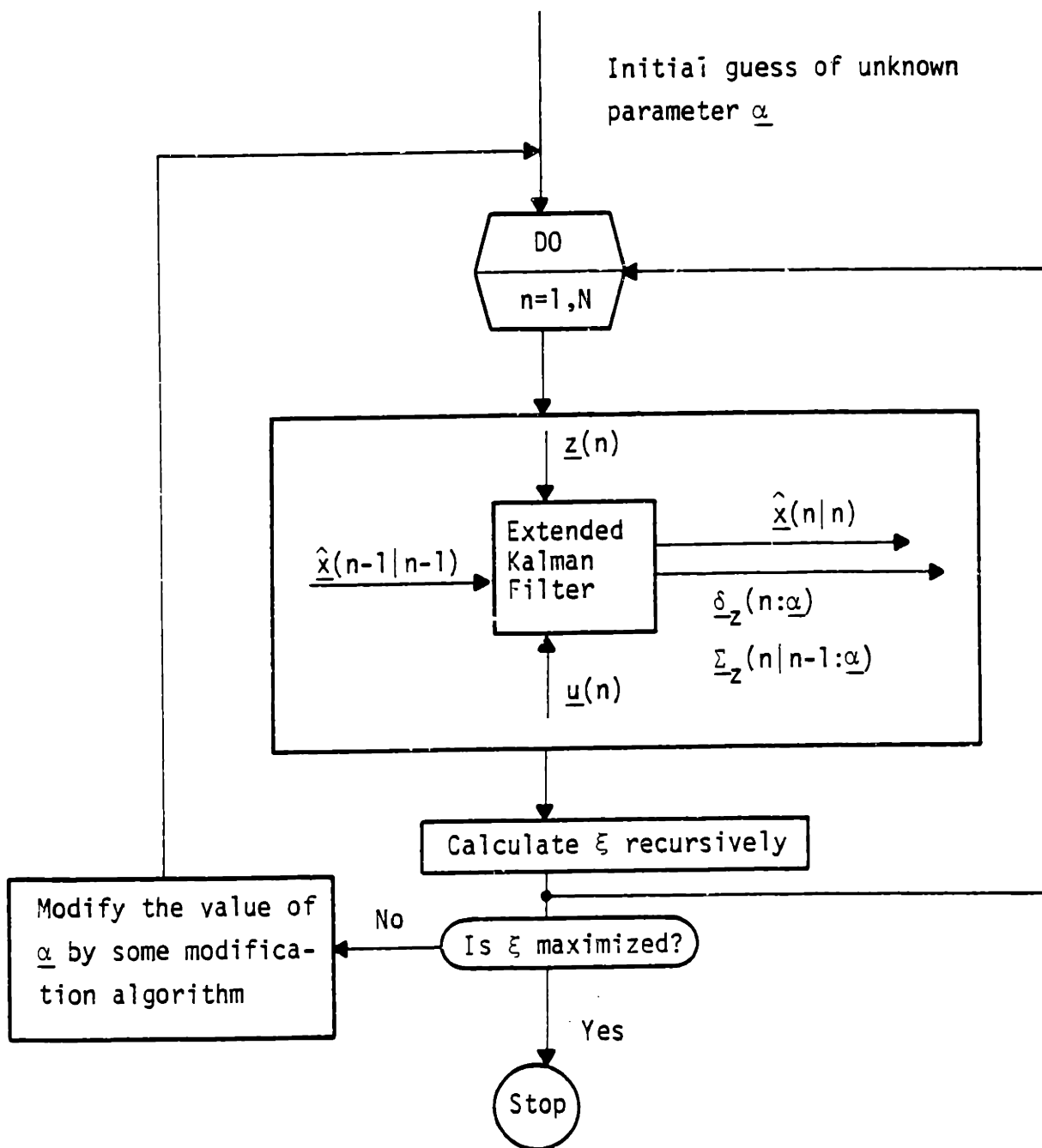
Figure 3.7 Procedure to search for the optimal $\hat{\alpha}$ to maximize $\xi(N:\underline{\alpha})$

1. Many passes of data processing are necessary to converge to the optimal solution, which makes MLM unsuitable as a real time parameter estimation technique.

2. Since $\underline{\alpha}$ is assumed constant in each pass, there is no way to track the time variation of parameters, which is a very useful information to reveal the defects in the model.

3.3 Validity Test

After the unknown parameter $\underline{\alpha}$ is estimated, the next step is to check its validity. The function of the validity test is not only to check whether the estimation is acceptable, but also to furnish the primitive diagonosis in case the model fails the test. Three types of validity tests will be discussed:

1. Statistical hypothesis testing,

2. Evaluation of parameter accuracy,

3. Engineering judgement.

3.3.1 Statistical Hypothesis Testing

For the model involving stochastic process, its test statictics is used to do the hypothesis testing. The test statistic is some quantity which can be computed from the measurements and the statistical properties of this quantity are known when the model is valid. If hypotheses H_0 and H_1 are defined as

H_0:   the structure is valid and the estimated $\underline{\alpha}$ is close to the

true $\underline{\alpha}$,

H_1: H_0 is not true,

the procedure of hypothesis testing is illustrated in the flow chart of Fig. 3.8. It is important to notice that even if all the chosen test statistics for this model gives consistent results, the only thing we can say is that we cannot reject H_0 by using the available measurements with the chosen set of test statistics. In other words, as long as one can find a new test statistic that the model does not give consistent results, then the model is not acceptable.

In the following, we list a few test statistics that Schweppe[1976] has suggested as a "good set" for the statistical hypothesis testing. First, let us define the residual as the difference between the actual measurement and the predicted measurement,

$$\underline{\delta}_z(n) = \underline{z}(n) - \underline{z}(n|n-1)$$

$$\underline{\Sigma}_z = E\{\underline{\delta}_z(n)\underline{\delta}_z^T(n)\}$$

(3.3.1)

1. "Individual Residual Magnitude" test statistics are defined by

$$\underline{r}_z(n) \equiv \underline{\Sigma}_z^{-\frac{1}{2}}\underline{\delta}_z(n) \qquad\qquad n=1,\ldots\ldots,N \qquad\qquad (3.3.2)$$

When H_0 is true,

$$\underline{r}_z(n) \sim N(\underline{0},\underline{I})$$

2. "Sum of Squared Residuals" test statistic is defined by

$$\zeta = \sum_{n=1}^{N} \underline{\delta}_z^T \underline{\Sigma}_z^{-1} \underline{\delta}_z = \sum_{n=1}^{N} \underline{r}_z^T(n)\underline{r}_z(n) \qquad\qquad (3.3.3)$$

When H_0 is true,

$$E\{\zeta\}=NK_z \qquad\qquad K_z: \text{dimension of } \underline{z}$$

$$E\{(\zeta-NK_z)^2\}=2NK_z$$

$$\zeta \sim N(NK,2NK) \qquad\qquad N \rightarrow \infty$$

3. "Residual Whiteness" test statistics are defined by

$$\underline{P}_{rr}(\tau)= \frac{1}{N}\sum_{n=1}^{N} \underline{r}_z(n)\underline{r}_z^T(n-\tau) \qquad \tau=0,1,\ldots\ldots \qquad (3.3.4)$$

When H_0 is true,

$$E\{\underline{P}_{rr}(\tau)\}=\begin{cases} \underline{I} & \tau=0 \\ \\ \underline{0} & \tau>0 \end{cases}$$

the $\underline{P}_{rr}(\tau)$ can be considered as normally distributed when $N \rightarrow \infty$.

Also,

$$\sigma_{\underline{p}(0)} = \sqrt{\frac{2}{N}} \qquad\qquad \text{for diagonal elements}$$

$$\sigma_{\underline{p}(0)} = \sqrt{\frac{1}{N}} \qquad\qquad \text{for off-diagonal elements}$$

$$\sigma_{\underline{p}(\tau\neq 0)} = \sqrt{\frac{1}{N} - \frac{\tau}{N^2}}$$

4. "Residual-Input Correlation" test statistics & "Residual-Output Correlation" test statistics are defined by

$$\underline{P}_{ru}(\tau)= \frac{1}{N}\sum_{n=1}^{N} r_z(n)\underline{u}^T(n-\tau) \qquad \tau=0,1,\ldots\ldots \qquad (3.3.5)$$

$$\underline{P}_{rz}(\tau)= \frac{1}{N}\sum_{n=1}^{N} r_z(n)\underline{z}^T(n-\tau) \qquad \tau=1,2,\ldots\ldots \qquad (3.3.6)$$

When H_0 is true,

$$E\{\underline{P}_{ru_j}(\tau)\}=\underline{0} \qquad \sigma_{\underline{P}_{ru_j}}(\tau)= \frac{1}{N}\sqrt{\sum_{n=1}^{N-\tau} u_j(n-\tau)^2} \qquad \tau=0,1,\ldots\ldots$$

$$E\{\underline{P}_{rz_j}(\tau)\}=\underline{0} \qquad \sigma_{\underline{P}_{rz_j}}(\tau)= \frac{1}{N}\sqrt{\sum_{n=1}^{N-\tau} z_j(n-\tau)^2} \qquad \tau=1,2,\ldots\ldots$$

5. "Information Matrix" test statistic is defined by the estimated information matrix $\hat{\underline{I}}$. When H_0 is true,

$$E\{\hat{\underline{I}}_\alpha\}=\underline{I}_\alpha$$

where $\underline{I}_\alpha$ is the actual information matrix. It is defined by

$$\underline{I}_\alpha=E\{\frac{\partial\xi(\underline{\alpha})}{\partial\underline{\alpha}}\cdot\frac{\partial\xi(\underline{\alpha})}{\partial\underline{\alpha}}^T\}$$

the $\xi(\underline{\alpha})$ is the log likelihood function in eq. (3.3.3).

To avoid the situation that the identified model is data specific, i.e., data file dependent, it is more convincing to have other data files of the system used for these tests and still verify the model validity.

3.3.2 Evaluation of Parameter Accuracy

The statistical hypothesis testing discussed in the last section is just an incomplete confirmation that the model is not rejectable based on the set of test statistics. The accuracy of the parameter estimation is not implied from those tests. Therefore, we now consider the evaluation of parameter accuracy.

The "Cramer-Rao" inequality is the testing criterion, under the assumption that the hypothesized structure is exact, for any unbiased

choose one test statistic

compute the value of test statistic by using the measurements

no

is the value consistent with the value of test statistic when H_0 is true?

accept H_1

yes

choose another test statistic
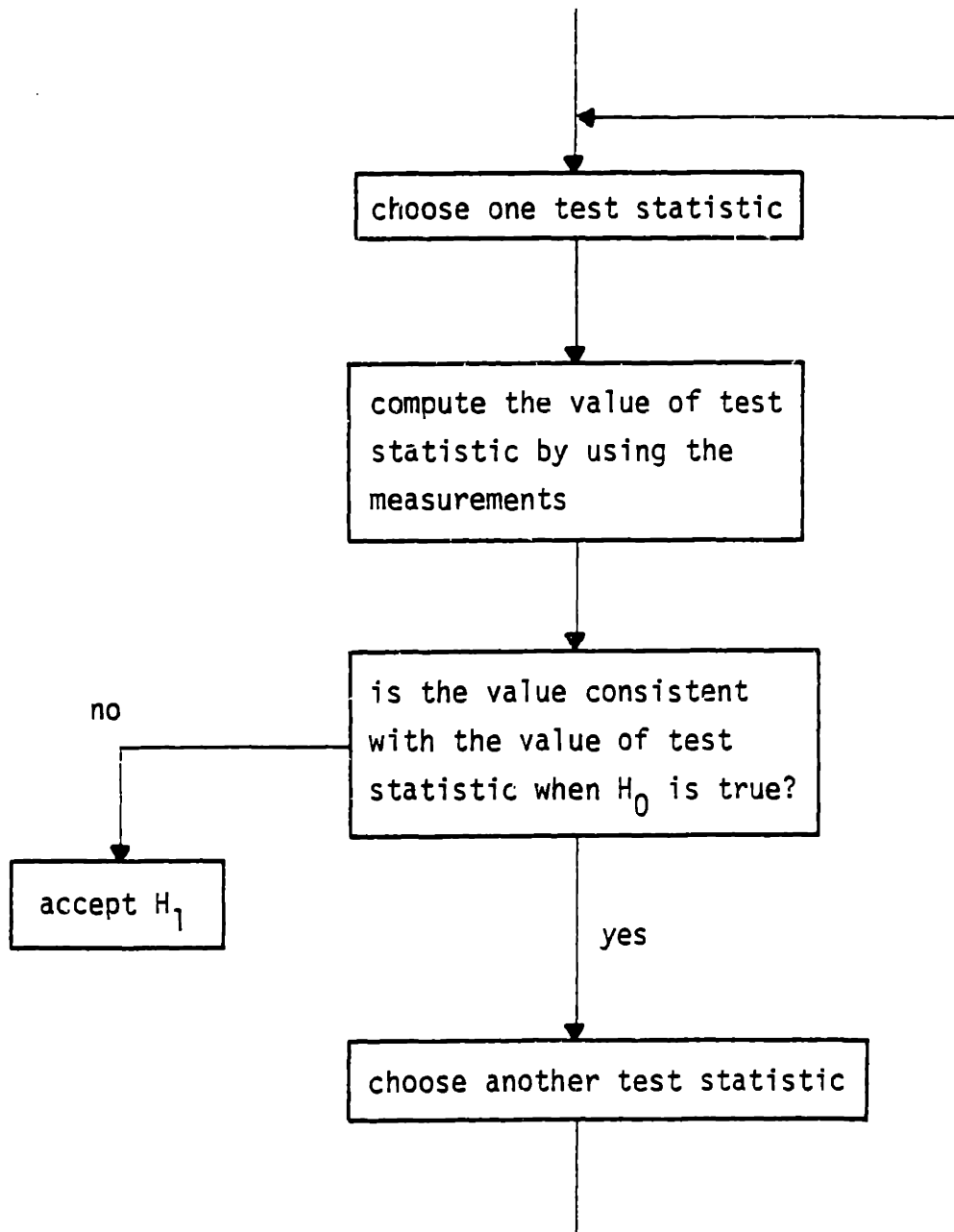
Figure 3.8   The procedure of hypothesis testing
(ref. Schweppe[1976])

estimate $\hat{\underline{\alpha}}$,

$$\underline{\Sigma}_\alpha = E\{(\hat{\underline{\alpha}} - \underline{\alpha}_{true})(\hat{\underline{\alpha}} - \underline{\alpha}_{true})^T \geq \underline{I}_\alpha^{-1} \qquad (3.3.4)$$

where $\underline{I}_\alpha$ is the information matrix defined in last section. If $\underline{I}_\alpha^{-1}$ has very large diagonal elements, this inequality says that the corresponding parameter estimates are not accurate or unidentifiable. In extreme case, if the information matrix $\underline{I}_\alpha$ is singular, then some of the parameters are completely unidentifiable. But how large are these elements that should call for our concern? This is resolved by the simulation as discussed by Morris[1978]. The EKF is "open looped" by setting the measurement error covariance $\underline{R}$ to very large value. The models accuracy of predicting the system output in the presence of any input is justified by checking how the real system output falls within the confidence bound from the model prediction.

For the SAEKF method, a less rigorous indication of the accuracy is to check the error covariance of $\underline{\alpha}$ at the end of filtering. Starting with a big initial error covariance, if the estimation does not improve the confidence bound significantly, the corresponding parameter is most likely unidentifiable and the resulting estimate is inaccurate.

3.3.3 Engineering Judgement

For a model of physical system structure, the unknown parameters bear some physical meaning which enables us to check the validity based on engineering judgement. At least two questions have to be checked,

1. Do these estimated parameter values make sense from the engineering

(physical) point of view?

2. Do the simulations based on this model agree with the engineering judgement and the existing system measurement?

Note that the importance of engineering judgement should not be disdained because of the lack of impressive mathematical formulation. There are possibilities that a wrongly hypothesized structure and erroneous parameter value can survive the tests in previous two sections.

3.4 Diagnostic Analysis

In case the model fails the validity test, diagnostic analysis is necessary to improve the model. The result of validity test provides valuable information for the diagnosis. In this section the discussion will be mainly based on this information. A more extensive study on the diagnostic analysis is refered to Schweppe[1976].

1. If the model passes all the tests except the whiteness test, the correlation of residuals in time implies that some system dynamics has not been modelled. Some important physical phenomena should be reconsidered or found.

2. If the model passes all the tests except the "residual-input correlation" test, then the assumption of exogeneousness for the input u may not be valid.

3. If the model passes all the tests except the "residual-output correlation" test, then the assumption that v is independent of w is questionable.

4. When the error covariance Q of process noise w is estimated, the

elements that have unusually large quantity may indicate the corresponding state variables are not modelled properly.

5. Using the SAEKF, if the parameter estimated is time dependent, which violates the assumption of constant, it is a trace that the modelling is not correct.

6. If a parameter is not identifiable for all the various input and a significant variation of its value does not affect the resulting simulation, most likely this parameter has negligible effect on the system. Therefore, it can be removed from the model.

3.5 Summary

In recent years, system identification has been a fast developing field. The progress is reflected in the large amount of publication on various theories and its applications. In this chapter the basic idea of system identification is reviewed and only a few estimation techniques about which this work is concerned are briefly introduced. Further reading has to be resorted to books and periodicals. In the following chapters, we will apply system identification techniques to the ship maneuvering problem.

4. STOCHASTIC MODEL STRUCTURE OF SHIP MANEUVERING PROBLEMS

Equation (2.5.22) is a deterministic discription of ship motion. When applying system identification to ship maneuvering problems, the first step is to apply eq. (2.5.22) to the stochastic model described in Fig. 3.2, and then hypothesize the necessary elements of the model structure in the preparation of parameter estimation. In this chapter, special considerations on hypothesizing the ship model will be discussed.

4.1 Input-output Classification

Since we are interested in finding the values of the optimal hydro-dynamic coefficients that best simulate the ship motion, the "physical input-output relationship" is a natural choice for this study. In order to simplify the model, the rudder deflection δ and the angular velocity of propeller are treated as exogeneous input. Thus, only u, v, r and ψ are chosen as the state variables. With this approach, it is not required to know the dynamics of propulsion device and the rudder gears. Newman [1977] has pointed out that the effect of rudder deflection speed is significant only in a short period of the order $\frac{chord}{u}$. If the measurements made on the system correspond directly to the state variables, u, v, r and ψ, the system dynamics and the measurement model can be written in the state-space notation as

$$\underline{x}(n+1) = \begin{bmatrix} u(n+1) \\ v(n+1) \\ r(n+1) \\ \psi(n+1) \end{bmatrix} = \underline{f}(\underline{x}(n),n_p(n),\delta(n))+\underline{w}(n) \qquad (4.1.1)$$

$$\underline{z}(n) = \underline{H}\ \underline{x}(n) + \underline{v}(n)$$

where $\underline{H}$ is an identity matrix and n_p is the propeller rotating speed. This is a fourth order system. However, when the unknown parameters are augmented to the real state vectors, the order of the system will be different, and is dependent on the number of parameters to be estimated,

$$\underline{x}'(n+1) = \begin{bmatrix} \underline{x}(n+1) \\ \underline{\alpha}(n+1) \end{bmatrix} = \begin{bmatrix} \underline{f}(\underline{x}(n), n_p(n), \delta(n), \underline{\alpha}(n)) \\ \underline{\alpha}(n) \end{bmatrix} + \begin{bmatrix} \underline{w}(n) \\ \underline{0} \end{bmatrix}$$

$$\underline{z}(n) = \underline{H}'\underline{x}'(n) + \underline{v}(n) \tag{4.1.2}$$

where

$$\underline{H}' = [\ \underline{I}\ |\ \underline{0}\ ]$$

Since $\underline{H}'$ is composed of the identity matrix $\underline{I}$ and the zero matrix $\underline{0}$, this simple expression for $\underline{H}'$ can significantly reduce the computation effort.

It is important to realize that, although the dynamics of ship motion is nonlinear, the noises are assumed to be linearly related to the system dynamics and the measurements. The linearity in noises helps to simplify the problem, but this assumption needs to be verified by validity tests.

In practice, measurements are usually taken at discrete time intervals. Therefore, the $\underline{z}(n)$ in Eq. (4.1.1) is an appropriate description of these measurement. However, the discrete-time expression of system dynamics is only an approximation of the real system. Instead of using finite difference expression to propagate the state vector and the covariance matrix, a numerical integration scheme, the Runge-Kutta method,

is used in this work to improve the accuracy. The trade-off is an increase
of computing burden, storage requirements and round-off errors. Because
eq. (2.5.22) is only accurate to the third order, Runge-Kutta method of
the third order is used in this analysis. The application of higher order
Runge-Kutta method will not improve the accuracy of ship motion simulation.

4.2 Nature of Disturbance

When we derived the simplified equations of ship motion, eq. (2.5.22),
the modelling error is attributed to

1. The negligence of environmental excitations, such as waves, wind, etc.,

2. The reduction of 6 degree of freedom system to a system which has
only 3 degrees of freedom in describing the ship motions,

3. The truncation error in performing Taylor series expansion,

4. The noises of exogeneous inputs.

Due to the tremendous inertia of the ship and the relatively small
direct contribution of control surface to the external force acting upon
the ship, the dynamics of the ship motions is rather slow. In other words,
the process to be modelled here is basicly of low order, but is nonlinear
and involves slow speed dynamics. Therefore, from the discussions made in
sec. 3.1.2, uncorrelated zero mean Gaussian white noise is a reasonable
assumption for the process noise.

As long as the observation time interval is long comparing to the
time constant of the noise and if the different sources of noise are
independent, the uncorrelated zero mean Gaussian white noise is still a
good assumption for the measurement noise. During the sea trial, the

time constants of all the sensor dynamics are shorter than 1 second, according to Åström & Källström[1976]. When $\Delta t \geq 4$ sec. is used during filtering, it is quite safe to assume that there is no time structure in the measurement noise, i.e., the noise is white.

Information on the resolution of the sensors is usually furnished by the manufacturer. However, the limitation on the measurement accuracy is not the only source of measurement error. For instance, a rough sea bottom could degrade the speed measurement of doppler sonar, ship hull vibration could affect the rate gyro, etc.. The covariance of measurement error is approximated by passing the data through a low pass filter. The RMS of the difference between the original data and the filtered data is used as the standard deviation of the measurement noise.

Compared to the measurement noise, the covariance of process noise is usually not as easy to approximate as the measurement noise. Since a direct identification of the uncertain covariance by SAEKF is impossible, the initial guess of Q is based on the judgement of engineering experience, the estimation of Q is accomplished by using the information fed back from statistical hypothesis testing.

4.3 Parameterization

In chapter 3, we have mentioned that SAEKF should not estimate too many unknown parameters at the same time. The number of operations required for matrix multiplication is proportional to pxqxm, where pxq and qxm are the orders of these two matrices. The computing burden increases eight times as each order of the matrices doubles.

In order to maintain the CPU time below 200 seconds for a 400 time step filtering on the Honeywell Multics system, the maximum order of augmented state vector is limited to no more than 14. Among the 14 state variables, 4 are used for the real state vector, 2 are used for the current magnitude and current direction, and 8 are reserved for the unknown hydrodynamic coefficients.

At the first glance, one may feel annoyed by the fact that there are 31 hydrodynamic coefficients in eq. (2.5.22) and there are only 8 coefficients identified at one time. In the following paragraphs, we will discuss the appropriate parameterizations that will give a systematic estimation of the hydrodynamic coefficients without requiring the simultaneous identification of all the 31 coefficients.

For most engineering problem, the linearized model is commonly used as the first order approximation. For a ship undergoing moderate maneuvers, such as 10°/10° zigzag maneuver, hydrodynamic forces and moments are usually dominated by the linear forces and moments. In a tight maneuver, such as 35° turning circle, the linear forces and moments remain important, but the contributions from nonlinear terms can not be neglected.

Therefore, it is advisable to begin the analysis with the estimation of linear hydrodynamic coefficients. In performing the estimation, the measurements of moderate maneuvers are processed, and the nonlinear coefficients are fixed at the model testing value. After the linear terms are identified, the measurements made on tight maneuvers are processed to

estimate the nonlinear terms, while the linear coefficients are held fixed at the identified value. The iteration is repeated until a further modification is minimal.

However, in each of linear and nonlinear hydrodynamic coefficient category, the number of parameters are still more than 8. More analysis is required to overcome this difficulty. As mentioned before, the exogeneous input decides not only whether the motion is linear or nonlinear but also which mode of the motion is excited most and which coefficient plays an important role corresponding to that input. Therefore, if the number of modes can be reduced by a proper choice of inputs, the number of relevent unknown parameters can also be reduced. Some maneuvers that have this kind of characteristecs are listed below:

a. *Straight forward motion and reverse spiral maneuver*. For a ship which has directional stability, during straight forward motion in calm water, $v=r=0$, the following relationship holds:

$$Y_0 + Y_\delta \delta = 0$$

$$N_0 + N_\delta \delta = 0$$

(4.3.1)

Since Y_δ is coupled with N_δ, and Y_0 is coupled with N_0 by the same relationship, there exists one δ that satisfies both the above equations. Thus a reasonably good estimate of Y_0 and N_0 can be acquired by measuring the rudder bias. In the presence of current, the ship heading can be directed into the current at a speed which is large enough to neglect the current effect, and yet small enough to give essentially constant drag

coefficient, such that rudder bias can still be measured accurately. For a directionally unstable ship, the rudder has to oscillate about a mean to achieve a zero turning rate, Burcher[1971]. Therefore, reverse spiral test helps to determine the rudder bias.

b. *Coasting with propeller windmilling.* When the ship is coasting with propeller windmilling, the ship is slowed down mainly by the hull resistance, together with a small resistance induced by the windmilling propeller, which is about 5% of the total drag.

c. *Coasting with locked propeller.* When the propeller is locked, the drag force upon a coasting ship consists of the drag force from the hull, appendages and from the propeller. As discussed in Sec. 2.5.2, the resistance induced by a locked propeller is usually as significant as 20% of the total drag.

d. *Acceleration.* If the hull resistance coefficient C_R can be determined by seperating it from the effect of windmilling propeller or locked propeller, which needs an extensive study that is beyond the scope of this thesis, then accelerating motion assists in estimating the coefficients n_1', n_2' and n_3' in Eq. (2.5.22). This is because the ship motion response is much slower than the propeller response to an adjustment of propeller rotating speed, thus the contributions of these terms are different. The estimation should be good, if acceleration and deceleration are alteranately performed during the trial.

e. *Steady turn at small rudder deflection.* Since $\dot{u}=\dot{v}=\dot{r}=0$, and the rudder deflection is small, Y_v', Y_r', Y_δ', Y_0', N_v', N_r', N_δ', N_0' and $X_{vr}'+m'$ are the

most important coefficients in this case.

Nevertheless, there are still many coefficients left behind in the above discussion, especially the nonlinear coefficients. The analysis of identifiability in Chap. 5 will make up this gap. Notice that the sensitivity of the ship motion to the variation of a certain hydrodynamic coefficient is not equivalent to the identifiability of that coefficient.

Recall that the strategy of systematically identifying the hydrodynamic coefficients is to design a series of model structures, each of them has different parameterization, such that certain coefficients can be accurately estimated by a proper choice of the model and the observation of specific inputs. Unfortunately, the sea trials conducted on ESSO OSAKA did not cover the maneuvers discussed in this section. Therefore, the identification of C_R could not be made. However, from the view point identifying an equivalent thrust-resistance relationship, the existing sea trials are sufficient to provide this information.

Based on the above discussion and the analysis in Chap. 5, a flow chart as shown in Fig. 4.1 is constructed to illustrate the parameterizations for the system identification of ESSO OSAKA.

4.4 A Priori Information

In order to use SAEKF, we have to provide statistical information on the parameters to the filter. For the model of a physical relationship, the elements of $\underline{\alpha}$ are usually known approximately. In ship maneuvering problems, the scaled model testing data from a towing tank provides a good initial guess of these parameters. The level of confidence in the

measurement is reflected in its covariance matrix. The measurement error covariance is a more difficult quantities to guess. Even if a vast quantity of experimental data for the model is available about these parameters, in general, it still may not reflect the real value of covariances. This is due to the intrinsic scale effect between the model and the full size ship. However, the effect of initial conditions decays with time if the filter becomes a time-invariant stable system. Fortunately, our experience with the identification of hydrodynamic coefficients shows that the filter does reach a steady state. Therefore, it is reasonable to estimate the initial covariance by engineering experience.

Notice that using a certain fraction of the initial parameter value as its standard deviation can be errorneous. In the extreme case, if the parameter is approximately zero, this percentage approximation of covariance will not allow the filter modify the parameters during the process of estimation.

Linear Category:

10°/10° zigzag &
20°/20° zigzag
(parallelly processed)

$\underline{\alpha}$ | Y_0', N_0', u_c, α

10°/10° zigzag

$\underline{\alpha}$ | n_1', n_2', n_3', u_c, α

10°/10° zigzag

$\underline{\alpha}$ | Y_v', Y_r', N_v', N_r', N_δ', $X_{vr}'+m'$, u_c, α

20°/20° zigzag for
checking the validity
of identified nonlinear
model

Nonlinear Category:

biased zigzag or tight
turning circle maneuvers

$\underline{\alpha}$ | X_{ee}', N_{eee}', Y_{vrr}', N_{vrr}', X_{vvrr}', u_c, α
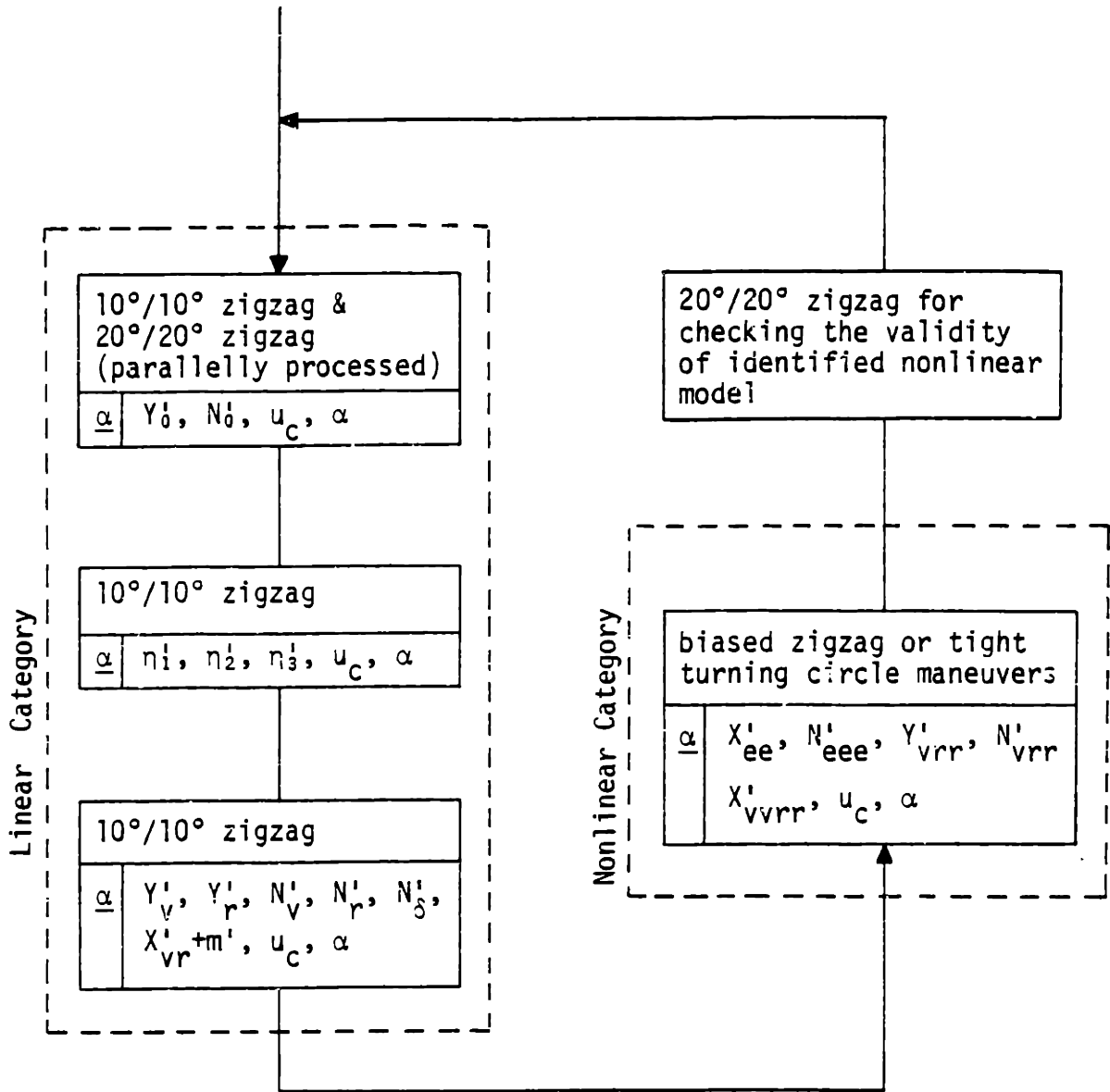
$\underline{\alpha}$: unknown parameter

α : current angle

Figure 4.1   Parameterizations for the system identification
of ESSO OSAKA.

5. IDENTIFIABILITY

The study of identifiability is very important. It can not be justi-
fied to spend time and energy to deal with a system model which is not
identifiable. After the estimation is completed, the identifiability of
parameters should be also checked. A significant deviation of these para-
meters is still possible to satisfy the input-output relationship.

The term "identifiability" should be used very carefully. An exam-
ple given by Schweppe[1973] best illustrates its definition from different
point of view. Consider a scalar system,

$$x(n+1)=\Phi x(n)+Bu(n)$$
$$z(n)=Hx(n)+v(n) \qquad\qquad (5.0.1)$$
$$x(0)=0$$

where the values of B and H are both assumed to be unknown. Equation
(5.0.1) can be rewritten as

$$z(N)=HB \sum_{n=0}^{N-1} \Phi^{N-n-1}u(n)+v(N) \qquad N=1,\ldots\ldots \qquad (5.0.2)$$

If it is desired to estimate the individual values of H and B, then the
system is said unidentifiable, because there is no unique solution of H
and B to describe the input-output relationship. However, if the identi-
fiability is defined in the sense that a system's input-output character-
istics can be predicted, then the system in Eq. (5.0.1) is identifiable,
because only the identification of the product HB is necessary and it is
possible in this case.

In this study of ship maneuvering problem, values of the hydrodynamic coefficients in Eq. (2.5.22) are to be estimated. Therefore, the identifiability is defined as: A parametric model is parameter identifiable if the parameters can be uniquely identified from the input-output relation.

For linear systems, controllability, observability and identifiability are well defined concept. Mathematical definition and criteria for these concepts can be referred to Gelb[1974], Eykhoff[1974] and Lee[1964]. For nonlinear systems, clear cut definitions are not available for these concepts. It is the purpose of this chapter to find out the unidentifiable parameters, and the conditions under which those parameters can be identified.

In Sec. 5.1, we will discuss the identifiability of inertia terms, such as $X_{\dot{u}}$, $Y_{\dot{v}}$, $N_{\dot{r}}$ and $N_{\dot{v}}$, when they are estimated together with the other coefficients. In Sec. 5.2, we will study the sensitivity of ship motion to the variation of a hydrodynamic coefficient. This analysis will help us to recognize the relative importance of one particular hydrodynamic coefficient among all the coefficients in the equation of ship motion during a specific maneuver. In Sec. 5.3, we will discuss the difficulties of identification due to the cancellation effect of hydrodynamic forces and moments induced by the accompanied sway and yaw motion of a maneuvering ship.

5.1 Identifiability of the Inertia Terms Together with the Other Hydrodynamic Coefficients

In order to reveal the problem, let us consider the simplest model for the ship motion. Assume that all the measurements of velocity is relative to the constant current and the ship is performing moderate maneuver, therefore a linearized expression is sufficient to describe the ship motion. Writing these equations in matrix form and omitting the subscript "r" for the velocity relative to water, we have

$$
\begin{bmatrix} m-Y_{\dot{v}} & mx_G-Y_{\dot{r}} \\ mx_G-N_{\dot{v}} & I_z-N_{\dot{r}} \end{bmatrix} \begin{bmatrix} \dot{v} \\ \dot{r} \end{bmatrix} = \begin{bmatrix} Y_v & Y_r-mu \\ N_v & N_r-mx_G \end{bmatrix} \begin{bmatrix} v \\ r \end{bmatrix} + \begin{bmatrix} Y_\delta \\ N_\delta \end{bmatrix} \delta \qquad (5.1.1)
$$

The relationship between the input δ and the output v, r will not be changed if this equation is premultiplied by an arbitrary non-singular matrix. Obviously, it is impossible to estimate simultaneously all the coefficient matrices in Eq. (5.1.1). However, if any one of these matrices can be experimentally determined to some reasonable accuracy, then the identification of the rest of the coefficients is possible. For non-linear models, although a clear input-output expression like Eq. (5.1.1) does not exist, similar arguments used in this section are still applicable to Eq. (2.5.22) for nonlinear systems.

This difficulty of identification can be resolved by some physical insight of the mechanism of hydrodynamic coefficients. The simplest way to estimate the added sway mass $Y_{\dot{v}}$ and yaw moment $N_{\dot{r}}$ is to apply the strip theory. However, Fujino, Takashina and Yamamoto[1974] have

shown that three-dimensional effect is not negligible, especially when water depth becomes shallow relative to the ship draft, see Fig. 5.1. This is because the strip theory predicts that the values of Y_v and N_r approach infinity when water depth approaches to zero. However, the complete blockage of fluid flow does not occur in practical situations. In the extreme case, the fluid flow will be diverted around the ends of ship and Y_v & N_r remain finite.

In deep water, there is still a 20% difference in sway added mass and 40% difference in yaw added moment of inertia between the experimental data and the theoretical prediction from strip theory. In Appendix C, it is shown that a 20% difference in inertia terms will significantly affect the ship performance, not to mention the 40% difference in the moment of inertia. Since the 3-dimensional finite element method gives an estimate of these quantities which are in consistent with the experimental value, it is reasonable to use the model testing value as an "accurate" measurement of Y_v & N_r for deep water maneuvering of a full scale ship. If necessary, the result can be verified by the 3-dimensional finite element method. By doing so, the rest of the hydrodynamic coefficients can be uniquely determined when there is only one optimal solution.

When the water depth to ship draft ratio becomes small, the difference in boundary layer between the model and the full scale ship can cause significant difference in Y_v and N_r, even if the experiment value is still close to the 3-dimensional finite element method's estimation. Therefore, we think that the identification Y_v and N_r is necessary in

Figure 5.1 Three-dimensional correction factors, C_y and C_{zz}, of the sway added mass and the yaw added moment of inertia. (Remarks in this figure designate the method to obtain the 3-dimensional added mass and added moment of inertia, ref. Fujino, Takashina and Yamamoto[1974]).
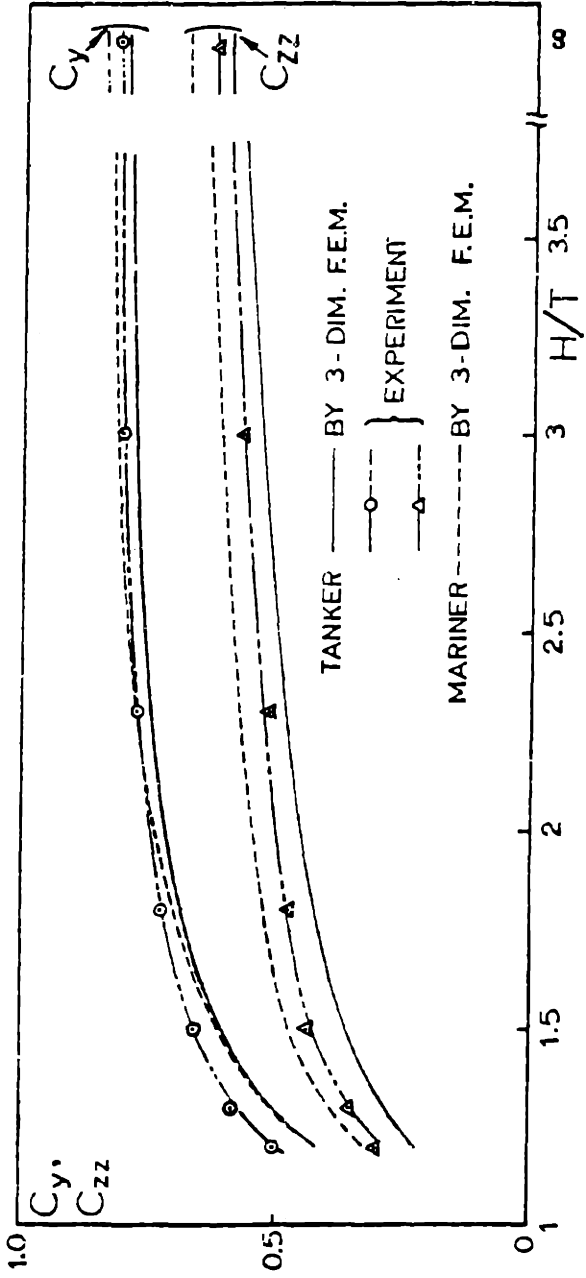
$$C_y = \frac{\text{3-Dimensional sway added mass}}{\text{Sway added mass by strip theory}}$$

$$C_{zz} = \frac{\text{3-Dimensional yaw added moment of inertia}}{\text{Yaw added moment of inertia by strip theory}}$$

both medium and shallow water ship maneuvers.

In Fig. 5.2, Fujino[1976] shows that shallow water also has a significant effect on the damping derivative terms. Therefore, the identification of these terms is indispensible in medium and shallow water cases. Fortunately, this phenomena does not apply to the derivatives with respect to rudder deflection, Y'_δ and N'_δ. Fujino[1976] and Dand[1976] have shown that water depth has insignificant effect on Y'_δ and N'_δ. This is because of the clearance between the rudder tip and the sea bottom is still relatively too large to cause a significant wall effect, even if the water depth to ship draft ratio is small. Consequently, Y'_δ, $Y'_{\delta\delta\delta}$, N'_δ, $N'_{\delta\delta\delta}$ and $X'_{\delta\delta}$ are nearly constant at different water depths. This statement is best verified by the model testing values of the hydordynamic coefficient at different water depth for the ship ESSO OSAKA, which are tabulated in Appendix B for comparison.

To avoid the non-uniqueness problem mentioned at the beginning of this section, the values of certain appropriate hydrodynamic coefficients are fixed on the best estimated value. In infinite deep water, the inertia terms are determined by model test or finite element method. The rest of the coefficients are identified by stochastic estimation theory. After that, the identified values of Y'_δ, $Y'_{\delta\delta\delta}$, N'_δ, $N'_{\delta\delta\delta}$ and $X'_{\delta\delta}$ in deep water are carried over to the processing of shallow water maneuvering data to estimate the rest coefficients in finite water depth.
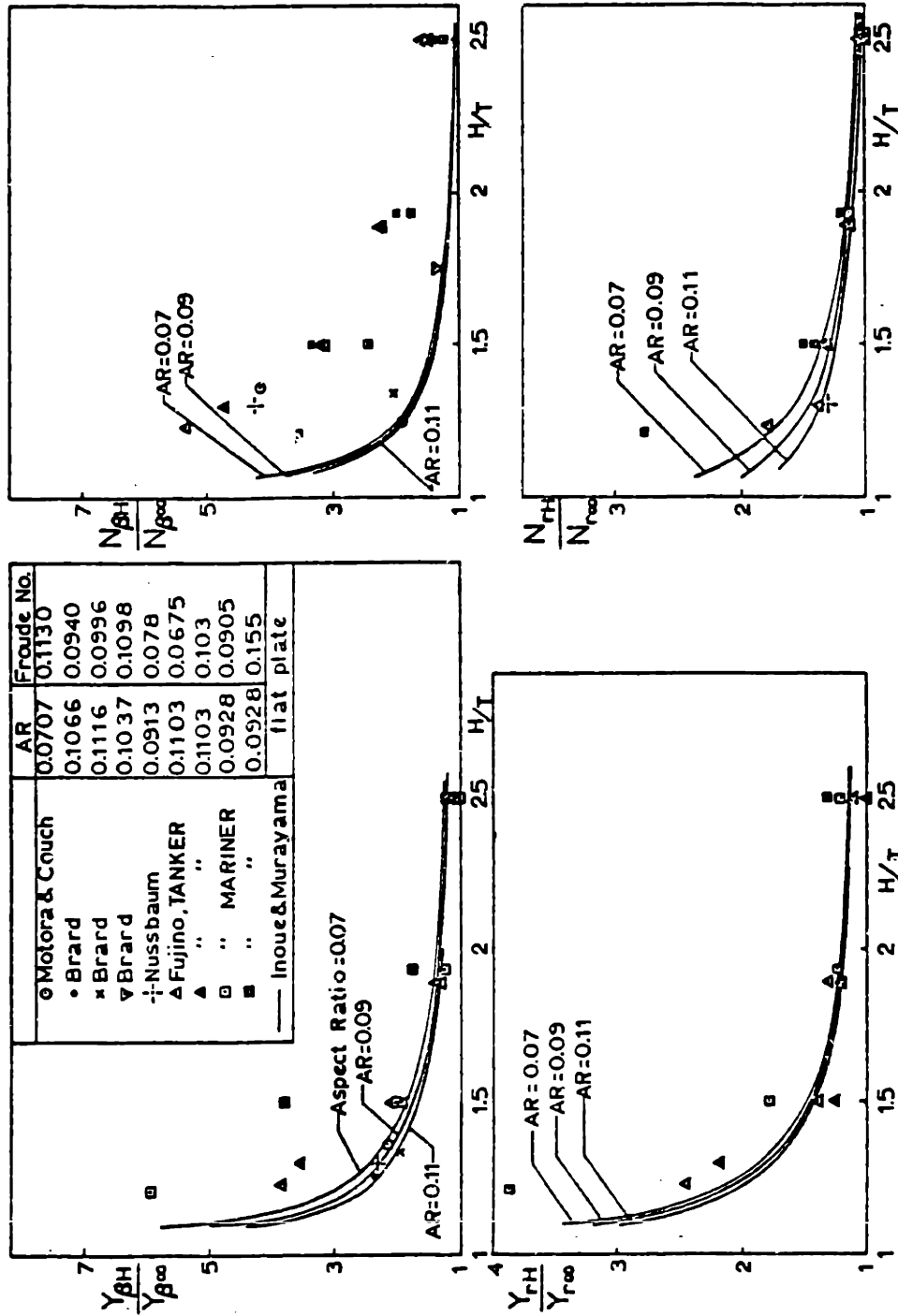
Figure 5.2 Shallow water effect on the linear damping derivatives(the aspect ratio is defined by 2T/L, ref. Fujino[1976]).

5.2 Sensitivity Analysis

The definition of "sensitivity analysis" may be some what different from what is commonly defined in control theories. In this study, sensitivity is defined as how sensitive is the ship response to the variation of a particular hydrodynamic coefficient. This analysis will help us to understand qualitatively which coefficients play the more important role in a specific maneuver of a specific ship. Thus an appropriate parameterization strategy can be designed in order to estimate the uncertain coefficients in a systematic, reliable and efficient manner. Notice that each coefficient has a different role in a different maneuver of a particular ship. Therefore, one must be careful when applying results from this kind of study.

A straightforward and yet very informative method is described here. The idea of this method is similar to Chen's[1969], but with many modifications.

*Step 1 Simulate the response of ship motion to rudder deflection based on the original set of hydrodynamic coefficients,

*Step 2 Perturb the value of ith coefficient by a certain amount, say 20% of the original value,

*Step 3 Simulate the ship motion by using the new set of coefficient values,

*Step 4 Restore the perturbed ith coefficient back to the original value,

*Step 5 Go to Step 2 for i+1th coefficient, unless this procedure has gone through all the hydrodynamic coefficients. Notice that we also

perturb the current magnitude and direction in the same manner as a hydrodynamic coefficient, because these two quantities are also considered as unknown parameters. However, we think that the percentage perturbation is not a proper way for current direction. Consider the case of current angle 270° from north, a 20% perturbation will amount to 54°. Therefore, instead of the percentage perturbation, we use a perturbation of 10° for current angle.

*Step 6 Plot the ship motion versus time for these perturbed set of coefficients together with the ship motion response of the original set of coefficients in the same figure(see Appencix C for these plots of a 20°/20° zigzag maneuver).

*Step 7 Measure the maximum difference between the perturbed and the original simulation of state variable u, v and r, and prepare a table, such as Table C.1.a for the 5°/5° zigzag maneuver.

*Step 8 Normalize each element in Table C.1.a by the sum of corresponding columns to obtain the relative sensitivity of u, v and r to the variance of 20% coefficient value. The overall relative sensitivity of a specified maneuver to the variance of a coefficient is defined as the sum of the relative sensitivity of u, v and r to the variance of coefficient value. The individual relative sensitivity of u, v and r and the overall sensitivity of 5°/5° zigzag maneuver to the variance of coefficients are shown in Table C.1.b.

*Step 9 Go to Step 1 for the other maneuver. In this study, four maneuvers are investigated on their sensitivity analysis. They are

LP	COEFFICIENT	35° CIRCLE	20°/20° Z	10°/10° Z	5°/5° Z
1	$m'-X'_{\dot{u}}$	0.208(4)	0.113(9)	0.044(15)	0.012(24)
2	n_1	0.023(23)	0.015(24)	0.025(18)	0.044(16)
3	Y'_{rrr}	0.115(9)	0.042(18)	0.016(21)	0.020(22)
4	$m'-Y'_{\dot{v}}$	0.085(14)	0.285(2)	0.183(6)	0.114(11)
5	$m'x'_G-Y'_{\dot{r}}$	0.012(24)	0.037(22)	0.016(21)	0.024(21)
6	Y'_v	0.095(12)	0.249(4)	0.390(2)	0.265(3)
7	Y'_r	0.046(17)	0.087(11)	0.156(8)	0.142(9)
8	Y'_δ	0.252(2)	0.202(6)	0.178(7)	0.134(10)
9	Y'_0	0.023(23)	0.024(23)	0.027(17)	0.061(14)
10	$m'x'_G-N'_{\dot{v}}$	0.012(24)	0.060(13)	0.011(23)	0.036(19)
11	$I'_z-N'_{\dot{r}}$	0.061(18)	0.260(3)	0.241(4)	0.151(8)
12	N'_v	0.114(10)	0.110(10)	0.446(1)	0.463(1)
13	N'_r	0.181(5)	0.204(5)	0.130(9)	0.202(6)
14	N'_δ	0.432(1)	0.436(1)	0.374(3)	0.261(4)
15	N'_{vrr}	0.113(11)	0.015(24)	0.016(21)	0.016(23)
16	n_2	0.028(22)	0.038(21)	0.059(13)	0.080(13)
17	n_3	0.170(6)	0.183(7)	0.195(5)	0.304(2)
18	X'_{vv}	0.023(23)	0.015(24)	0.016(21)	0.008(24)
19	$X'_{rr}+m'x'_G$	0.012(24)	0.007(25)	0.005(25)	0.004(25)
20	$X'_{\delta\delta}$	0.142(8)	0.052(16)	0.014(22)	0.012(23)
21	$X'_{vr}+m'$	0.209(3)	0.138(8)	0.058(14)	0.040(17)
22	$X'_{v\delta}$	-	-	-	-
23	N'_{rrr}	0.163(7)	0.003(26)	0.006(24)	0.000(26)
24	N'_0	0.023(23)	0.057(14)	0.077(11)	0.204(5)
25	Y'_{vvv}	0.035(19)	0.042(18)	0.022(19)	0.029(20)
26	$Y'_{\delta\delta\delta}$	0.023(23)	0.015(24)	0.016(21)	0.000(26)
27	Y'_{rvv}	0.023(23)	0.015(24)	0.016(21)	0.000(26)
28	$Y'_{\delta vv}$	-	-	-	-
29	$Y'_{v\delta\delta}$	-	-	-	-
30	N'_{vvv}	0.000(25)	0.000(26)	0.000(26)	0.000(26)
31	$N'_{\delta\delta\delta}$	0.081(15)	0.038(21)	0.006(24)	0.000(26)
32	N'_{rvv}	0.035(21)	0.049(17)	0.006(24)	0.000(26)
33	$N'_{\delta vv}$	-	-	-	-
34	$N'_{v\delta\delta}$	-	-	-	-
35	Y'_{vrr}	0.087(13)	0.072(12)	0.021(20)	0.040(17)
36	C'_R	0.039(20)	0.056(15)	0.102(10)	0.170(7)
38	α	0.067(16)	0.041(19)	0.070(12)	0.111(12)
39	u_c	0.066(17)	0.039(20)	0.041(16)	0.052(15)

Table 5.1 Overall relative sensitivity in different maneuvers for OSAKA

a. 5°/5° zigzag maneuver   (Table C.1.a & C.1.b)

b. 10°/10° zigzag maneuver   (Table C.2.a & C.2.b)

c. 20°/20° zigzag maneuver   (Table C.3.a & C.3.b)

d. 35° turning circle maneuver (Table C.4.a & C.4.b)

In order to compare the importance of each coefficient in different maneuvers, we tabulate the overall relative sensitivity of each coefficient of the four maneuvers in one table(Table 5.1) and rank them by their relative importance in each maneuver. By a somewhat arbitrarily designed rule as in Table 5.2, the overall sensitivity are categorized into five groups-very important, important, significant, minor and negligible. This categorization is shown in Table 5.3. It must be kept in mind that this indication of importance is only a relative comparison. For instance, Y_v' is a "very important" coefficient for 10°/10° zigzag maneuver, while for 20°/20° zigzag maneuver, Y_v' is marked only as "important". But on the absolute scale, a 20% variance of Y_v' causes larger deviation of ship motion response from the original.

x	-1.2	-1.7	-2.3	-3.0
overall sensitivity e^x	0.301	0.183	0.100	0.050

VI ← | ← I → | ← S → | ← M → | → N

Table 5.2 The rule for categorization

LP	COEFFICIENT	DIMENSIONAL FACTOR	35° CIRCLE	20°/20° Z	10°/10° Z	5°/5° Z
1	$m'-X'_{\dot{u}}$	$0.5\rho L^3$	I	S	N	N
2	$\dot{n}_1$	$0.5\rho L^2$	N	N	N	N
3	Y'_{rrr}	$0.5\rho L^5 U^{-1}$	S	N	N	N
4	$m'-Y'_{\dot{v}}$	$0.5\rho L^3$	M	I	I	S
5	$m'x'_G-Y'_{\dot{r}}$	$0.5\rho L^4$	N	N	N	N
6	Y'_v	$0.5\rho L^2 U$	M	I	VI	I
7	Y'_r	$0.5\rho L^3 U$	N	M	S	S
8	Y'_δ	$0.5\rho L^2 c^2$	I	I	S	S
9	Y'_0	$0.5\rho L^2 U^2$	N	N	N	M
10	$m'x'_G-N'_{\dot{v}}$	$0.5\rho L^4$	N	N	N	N
11	$I'_z-N'_{\dot{r}}$	$0.5\rho L^5$	M	I	I	S
12	N'_v	$0.5\rho L^3 U$	S	S	VI	VI
13	N'_r	$0.5\rho L^4 U$	I	I	S	I
14	N'_δ	$0.5\rho L^3 c^2$	VI	VI	VI	I
15	N'_{vrr}	$0.5\rho L^5 U^{-1}$	S	N	N	N
16	$\dot{n}_2$	$0.5\rho L^3$	N	N	M	M
17	$\dot{n}_3$	$0.5\rho L^4$	S	I	I	VI
18	X'_{vv}	$0.5\rho L^2$	N	N	N	N
19	$X'_{rr}+m'x'_G$	$0.5\rho L^4$	N	N	N	N
20	$X'_{\delta\delta}$	$0.5\rho L^2 c^2$	S	M	N	N
21	$X'_{vr}+m'$	$0.5\rho L^3$	I	S	M	N
22	$X'_{v\delta}$	$0.5\rho L^2 c$	-	-	-	-
23	N'_{rrr}	$0.5\rho L^5 U^{-1}$	S	N	N	N
24	N'_0	$0.5\rho L^3 U^2$	N	M	M	I
25	Y'_{vvv}	$0.5\rho L^2 U^{-1}$	N	N	N	N
26	$Y'_{\delta\delta\delta}$	$0.5\rho L^2 c^2$	N	N	N	N
27	Y'_{rvv}	$0.5\rho L^3 U^{-1}$	N	N	N	N
28	$Y'_{\delta vv}$	$0.5\rho L^2$	-	-	-	-
29	$Y'_{v\delta\delta}$	$0.5\rho L^2 U$	-	-	-	-
30	N'_{vvv}	$0.5\rho L^3 U^{-1}$	N	N	N	N
31	$N'_{\delta\delta\delta}$	$0.5\rho L^3 c^2$	M	N	N	N
32	N'_{rvv}	$0.5\rho L^4 U^{-1}$	N	N	N	N
33	$N'_{\delta vv}$	$0.5\rho L^3$	-	-	-	-
34	$N'_{v\delta\delta}$	$0.5\rho L^3 U$	-	=	-	-
35	Y'_{vrr}	$0.5\rho L^4 U^{-1}$	M	M	N	N
36	C'_R	$0.5\rho Su^2$	N	M	M	S
38	α		M	N	N	S
39	u_c		M	N	N	M

Table 5.3 Relative importance of each coefficient categorized by the rules in Table 5.2.

To observe the trend of transition from moderate maneuver to tight maneuver, the overall relative sensitivity of 5°/5°, 10°/10° and 20°/20° zigzag maneuvers are shown in Fig. 5.3. Some useful information is uncovered by carefully examining Table 5.1, Table C.1 to Table C.4 and Fig. 5.3,

(1) Inertia terms, $m-X_{\dot{u}}$, $m-Y_{\dot{v}}$ and $I_z-N_{\dot{r}}$ become more and more impor-tant, when the maneuver is becoming tight.

(2) The thrust force coefficient n_3 is the most important among n_1, n_2, n_3. The ship motion response is more sensitive to them, when the maneuver is very mild. The same statement applies to C_R. It is concei-vable when the ship moves at constant heading, these thrust coefficients and drag coefficient will be the dominant coefficients in this extreme case.

(3) The nonlinear coefficients play a more important role in tight maneuver, which is consistent with the definition of the nonlinear terms. However, one must not conclude that nonlinear terms are not necessary for the simulation of moderate maneuvers such as 10°/10° zigzag, more than 25% speed loss is acquired at steady state of this maneuver for OSAKA.

(4) In moderate maneuver, unbalanced yaw moment N_0 is important. It suggests that the estimation of N_0 is indispensible. However, the unbalanced sway force does not affect the ship motion response as much as N_0 does.

(5) It is found that $Y_{\delta}^{\prime}$ is less influential over the ship motion than $N_{\delta}^{\prime}$. This can be used to our advantage to make $Y_{\delta}^{\prime}$ dependent of $N_{\delta}^{\prime}$
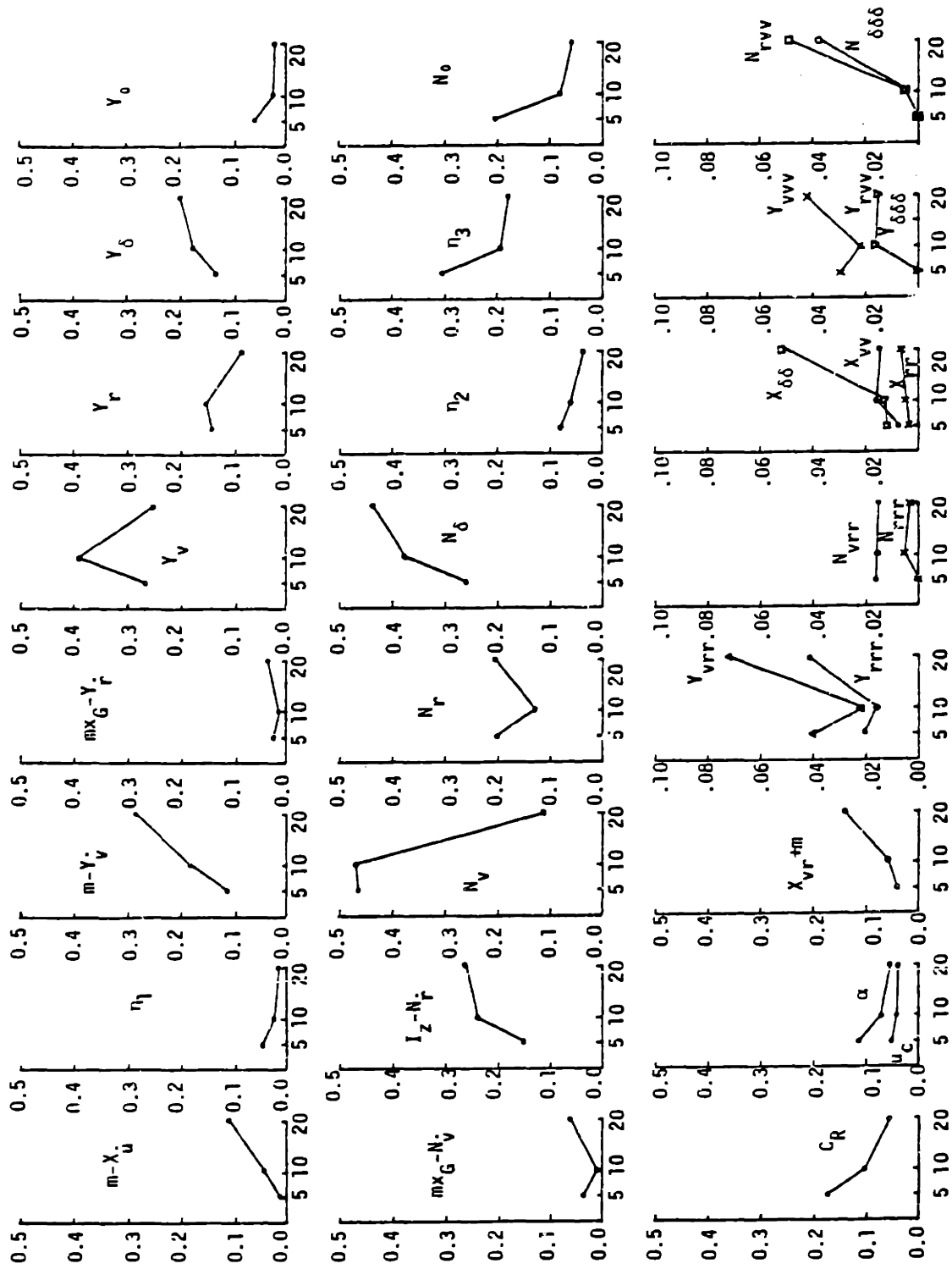
Figure 5.3 Overall relative sensitivity in the zigzag maneuvers of different tightness

(through a fixed moment arm) without introducing any significant error, thereby reducing the number of unknown parameters to be estimated.

(6) Although the 35° turning circle maneuver is a very tight maneuver, $m-X_{\dot{u}}$ is the only important inertia term. This is because of the fact that the transient periord of v and r is rather short compared to that of the surge velocity during a turning circle maneuver.

(7) For moderate ship motions and the turning circle maneuver, both current direction and magnitude have non-negligible effect on the ship motion. Because the data collected by current meters is not reliable, e.g., a difference of 30° in current direction and 0.3∿0.4 knots in current magnitude between the two current meters at different water depths, but at the same buoy system, is not unusual. We believe the bulk effect of current on the ship motion should be the net effect of these distributed elemets. This is the reason why current direction and magnitude are included as parameters to be identified. We have to emphasize that the analysis here is incomplete for the current, because the initial heading of ship is always about the opposite direction of current in the simulation, which is the case for the sea trial of the OSAKA. In general, all current directions should be included in this study.

(8) Notice that Y_v' is always more important than Y_r' in all maneuvers, because Y_r' is just a small portion of $Y_r'-m'u'$. However, the role of N_v' and N_r' exchanges when the maneuver becomes more violent.

(9) Contrary to the other linear derivatives, Y_δ' and N_δ' become more influential on the ship motion when the maneuver is tighter.

Since our analysis is based on the model testing value of OSAKA, the sensitivity of ship motions to the variation of certain coefficient is not available because of the lack of data. We believe these coefficient belongs to the category of "minor" or "negligible" effect for these maneuvers, otherwise their importance should win the notice of analyzer of the model testing data in Stevens Institute of Technology. Nevertheless, we left the definite conclusion open for these coefficient, unless a positive confirmation is available.

Notice that the sensitivity of ship motion response to the variation of a particular coefficient for a specific maneuver should not be confused with the identifiability of a hydrodynamic coefficient. In Sec. 5.3, a good example is given to show that two coefficients, both of which contribute significant amount of force or moment in a maneuver, are not identifiable by using this specific maneuvering model. Therefore, a parameter to which the system is not sensitive is most likely to be unidentifiable. However, the unidentifiability does not necessarily imply that the system is not sensitive to the parameter's variation.

A final remark on the analysis in this section is to call to the reader's attention that the model used in this section is slightly different from Eq.(2.5.22) in Chap. 2, this is because of the sensitivity analysis was done before all the modification proposed in Chap. 2 were incorporated in the model. The only modifications included in this model are those discussed in Sec. 2.5.1 and Sec. 2.5.2. Since modifications other than the above do not change the ship behavior significantly, the

results shown in Table 5.3 are still qualitatively valid.

5.3 Simultaneous Drifting and Cancellation Effect

When the stochastic model described in Chap. 4 was used to estimate the hydrodynamic coefficients, a troublesome and yet interesting phenomenon occured. If Y_v' and Y_r' or N_v' and N_r' are estimated simultaneously, at a certain point during the estimation, these two coefficients will start to drift together in a similar pattern, although the measurement of state variable can be filtered very well. Figure 5.4 is an illustration of this "simultaneous drifting", in which the simulated $10°/10°$ zigzag maneuvering data of ESSO OSAKA is processed. This implies that the value of Y_v' and Y_r' or N_v' and N_r' can be increased or decreased simultaneously according to certain implicit rules and still result in the same ship motion responses to the rudder defletion. In other words, there is a problem of nonuniqueness or identifiability.

Some difficulties involved in the estimation were mentioned by Åström and Källström[1976]. They attempted to identify the linear coefficients Y_v', $Y_r'-m'$, N_v', $N_r'-m'x_G'$, Y_δ' and N_δ' simultaneously, using a linear model. The failure was attributed to "the nonlinear effects during the course change in the middle of the experiment". This argument may be justified if the sea trial had involved tight maneuvers. Nevertheless, the execution of rudder rarely exceeded $5°$ in their test. Therefore, it is doubtful that such argument can be fully justified. However, Åström and Källström failed to point out that Y_v' and $Y_r'-m'$ showed similar trend at the end of identification(so did the N_v' and $N_r'-m'x_G'$), Y_v' and $Y_r'-m'$

```
******************************************************************
*                                                                *
*    PARAMETRIC IDENTIFICATION - EXTENDED KALMAN FILTER    *
*                                                                *
******************************************************************
```

SYSTEM: 280,000 DWT. TANKER - ESSO OSAKA

MANEUVER: ZIG-ZAG RUDDER, AT RUDDER RATE -2.00 DEG./SEC.,
                                  10.00/ 10.00 ZIG-ZAG
            1.35 FT/SEC. OF CURRENT
            86.00DEGREES FROM NOMINAL ZERO

TRIAL PERIOD: 1600.00 SECONDS AT 4.00 SECONDS OF TIME INTERVAL
IDENTIFICATION: STATE VARIABLES -U,V,R,PS

UNKNOWN PARAMETERS -

$NP = 6$: Y'_V

$NP = 7$: Y'_R

$NP = 12$: N'_V

$NP = 13$: N'_R

$NP = 14$: N'_D

$NP = 21$: $X'_{VR} + M'$

$NP = 38$: ALPHA(DEGREE)

$NP = 39$: U_c (FT./SEC.)

Table 5.4   Results of identification to illustrate the phenomenon
            of "simultaneous drifting".

NP = 13   MODEL VALUE = -0.50000D-02

STARTING VALUE = -0.40000D-02 + OR - 0.10000D-02
FILTERED VALUE = -0.45826D-02 + OR - 0.29637D-03
IDENTIFIED WITHIN 8.35% OF THE MODEL VALUE

NP = 14   MODEL VALUE = -0.24200D-02

STARTING VALUE = -0.19400D-02 + OR - 0.48000D-03
FILTERED VALUE = -0.24102D-02 + OR - 0.73163D-04
IDENTIFIED WITHIN 0.40% OF THE MODEL VALUE

NP = 21   MODEL VALUE = 0.30700D-01

STARTING VALUE = 0.24600D-01 + OR - 0.61000D-02
FILTERED VALUE = 0.30437D-01 + OR - 0.71363D-03
IDENTIFIED WITHIN 0.86% OF THE MODEL VALUE

NP = 39   MODEL VALUE = 0.13500D+01

STARTING VALUE = 0.16200D+01 + OR - 0.20000D+00
FILTERED VALUE = 0.13730D+01 + OR - 0.46808D-01
IDENTIFIED WITHIN 1.70% OF THE MODEL VALUE

NP = 38   MODEL VALUE = 0.86000D+02

STARTING VALUE = 0.68800D+02 + OR - 0.40000D+01
FILTERED VALUE = 0.86368D+02 + OR - 0.48540D+00
IDENTIFIED WITHIN 0.43% OF THE MODEL VALUE

NP = 6   MODEL VALUE = -0.28280D-01

STARTING VALUE = -0.22620D-01 + OR - 0.56000D-02
FILTERED VALUE = -0.27185D-01 + OR - 0.13469D-02
IDENTIFIED WITHIN 3.87% OF THE MODEL VALUE

NP = 7   MODEL VALUE = 0.39160D-02

STARTING VALUE = 0.31200D-02 + OR - 0.78000D-03
FILTERED VALUE = 0.38721D-02 + OR - 0.55514D-03
IDENTIFIED WITHIN 0.97% OF THE MODEL VALUE

NP = 12   MODEL VALUE = -0.10900D-01

STARTING VALUE = -0.87200D-02 + OR - 0.22000D-02
FILTERED VALUE = -0.48367D-02 + OR - 0.61227D-03
IDENTIFIED WITHIN 9.75% OF THE MODEL VALUE

Table 5.4 Continued
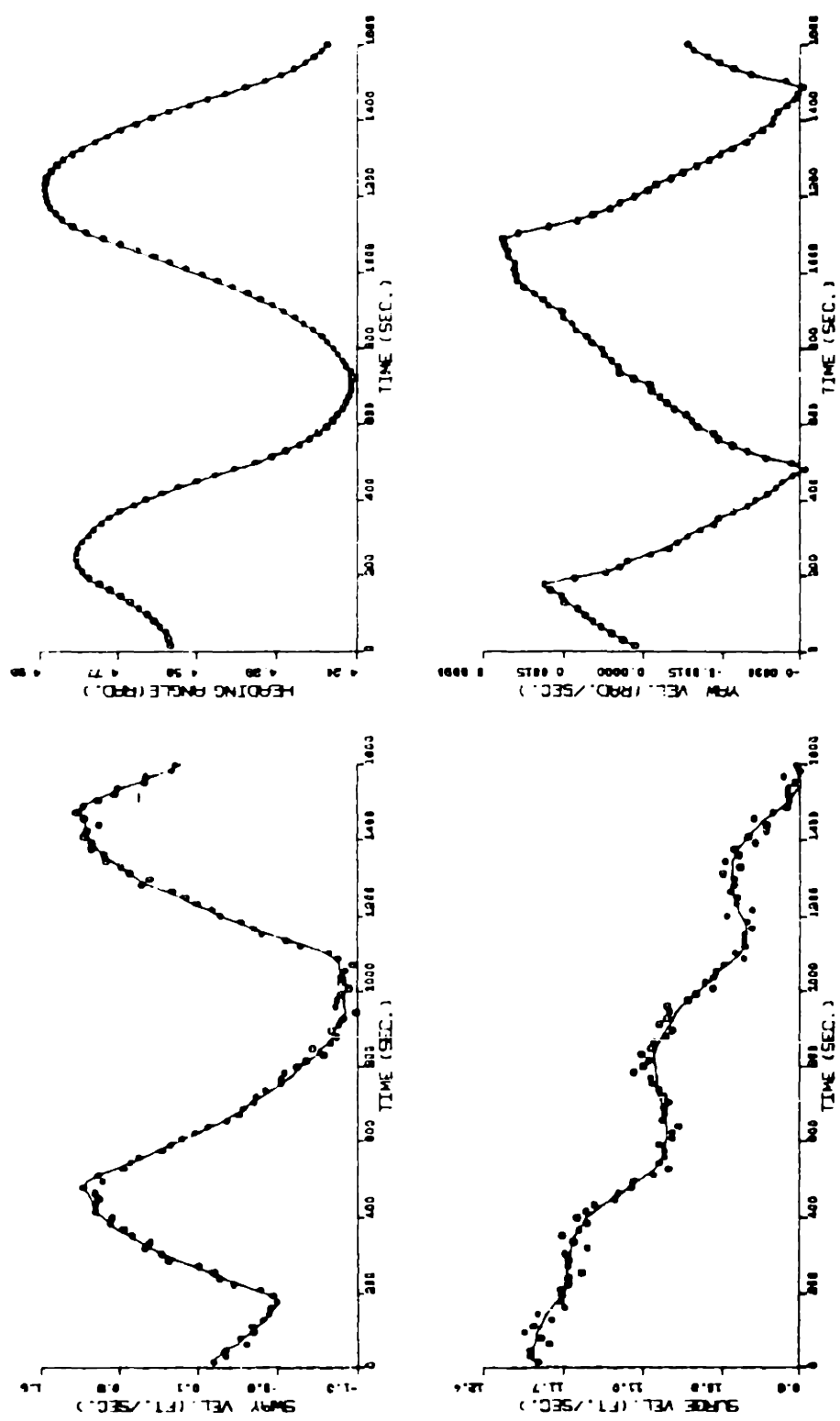
Figure 5.4.a Results of identification to illustrate the phenomenon of "simultaneous drifting" - the filtering of state measurements.
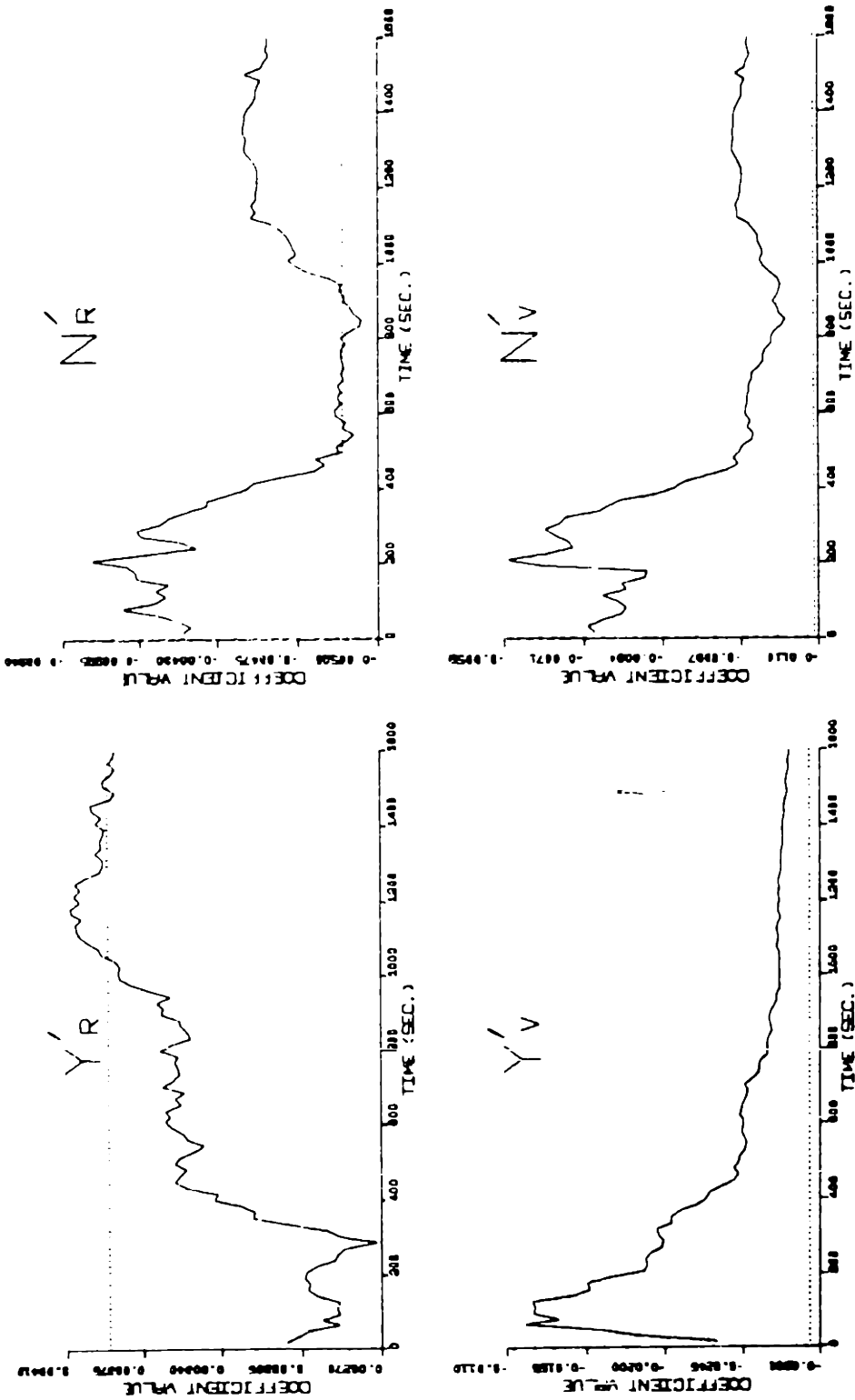
Figure 5.4.b Results of identification to illustrate the phenomenon of "simultaneous drifting" - the estimation of coefficient
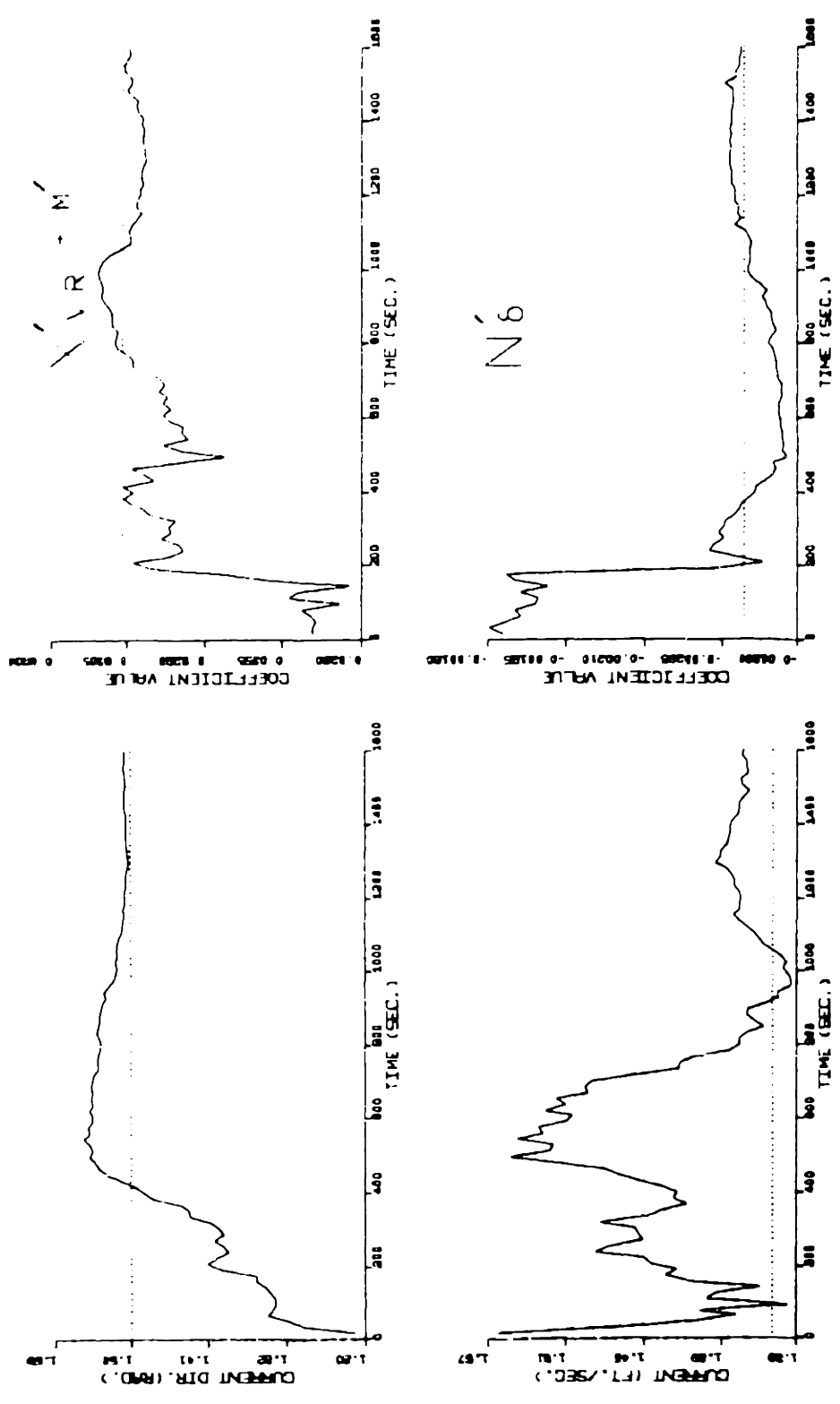
······ True value

────── Estimation

Figure 5.4.c Results of identification to illustrate the phenomenon of "simultaneous drifting" - the estimation of coefficients and current.

- 131 -

either increase or decrease together by similar percentage.

In the study by Norrbin, Åström, Byström and Källström[1977] and by Byström & Källström[1978], where a nonlinear model was used to process the 20°/20° zigzag maneuvering data, similar problem was revealed in their estimation of the values for the hydrodynamic coefficients.

Since these estimated values of different works showed consistent behavior, there must be some physical explanation. A report by Leeuwen [1972] suggested the idea of exploring this problem from the contribution of each hydrodynamic coefficient. He showed that during a turning circle maneuver, the time histories of $Y_v'v'$ and $(Y_r'-m')r'$ or $N_v'v'$ and $N_r'r'$ have behaved in the same pattern and are of the similar order of magnitude, except of opposite sign. These figures are reproduced in Fig. 5.5.

Figure 5.5 provided a clear explanation why circular turning maneuvers are not suitable for parameter estimation: the same resultant Y force and N moment can be obtained by different combinations of these hydrodynamic coefficient values. Apparently, the cancellation effect has caused the simultaneous drifting problems occurred to Lundblad[1974] when the maneuvering data of turning circle was processed. Therefore, the "simultaneous drift" shown in Fig. 5.4 strongly suggests that the cancellation effect is not a consequence of constant rudder deflection, but is more likely due to an intrinsic nature of the ship dynamics.

To confirm this speculation, a similar study to Fig. 5.5 was made on 10°/10° zigzag, 20°/20° zigzag and biased zigzag maneuver to investigate the contribution of these hydrodynamic coefficients in each case.

coeff. Y'....	rvv	vvvu	rrr	au	δrr	rvvu	vrδ	rrru	vδδ	δvv	δδ	vδδu	δδδ	δδu	δδδu
maximum contribution	10.5	9.1	8.9	7.3	-6.4	5.0	5.2	5.0	-3.9	-3.6	3.1	1.2	1.2	-1.0	- 4

coeff. N'....	rvvu	vrr	rrru	δrr	vrδ	vrru	δvv	vvv	vδδ	δδ	δδδ	vvvu	δδu	vδδu	δδδu
maximum contribution	-5.1	-3.7	-3.3	3.1	-2.9	-2.1	1.3	1.1	1.0	-.9	-.7	.6	.3	-.3	.2
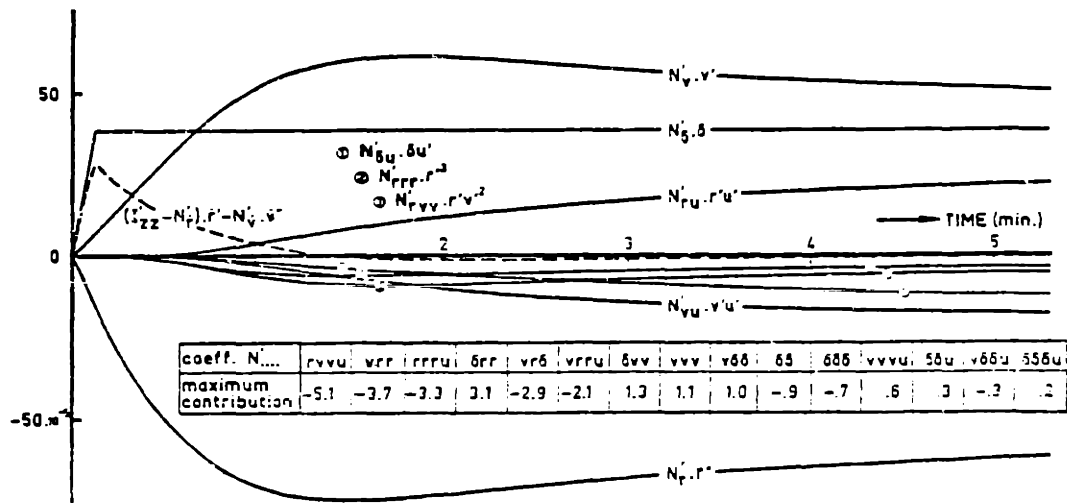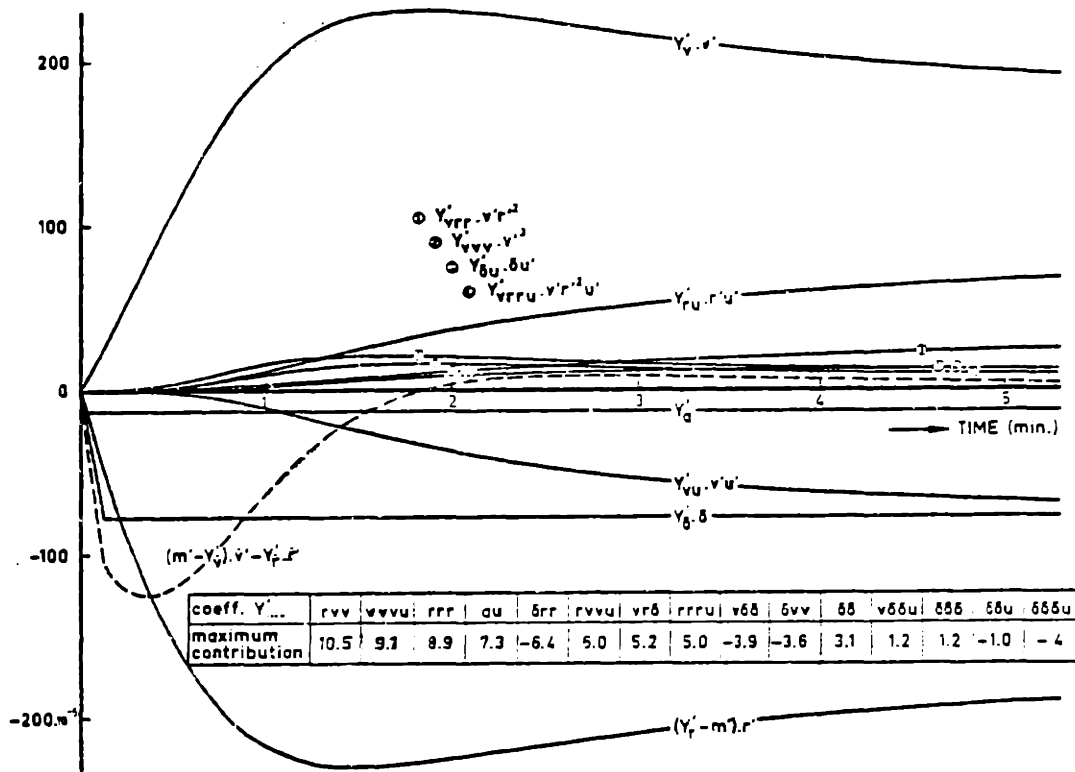
Figure 5.5   Time histories of separate terms of force and moment equation during a 19° rudder turning circle, rpm=100, u_0=8m/sec. (Ref. Leeuwen[1972]).

- 133 -

(see Fig. 5.6, Fig. 5.7 and Fig. 5.8). Again, the model testing values of hydrodynamic coefficients are used to do the simulation for convenience.

It is surprising to find that the cancellation effect does not discriminate between the maneuver of constant rudder deflection and the maneuver of continuous rudder execution at all. This accounts for the resulting simultaneous drift when zigzag maneuvering data is processed.

Once it was believed that the idea of "parallel processing", which will be discussed in Chap. 6, can be applied to eliminate this trouble-some simultaneous drift. Because the contributions of each hydrodynamic coefficient is of different pattern for different maneuvers, it was taken for granted that when two data files are processed together to estimate the same set of coefficients, the chance of simultaneous drift should be small. Unforturnately, when the parallel processing technique was applied, simultaneous drift still occurred. This is a further confirmation of the existance of the cancellation effect.

Realizing that the cancellation effect causes the simultaneous drift, it is required to explain why the contributions tend to cancel with each others. The slender body theory in hydrodynamics is probably the handiest tool to tackle this problem. A detail discussion on this theory is referred to the book by Newman[1977]. Following the sign convention in Fig. 2.1, the hydrodynamic sway force and yaw moment upon a ship in maneuvers are:

$$Y = -\dot{v}m_{22}^S + \dot{r}m_{26}^S - uvm_{22}(x_T) - urx_Tm_{22}(x_T) + m_Tu^2\delta \qquad (5.3.1)$$
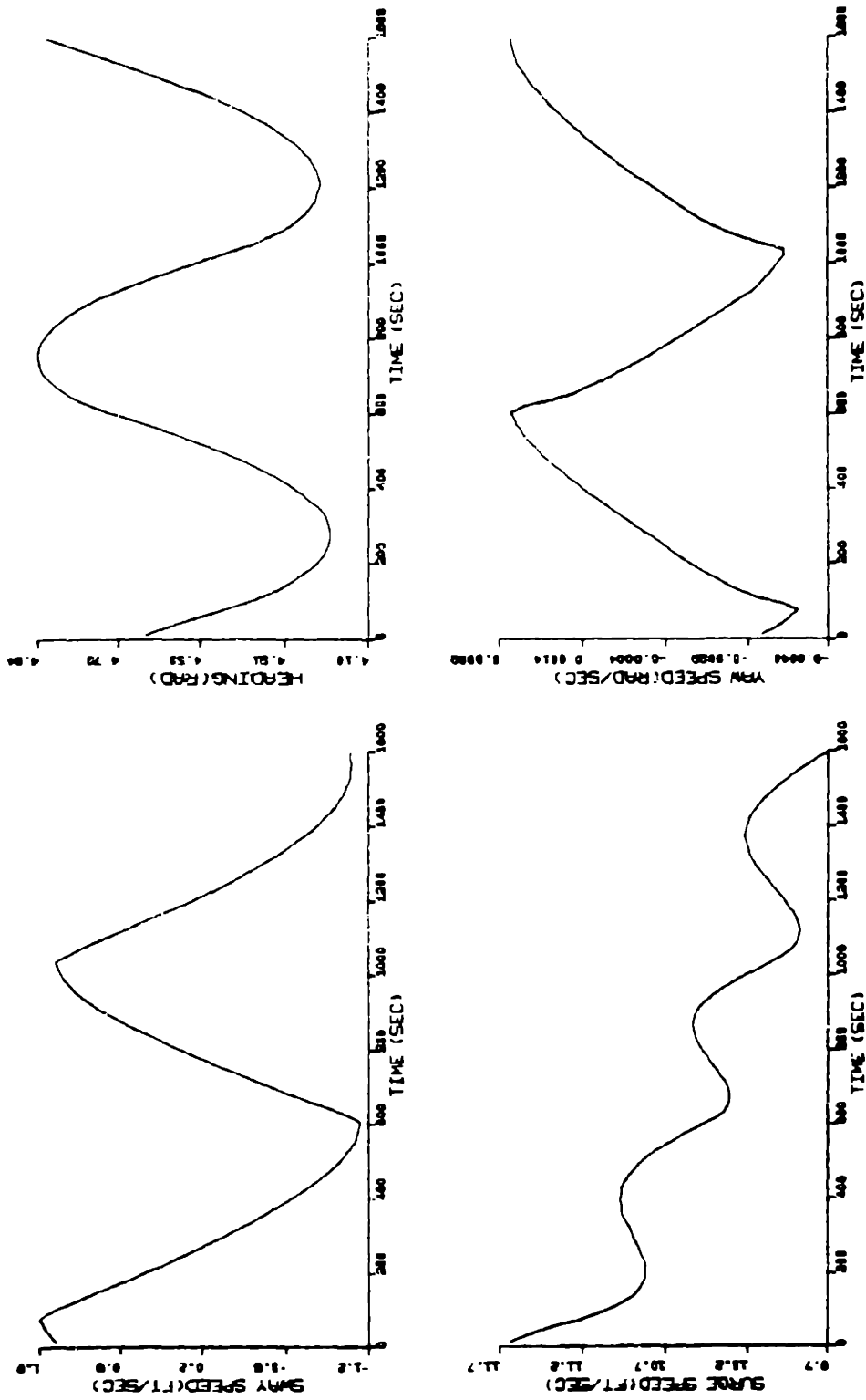
Figure 5.6.a   Simulated 10°/10° zigzag maneuver for ESSO OSAKA at rps=0.690
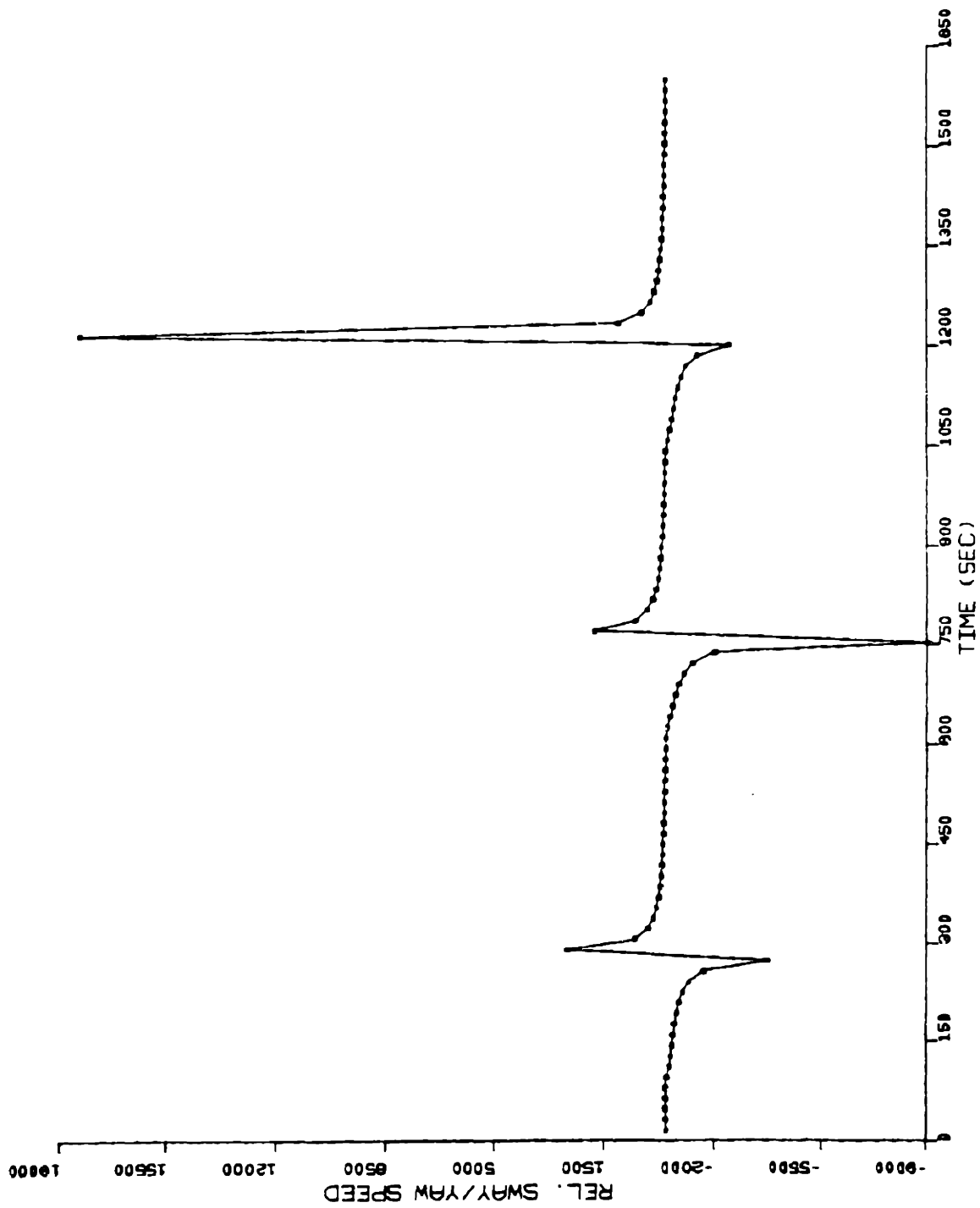
Figure 5.6.b Position of the instantaneous pivot point during the 10°/10° zigzag
maneuver in Fig. 5.6.a. Ship length=1066.27 ft.
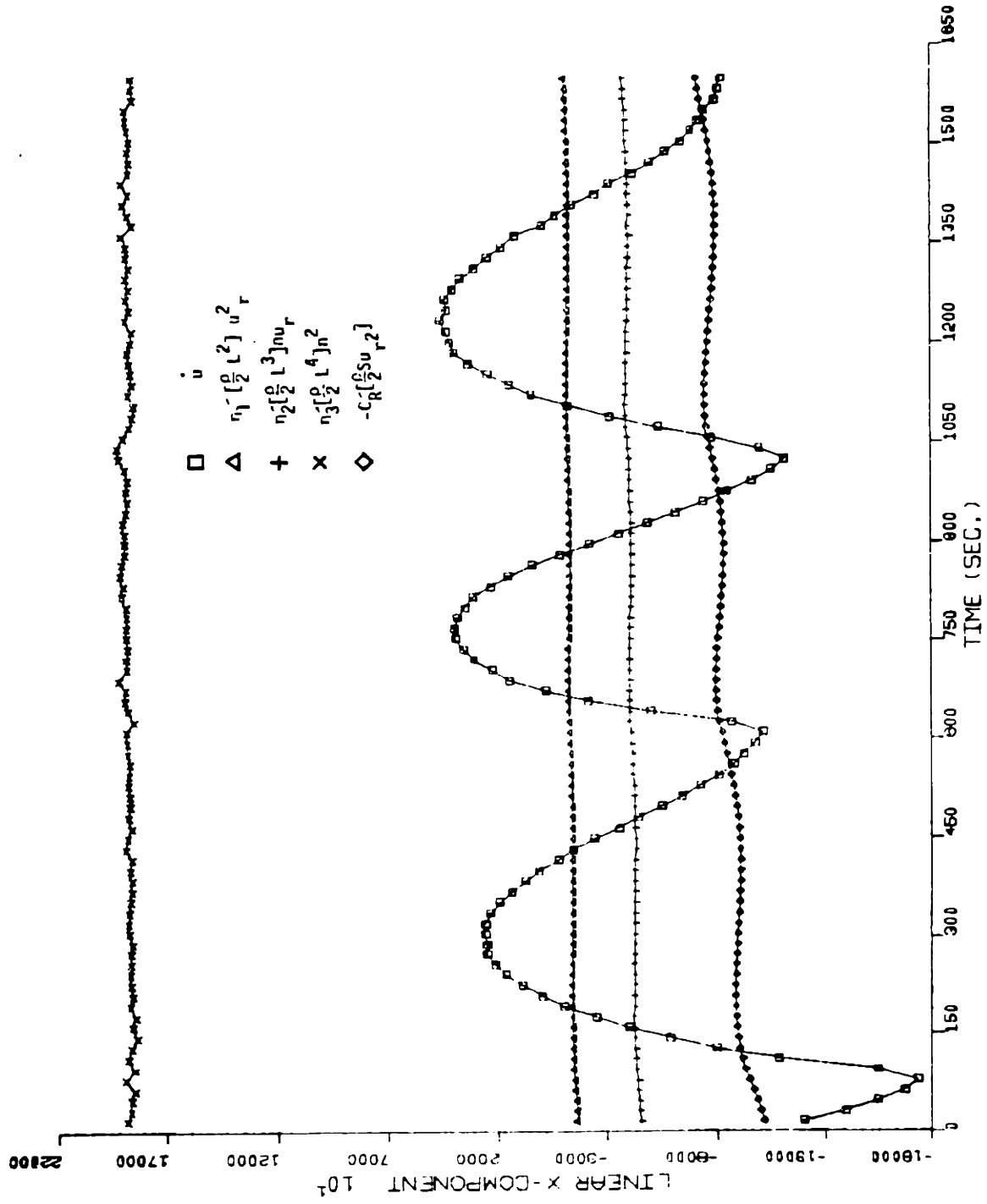
Figure 5.6.c Time histories of linear terms of X-force in Eq. (2.5.22) during the 10°/10° zigzag maneuver in Fig. 5.6.a.

- 137 -
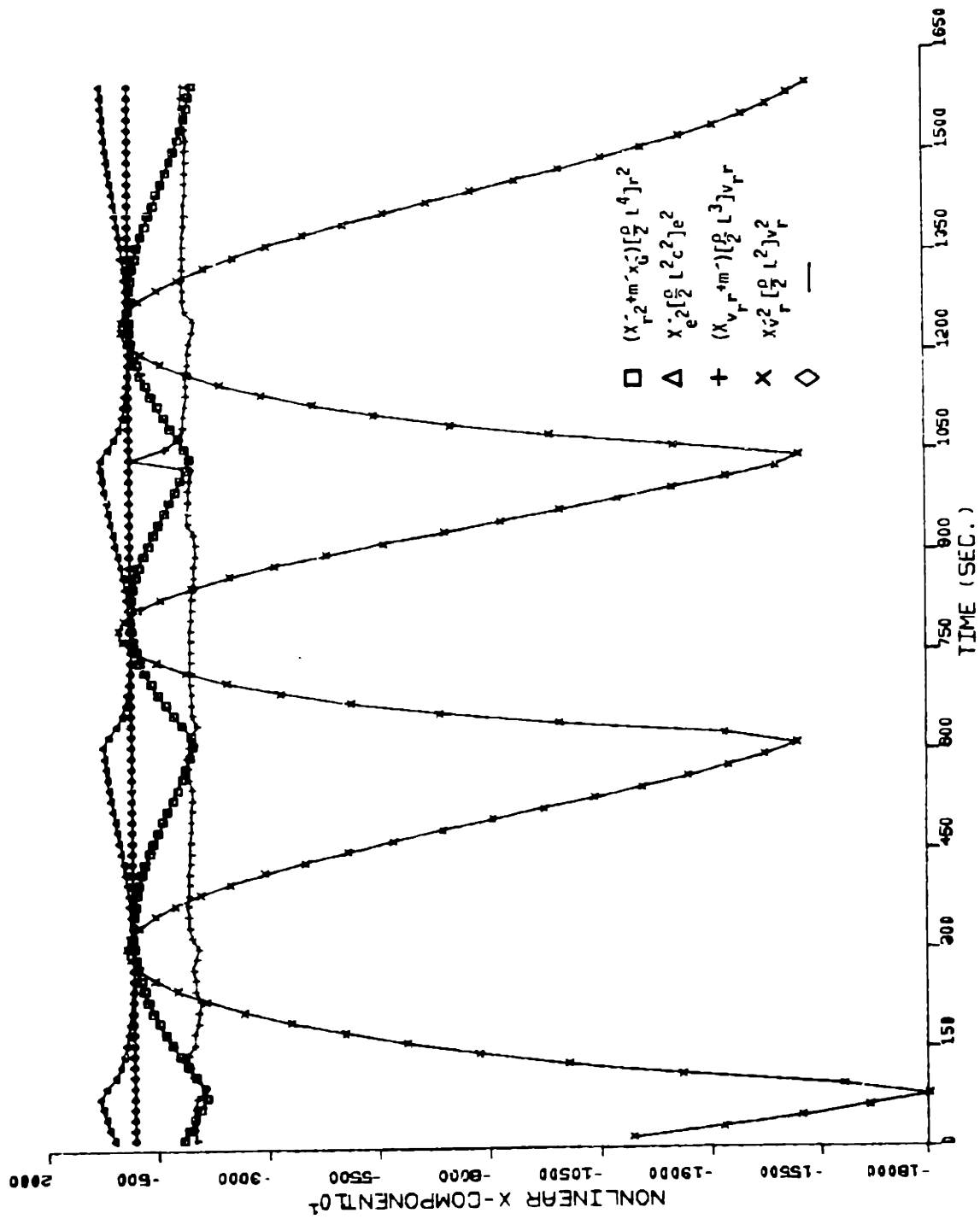
Figure 5.6.d Time histories of nonlinear terms of X-force in Eq. (2.5.22) during the 10°/10° zigzag maneuver in Fig. 5.6.a.
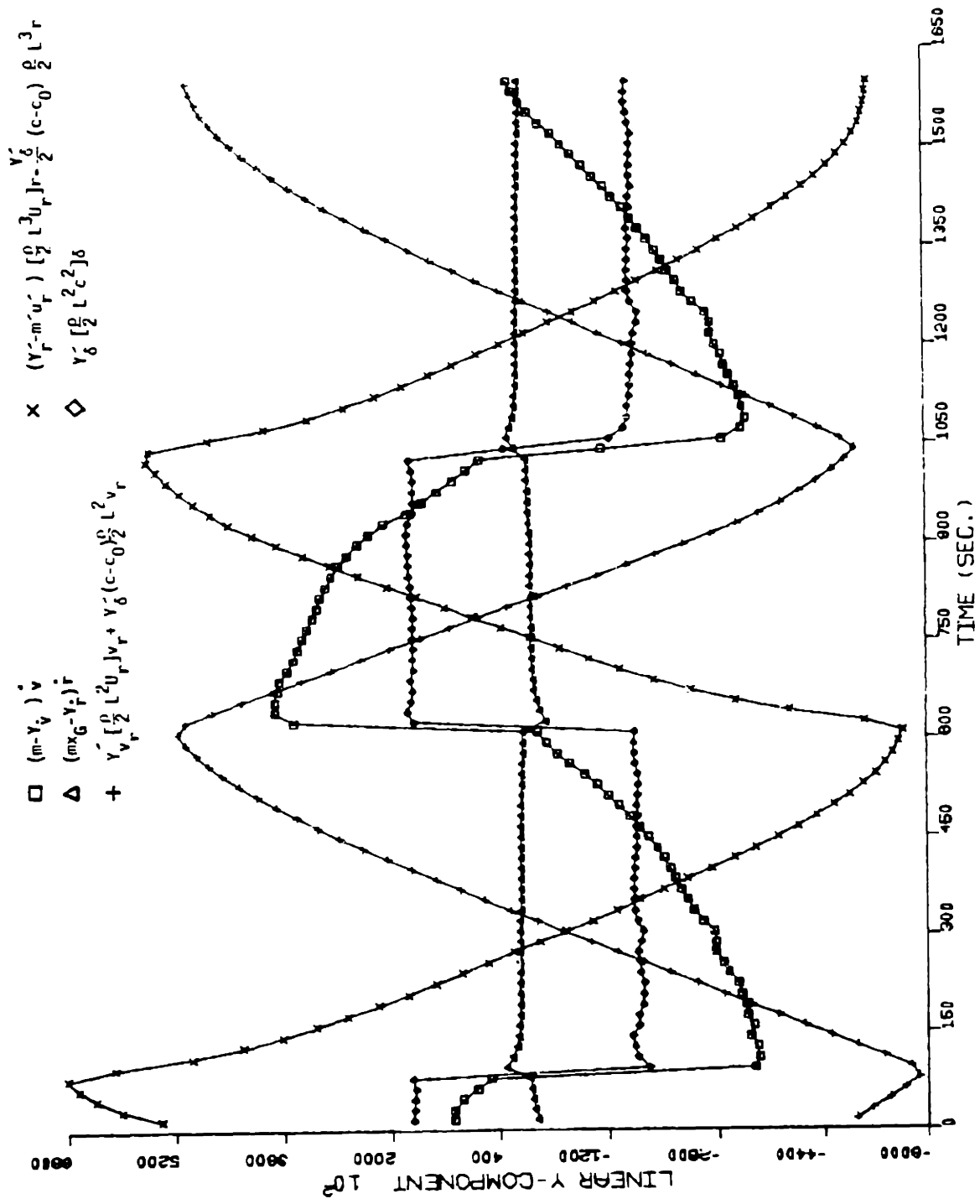
Figure 5.6.e Time histories of linear terms of Y-force in Eq. (2.5.22) during the 10°/10° zigzag maneuver in Fig. 5.6.a.
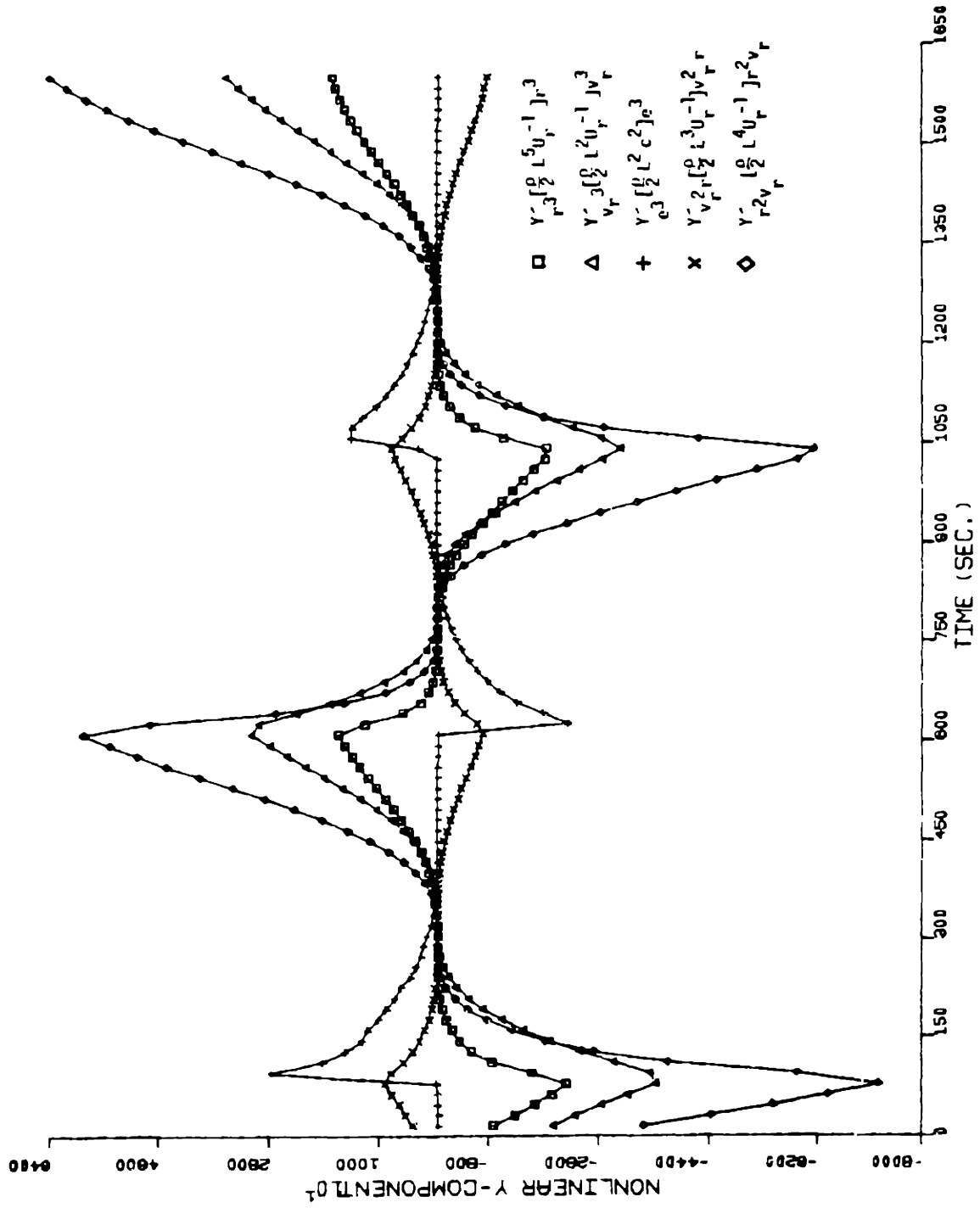
Figure 5.6.f Time histories of nonlinear terms of Y-force in Eq. (2.5.22) during the 10°/10° zigzag maneuver in Fig. 5.6.a.
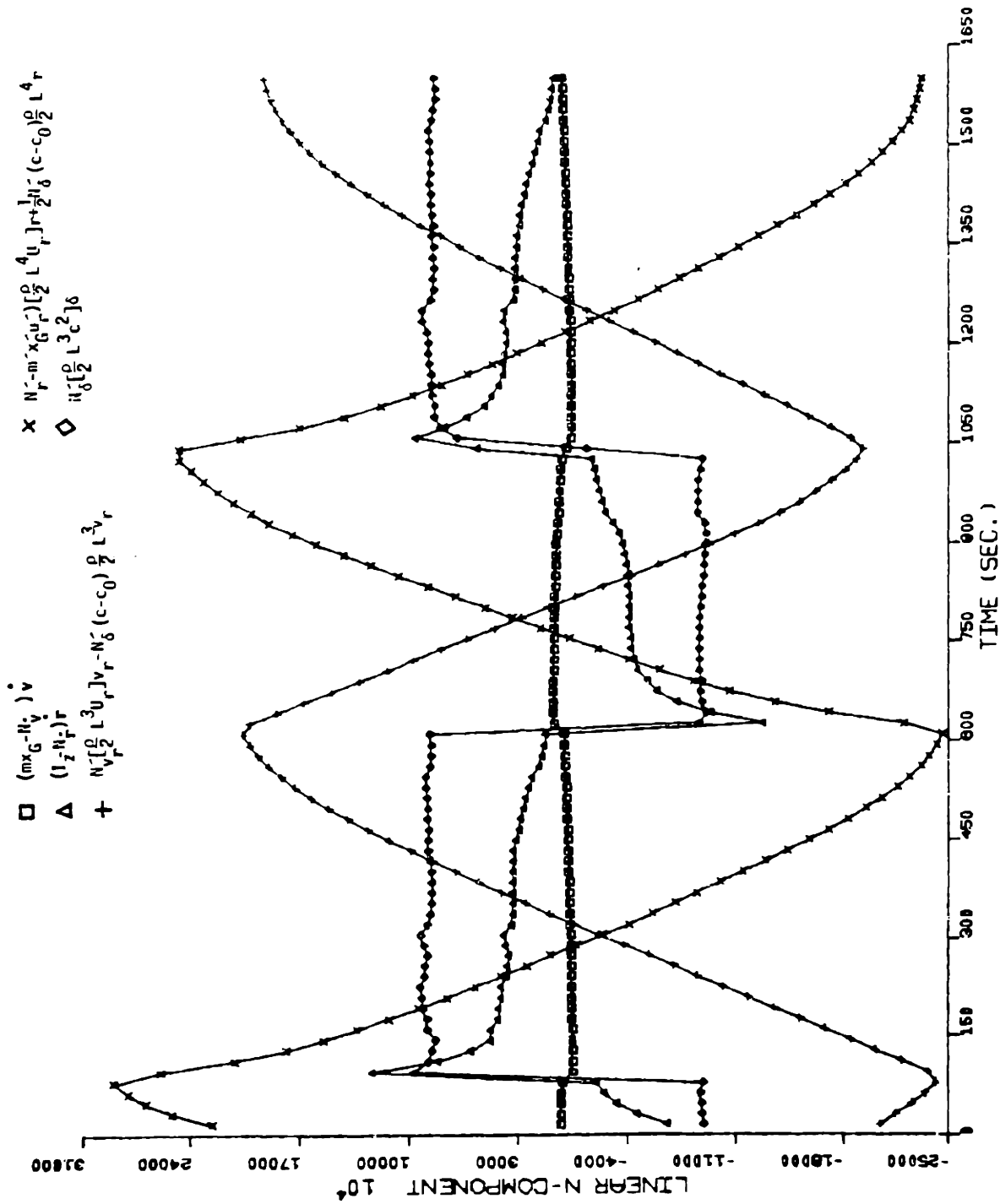
Figure 5.6.g Time histories of linear terms of N-moment in Eq. (2.5.22) during
the 10°/10° zigzag maneuver in Fig. 5.6.a.
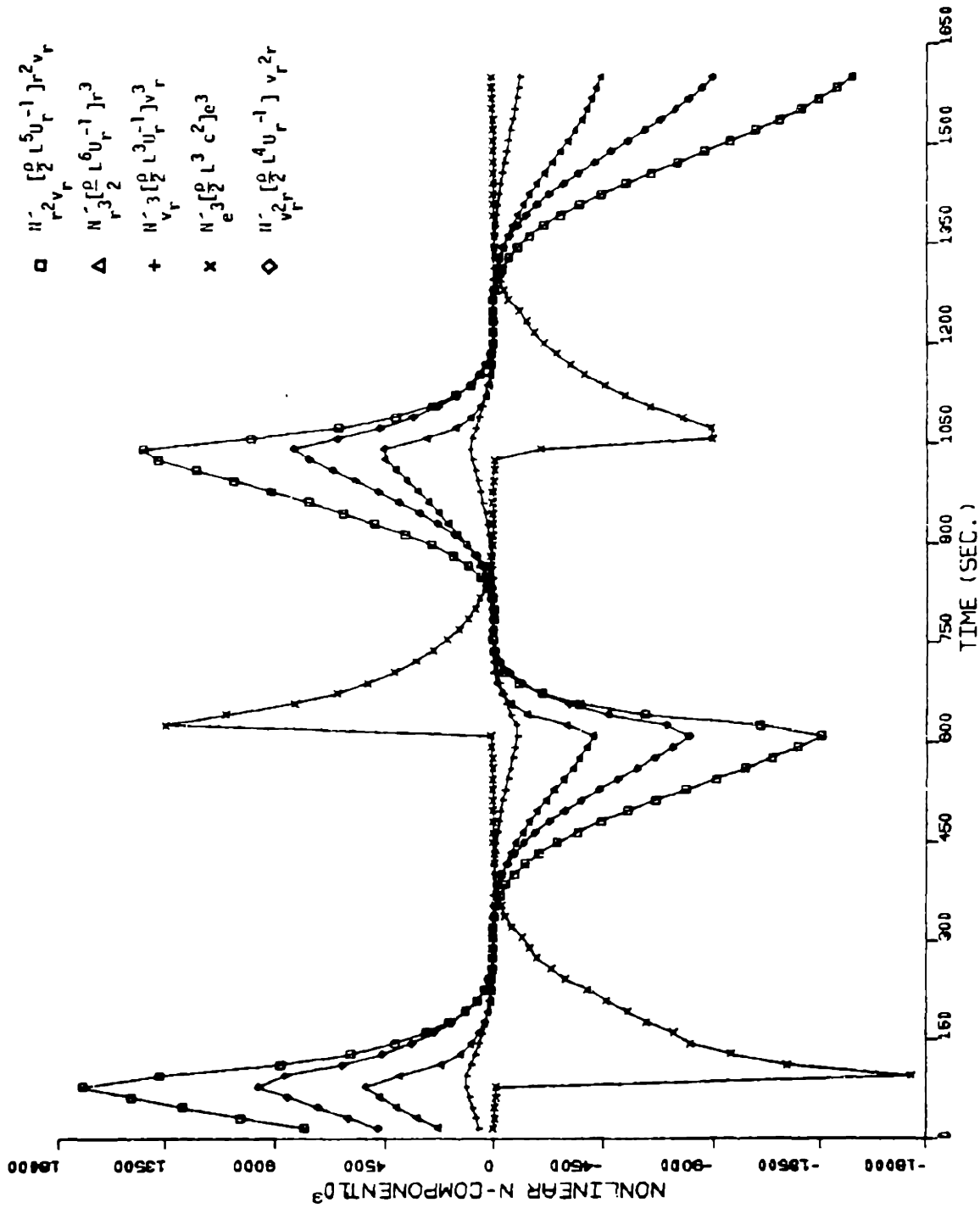
Figure 5.6.h Time histories of nonlinear terms of N-moment in Eq. (2.5.22) during the 10°/10° zigzag maneuver in Fig. 5.6.a.
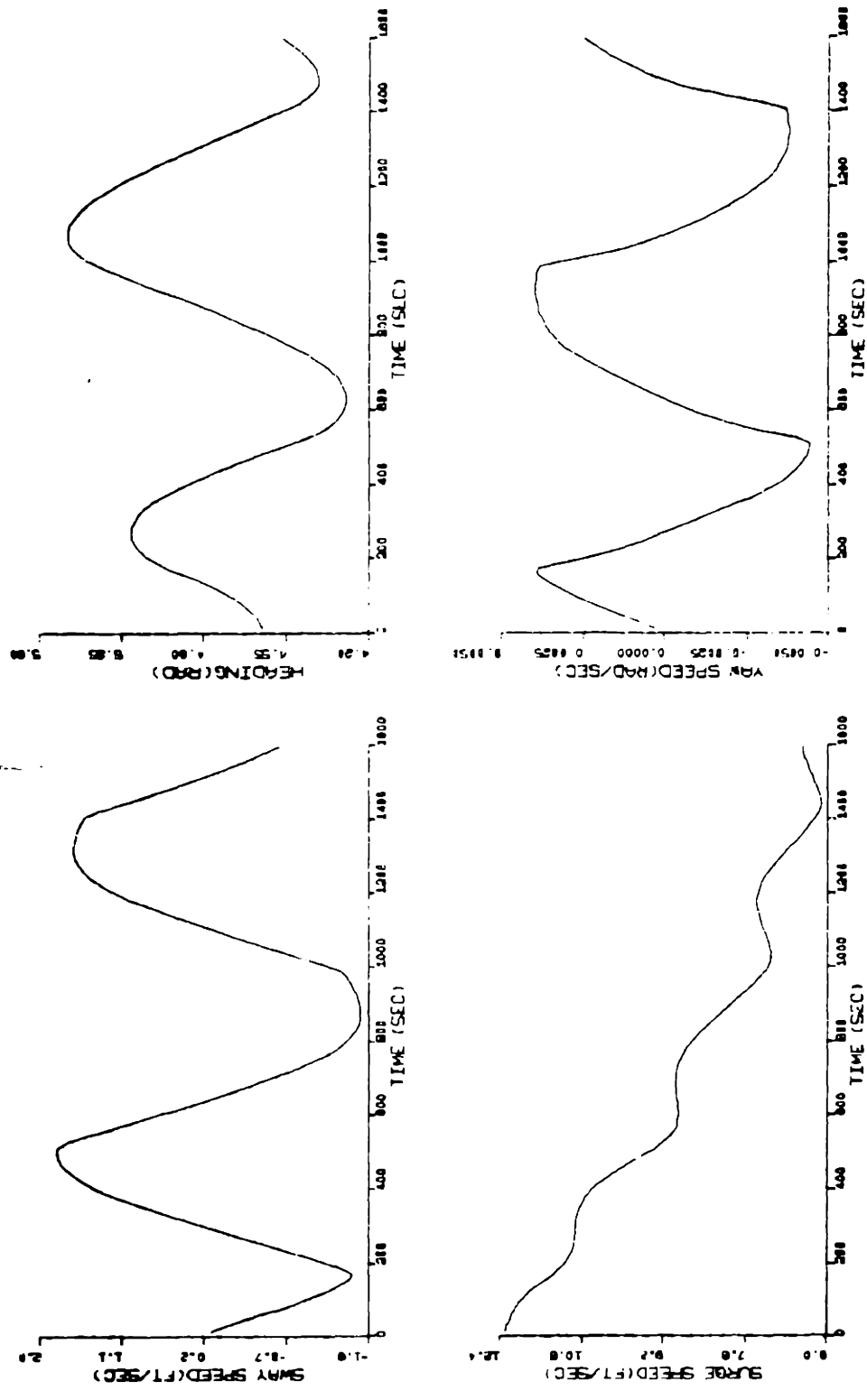
Figure 5.7.a   Simulated 20°/20° zigzag maneuver for ESSO OSAKA at rps=0.675
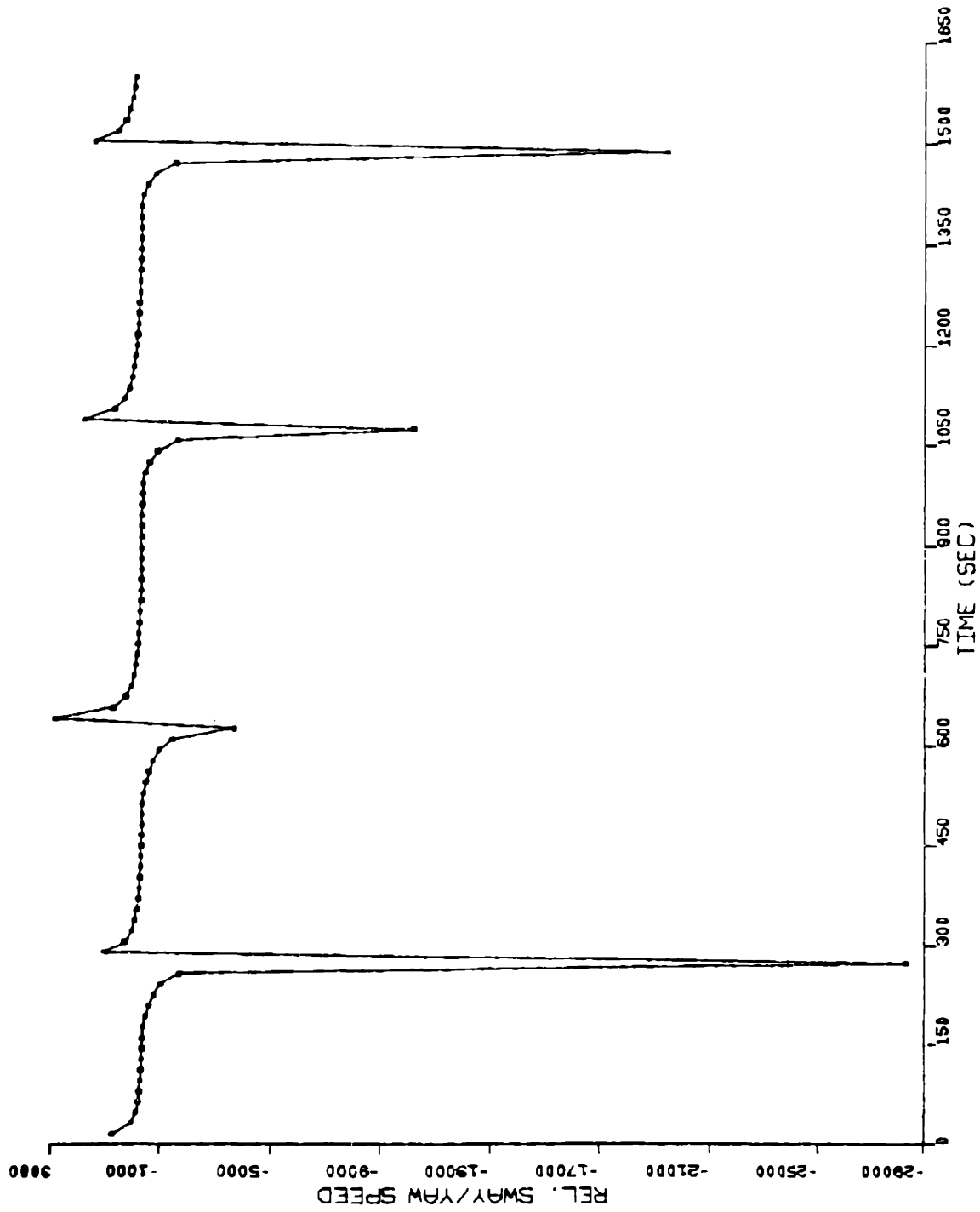
Figure 5.7.b   Position of the instantaneous pivot point during the 20°/20° zigzag
maneuver in Fig. 5.7.a.   Ship length=1066.27 ft.
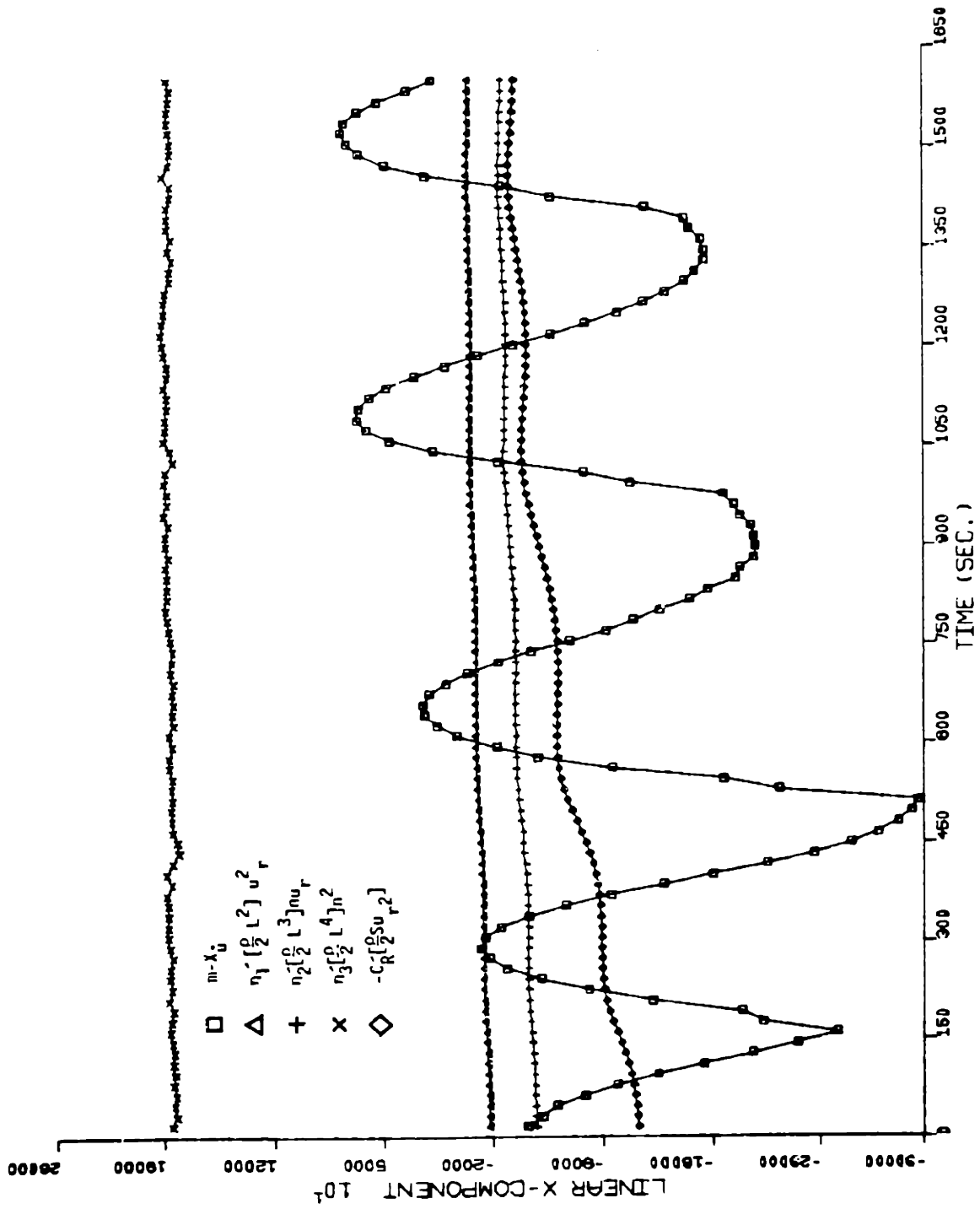
Figure 5.7.c Time histories of linear terms of X-force in Eq. (2.5.22) during the 20°/20° zigzag maneuver in Fig. 5.7.a.

- 145 -
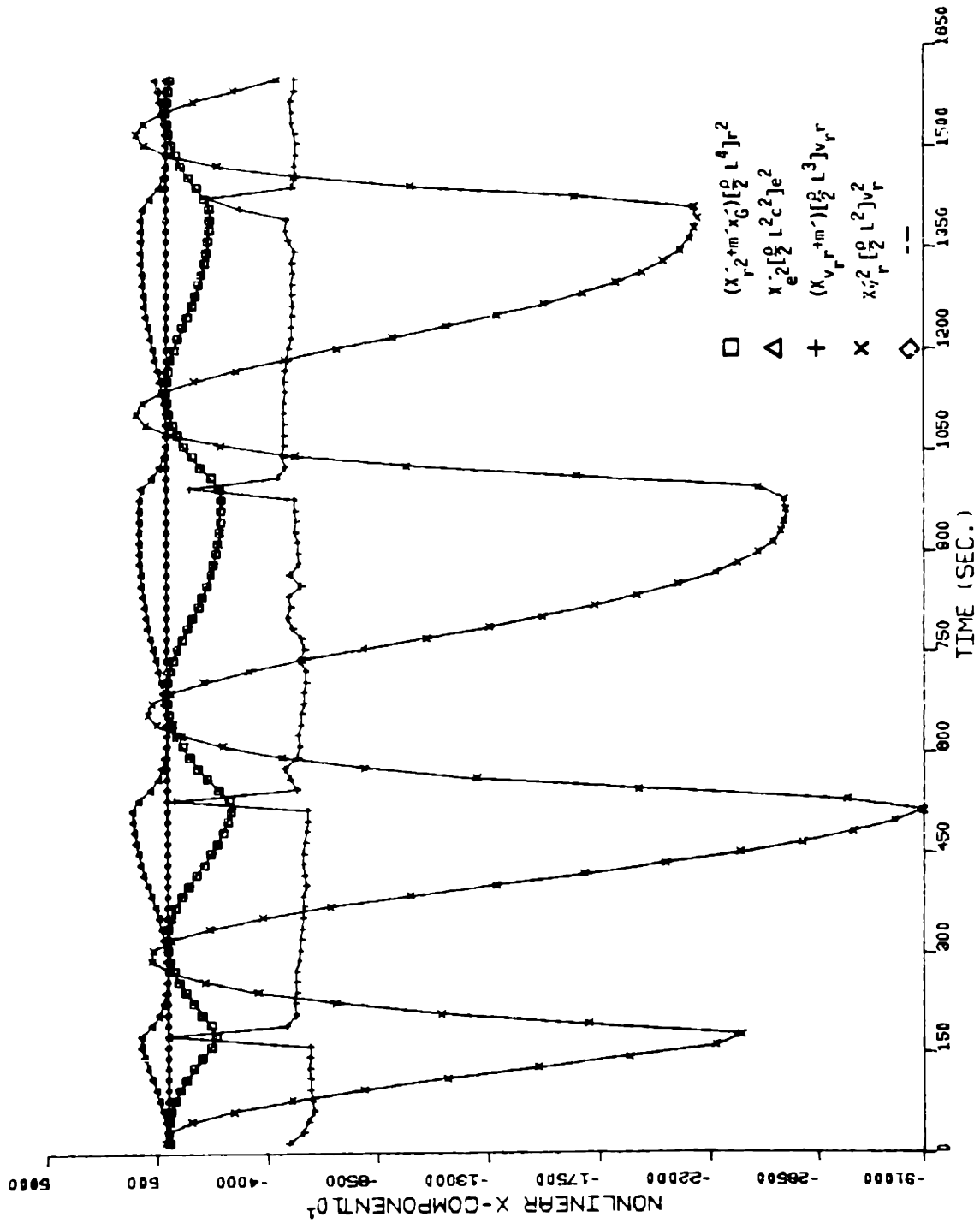
Figure 5.7.d   Time histories of nonlinear terms of X-force in Eq. (2.5.22) during the 20°/20° zigzag maneuver in Fig. 5.7.a.
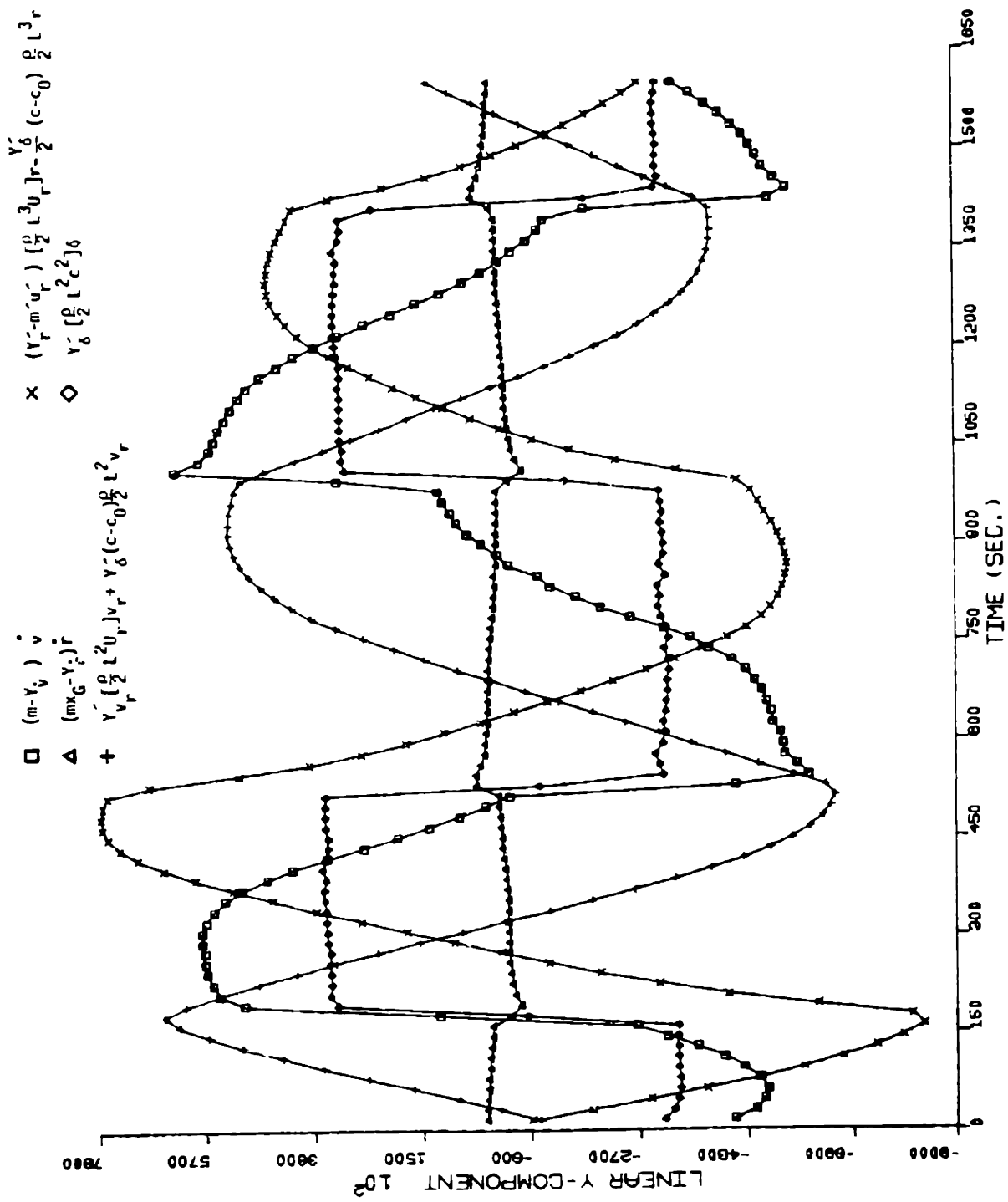
Figure 5.7.e Time histories of linear terms of Y-force in Eq. (2.5.22) during the 20°/20° zigzag maneuver in Fig. 5.7.a.

- 147 -
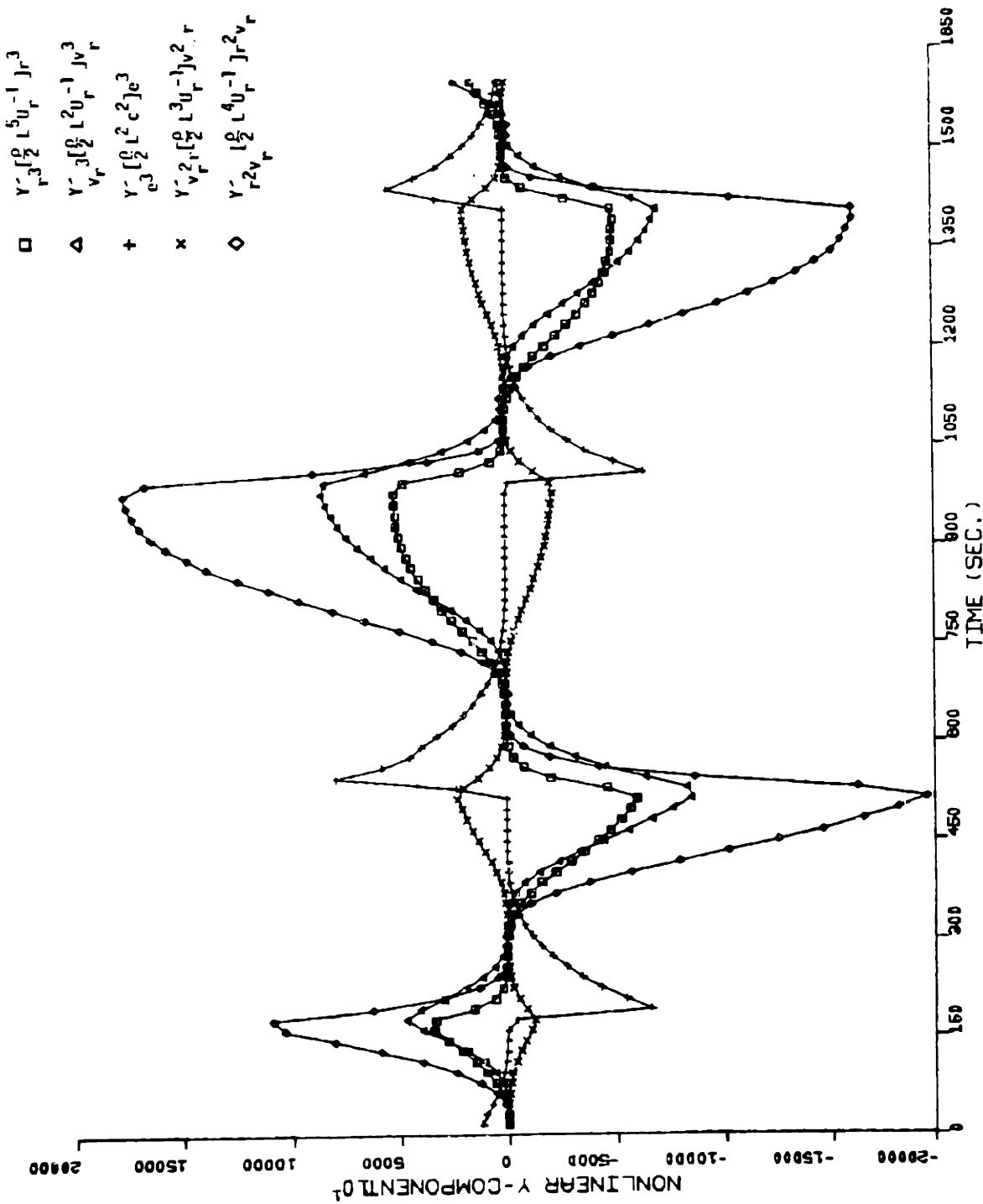
Figure 5.7.f Time histories of nonlinear terms of Y-force in Eq. (2.5.22) during the 20°/20° zigzag maneuver in Fig. 5.7.a.

- 148 -
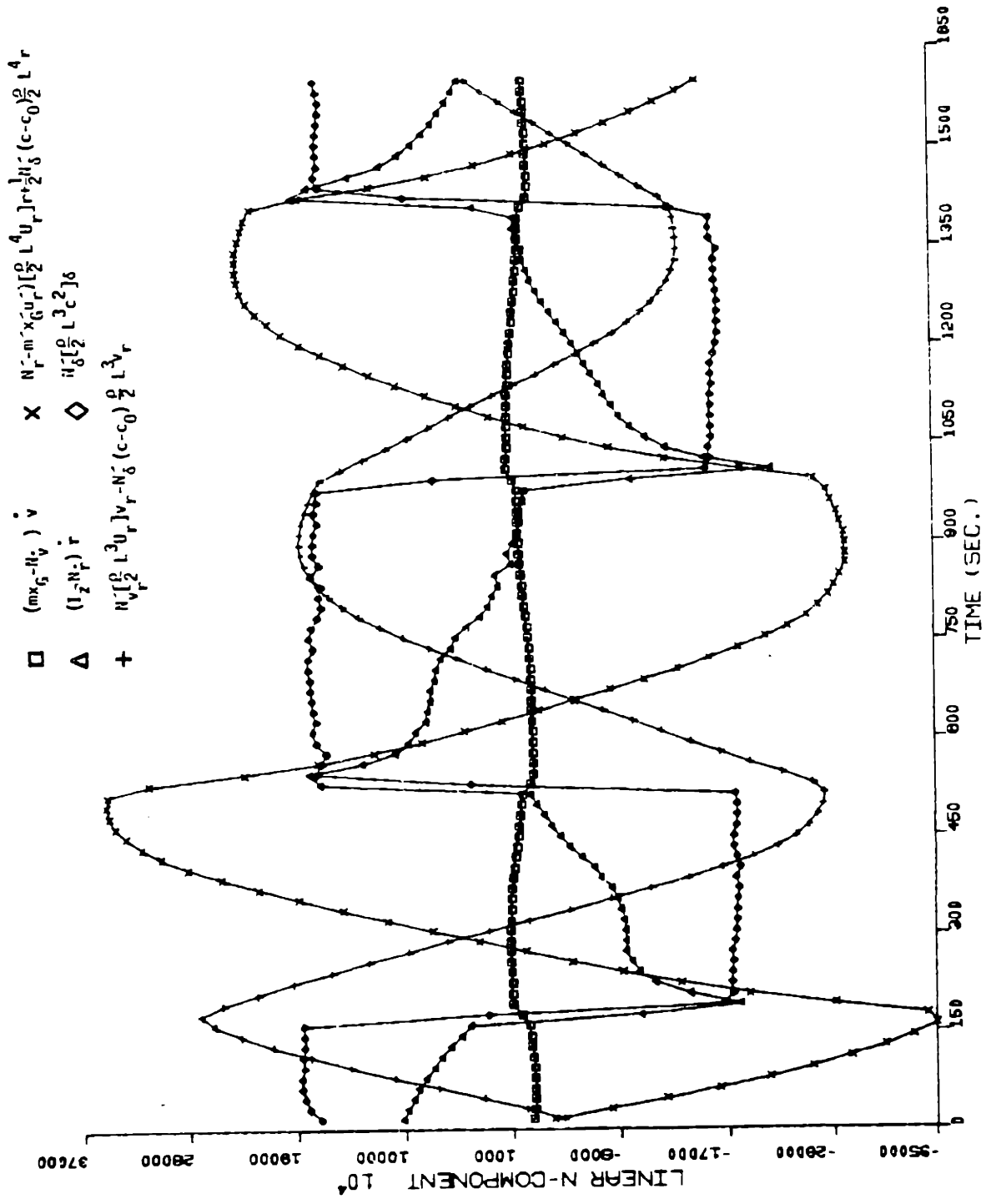
Figure 5.7.g   Time histories of linear terms of N-moment in Eq. (2.5.22) during 20°/20° zigzag maneuver in Fig. 5.7.a.
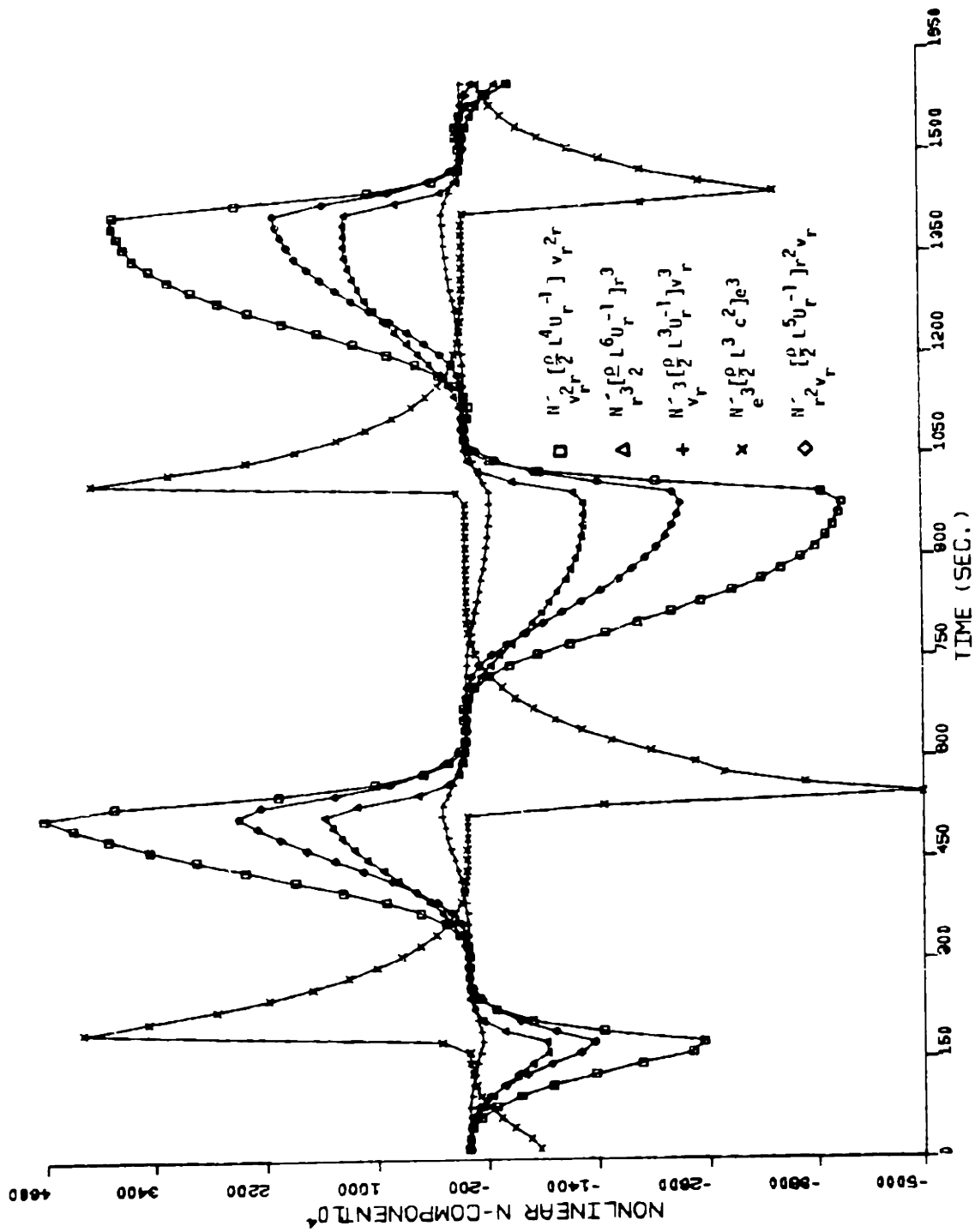
Figure 5.7.h Time histories of nonlinear terms of N-moment in Eq. (2.5.22) during the 20°/20° zigzag maneuver in Fig. 5.7.a.

- 150 -
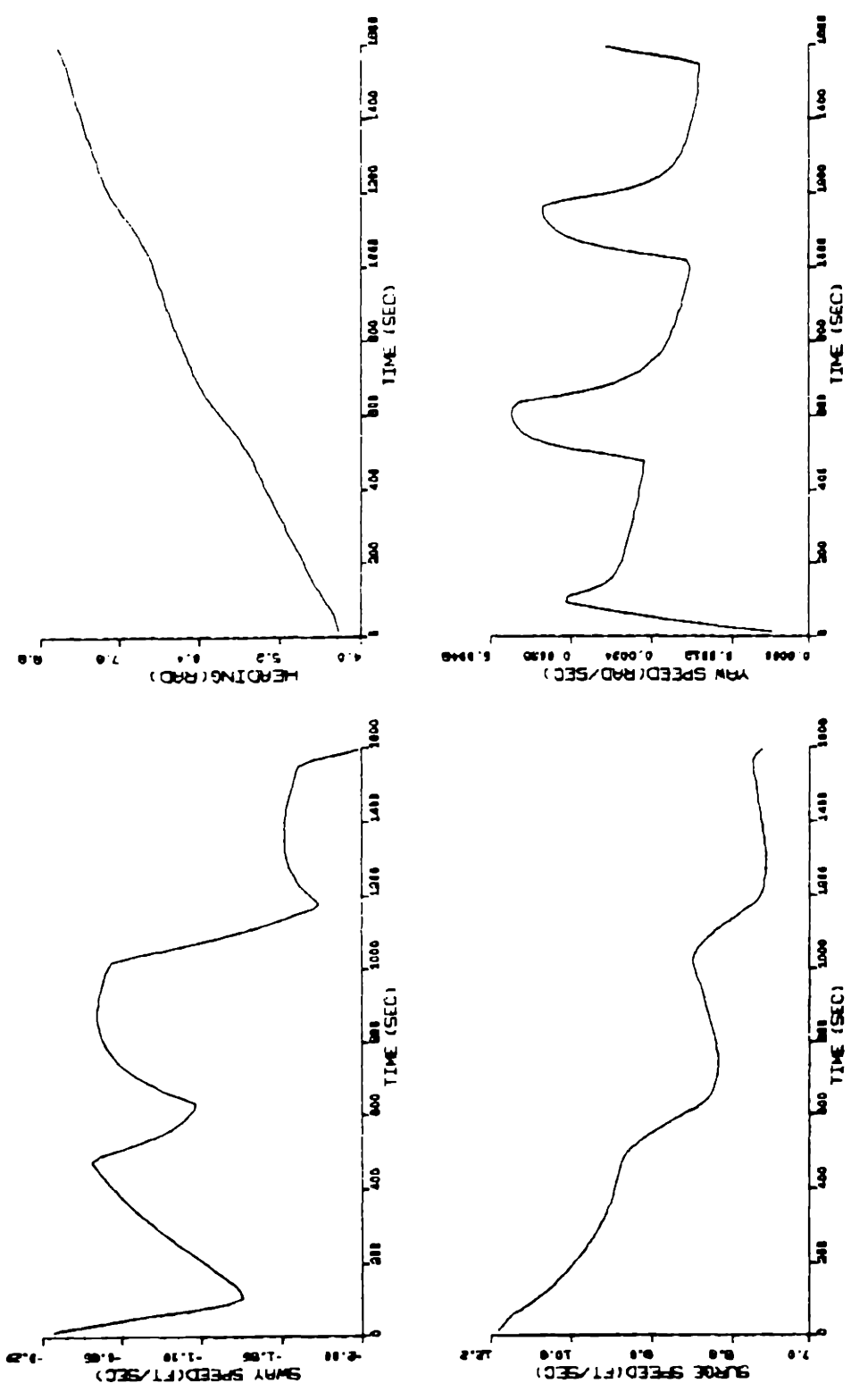
Figure 5.8.a   Simulated biased zigzag(15°±10°) maneuver for ESSO OSAKA at rps=0.673
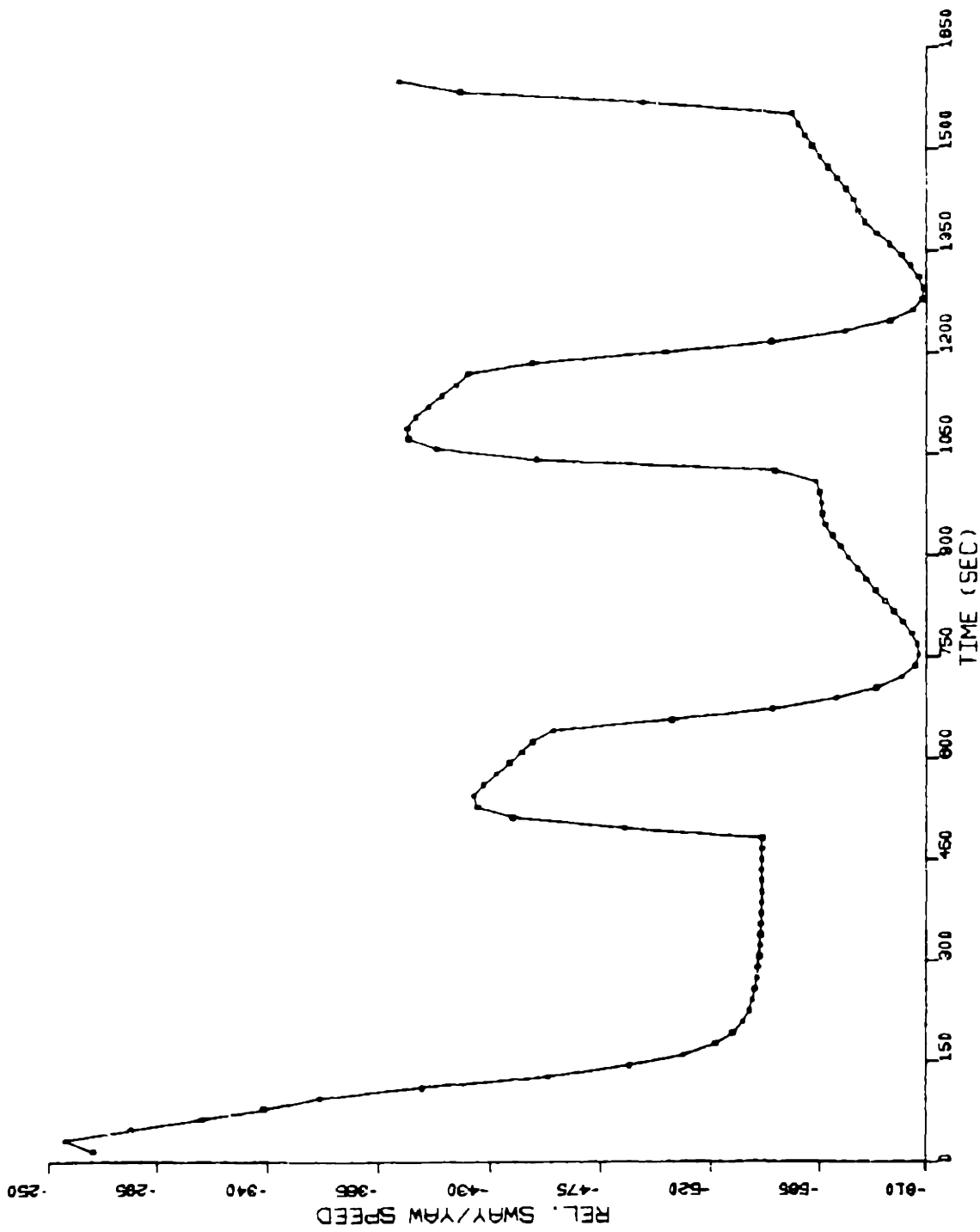
Figure 5.8.b Position of the instantaneous pivot point during the biased zigzag maneuver in Fig. 5.8.a. Ship length=1066.27 ft.

- 152 -
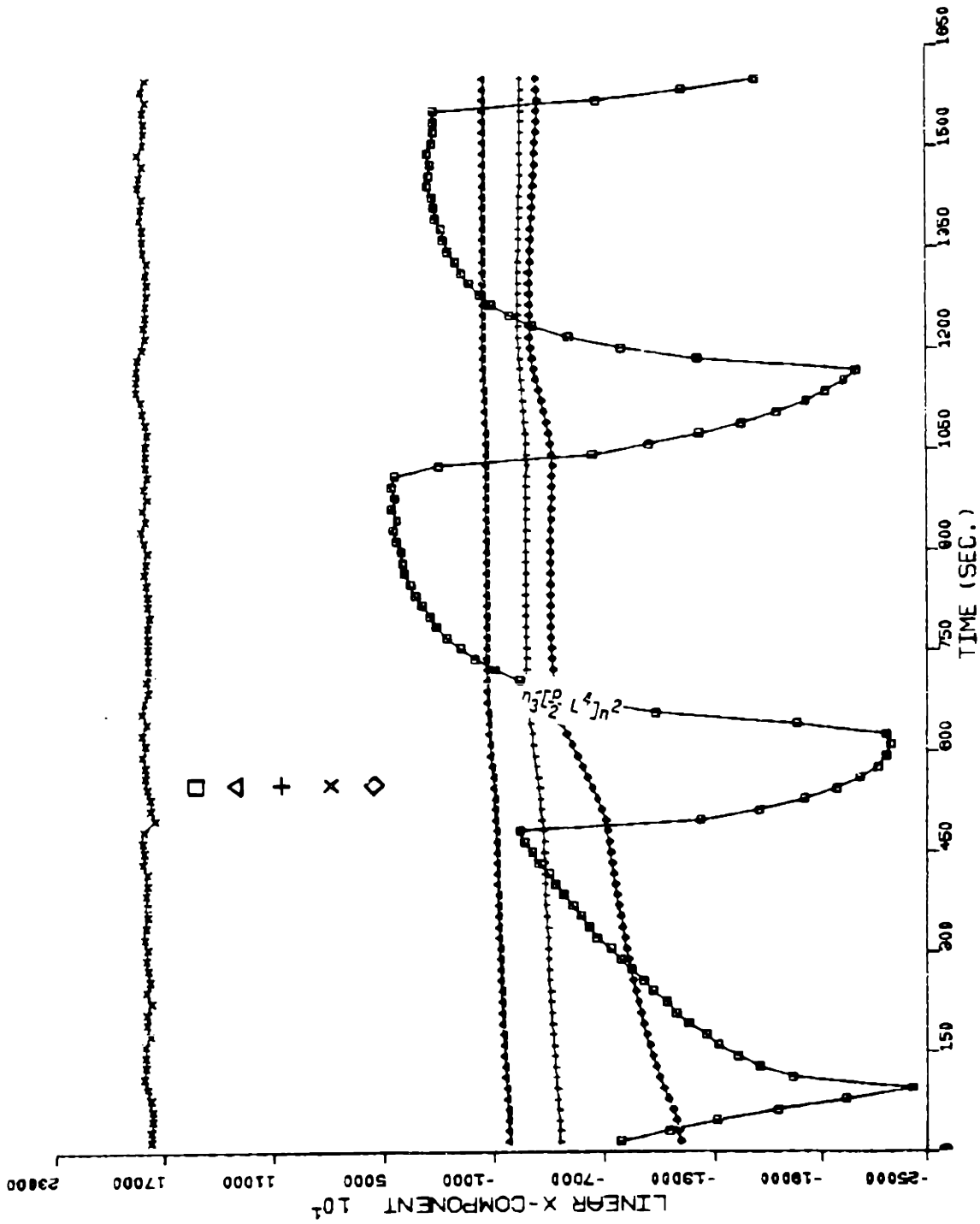
Figure 5.8.c   Time histories of linear terms of X-force in Eq. (2.5.22) during the biased zigzag maneuver in Fig. 5.8.a.
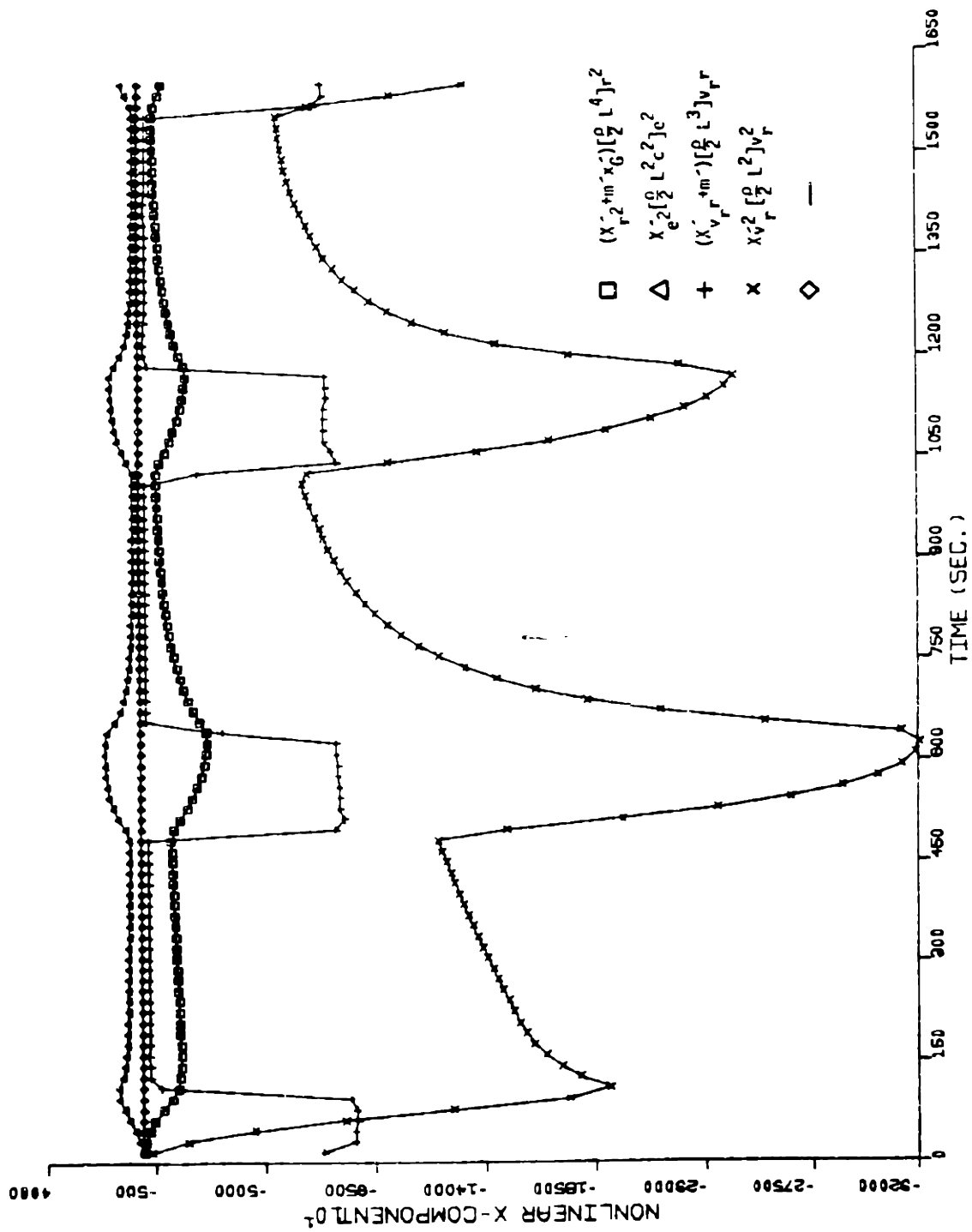
Figure 5.8.d   Time histories of nonlinear terms of X-force in Eq. (2.5.22) during the biased zigzag maneuver in Fig. 5.8.a.
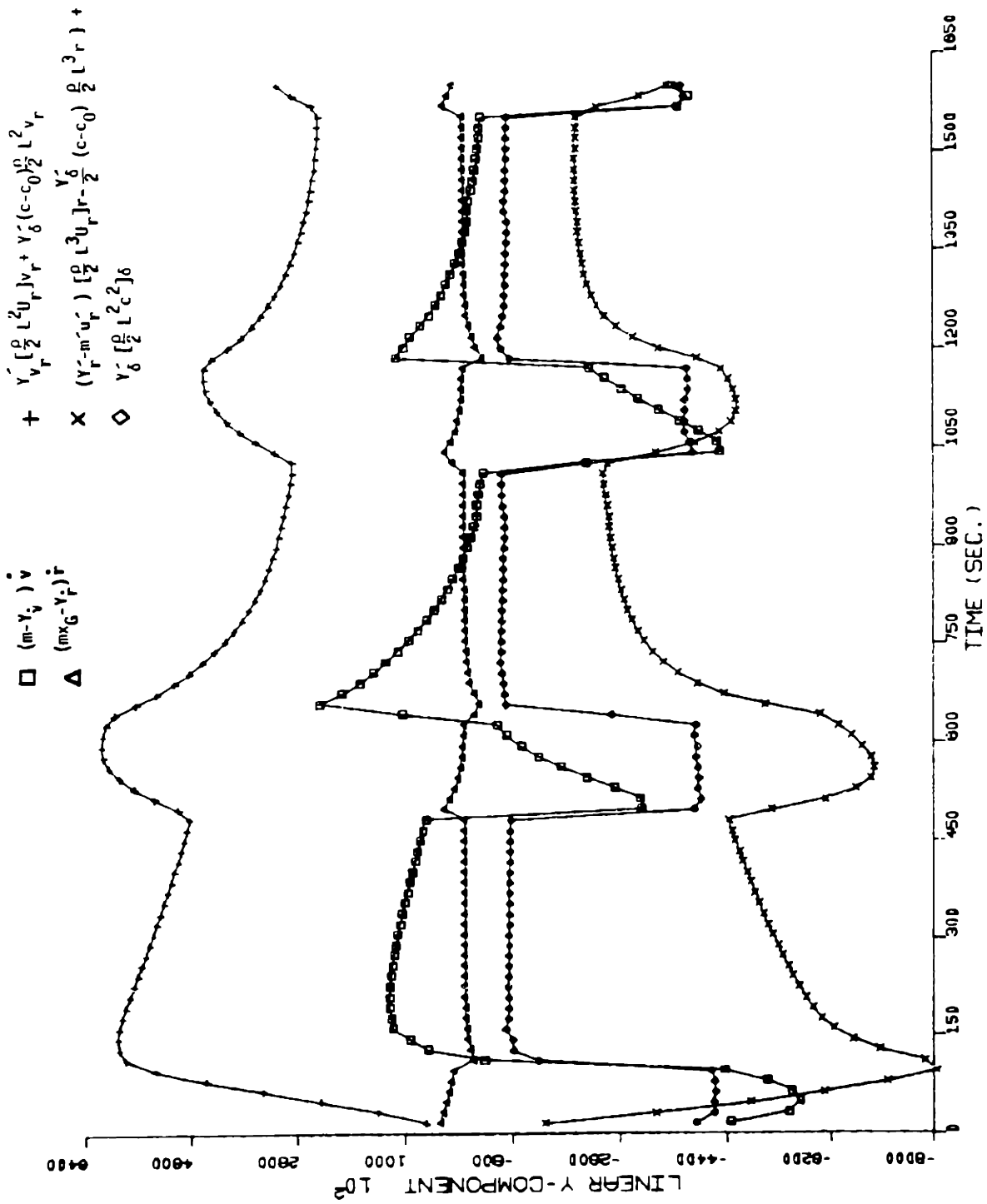
Figure 5.8.e Time histories of linear terms of Y-force in Eq. (2.5.22) during the biased zigzag maneuver in Fig. 5.8.a.

- 155 -
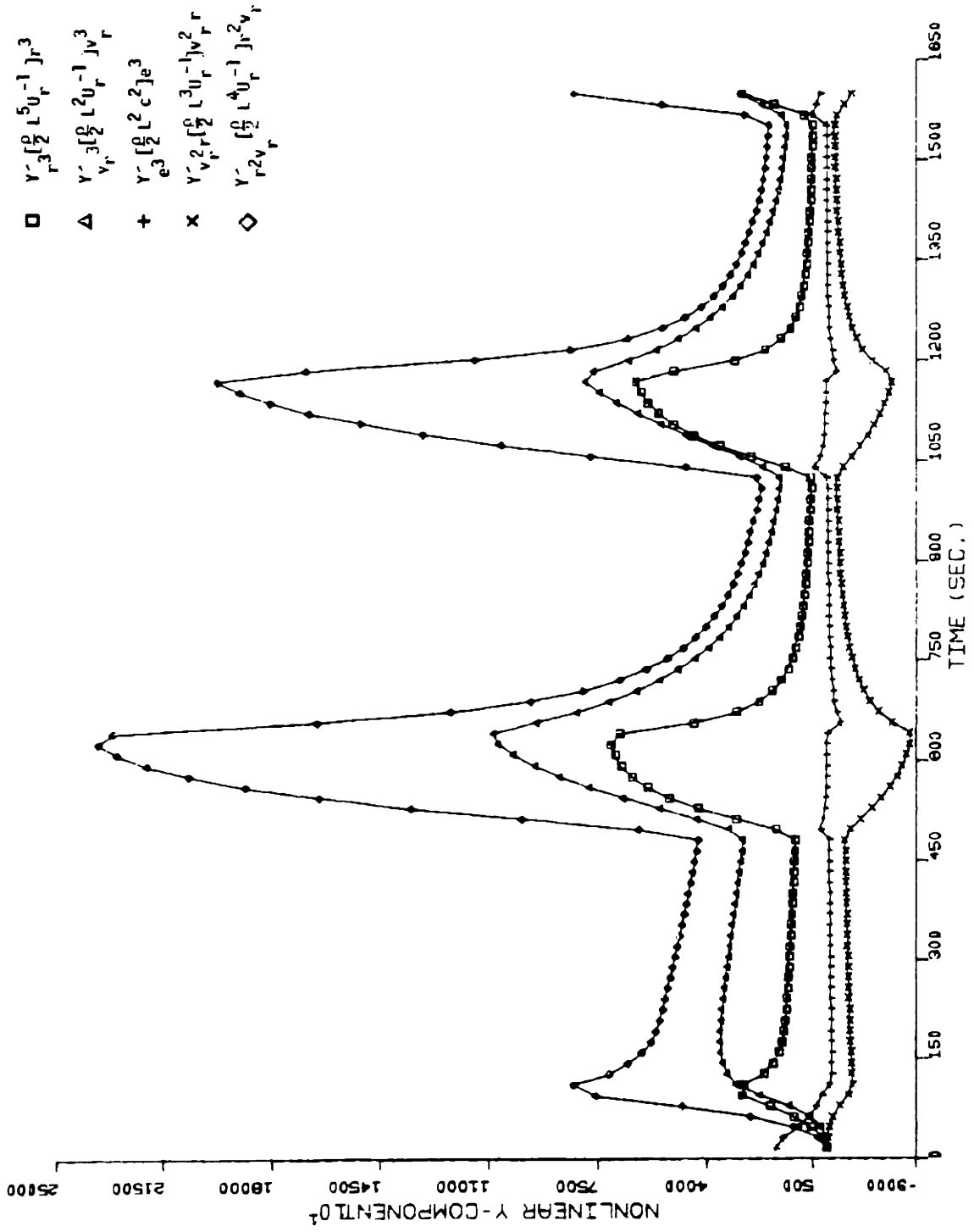
Figure 5.8.f Time histories of nonlinear terms of Y-force in Eq. (2.5.22) during the biased zigzag maneuver in Fig. 5.8.a.
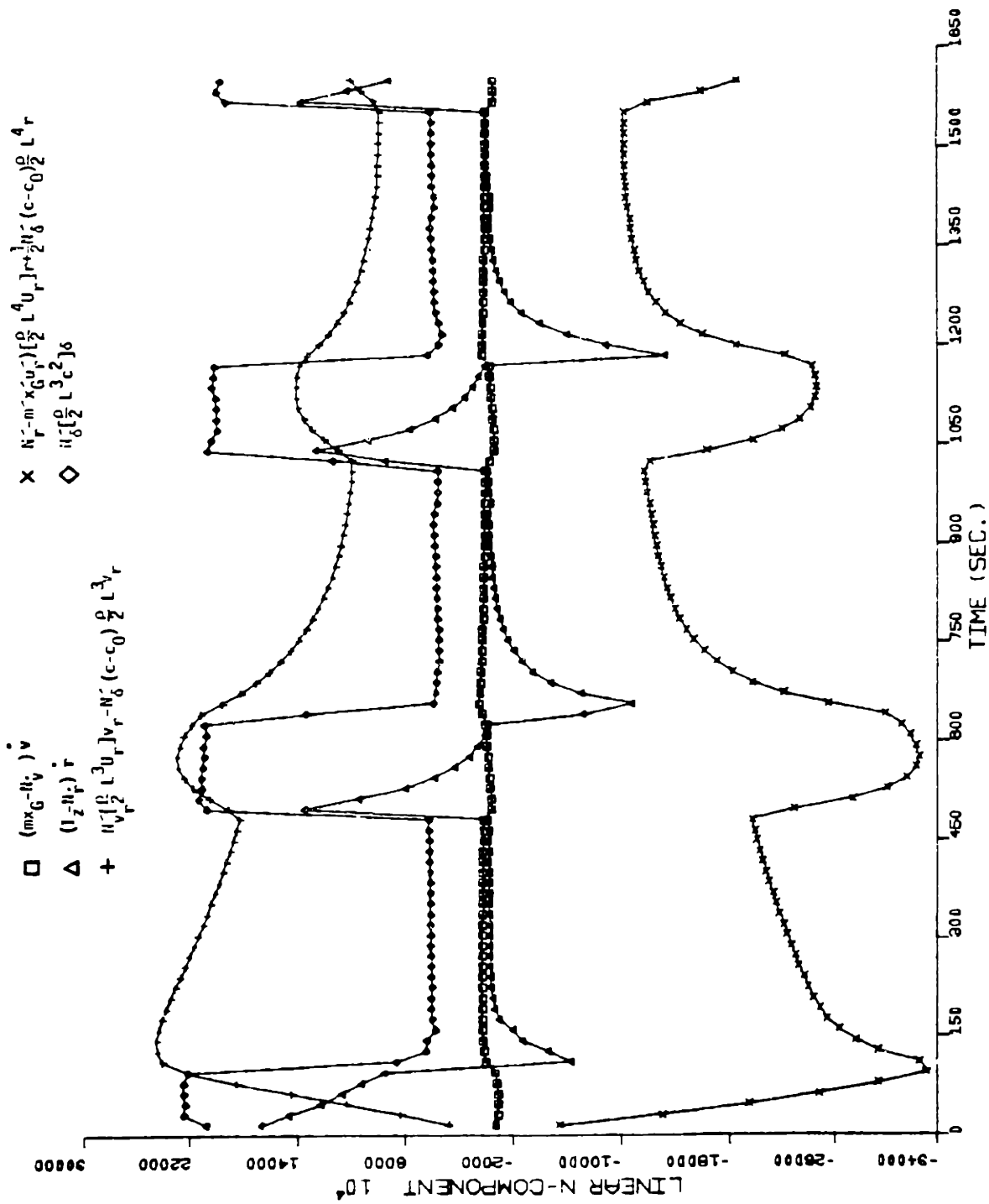
Figure 5.8.g Time histories of linear terms of N-moment in Eq. (2.5.22) during the biased zigzag maneuver in Fig. 5.8.a.
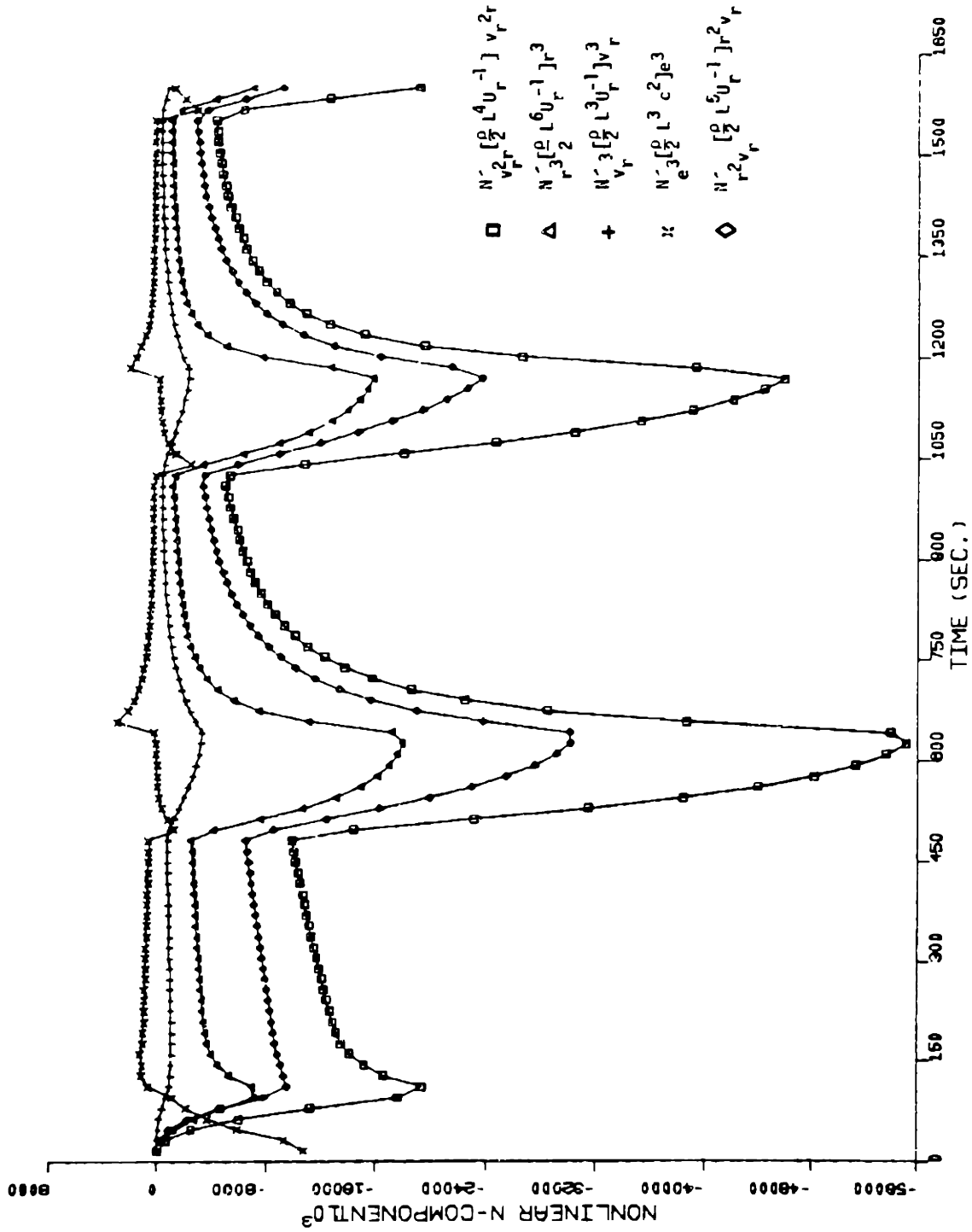
Figure 5.8.h   Time histories of nonlinear terms of N-moment in Eq. (2.5.22) during the biased zigzag maneuver in Fig. 5.8.a.

$$N = -\dot{v}m^S_{26} + \dot{r}m^S_{66} + uv[m^S_{22} + x_T m_{22}(x_T)] \tag{5.3.2}$$

$$+ ur[m^S_{26} - x^2_T m_{22}(x_T)] + m_{22}(x_T)u^2\delta\, x_T$$

$$m^S_{22} = \int_L m_{22}(x)dx \tag{5.3.3}$$

$$m^S_{66} = \int_L m_{22}(x)x^2 dx \tag{5.3.4}$$

$$m^S_{26} = -\int_L m_{22}(x)x\,dx \tag{5.3.5}$$

where

$m_{22}(x)$ is the two dimensional added mass in y-direction,

δ is the rudder deflection,

x_T is the value of x at the effective trailing edge,

the superscript "s" over the added mass denotes the added mass

from strip theory.

Equating these hydrodynamic force and moment to the inertia force

and moment, the equations of motion are found to be

$$uvm_{22}(x_T) + u[x_T m_{22}(x_T) + m]r + (m^S_{22} + m)\dot{v}$$

$$-(m^S_{26} + M_{26})\dot{r} = m_{22}(x_T)u^2\delta \tag{5.3.6}$$

$$-uv(m^S_{22} + x_T m_{22}(x_T)) + u[m^S_{26} + M_{26} - (x_T)^2 m_{22}(x_T)]r$$

$$+ (m^S_{26} + M_{26})\dot{v} - (m^S_{66} + M_{66})\dot{r} = m_{22}(x_T)u^2\delta\, x_T \tag{5.3.7}$$

where

M_{66} is the moment of inertia in z direction,

M_{26} equals to mx_G

According to Eq. (5.3.6) and (5.3.7),

$$Y_v v + (Y_r - mu)r = [-um_{22}(x_T)]v + [-ux_T m_{22}(x_T) - mu]r \tag{5.3.8}$$

$$N_v v + (N_r - mx_G u)r = [um_{22}^S + ux_T m_{22}(x_T)]v \tag{5.3.9}$$

$$+ [-um_{26}^S - mx_G u + ux_T^2 m_{22}(x_T)]$$

If $Y_v v$ cancels $(Y_r - mu)r$ completely and $N_v v$ cancels $(N_r - mx_G u)r$ completely, it requires that

$$m_{22}(x_T)v + [x_T m_{22}(x_T) + m]r = 0 \tag{5.3.10}$$

$$[m_{22}^S + x_T m_{22}(x_T)]v + [-m_{26}^S - mx_G + x_T^2 m_{22}(x_T)]r = 0 \tag{5.3.11}$$

Assume the slender body has a circular cross section and a constant draft T, except that at the bow it has a rounded end. Also, assume that the origin is located at midship and the ship mass is of the same magnitude as the sway added mass m_{22}^S, which is a fairly realistic approximation for the real ship configurations, then

$$m_{22}(x) = \frac{\rho}{2} \pi T$$

$$m_{26}^S(x) = 0$$

$$X_T = -0.5L \tag{5.3.12}$$

$$X_G = 0$$

Substitute Eq. (5.3.12) into Eq. (5.3.10) and (5.3.11), it follows that

$$v + 0.5rL = 0 \qquad (5.3.13)$$

Suppose that there are two sensors installed at the bow and stern to measure the local sway velocity, as is illustrated in Fig. 5.9, the sway velocity v at midship and the yaw velocity r can be expressed as follows:

$$v = \frac{v_1 + v_2}{2}$$
$$(5.3.14)$$
$$r = \frac{v_1 - v_2}{L}$$

Substitute Eq. (5.3.14) into Eq. (5.3.13), it results in

$$v_1 = 0 \qquad (5.3.15)$$
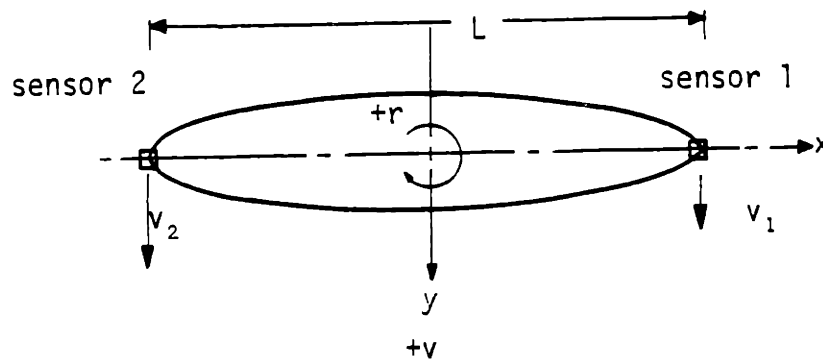
Figure 5.9   Relationship between v, r and the local

sway speed v_1 and v_2 at bow and stern

Therefore, if the pivoting point is located at the bow of a plate maneuvering in an ideal fluid, $Y_v v$ and $(Y_r - mu)r$ or $N_v v$ and $(N_r - mx_G u)r$ will cancel each other entirely. In other words, in this special case, the inertia forces and moments are completely balanced by rudder force and moment. Since this is an over simplified case, the conclusion can not be applied to real ships without modifications. However, since we realized that $Y_v v$ and $(Y_r - mu)r$ or $N_v v$ and $(N_r - mx_G u)r$ cancel each other to a large extent, it is expected that the pivot point of a ship must be near the bow. Table 5.5 is the normalized pivot point position(in front of the origin) of the three simulated maneuvers in Fig. 5.6, 5.7 and 5.8. Notice that the sway velocity relative to current is used to calculate the pivot position. Figure 5.10 is a plot of the pivot position after bow during the turning circle maneuver of BRITISH BOMBARDIER that Leeuwen used in Fig. 5.5. The procedure to apply the time history of $Y_v' v'$, $(Y_r' - m')r'$, $N_v' v'$ and $(N_r' - m'x_G')r'$ to obtain the pivot position is described in Appendix D.

The earlier postulate has been confirmed by the plots of instantaneous position of pivot point. Therefore, as long as the pivot point is near the bow, $Y_v' v'$ and $(Y_r' - m')r'$ or $N_v' v'$ and $(N_r' - m'x_G')r'$ will cancel each other to a large extent.

Examining Fig. 5.5 to 5.10 closely, there are several things worth noticing:

1. The singular behavior of pivot position at the beginning of turning circle maneuver or during the progress of zigzag maneuvers shows

TIME	10°/10° ZIGZAG	20°/20° ZIGZAG	BIASED ZIGZAG	TIME	10°/10° ZIGZAG	20°/20° ZIGZAG	BIASED ZIGZAG
0.160E+02	-0.458E+00	0.670E+00	-0.252E+00	0.816E+03	-0.630E-01	-0.364E+00	-0.559E+00
0.320E+02	-0.444E+00	0.797E-02	-0.241E+00	0.832E+03	-0.158E+00	-0.379E+00	-0.555E+00
0.480E+02	-0.436E+00	-0.145E+00	-0.266E+00	0.848E+03	-0.221E+00	-0.389E+00	-0.552E+00
0.640E+02	-0.435E+00	-0.223E+00	-0.294E+00	0.864E+03	-0.265E+00	-0.397E+00	-0.548E+00
0.800E+02	-0.437E+00	-0.269E+00	-0.317E+00	0.880E+03	-0.298E+00	-0.406E+00	-0.545E+00
0.960E+02	-0.490E+00	-0.304E+00	-0.338E+00	0.896E+03	-0.323E+00	-0.412E+00	-0.541E+00
0.112E+03	-0.547E+00	-0.330E+00	-0.378E+00	0.912E+03	-0.344E+00	-0.417E+00	-0.538E+00
0.128E+03	-0.577E+00	-0.351E+00	-0.426E+00	0.928E+03	-0.360E+00	-0.423E+00	-0.535E+00
0.144E+03	-0.636E+00	-0.368E+00	-0.456E+00	0.944E+03	-0.377E+00	-0.427E+00	-0.532E+00
0.160E+03	-0.673E+00	-0.383E+00	-0.477E+00	0.960E+03	-0.390E+00	-0.430E+00	-0.531E+00
0.176E+03	-0.716E+00	-0.410E+00	-0.489E+00	0.976E+03	-0.400E+00	-0.433E+00	-0.531E+00
0.192E+03	-0.770E+00	-0.501E+00	-0.496E+00	0.992E+03	-0.409E+00	-0.444E+00	-0.530E+00
0.208E+03	-0.846E+00	-0.620E+00	-0.500E+00	0.101E+04	-0.417E+00	-0.533E+00	-0.528E+00
0.224E+03	-0.959E+00	-0.768E+00	-0.502E+00	0.102E+04	-0.423E+00	-0.700E+00	-0.512E+00
0.240E+03	-0.114E+01	-0.101E+01	-0.503E+00	0.104E+04	-0.436E+00	-0.968E+00	-0.421E+00
0.256E+03	-0.160E+01	-0.163E+01	-0.504E+00	0.106E+04	-0.496E+00	-0.163E+01	-0.384E+00
0.272E+03	-0.355E+01	-0.266E+02	-0.505E+00	0.107E+04	-0.563E+00	-0.968E+01	-0.373E+00
0.288E+03	0.248E+01	0.898E+00	-0.506E+00	0.109E+04	-0.625E+00	0.154E+01	-0.372E+00
0.304E+03	0.473E+00	0.203E+00	-0.506E+00	0.110E+04	-0.633E+00	0.503E+00	-0.375E+00
0.320E+03	0.828E-01	-0.252E-01	-0.506E+00	0.112E+04	-0.743E+00	0.180E+00	-0.380E+00
0.336E+03	-0.840E-01	-0.141E+00	-0.507E+00	0.114E+04	0.816E-01	0.187E-01	-0.386E+00
0.352E+03	-0.180E+00	-0.211E+00	-0.507E+00	0.115E+04	-0.914E+00	-0.801E-01	-0.391E+00
0.368E+03	-0.242E+00	-0.259E+00	-0.507E+00	0.117E+04	-0.107E+01	-0.148E+00	-0.395E+00
0.384E+03	-0.286E+00	-0.293E+00	-0.507E+00	0.118E+04	-0.137E+01	-0.198E+00	-0.419E+00
0.400E+03	-0.317E+00	-0.320E+00	-0.507E+00	0.120E+04	-0.234E+01	-0.236E+00	-0.470E+00
0.416E+03	-0.341E+00	-0.341E+00	-0.507E+00	0.122E+04	0.171E+02	-0.266E+00	-0.511E+00
0.432E+03	-0.360E+00	-0.359E+00	-0.507E+00	0.123E+04	0.957E+00	-0.291E+00	-0.540E+00
0.448E+03	-0.375E+00	-0.374E+00	-0.507E+00	0.125E+04	0.255E+00	-0.312E+00	-0.558E+00
0.464E+03	-0.387E+00	-0.384E+00	-0.507E+00	0.126E+04	0.118E-01	-0.330E+00	-0.567E+00
0.480E+03	-0.398E+00	-0.396E+00	-0.507E+00	0.128E+04	-0.115E+00	-0.343E+00	-0.570E+00
0.496E+03	-0.407E+00	-0.404E+00	-0.455E+00	0.130E+04	-0.175E+00	-0.358E+00	-0.571E+00
0.512E+03	-0.416E+00	-0.412E+00	-0.412E+00	0.131E+04	-0.250E+00	-0.369E+00	-0.569E+00
0.528E+03	-0.423E+00	-0.445E+00	-0.399E+00	0.133E+04	-0.287E+00	-0.379E+00	-0.566E+00
0.544E+03	-0.429E+00	-0.538E+00	-0.398E+00	0.134E+04	-0.318E+00	-0.387E+00	-0.562E+00
0.560E+03	-0.435E+00	-0.649E+00	-0.401E+00	0.136E+04	-0.341E+00	-0.394E+00	-0.557E+00
0.576E+03	-0.442E+00	-0.783E+00	-0.406E+00	0.138E+04	-0.360E+00	-0.401E+00	-0.553E+00
0.592E+03	-0.447E+00	-0.987E+00	-0.411E+00	0.139E+04	-0.375E+00	-0.406E+00	-0.548E+00
0.608E+03	-0.151E+00	-0.143E+01	-0.416E+00	0.141E+04	-0.380E+00	-0.411E+00	-0.545E+00
0.624E+03	-0.493E+00	-0.352E+01	-0.420E+00	0.142E+04	-0.398E+00	-0.467E+00	-0.544E+00
0.640E+03	-0.583E+00	0.259E+01	-0.428E+00	0.144E+04	-0.407E+00	-0.611E+00	-0.541E+00
0.656E+03	-0.668E+00	0.575E+00	-0.473E+00	0.146E+04	-0.415E+00	-0.869E+00	-0.537E+00
0.672E+03	-0.756E+00	0.158E+00	-0.511E+00	0.147E+04	-0.422E+00	-0.193E+01	-0.534E+00
0.688E+03	-0.861E+00	-0.239E-01	-0.537E+00	0.149E+04	-0.429E+00	-0.183E+02	-0.530E+00
0.704E+03	-0.101E+01	-0.127E+00	-0.552E+00	0.150E+04	-0.434E+00	0.123E+01	-0.527E+00
0.720E+03	-0.126E+01	-0.194E+00	-0.562E+00	0.152E+04	-0.479E+00	0.417E+00	-0.524E+00
0.736E+03	-0.191E+01	-0.241E+00	-0.567E+00	0.154E+04	-0.445E+00	0.151E+00	-0.521E+00
0.752E+03	-0.848E+01	-0.276E+00	-0.569E+00	0.155E+04	-0.458E+00	0.105E-01	-0.517E+00
0.768E+03	0.166E+01	-0.305E+00	-0.568E+00	0.157E+04	-0.454E+00	-0.775E-01	-0.453E+00
0.784E+03	0.447E+00	-0.328E+00	-0.566E+00	0.158E+04	-0.459E+00	-0.143E+00	-0.392E+00
0.800E+03	0.101E+00	-0.349E+00	-0.563E+00	0.160E+04	-0.463E+00	-0.191E+00	-0.369E+00

Table 5.5 Normalized position of instantaneous pivot point during the different maneuvers illustrated in Fig. 5.6.a, Fig. 5.7.a and Fig. 5.8.a.

that although the pivot point is near the bow during most of the time of maneuver, it is not defined when the yaw speed approaches zero. From a kinematic viewpoint, the ship motion is of almost pure sway and the center of rotation is at infinity. An extreme case is the constant heading movement of ship at constant forward speed, in which the unbalanced hydrodynamic force Y_0 and moment N_0 are balanced by the rudder bias induced force $Y_\delta \delta$ and moment $N_\delta \delta$ as well as by the sway induced force $Y_v v$ and moment $N_v v$. It is deducible that the cancellation effect is weak around the period of singular behavior of pivot point for other kinds of maneuvers. This statement can be verified by examining Fig. 5.6 and 5.7.

2. During this study, the current effect has shown to be of some importance. Fig. 5.11 and 5.12 are plots of pivot point position of OSAKA in a biased zigzag maneuver and a turning circle maneuver, based on her sea trial data. In Fig. 5.9 and 5.10, we have seen the behaviors of pivot point position during the biased zigzag maneuver and the turning circle maneuver from simulation with complete current infomation. Since the pivot position shifted away from the bow region toward midship in Fig. 5.11 and the pivot position in Fig. 5.12 did not stablize after the transient period, the difference between the pivot position of sea trial data and the pivot position of simulation indicates that without accurate current information, the estimation of hydrodynamic coefficients can not be satisfactory.

3. The estimation of nonlinear hydrodynamic coefficients is more difficult than that of the linear coefficients. This is not only because
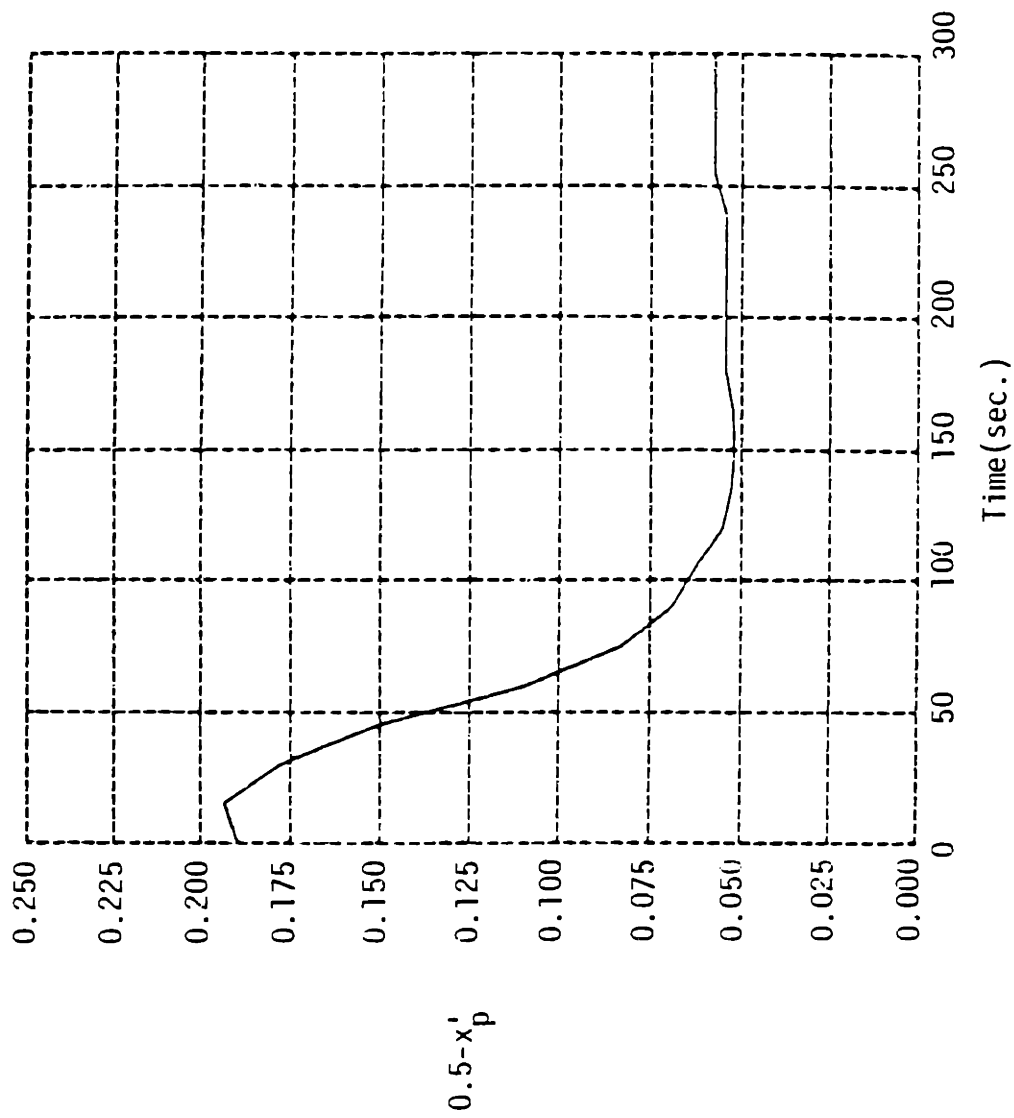
Figure 5.10 Nondimensionalized position of pivot point during the turning circle maneuver of BRITISH BOMBARDIA in Fig. 5.5.
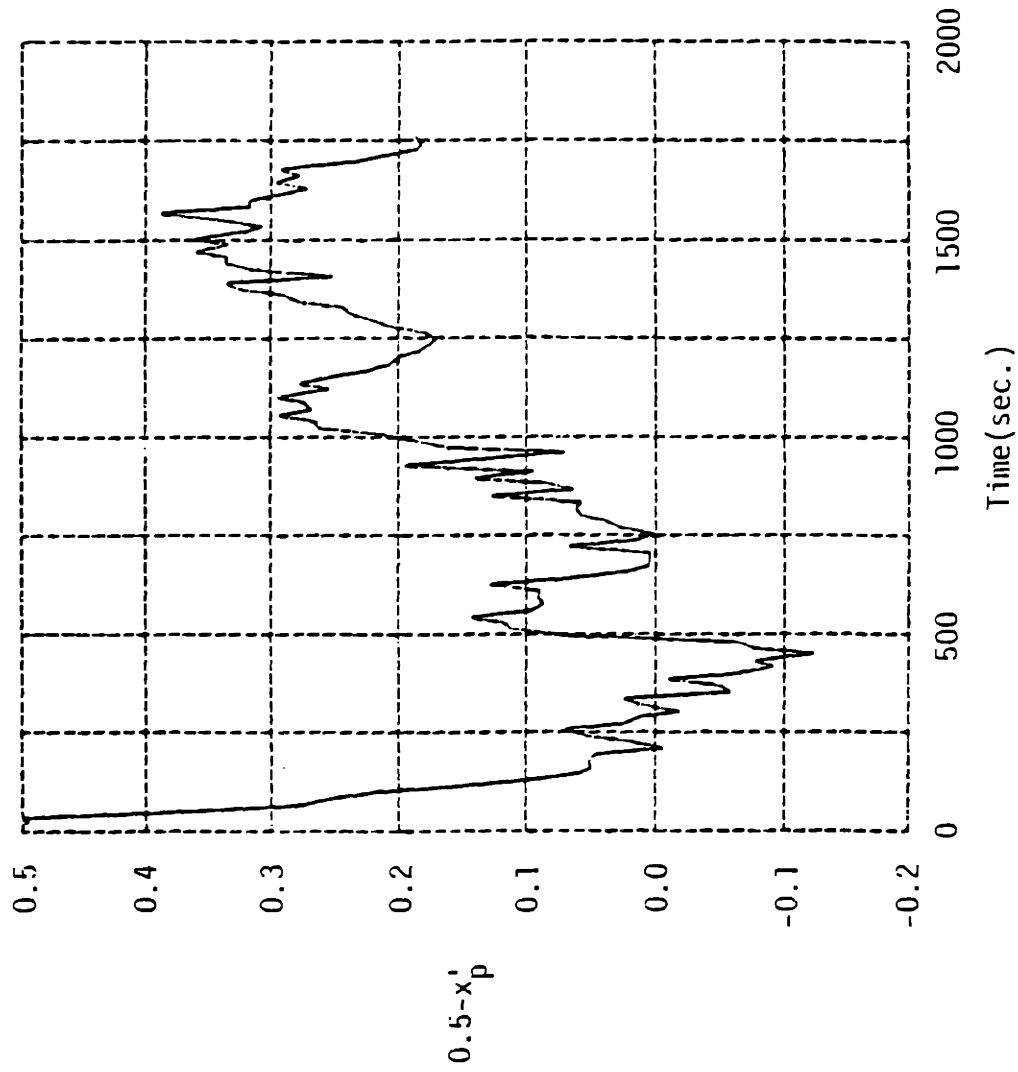
Figure 5.11   Nondimensionalized position of pivot point
during the sea trial biased zigzag maneuver of
ESSO OSAKA.
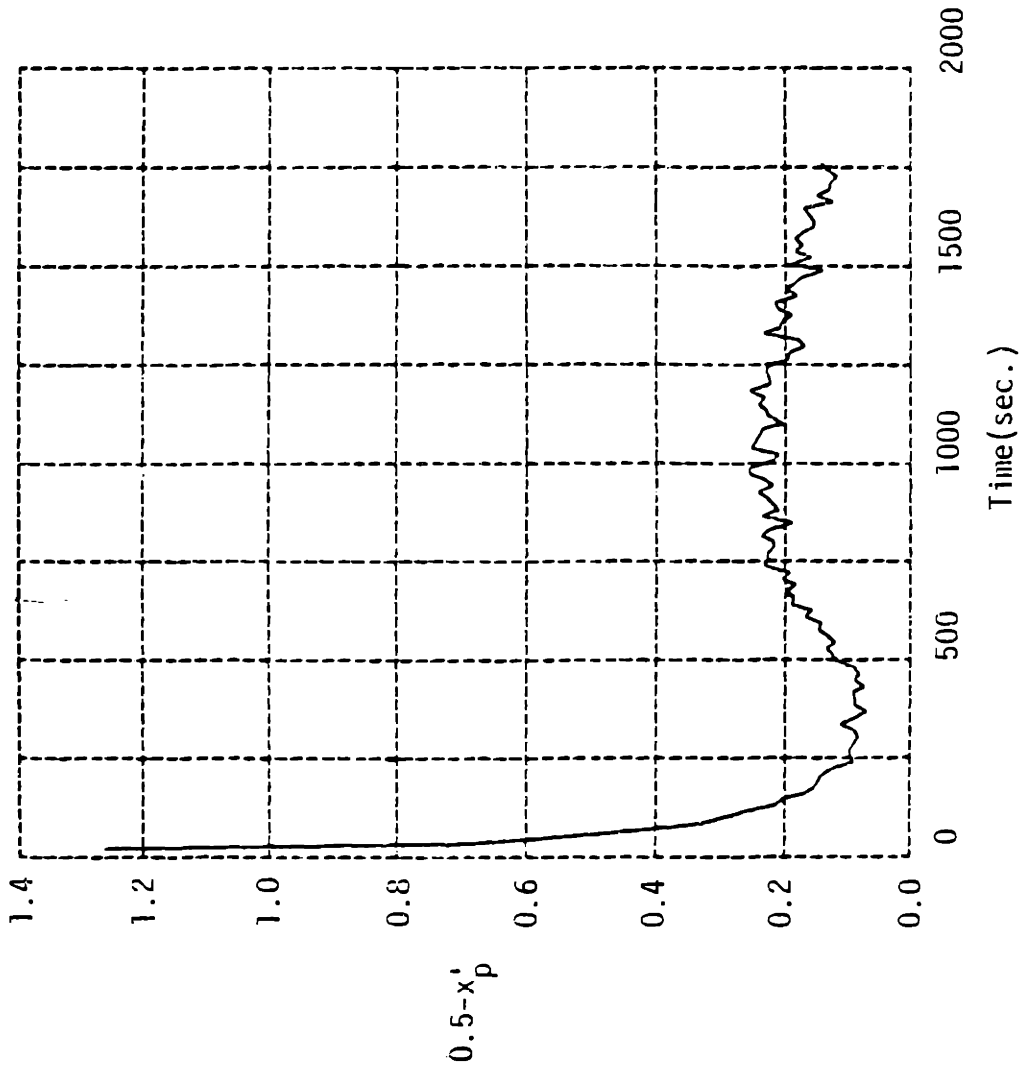
Figure 5.12 Nondimensionalized position of pivot point during the sea trial 35° rudder turning maneuver of ESSO OSAKA.

of the estimation error of the linear terms can exceed the contribution of nonlinear terms, but also because of the "simultaneous drift" of the nonlinear hydrodynamic coefficients. Since the yaw velocity has similar pattern to that of the sway velocity, execpt with an approximate phase shift of 180°, it is extremely difficult to determine the individual contribution of each nonlinear coefficient and to identify their values. In Fig. 5.5 to 5.8 , it is obvious that the contribution of Y'_{vvv}, Y'_{rrr},·· ...etc., except Y'_{eee}, can "compensate" each other to give the same resultant nonlinear Y-force. A simultaneous estimation of all the non-linear coefficients will most likely be impossible.

Since the "cancellation effect" has been identified as the major cause for the "simultaneous drift" of the linear coefficients, some technique is required to overcome this problem of unidentifiability. In Chap. 6, we will discuss the "parallel processing","exaggerated over- and under-initial estimation" and "parameter transformation" techniques for this purpose.

Since the "compensation effect" is the cause of "simultaneous drift" of nonlinear coefficients, we will also develop a practical way to estimate the nonlinear effect in Chapter 6.

6. REMEDY FOR SIMULTANEOUS DRIFT

Chronologically, "parallel processing", "exaggerated over- and under-estimated initial guess" and "parameter transformation" were studied in order to eliminate the "simultaneous drift" discussed in Chapter 5.

"parallel processing" technique did not successfully prevent the occurance of simultaneous drift due to the instinctive nature of cancellation effect, although it can delay the happening of simultaneous drift. But the idea of using this scheme to estimate the resistance coefficient is a valuable by-product of this study.

"Exaggerated over- and under-estimated initial guess" is a less rigorous technique, but practically it has given a very good estimation when simulated data is processed.

"Parameter transformation" is a more formal way to eliminate the "simultaneous drift". A nonlinear transformation is introduced as suggested by the phenomenon of simultaneous drift.

The discussion in the last section will be devoted to designing an effective way to estimate nonlinear effects instead of determining the magnitude of the individual nonlinear coefficients.

6.1 Parallel Processing

In Chapter 5, the cancellation effect between the contributions of hydrodynamic coefficients has been discussed. For the turning circle maneuver, the cancellation persists through out the maneuver. Therefore, the estimation of Y'_v together with $Y'_r-m'u'$ or the estimation of N'_v together with N'_r is difficult.

For zigzag maneuver, the cancellation still occurs most of the time during a cycle, but there are two very small time intervals during which cancellation does not occur. At one end of the intervals, the force and moment derivatives with respect to v prevails; While at the other end, only the force and moment derivatives with respect to r prevails. Between the ends of the small time interval, the contribution of Y_v' and $Y_r'-m'u'$ or the contribution of N_v' and N_r' have the same sign. Therefore, the cancellation effect does not exist during these very small time intervals. This observation suggests that for two different maneuvers, the contribution of the same coefficient is of different pattern, therefore if the maneuvering data of two different maneuvers is processed at the same time, the phenomenon of simultaneous drift may be improved.

As mentioned in the discussion of parameterization, the role of a coefficient can be of different importance for different maneuvers. Consequently, the estimation of the same coefficient may have different value when different maneuvering data is processed. If two maneuvering data files are processed simultaneously to estimate the same set of coefficients, the problem of data file dependence can also be resolved.

6.1.1 Inspiration of Parallel Processing

Intuitively speaking, the more information we have about an system the better we can describe this system. Therefore, in order to estimate a quantity accurately, we tend to measure that quantity as many times as possible or to measure that quantity by more than one sensor. Gelb[1974] gave a good example of this idea. Let us consider the problem of optimal

estimation of an unknown constant x by using two independent sensors that their measurements are contaminated by unbiased random noise. Its mathematical formulation can be written as

Sensor 1: $z_1 = x + v_1$ x is the unknown constant

Sensor 2: $z_2 = x + v_2$

$$E\{v_1^2\} = \sigma_1^2 \qquad\qquad E\{v_1\} = E\{v_2\} = 0$$

$$E\{v_2^2\} = \sigma_2^2$$

$$\hat{x} = ? \qquad\qquad E\{(x-\hat{x})^2\} = E\{\tilde{x}^2\} = ?$$

Let x be a weighted sum of these two measurement,

$$\hat{x} = k_1 z_1 + k_2 z_2$$

By requesting an unbiased estimation, we can express k_2 in terms of k_1,

$$k_2 = 1 - k_1$$

By minimizing the error covariance $E\{(x-\hat{x})^2\}$, k_1 can be expressed in terms of the error covariances of measurements. The final expression of $\hat{x}$ and $E\{\tilde{x}^2\}$ are as follows:

$$\hat{x} = \left(\frac{\sigma_2^2}{\sigma_1^2 + \sigma_2^2} \right) z_1 + \left(\frac{\sigma_1^2}{\sigma_1^2 + \sigma_2^2} \right) z_2 \qquad (6.1.1)$$

$$E\{\tilde{x}^2\} = \left(\frac{1}{\sigma_1^2} + \frac{1}{\sigma_2^2} \right)^{-1} \qquad (6.1.2)$$

Since $E\{\tilde{x}^2\}$ is smaller than either σ_1^2 or σ_2^2, the x in Eq. (6.1.1) is a better estimation then either of the original measurements.

For a dynamic quantity, the multi-sensor argument still applies. But here we will consider another problem for a dynamic system. For a linear dynamic, the Kalman filter provides an optimal estimation of the state vector, $\hat{\underline{x}}(n|n)$, by using the measurements up to the time step n. Could one obtain better estimation than this by using more information? one of the answer is through the usage of optimal smoothing, an off-line processing scheme which uses all the measurements between time 0 to T to estimate the state variable at time t, $0 \leq t \leq T$. The optimal smoother can be considered as a combination of forward filter and a backward filter as shown in Figure 6.1.

$$\hat{\underline{x}}(t|T)$$

0	t	T

$$\hat{\underline{x}}(t) \quad \hat{\underline{x}}_b(t)$$

forward filter   backward filter
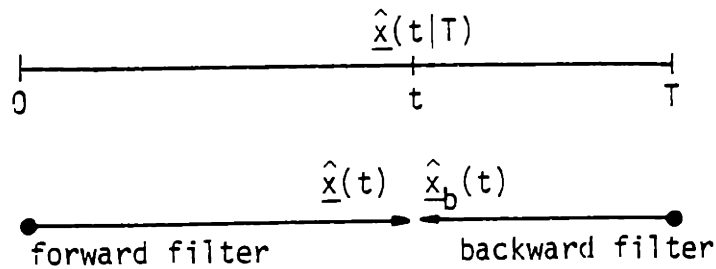
Figure 6.1 Optimal smoother(ref. Gelb[1974])

Let $\hat{\underline{x}}(t|T)$ represents the estimation from the smoother, then

$$\hat{\underline{x}}(t|T) = \underline{A}\, \hat{\underline{x}}(t) + \underline{A}'\, \hat{\underline{x}}_b(t) \qquad (6.1.3)$$

- 172 -

where $\underline{A}$ and $\underline{A}'$ are the weighting factors to be determined by requesting an unbiased error, $\underline{\tilde{x}}(t|T)=\underline{\hat{x}}(t|T)-\underline{x}(t)$, and by the minimization of the trace of the smoother error covariance $\underline{P}(t|T)$, $\underline{P}(t|T)=E\{\underline{\tilde{x}}(t|T)\underline{\tilde{x}}^T(t|T)\}$. After some algebraic manipulation, we find that

$$\underline{\hat{x}}(t|T)=\underline{\hat{P}}(t|T)[\underline{P}^{-1}(t)\underline{\hat{x}}(t)+\underline{P}^{-1}(t)\underline{\hat{x}}_b(t)] \tag{6.1.4}$$

$$\underline{P}^{-1}(t|T)=\underline{P}^{-1}(t)+\underline{P}_b^{-1}(t) \tag{6.1.5}$$

The derivation of the backward filter and the error covariance propagation is omitted here. Further study is referred to Gelb[1974], Schweppe[1973]. What we want to emphasize here is that the error covariance of smoothed state variable, $\underline{P}(t|T)$, is always less than or equal to the error covariance of either the forward filter or the backward filter. In other words, the smoother estimated state is always better than or equal to the estimations of filters. In Fig. 6.2 is an illustration of the advantage of performing the optimal smoothing.

Inspired by these two examples, we come up with the idea of parallel processing of two measurement data files of a system simultaneously. Although the system dynamics is the same and the only difference is the exogeneous input for these two files, we treat the state variables of these two files as different variables and keep the unknown parameters in common. Therefore, the formulation of this stochastic model has the following form:
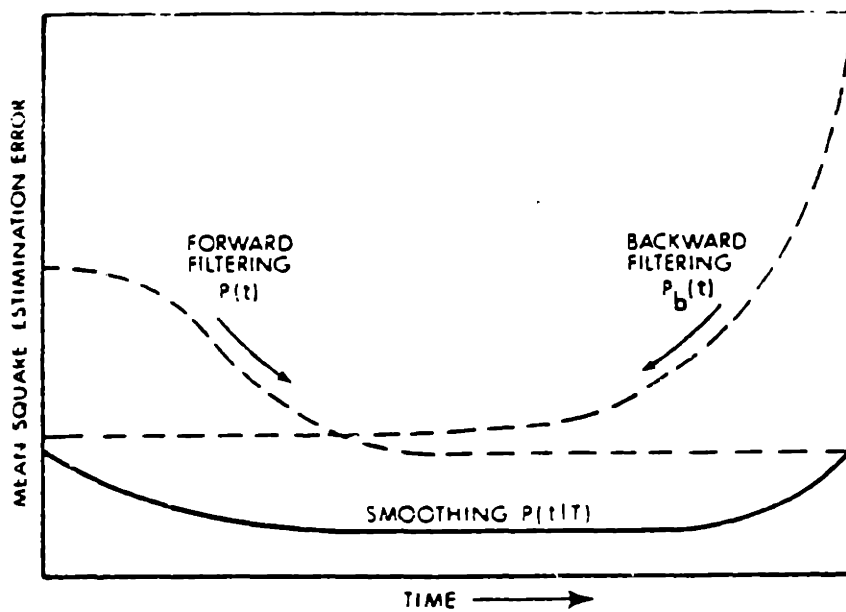
Figure 6.2 The advantage of performing optimal
smoothing(ref. Gelb[1974]).

$$\underline{x}'(n+1)=\begin{bmatrix} \underline{x}_1(n+1) \\ \underline{x}_2(n+1) \\ \underline{\alpha}(n+1) \end{bmatrix} = \begin{bmatrix} \underline{f}(\underline{x}_1(n),\ \underline{\alpha}(n),\ n_{p1}(n),\delta_1(n)) \\ \underline{f}(x_2(n),\ \underline{\alpha}(n),\ n_{p2}(n),\delta_2(n)) \\ \underline{\alpha}(n) \end{bmatrix} + \begin{bmatrix} \underline{w}_1(n) \\ \underline{w}_2(n) \\ \underline{0} \end{bmatrix}$$

$$\text{(6.1.6)}$$

$$\underline{z}'(n)=\begin{bmatrix} \underline{z}_1(n) \\ z_2(n) \end{bmatrix} = \underline{H}'\ \underline{x}'(n)+ \begin{bmatrix} \underline{v}_1(n) \\ \underline{v}_2(n) \end{bmatrix} \qquad\text{(6.1.7)}$$

where

$$\underline{H}' = \begin{bmatrix} \underline{I} & \underline{0} & \underline{0} \\ \underline{0} & \underline{I} & \underline{0} \end{bmatrix}$$

From Appendix B, we find that the gain matrix can be written as

$$\underline{K}'(n)=\underline{P}(n^-)\underline{H}^T(n)[\underline{H}(n)\underline{P}(n^-)\underline{H}^T(n)+\underline{R}(n)]^{-1}$$

$$= \begin{bmatrix} \underline{P}_{x_1x_1} & \underline{P}_{x_1x_2} & \underline{P}_{x_1\alpha} \\ \underline{P}_{x_2x_1} & \underline{P}_{x_2x_2} & \underline{P}_{x_2\alpha} \\ \underline{P}_{\alpha x_1} & \underline{P}_{\alpha x_2} & \underline{P}_{\alpha\alpha} \end{bmatrix} \begin{bmatrix} \underline{I} & \underline{0} \\ \underline{0} & \underline{I} \\ \underline{0} & \underline{0} \end{bmatrix} [\underline{H}(n)\underline{P}(n^-)\underline{H}^T(n)+ \begin{bmatrix} \underline{R}_1 & \underline{0} \\ \underline{0} & \underline{R}_2 \end{bmatrix}]^{-1}$$

$$= \begin{bmatrix} \underline{P}_{x_1x_1} & \underline{0} \\ \underline{0} & \underline{P}_{x_2x_2} \\ \underline{P}_{x_1\alpha} & \underline{P}_{x_2\alpha} \end{bmatrix} \begin{bmatrix} \underline{P}_{x_1x_1}+\underline{R}_1 & \underline{0} \\ \underline{0} & \underline{P}_{x_2x_2}+\underline{R}_2 \end{bmatrix}^{-1} \qquad\text{(6.1.8)}$$

Define λ as

$$\underline{\lambda} \equiv \begin{bmatrix} \underline{P}_{x_1 x_1} + \underline{R}_1 & \underline{0} \\ \underline{0} & \underline{P}_{x_2 x_2} + \underline{R}_2 \end{bmatrix}^{-1} = \begin{bmatrix} \underline{\lambda}_{11} & \underline{\lambda}_{12} \\ \underline{\lambda}_{21} & \underline{\lambda}_{22} \end{bmatrix} \tag{6.1.9}$$

then

$$\underline{\lambda}_{11} = (\underline{P}_{x_1 x_1} + \underline{R}_1)^{-1}$$

$$\underline{\lambda}_{22} = (\underline{P}_{x_2 x_2} + \underline{R}_2)^{-1} \tag{6.1.10}$$

$$\underline{\lambda}_{12} = \underline{\lambda}_{21}^T = \underline{0}$$

Substitute eq. (6.1.10) into eq. (6.1.8) and use the expression for the updated error covariance matrix $\underline{P}(n^+)$ in Appendix B, we have that

$$\underline{P}(n^+) = \begin{bmatrix} \underline{P}_{11} - \underline{P}_{11}\underline{\lambda}_{11}\underline{P}_{11}(n^-) & \underline{0} & \underline{P}_{1\alpha} - \underline{P}_{11}\underline{\lambda}_{11}\underline{P}_{1\alpha}(n^-) \\ \underline{0} & \underline{P}_{22} - \underline{P}_{22}\underline{\lambda}_{22}\underline{P}_{22}(n^-) & \underline{P}_{2\alpha} - \underline{P}_{22}\underline{\lambda}_{22}\underline{P}_{2\alpha}(n^-) \\ -\underline{P}_{1\alpha}\underline{\lambda}_{11}\underline{P}_{11} + \underline{P}_{\alpha 1}(n^-) & -\underline{P}_{2\alpha}\underline{\lambda}_{22}\underline{P}_{22} + \underline{P}_{\alpha 2}(n^-) & -\underline{P}_{1\alpha}\underline{\lambda}_{11}\underline{P}_{1\alpha} - \underline{P}_{2\alpha}\underline{\lambda}_{22}\underline{P}_{2\alpha} + \underline{P}_{\alpha\alpha} \end{bmatrix}$$

$$\tag{6.1.11}$$

Because

$$-\underline{P}_{1\alpha}\underline{\lambda}_{11}\underline{P}_{1\alpha} - \underline{P}_{2\alpha}\underline{\lambda}_{22}\underline{P}_{2\alpha} + \underline{P}_{\alpha\alpha} < -\underline{P}_{1\alpha}\underline{\lambda}_{11}\underline{P}_{1\alpha} + \underline{P}_{\alpha\alpha}$$

$$-\underline{P}_{1\alpha}\underline{\lambda}_{11}\underline{P}_{1\alpha} - \underline{P}_{2\alpha}\underline{\lambda}_{22}\underline{P}_{2\alpha} + \underline{P}_{\alpha\alpha} < -\underline{P}_{2\alpha}\underline{\lambda}_{22}\underline{P}_{2\alpha} + \underline{P}_{\alpha\alpha} \quad ,$$

we now have a faster improvement of the confidence bound for the unknown parameters than the original filtering process does. Therefore, the estimation of unknown parameter is better. However, notice that this

technique does not improve the estimation of state variables, because the covariance matrices for $\hat{\underline{x}}_1$ and $\hat{\underline{x}}_2$ stay the same as that of the original filtering process.

Since the "paralell processing" scheme is developed to give a better estimation, its usage is not limited to processing two different maneuvering data files. We can also use the same data file but shift the phase of the file to use it as the second file. Or we can break one file into two files of equal length and then process them at the same time. The strategy of application quite depends on the special consideration on each case. In the following sections, we will illustrate a few examples of the usage of this parallel processing scheme.

6.1.2 Estimation of the Ship Resistance Coefficient

Due to the scale effect, it is not accurate to use the resistance coefficient of a scaled model as an estimation for the full scale ship. Froude Hypothesis provides a pratical scheme to reduce the scale effect on the estimation by decoupling the frictional drag and the residual drag. Nevertheless, considering the substantial difference in Reynolds number between the full scale ship and model, we are not surprised by the over prediction of resistance reported by Hughes [1930] for LUCY ASHTON.

Rawson and Tupper [1966] pointed out that the conventional speed trial over a measured distance in calm water only confirms the accuracy of the prediction of ship speed for a given power. It cannot prove that the estimation of effective horse power (EHP) is accurate and so is true for the resistance coefficient, because an erroneous estimation of both

could bring out an acceptable result. Therefore, an experiment to measure the resistance of a full scale ship is necessary to find the real resistance coefficient. For instance, this can be carried out by towing the full scale ship or by fitting jet engines aboard the ship.

However, the development of system identification provides a direct and economic way to estimate the ship resistance. We can run the ship on a straight course and at a steady speed. At the start of the execution, shut off the engine and let the propeller windmill. Since on a straight course the dominant mechanism to slow down the ship is the resistance of hull plus appendages, C_R^{+} and $m-X_{\dot{u}}$ are the only two hydrodynamic coefficients to be estimated. Notice that the added mass $X_{\dot{u}}$ is ususally between 4% and 8% of the ship mass. In extreme case, the error of $m-X_{\dot{u}}$ can hardly exceed 4% of m. Therefore, the information of $m-X_{\dot{u}}$ is usually good. On account of this, the drag coefficient C_R becomes the essential hydrodynamic coefficient to be estimated.

Nevertheless, the problem is slightly more complicated than it looks like. This is because of the current plays a very important role for this special type of "maneuver". Consider a ship which is running parallelly to the current direction. If the mathematical model does not include the current effect, the error of C_R estimation is at least 15% for a ship sailing at 15 knots into 1 knot current ocean.

Including the current into mathematical model and trying to estimate the current direction and magnitude do not solve the problem completely, because the error of a wrongly estimated current magnitude and direction

---

† The C_R considered here actually contains the effect of windmilling propeller.

can be absorbed by a wrongly estimated C_R. This is where the parallel processing scheme helps us to resolve this difficulty. Suppose we conducted two similar sea trials of this kind on the same route but of opposite ship heading within half an hour, see Fig. 6.3. Since the duration of trial is relatively short to have a significant change of current, the current can be considered as constant. When the data of these two trials are processed simultaneously, the current being estimated has to satisfy both cases. In other words, the information of one trial serves as a constraint for the other file. Therefore, the current effect can be reduced to certain extent by using this parallel processing scheme.

This similar procedure can also be used for estimating the locked propeller resistance coefficient n_1 in Eq. (2.5.22), after the C_R has been estimated accurately. For zigzag maneuvers and turning circle maneuvers, the current effect on the absolute surge and sway velocity is not constant anymore. Therefore, the influence of current is easier to detect than the case of straight motion. In the next section, we will discuss how parallel processing scheme can improve the estimation when zigzag maneuvers are dealt with.

6.1.3 Parallel Processing Scheme for Zigzag Maneuvers

As shown in Fig. 5.6 to 5.7, the cancellation between $Y_v'v'$ and $(Y_r'-m'u')r'$ or between $N_v'v'$ and $N_r'r'$ occur in most of the time during a zigzag meneuver. The individual contributions of each term manifest themself over only a short period. Although this period is short, it is

believed that this short period makes the zigzag maneuvers better than turning circle maneuvers for estimating Y_v' and $Y_r'-m'u'$ or N_v' and N_r' simultaneously. In order to artificially increase the period of no cancellation, the idea of parallel processing is adopted again.

Because the nonlinear effect is different for moderate and for tight maneuver, being consistent, we prefer to use the files of similar tightness of maneuver. Therefore, a parallel processing of $10^o/10^o$ zigzag data and $20^o/20^o$ zigzag data is not suggested.

To use two different files of similar maneuvers is not the best idea either. In that case, we need to increase the time and budget for conducting the experiment. Besides, the currents to be identified are two instead of one, if these two trials are not conducted within a short time. These considerations motivated the idea of parallelly processing a data file and the same file with phase shift. Consider a zigzag maneuver, the same file with a phase shift is treated as the second data file. In Fig. 6.4 is a plot of the force components $Y_v'v'$, $(Y_r'-m'u')r'$ and Y_δ' of both files.

To avoid the overlap of no cancellation period, an appropriate phase shift is chosen. The resulting increment of no cancellation period and the fact that only one current to be estimated make the parallel processing scheme benificial to the parameter estimation when zigzag maneuvering data is processed.
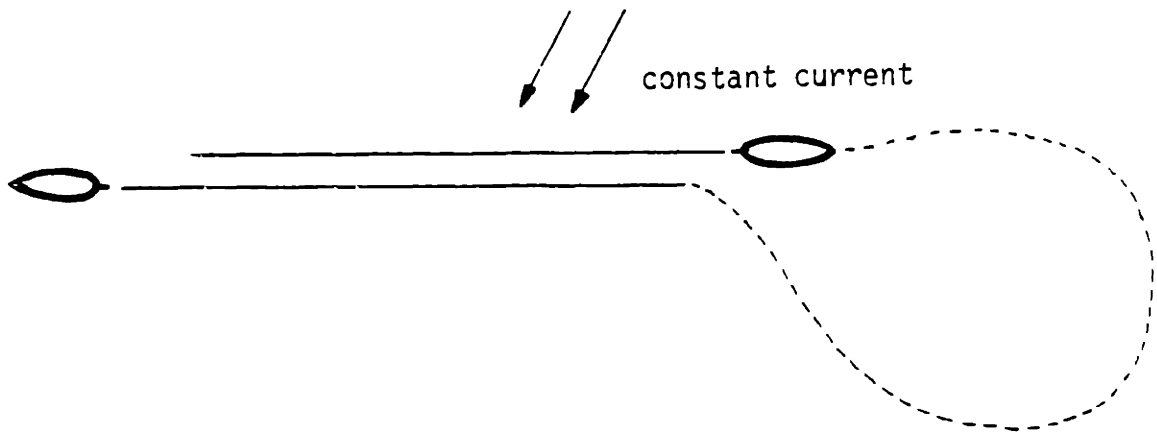
Figure 6.3   Trials for the estimation of C_R
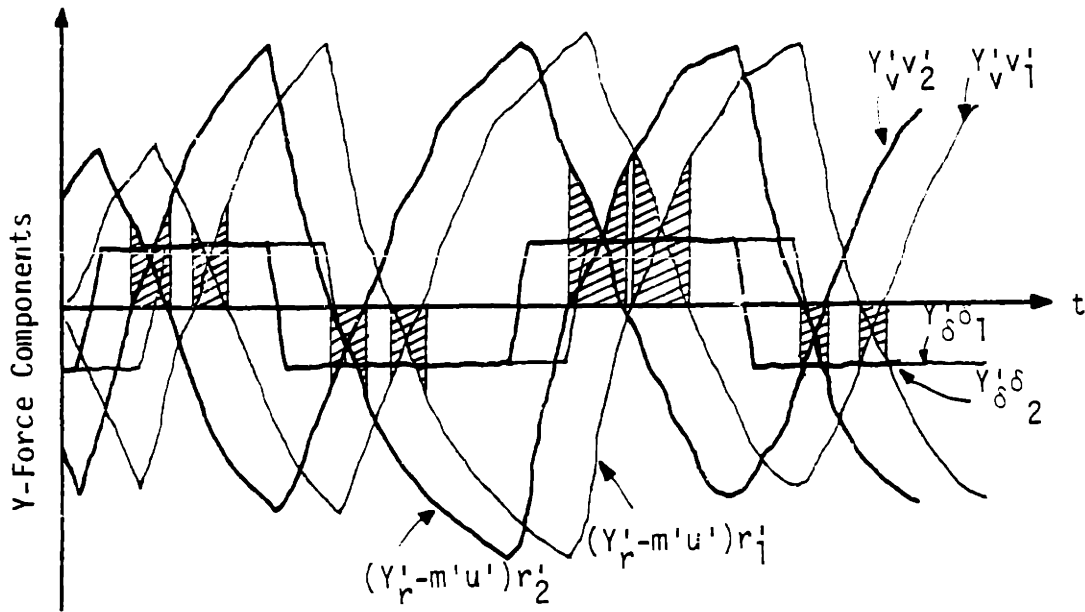
Figure 6.4   Increase the no cancellation period
             by shifting the phase

6.1.4 Parallel Processing Scheme for Biased Zigzag Maneuver and Turning Circle Maneuver

For biased zigzag maneuver and turning circle maneuver the ship motion is restricted within a region much smaller than that of a zigzag maneuver. Take ESSO OSAKA as an example, the advance of 1600 seconds is more than 4 km for $20^O/20^O$ zigzag maneuver in deep water, while the advance is about 1.1 km for a 35° degree rudder turning circle maneuver. Therefore, the variance of current should be smaller for turning circle or biased zigzag maneuver. Since within 1600 seconds, the ship changed her heading for more than 360°, the whole file can be splitted into two parts that are about 180° out of phase in the heading. When these two files are parallelly processed, the current has to satisfy both files simultaneously. From the experience of estimating resistance, we know that this scheme will help to zero in the true value of current and thus improve the estimation accuracy of the other coefficients. This idea is illustrated in Figure 6.5.
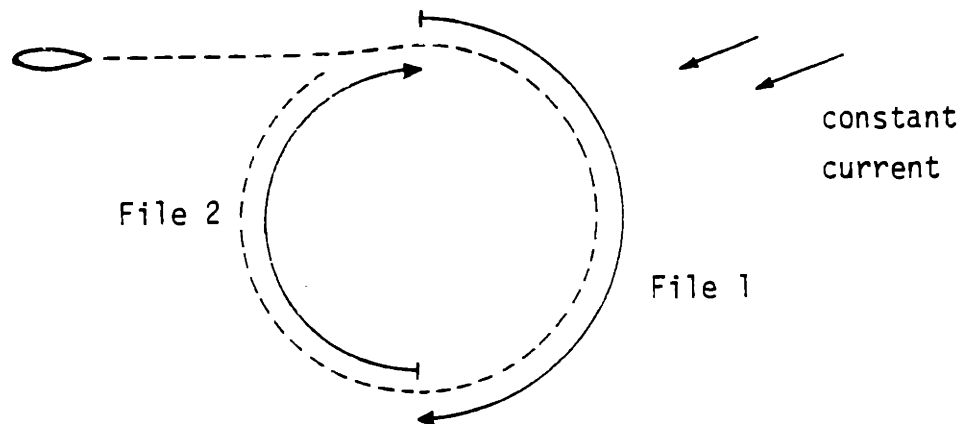
Figure 6.5 The application of "parallel processing" to one biased zigzag maneuver or one turning circle maneuver.

6.2 Exaggerated Over- and Under-estimated Initial Guess

In Fig. 5.4, the phenomenon of "simultaneous drift" has been demonstrated. The different behavior of Y_v', Y_r' pair and N_v', N_r' pair motivated the "exaggerated over- and under-estimated initial guess" scheme.

Notice that it is $(Y_r'-m'u')r'$ that counteracts $Y_v'v'$. Thus, when 0% of the true value of Y_v', Y_r', Y_v', N_r', etc. are used as the initial guess, it is actually an over estimation for $Y_r'-m'u'$. The fact that v is about 180° out of phase with r has made these initial guess of N_v' and N_r' an acceptable pair for the model, because the error in $N_{v_i}'v'$ is almost cancelled by the error in $N_{r_i}'r'$, where the subscript i indicates initial guess. However, the error of Y_{v_i}' and Y_{r_i}' will be felt by the filter, because the error in $Y_{v_i}'v$ and $(Y_{r_i}'-m'u')r$ is not cancelled. That explains why Y_v' and Y_r' converge to the true value while N_v' and N_r' starts to drift together almost from the very beginning of estimation.

Based on this observation, the scheme of "exaggerated over- and under-estimated initial guess" is formulated as follows:

1. Over estimate one of Y_v' and $Y_r'-m'u'$ to a large extent and under estimate the other one to a large extent as initial guesses, the same thing is also applied to N_v' and N_r'. The exaggeration of under estimation and over estimation is to prevent the initial guesses from both being under estimated or both over estimated.

2. Proceed the data processing.

3. Go through the time history of estimation and locate the spot from which the simultaneous drift begins, usually there will be a certain

period of stability and then the two curves starts to move up and down in company.

4. Measure the coefficient value at the starting point of simultaneous drift and enter them as the estimated value for these coefficients.

Although this method works well for simulated data, it is not a rigorous approach though. In the next section, a more formal way to overcome the problem of simultaneous drift will be presented.

6.3 Parameter Transformation

When "simultaneous drift" occurred, it is found that the percentage variance of N_v' and N_r' is always very close. In other words, if N_v' is 15% less than the true value, then N_r' is also 15% less than the true value. Y_v' and Y_r' do not have this relationship, but Y_v' and $Y_r'-m'u'$ do have.

Based on these observations, we introduce two new parameters. Define μ_Y and μ_N as follows:

$$\mu_Y \equiv \frac{Y_r'-m'u'}{Y_v'}$$

$$\mu_N \equiv \frac{N_r'-m'x_G'u'}{N_v'}$$

(6.3.1)

then

$$Y_v'[\frac{\rho}{2}L^2U]v+(Y_r'-m'u')[\frac{\rho}{2}L^3U]r=Y_v'[\frac{\rho}{2}L^2U](v+\mu_YLr)$$

(6.3.2)

$$N_v'[\frac{\rho}{2}L^3U]v+(N_r'-m'x_G'u')[\frac{\rho}{2}L^4U]r=N_v'[\frac{\rho}{2}L^3U](v+\mu_NLr)$$

Since the transformation spoils the original linear dependent relationship between Y_v' and $Y_r'-m'u'$ and between N_v' and $N_r'-m'x_G'u'$, such that

the local geometry of log likelihood surface around the true value is not

a horizontal ridge with respect Y'_v and μ_Y or with respect to N'_v and μ_N,

the new set of coefficient is more identifiable than the original one.

6.4 Nonlinear Hydrodynamic Coefficient

In last chapter, it has been mentioned that the estimation of non-

linear coefficients is more complicated than the linear case. In Fig. 7.3

is the estimation result from a simulated biased zigzag maneuver, which

is supposed to be the best maneuver to estimate the nonlinear terms.

Except N_{vrr} is pretty identifiable, the rest coefficients are just a

combination of wrong values. "Parallel processing" does not help very

much, Fig. 7.4 is the estimation from the same simulated maneuvering data

by using the idea of section 6.1.3, which further verifies the argument of

"simultaneous drift" and "compensation effect" in section 5.3.

Since we have so many nonlinear coefficients in the model, the

"exaggerated over- and under-estimated initial guess" scheme is just

not practicable. "Parameter transformation" will not work either, because

when more than one coefficient is transformed, the μ'_Ys and μ'_Ns still can

compensate each other to give an equivalent nonlinear contribution.

When X'_{ee}, Y'_{eee} and N'_{eee} replace $X'_{\delta\delta}$, $Y'_{\delta\delta\delta}$,$N'_{\delta\delta\delta}$ and other related

terms, their contribution to the forces and moment is of different pattern

with the other's. Therefore, we believe it is important to have them

identified.

For the rest of the nonlinear coefficients, having realized that the

identification of each term is very difficult, we would rather estimate

the effective resulting nonlinear contribution. Since the contributions of the v and r cross related nonlinear coefficients have the same phase or opposite phase, the adjustment of only one coefficient is sufficient to absorb the error of the rest. Therefore, X'_{ee}, $X'_{vr}+m'$, X'_{vvrr}, Y'_{eee}, Y'_{vrr}, N'_{eee} and N'_{vrr} will be estimated to give the correct nonlinear contribution. Notice that X'_{vvrr} is retained here, because the dimensional quantity of $X'_{vr}+m'$ is independent of ship speed, while X_{vvrr} increases as the ship speed decreases.

7. RESULTS OF ESTIMATION

In order to illustrate the performance of those schemes discussed in Sec. 6.1 to Sec. 6.3, the simulated maneuvering data of ESSO OSAKA is utilized in the former part of this chapter, such that we have the "true" value of "unknown" parameters for comparison. Instead of using Szeto's [1977] convention, which uses a certain percentage of the maximum amplitude of the state variable as the intensity of noise, the noise information obtained from processing the sea trial data is employed.

The full size ship hydrodynamic coefficients of ESSO OSAKA are estimated by processing the sea trial data provided by MARAD. The results are presented in the later part of this chapter. The accuracy of estimation is checked by simulation.

7.1 Results of Parallel Processing

In Fig. 5.5, we already showed the "simultaneous drift" phenomenon. When parallel processing scheme is applied to treat the same data file and its copy of shifted phase, we found that it could delay the occurence of simultaneous drift as shown in Fig. 7.1. But using the estimated value as the initial guess, further passes did not prevent the occurence of simultaneous drift, see Fig. 7.2. This is an indirect proof that the cancellation effect is an intrinsic nature of ship maneuvering dynamics.

The idea of breaking one biased zigzag maneuvering file or turning circle maneuvering file into two pieces of 180° heading angle difference is tested to estimate the nonlinear coefficients. Comparing the results of ordinary processing in Fig. 7.3 and the results of parallel processing

in Fig. 7.4, we found no improvement for the combination of erroneous coefficient values. This indicates not only that the most of the coefficients have minor contribution to the motion, but also the "simultaneous drift" also happens to the nonlinear hydrodynamic coefficients. Therefore, when sea trial data is processed, we seek the equivalent nonlinear effect of true system by adjusting a few nonlinear coefficients that forms an identifiable set.

7.2 Results of Exaggerated Over- and Under-estimated Initial Guess

Apply the scheme of "exaggerated over- and under-estimated initial guess" to a simulated $10°/10°$ zigzag maneuver, we have the result as shown in Fig. 7.5. All the estimated value has very small error except Y_r'. This is because Y_r' is just a small portion of $Y_r'-m'u'$ and is not easy to be identified very accurately. Notice that the simultaneous drift of N_v' and N_r' has started from the 270th time step, although the end value did not wander away. A few validity tests for this run is plotted in Fig. 7.6. To check the optimality of this result, we calculate the log likelihood based on the estimated value and the log likelihood based on true coefficient values. Since

$$\xi_{true} = 9611 \qquad \hat{\xi} = 9613,$$

the extended Kalman filtering technique does give us optimal estimation result for this ship maneuvering dynamic system.

In order to see whether the simultaneous drifting pair of N_v' and N_r' also gives equal optimality, we let the simultaneous drift happen by

under-estimating both N_v' and N_r' on purpose at the beginning of process. The result is shown in Fig. 7.7. Further more, we perturb the resulting value of N_v' and N_r' in different combination and calculate the log likelihood. If the log likelihood surface is projected onto $N_v'-N_r'$ plane, the log likelihood for each combination is illustrated in Fig. 7.8. Here we can see that the simultaneous drift of N_v' and N_r' is equivalent to walking on a horizontal ridge of the log likelihood surface. That explains why simultaneous drift could happen and an underestimated pair of N_v' and N_r' accelerates the occurence of simultaneous drift.

In case the initial guesses of N_v' and N_r' have different percentage of error, e.g., N_v' is over estimated by 15% and N_r' is under estimeted by 25%, the simultaneous drift could occur while both N_v' and N_r' had 3 to 4% error, although the final values of N_v' and N_r' have very small error, see Fig. 7.8-1.a and b. Therefore, the argument in Sec. 6.2 is not valid in general. However, it was found that if the idea of parallel processing by phase shift in Sec. 6.1.3 was applied together with the scheme of "exaggerated over- and under-estimated initial guesses", the coefficients' values could converge to the true values after multiple passes of data processing. The Fig. 7.8-2.a and b show the results of second pass.

In Sec. 3.2.2, it was mentioned that the EKF had the feature of tracking the time varying parameters. To confirm that, the dynamics of current magnitude and the dynamics of current direction were given a proper process noise strength, i.e.,

$$\dot{u}_c = w_{u_c}$$

$$\dot{\alpha} = w_\alpha$$

$$E\{w_{u_c}\} = E\{w_\alpha\} = 0 \tag{7.2.1}$$

$$E\{w_{u_c}^2\} = Q_{u_c} \qquad E\{w_\alpha^2\} = Q_\alpha$$

when the same simulated data as in Fig. 7.5 is processed via this modified model, we found that the filter indeed tracked the "varying" current without degrading the estimation of hydrohynamic coefficient significantly. The result is presented in Fig. 7.9. Notice that the occurence of simultaneous drift for N_v' and N_r' has delayed by the introduction of w_{u_c} and w_α, which is consistent with our knowledge that larger process noise slows down the convergence speed.

7.3 Estimation of Resistance Coefficient

In sec. 6.2.2, we already discussed the benefit of using parallel processing scheme when ship resistance is estimated. If we write down the governing equation of a coasting ship with windmilling propeller, since $v_r \approx 0$, $r \approx 0$,

$$(m-X_{\dot{u}})\dot{u} = -C_R \frac{\rho}{2} u_r^2 S \qquad (7.3.1)$$

is the essential part of the dynamics[†]. One can easily see the problem of identifiability when both $m-X_{\dot{u}}$ and C_R are estimated together. However, since $X_{\dot{u}}$ usually lies between 0.04m and 0.08m, a 2% error in $m-X_{\dot{u}}$ should be a representative figure in reality. To avoid the problem of nonuniqueness, we first try the estimation of C_R with fixed $m-X_{\dot{u}}$ of 2% error. The estimation of C_R in the presence of three different current is shown in Fig. 7.10(s) to 7.18(s). For each current, two simulated data files of opposite ship heading are processed alone first. Afterwards, the parallel processing scheme is applied to these two files. The results of different current are summarized in Table 7.3 to Table 7.5. The results have proved that parallel processing does provide better estimation.

By cross examining Table 7.3 to 7.5, we find that when ship sails parallel to the current, the estimation of C_R is the best among three cases. This is a useful information for designing the sea trial of this purpose later on.

[†] As discussed in Sec. 6.2.2, this C_R includes the effect of windmilling propeller.

Notice that the estimation error of C_R has not been less than 2%, which is the percentage error of fixed $m-X_{\dot{u}}$. Therefore a better estimation of C_R requires the improvement of $m-Y_{\dot{u}}$.

When both C_R and $m-X_{\dot{u}}$ are estimated, as we expected, the estimation results have degraded, Fig. 7.10c and 7.12c are the typical results of this kind. In some cases, "simultaneous drift" had occured. The argument of "over- and under-estimated initial guess" is still valid here. Apply this scheme to the same data files in Fig. 7.18, the results of different initial guess are shown in Fig. 7.19 to Fig. 7.22 and summarized in Table 7.6 for comparison. Notice that the error of estimation for both C_R and $m-X_{\dot{u}}$ are less than 2%, and the better the initial guess the more accurate the results. A validity test for Fig. 7.21 is shown in Fig. 7.23 as an representative for the similar test.

Since C_R and $m-X_{\dot{u}}$ converge to their final value very quickly, 100 time steps of 4 second interval is quite sufficient to obtain a good estimation, which is a favorable condition to assume a constant current.

7.4 <u>Results of Parameter Transformation</u>

Using the model proposed in Sec. 6.4 and the same data file in Fig. 7.5, we estimated Y_v', N_v', N_δ', $X_{vr}'+m'$ and μ_Y, μ_N. Figure 7.24 shows the result of first pass. In order to see whether "simultaneous drift" could happen, the estimated coefficients were fed into the filter as initial guess and do the second pass. In Fig. 7.25, one can see that no such "simultaneous drift" exists for N_v' and μ_N even if the initial guess is very close to the true value of these coefficients.

In Fig. 7.7, the initial guess of N_v' and N_r' are chosen to give apparent "simultaneous drift". However, when the corresponding initial guess of μ_N is fed into the estimator, it is found that both N_v' and μ_N have converged to the true value very quickly as in Fig. 7.26. Therefore, the "parameter transformation" is the most reliable scheme among the three methods that were discussed in Chap. 6 to overcome the "simultaneous drifting" problem.

7.5 Estimation from the Sea Trial Data

In the previous sections, it has been quite successful to estimate the hydrodynamic coefficients form the simulated maneuvering data of ESSO OSAKA. After all, the simulated data is different from the real data. The difficulties of processing sea trial data are as follows:

1. Since the program does not estimate all the coefficients for each pass, the value of the coefficients that are not estimated has to be assumed. In processing the simulated data, those fixed coefficients are taken to be equal to those used in generating the noisy data. When the sea trial data is processed, the fixed coefficients are assumed equal to those acquired from the model test, which may differ from their "true" value.

2. The statistical properties of the simulated process noise and the measurement noise received by the estimator are more accurately modelled than the real noise in sea trial data.

3. The current is constant in the simulated data, whereas the current is a function of geographical position and water depth in the real world,

even if it is measured at the same time.

These have handicapped the estimation of hydrodynamic coefficients from the sea trial data. In order to reduce the error introduced by assuming fixed value for some coefficients, it is necessary to decouple their effects from the process by choosing appropriate maneuvers and estimating those coefficients which contribute most significantly toward a given type of maneuver. The sensitivity analysis in Chap. 5 has helped us to resolve this difficulty.

Although the statistical characteristics of process noise and measurement noise is incomplete for the case of sea trial data, the low-pass filtered measurement is used to estimate the measurement noise strength and the process noise strength is adjusted according to the information from hypothesis tests.

From the experience of processing the simulated data, we found that current direction and magnitude can be estimated very accurately. And in addition, they converge to the true value pretty rapidly. We do not have this luck when sea trial data is processed. The variation of current during the maneuver has degraded the estimation, and misleading results are sometimes obtained. However, if we only use the portion of trial data over which the current is essentially constant, the estimation is pretty successful.

In order to simplify the model, we let Y'_δ depend on N'_δ, Y'_0 depend on N'_0 and Y'_{eee} depend on N'_{eee}. Although Ogawa[1978] has found that N'_δ/Y'_δ is slightly more than 0.5, since Y'_δ is less influential upon the ship motion,

the approximation

$$Y'_\delta = 2N'_\delta \qquad (7.4.1)$$

is a practical assumption. Similar argument is applicable to Y'_{eee} and Y'_0.

Because the sea trial of ESSO OSAKA does not cover all the test

suggested in Table 4.1, some coefficients have to be determined from the

existing data files or from the available ship information. Among which,

the effective thrust coefficients n_1, n_2 and n_3 are first determined from

the propeller characteristic curve and the drag coefficient is determined

by equilibrium operating condition. The estimation of their values is

obtained from processing the zigzag maneuvers.

The rudder bias Y'_0 and N'_0 is estimated by parallelly processing the

10°/10° zigzag data and 20°/20° zigzag data. We have found that if Y'_0

is also estimated as an independent coefficient, it will mess up the

estimation of current. This is a natural consequence of constant current

model, because Y'_0 gives the ship a constant drift that a constant current

will also do by different mechanism. Therefore, the assumption

$$Y'_0 = 2N'_0 \qquad (7.4.2)$$

not only simplifies the model but also helps to resolve the problem of

identifiability. The estimation of N'_0 does not have this trouble, because

a constant current only gives the ship a linear drift and no yawing motion.

Notice that N'_δ and $X'_{vr}+m'$ are estimated together with N'_0 in order to match

the amplitude of force and moment that the adjustment of N'_0 can not

accomplish. Fig. 7.27 is the result of this estimation.

By tracking the current, we found the current direction has a dramastic change about 13° after the first 800 seconds in 10°/10° zigzag maneuvering data, see Fig. 7.28. Therefore, only the data of the first 800 seconds is utilized to estimate the major linear coefficients together with $X'_{vr}+m'$. Fig. 7.29 shows the results of this estimation. Notice that simultaneous drift has occurred at t≈660 seconds.

Fixing these coefficient value on the estimated, we proceed further to estimate the nonlinear coefficient N'_{vrr}, X'_{ee}, X'_{vvrr}, N'_{eee} and Y'_{vrr} by using the data of 35° turning circle maneuver. This parameterization is based on the discussion in Sec. 6.4. In Fig. 7.30, one can see clearly that X'_{ee} and N'_{eee} have stablized value in the earlier stage of estimation, while Y'_{vrr}, X'_{vvrr} and N'_{vrr} are stabilized during the later stage, which is consistent with the contribution of these coefficient in a turning circle maneuver.

Having determined the hydrodynamic coefficient values, we go back to each file and estimate the current by portions. The results are tabulated in Table 7.9. In order to check the accuracy of estimation, the simulation of each maneuver is checked against the sea trial data in Fig. 7.31, 7.32 and 7.33 for 10°/10° zigzag maneuver, 20°/20° zigzag maneuver and turning circle maneuver. Considering the fact that the major linear coefficients are estimated from 10°/10° zigzag maneuver and the nonlinear coefficients are estimated from turning circle maneuver, the simulation of 20°/20° zigzag maneuver is a pretty good one.

	Model Test	Estimated	Data File(s) Used
Y'_v	-0.02828	-0.02608	10°/10° zigzag
Y'_r	0.00391	0.00365	"
N'_v	-0.01090	-0.01046	"
N'_r	-0.00500	-0.00480	"
N'_δ	-0.00242	-0.00283	"
$X'_{vr}+m'$	0.03070	0.02660	"
N'_o	-0.00116	-0.00028	10°/10° Z & 20°/20° Z
N'_{vrr}	0.00905	0.00611	35° turning circle
X'_{ee}	-0.00249	-0.00224	"
X'_{rrvv}	-	-0.00715	"
N'_{eee}	0.00110	0.00116	"
Y'_{vrr}	-0.04126	-0.04503	"

		u_c (ft./sec.)	α
10°/10° zigzag	0 ∿ 800 sec.	0.821	73.3°
	800 ∿ 1600 sec.	0.958	86.5°
20°/20° zigzag	0 ∿ 180 sec.	1.178	79.1°
	180 ∿ 440 sec.	0.479	79.4°
	440 ∿ 1600 sec.	0.861	93.4°
35° turning circle	0 ∿ 500 sec.	1.264	66.2°
	500 ∿ 1600 sec.	1.042	74.6°

Table 7.9 Estimated coefficient values for ESSO OSAKA

```
************************************************************
*                                                          *
*   PARAMETRIC IDENTIFICATION - EXTENDED KALMAN FILTER     *
*   TWO DATA FILES ARE PARALLELY PROCESSED IN THIS RUN     *
*                                                          *
************************************************************
```

SYSTEM: 280,000 DWT. TANKER - ESSO OSAKA

MANEUVER: ZIG-ZAG RUDDER, AT RUDDER RATE   -2.00 DEG./SEC.,
                                    10.00/ 10.00 ZIG-ZAG
               1.35 FT/SEC. OF CURRENT
               86.00DEGREES FROM NOMINAL ZERO

TRIAL PERIOD: 1200.00 SECONDS AT 4.00 SECONDS   OF TIME INTERVAL
IDENTIFICATION: STATE VARIABLES   -U,V,R,PS

                UNKNOWN PARAMETERS -

                              $NP = 6$: Y'_V

                              $NP = 7$: Y'_R

                              $NP = 12$: N'_V

                              $NP = 13$: N'_R

                              $NP = 14$: N'_D

                              $NP = 21$: $X'_{VR} + M'$

                              $NP = 38$:   ALPHA(DEGREE)

                              $NP = 39$: U_C (FT./SEC.)

Table 7.1   Results of parallelly processing two identical files that
            have a phase shift.

- 198 -

NP = 13   MODEL VALUE =   -0.50000D-02

STARTING VALUE =   -0.40000D-02   + OR -   0.10000D-02
FILTERED VALUE =   -0.45867D-02   + OR -   0.27847D-03
IDENTIFIED WITHIN   8.27% OF THE MODEL VALUE

NP = 14   MODEL VALUE =   -0.24200D-02

STARTING VALUE =   -0.19400D-02   + OR -   0.48000D-03
FILTERED VALUE =   -0.24080D-02   + OR -   0.67848D-04
IDENTIFIED WITHIN   0.50% OF THE MODEL VALUE

NP = 21   MODEL VALUE =   0.30700D-01

STARTING VALUE =   0.24550D-01   + OR -   0.61000D-02
FILTERED VALUE =   0.29913D-01   + OR -   0.64329D-03
IDENTIFIED WITHIN   2.56% OF THE MODEL VALUE

NP = 39   MODEL VALUE =   0.13500D+01

STARTING VALUE =   0.16200D+01   + OR -   0.20000D+00
FILTERED VALUE =   0.13846D+01   + OR -   0.39322D-01
IDENTIFIED WITHIN   2.55% OF THE MODEL VALUE

NP = 38   MODEL VALUE =   0.86000D+02

STARTING VALUE =   0.68800D+02   + OR -   0.40000D+01
FILTERED VALUE =   0.86132D+02   + OR -   0.39346D+00
IDENTIFIED WITHIN   0.15% OF THE MODEL VALUE

NP = 6   MODEL VALUE =   -0.28280D-01

STARTING VALUE =   -0.22620D-01   + OR -   0.56000D-02
FILTERED VALUE =   -0.28397D-01   + OR -   0.13063D-02
IDENTIFIED WITHIN   0.41% OF THE MODEL VALUE

NP = 7   MODEL VALUE =   0.39100D-02

STARTING VALUE =   0.31200D-02   + OR -   0.78000D-03
FILTERED VALUE =   0.36204D-02   + OR -   0.52964D-03
IDENTIFIED WITHIN   7.41% OF THE MODEL VALUE

NP = 12   MODEL VALUE =   -0.10900D-01

STARTING VALUE =   -0.87200D-02   + OR -   0.22000D-02
FILTERED VALUE =   -0.98447D-02   + OR -   0.57212D-03
IDENTIFIED WITHIN   9.68% OF THE MODEL VALUE

Table 7.1   Continued.
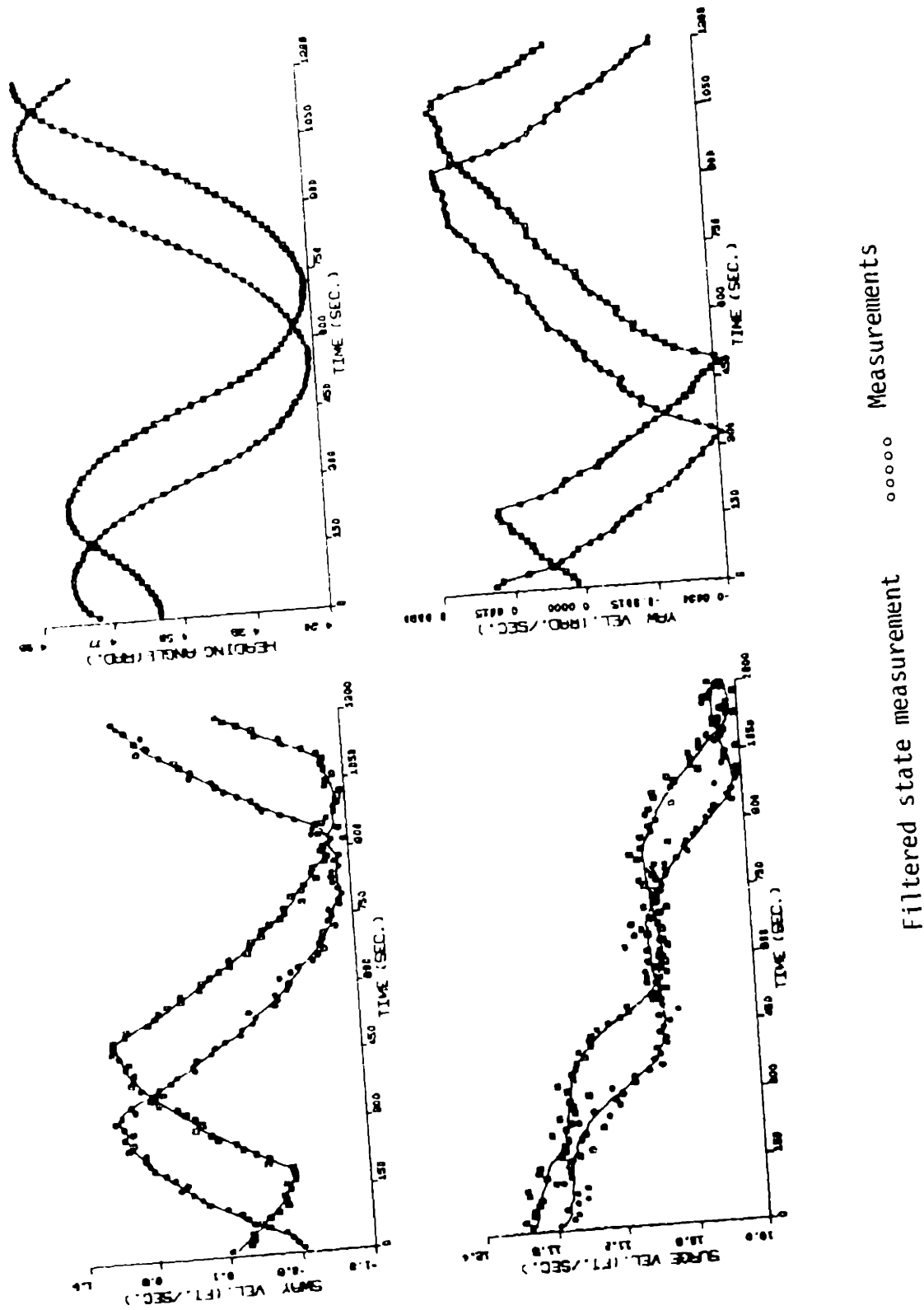
Figure 7.1.a Results of parallelly processing two identical files that have a phase shift - the filtering of state measurements.

_____ Filtered state measurement   ooooo Measurements
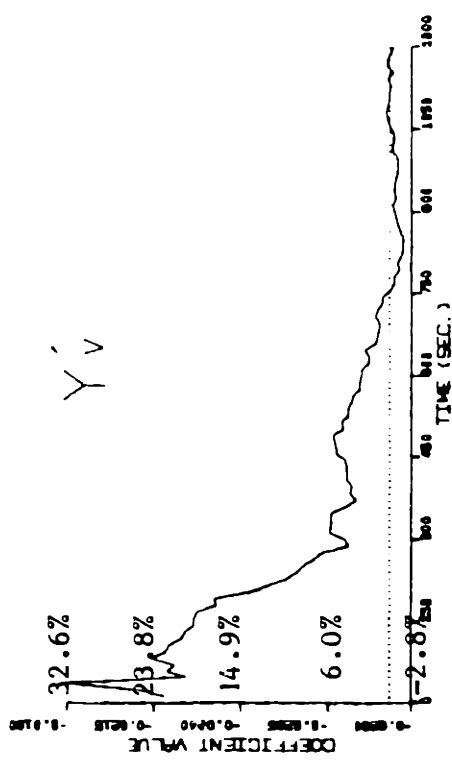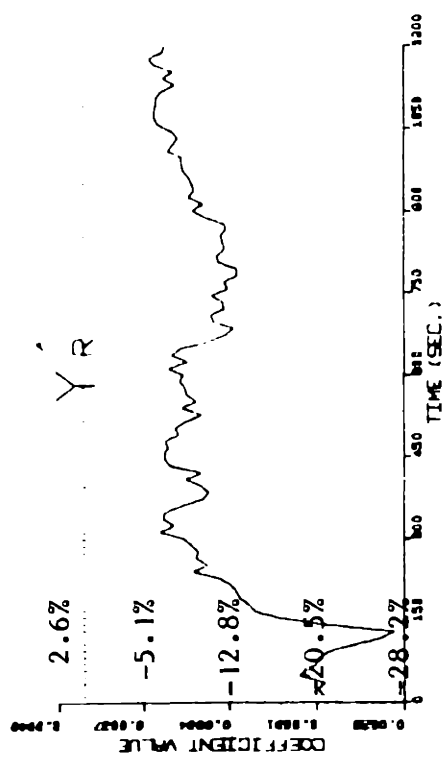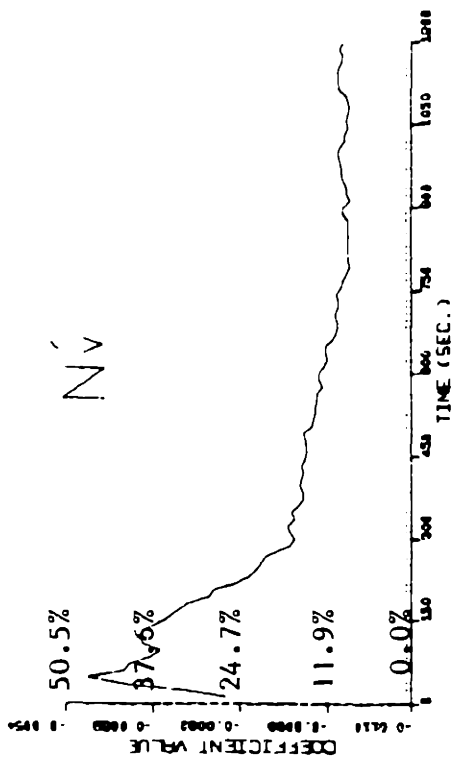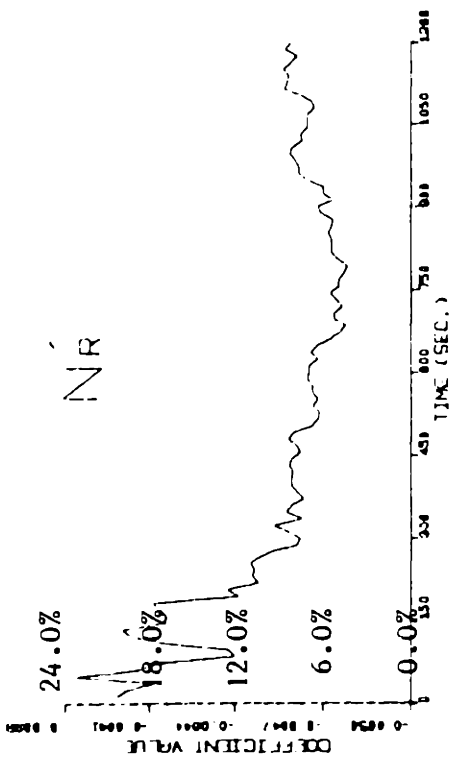
Figure 7.1.b Results of parallelly processing two identical files that have a phase
shift - the estimation of coefficients.
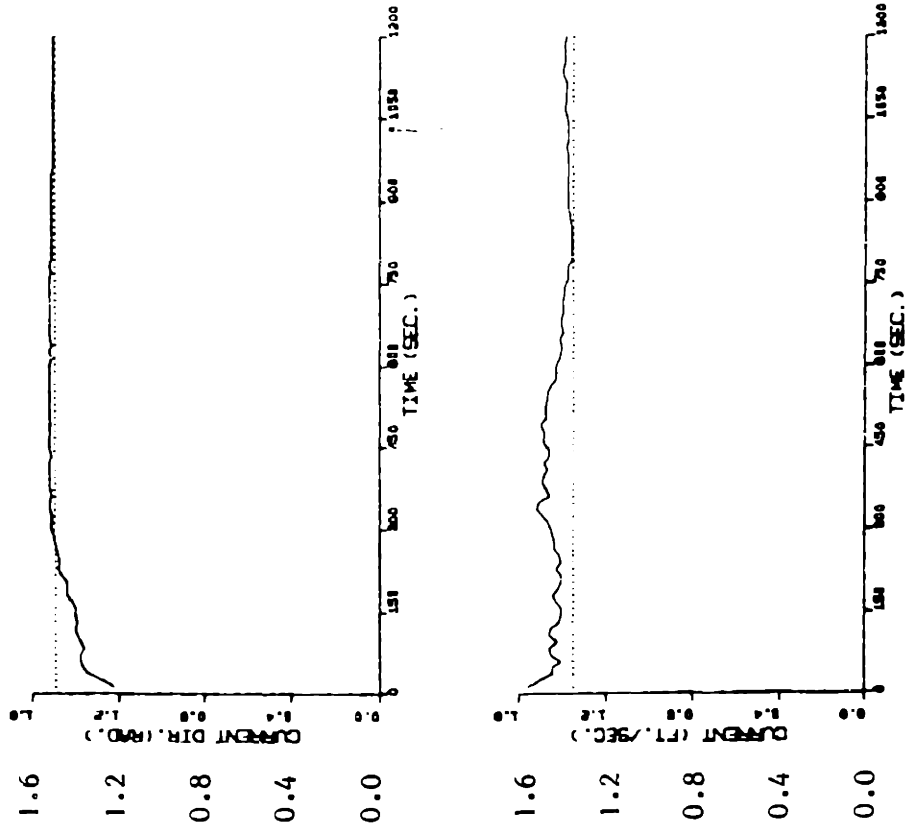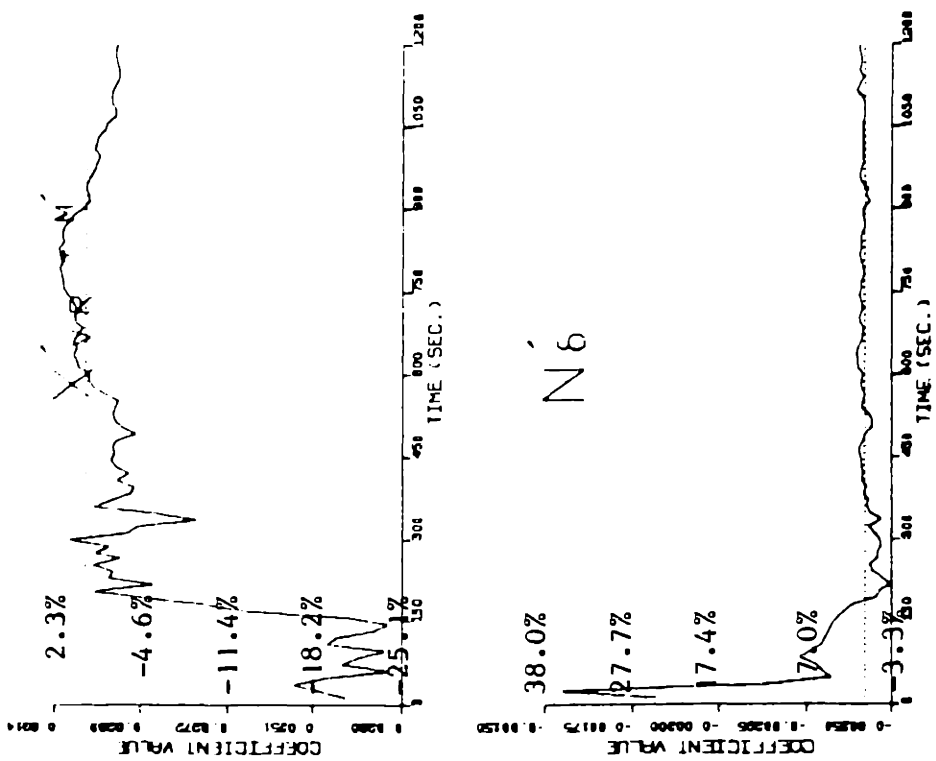
Figure 7.1.c Results of parallelly processing two identical files that have a phase
shift – the estimation of coefficients and current.

——— Estimation   ⋯⋯ True value

NP = 39   MODEL VALUE =   0.13500D+01

STARTING VALUE =   0.13570D+01 + OR -   0.20000D+00
FILTERED VALUE =   0.13450D+01 + OR -   0.33316D-01
IDENTIFIED WITHIN   0.37% OF THE MODEL VALUE

NP = 38   MODEL VALUE =   0.86000D+02

STARTING VALUE =   0.86500D+02 + OR -   0.40000D+01
FILTERED VALUE =   0.86712D+02 + OR -   0.31281D+00
IDENTIFIED WITHIN   0.83% OF THE MODEL VALUE

NP = 6   MODEL VALUE =   -0.28280D-01

STARTING VALUE =   -0.27540D-01 + OR -   0.56000D-02
FILTERED VALUE =   -0.26061D-01 + OR -   0.13213D-02
IDENTIFIED WITHIN   7.85% OF THE MODEL VALUE

NP = 7   MODEL VALUE =   0.39100D-02

STARTING VALUE =   0.43600D-02 + OR -   0.78000D-03
FILTERED VALUE =   0.51721D-02 + OR -   0.54263D-03
IDENTIFIED WITHIN   32.28% OF THE MODEL VALUE

NP = 12   MODEL VALUE =   -0.10900D-01

STARTING VALUE =   -0.12590D-01 + OR -   0.22000D-02
FILTERED VALUE =   -0.13459D-01 + OR -   0.86949D-03
IDENTIFIED WITHIN   23.48% OF THE MODEL VALUE

NP = 13   MODEL VALUE =   -0.50000D-02

STARTING VALUE =   -0.58600D-02 + OR -   0.10000D-02
FILTERED VALUE =   -0.62595D-02 + OR -   0.41425D-03
IDENTIFIED WITHIN   25.19% OF THE MODEL VALUE

NP = 14   MODEL VALUE =   -0.24200D-02

STARTING VALUE =   -0.26400D-02 + OR -   0.48000D-03
FILTERED VALUE =   -0.27060D-02 + OR -   0.94269D-04
IDENTIFIED WITHIN   11.82% OF THE MODEL VALUE

NP = 21   MODEL VALUE =   0.30700D-01

STARTING VALUE =   0.30270D-01 + OR -   0.61000D-02
FILTERED VALUE =   0.0407D-01 + OR -   0.59732D-03
IDENTIFIED WITHIN   0.96% OF THE MODEL VALUE

Table 7.2   Results of parallelly processing two identical files that have a phase
shift - 3rd pass of the estimation.
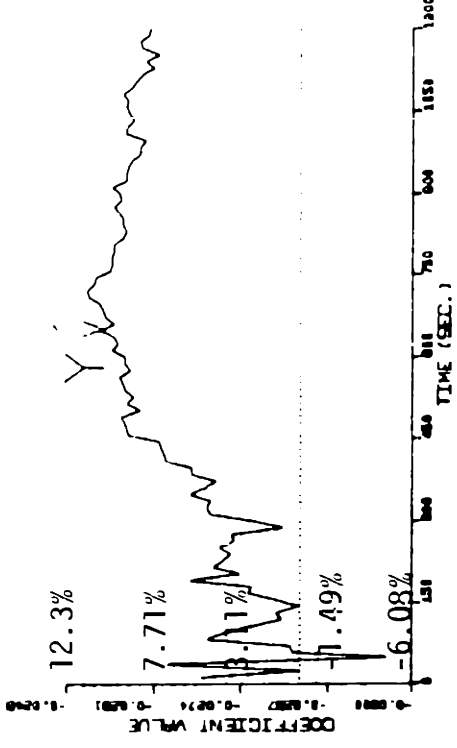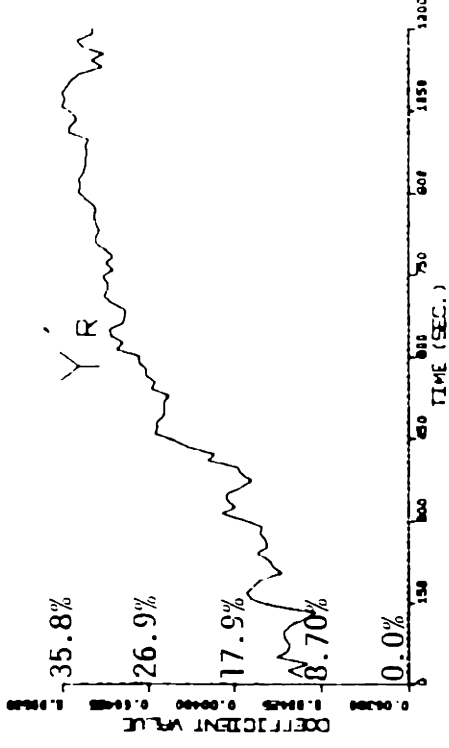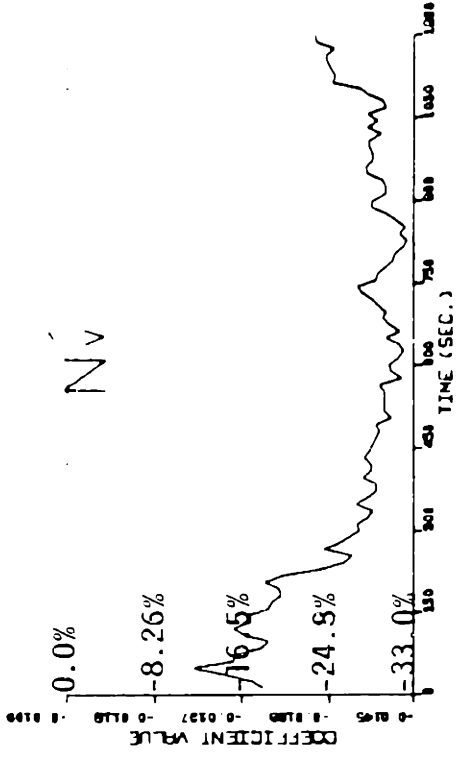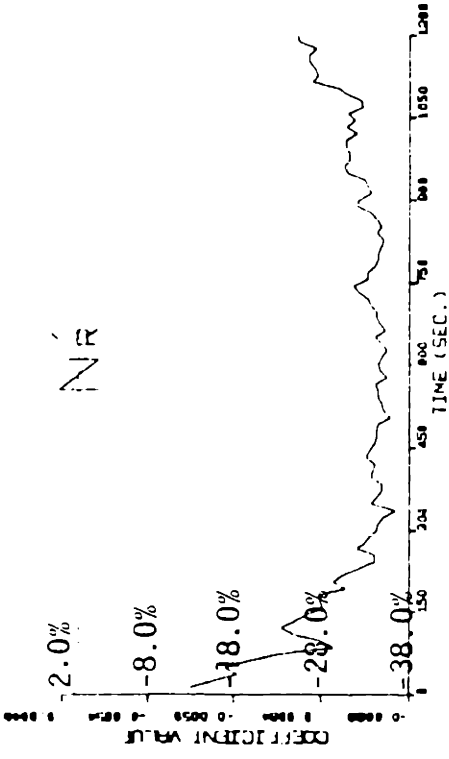
Figure 7.2.a   Results of parallelly processing two identical files that have a phase shift - 3rd pass of the estimation of coefficients.
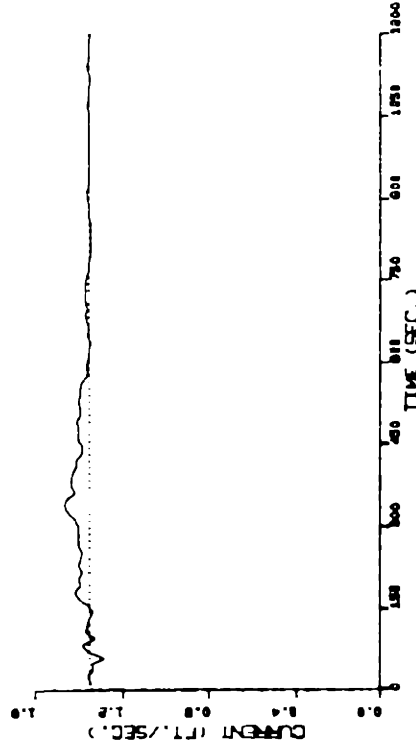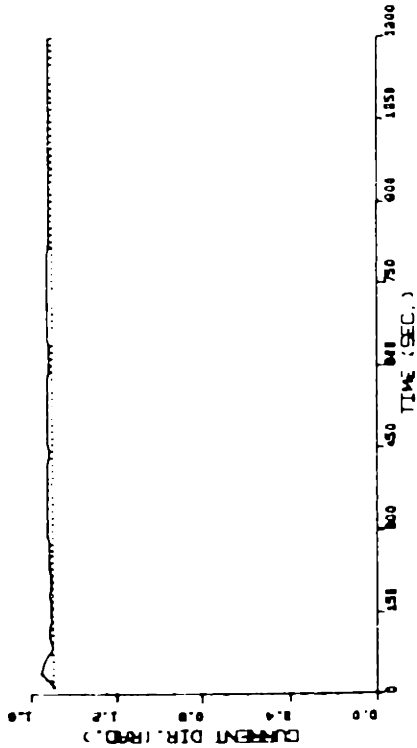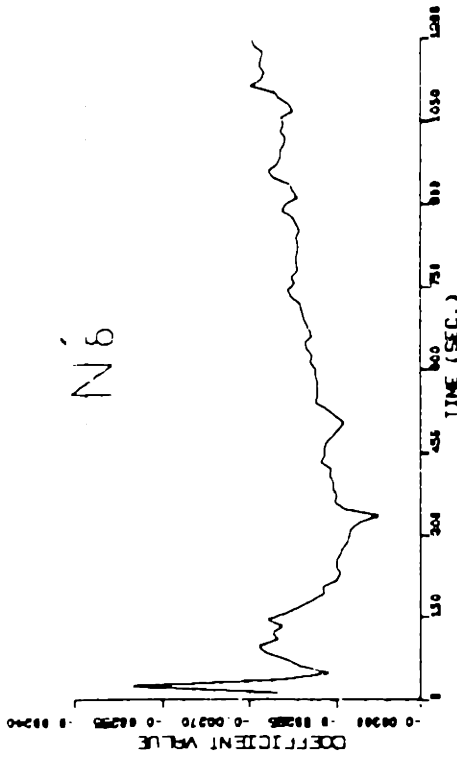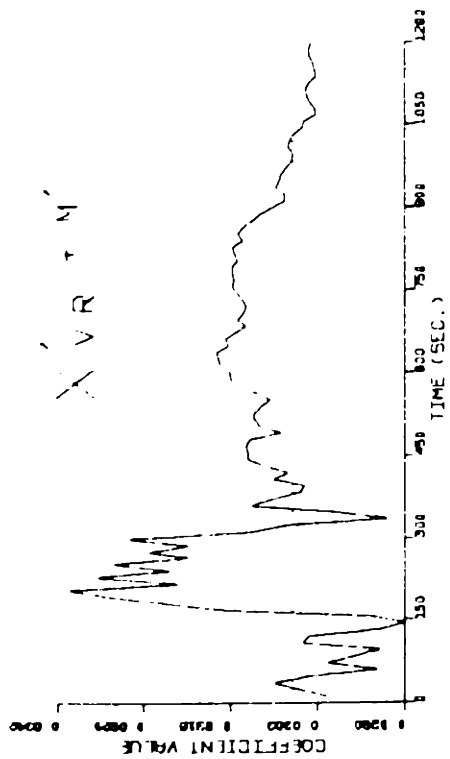
────── Estimation   ...... True value

Figure 7.2.b   Results of parallelly processing two identical files that have a phase
shift – 3rd pass of the estimation of coefficients and current.
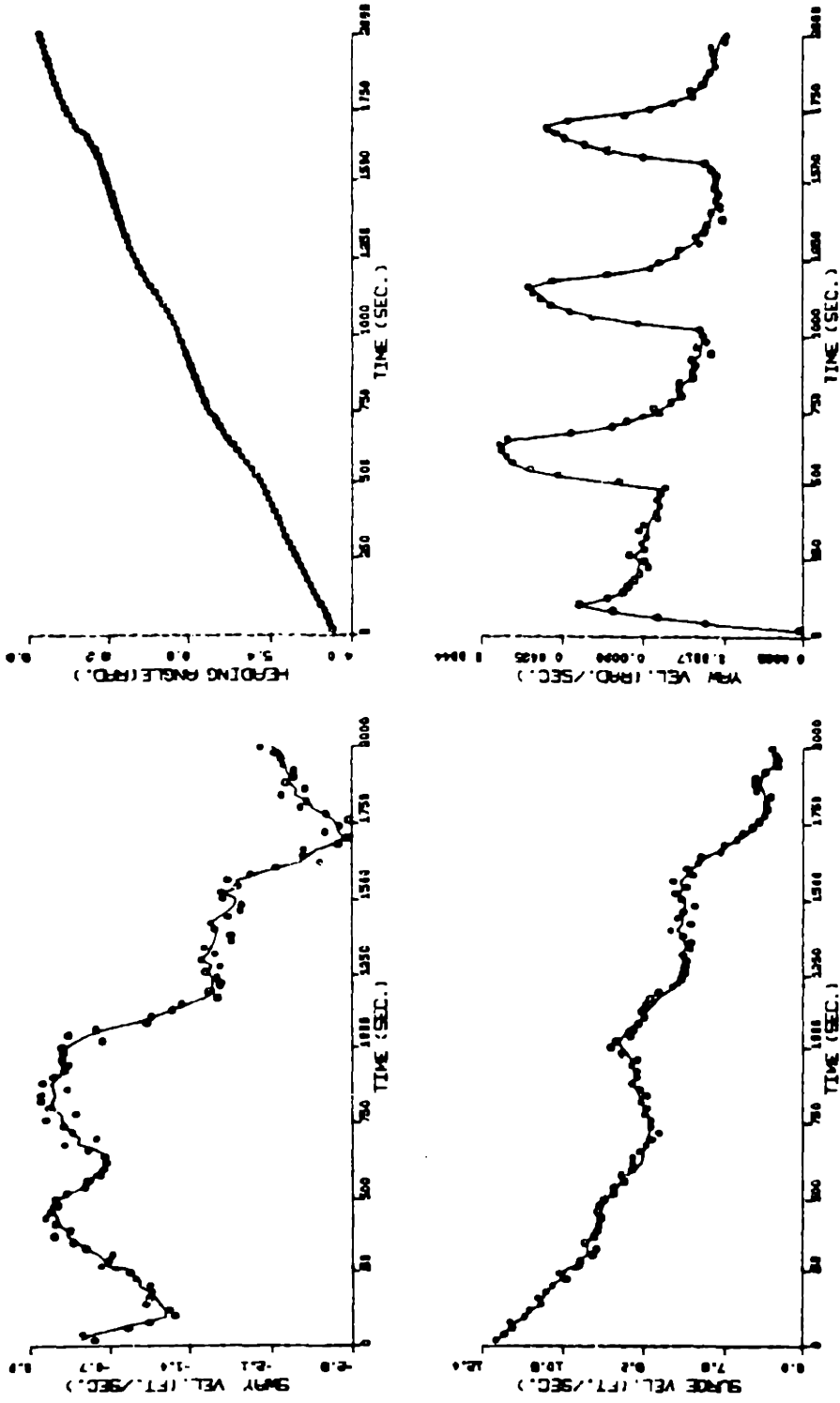
—————— Estimation   ⋯⋯⋯ True value

Figure 7.3.a Results of identification. Biased zigzag maneuvering data (simulated)
is processed to estimate the nonlinear coefficient.

ooooo Measurement

——— Filtered state measurement
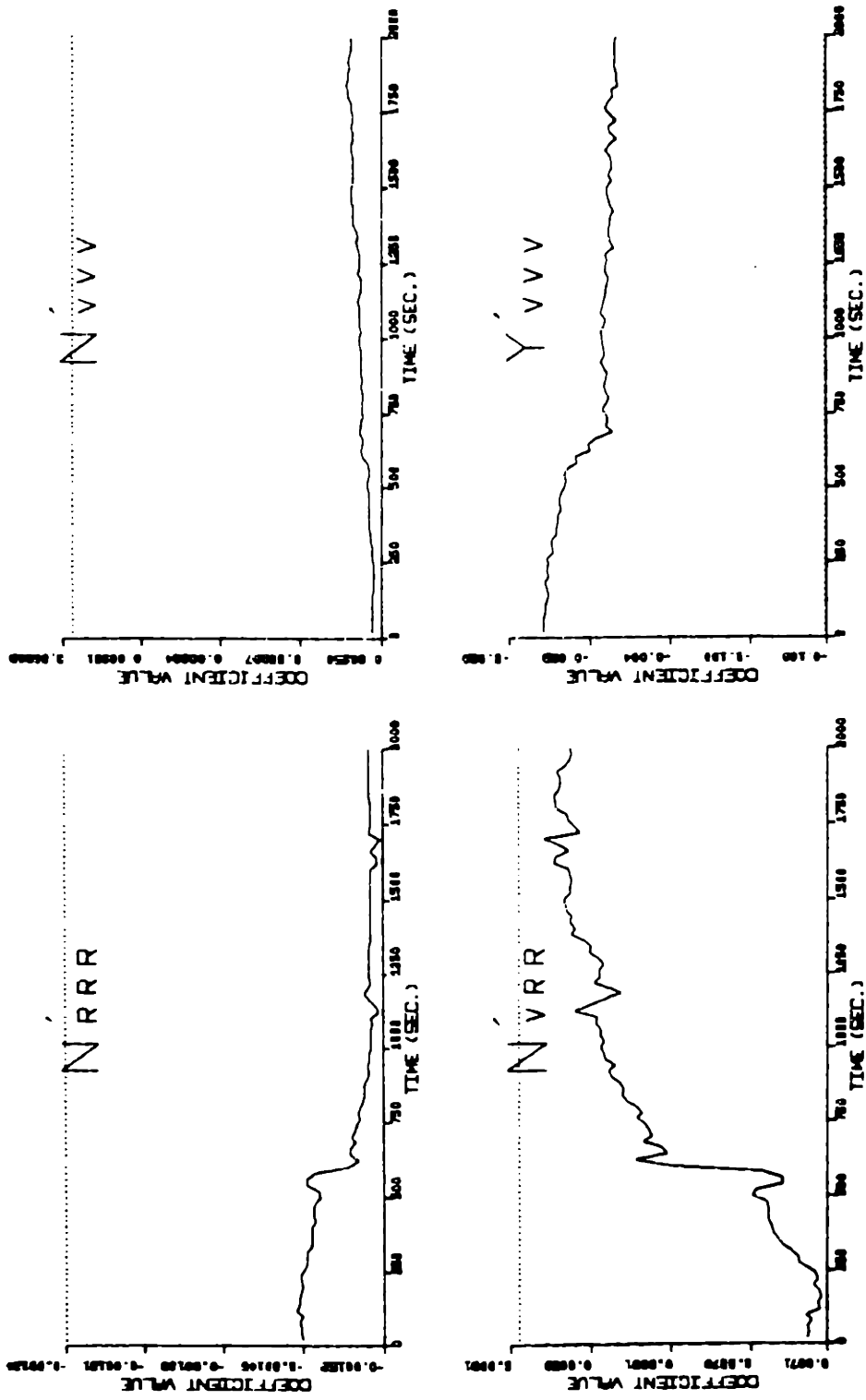
Figure 7.3.b Results of identification. Biased zigzag maneuvering data(simulated) is processed to estimate the nonlinear coefficients.
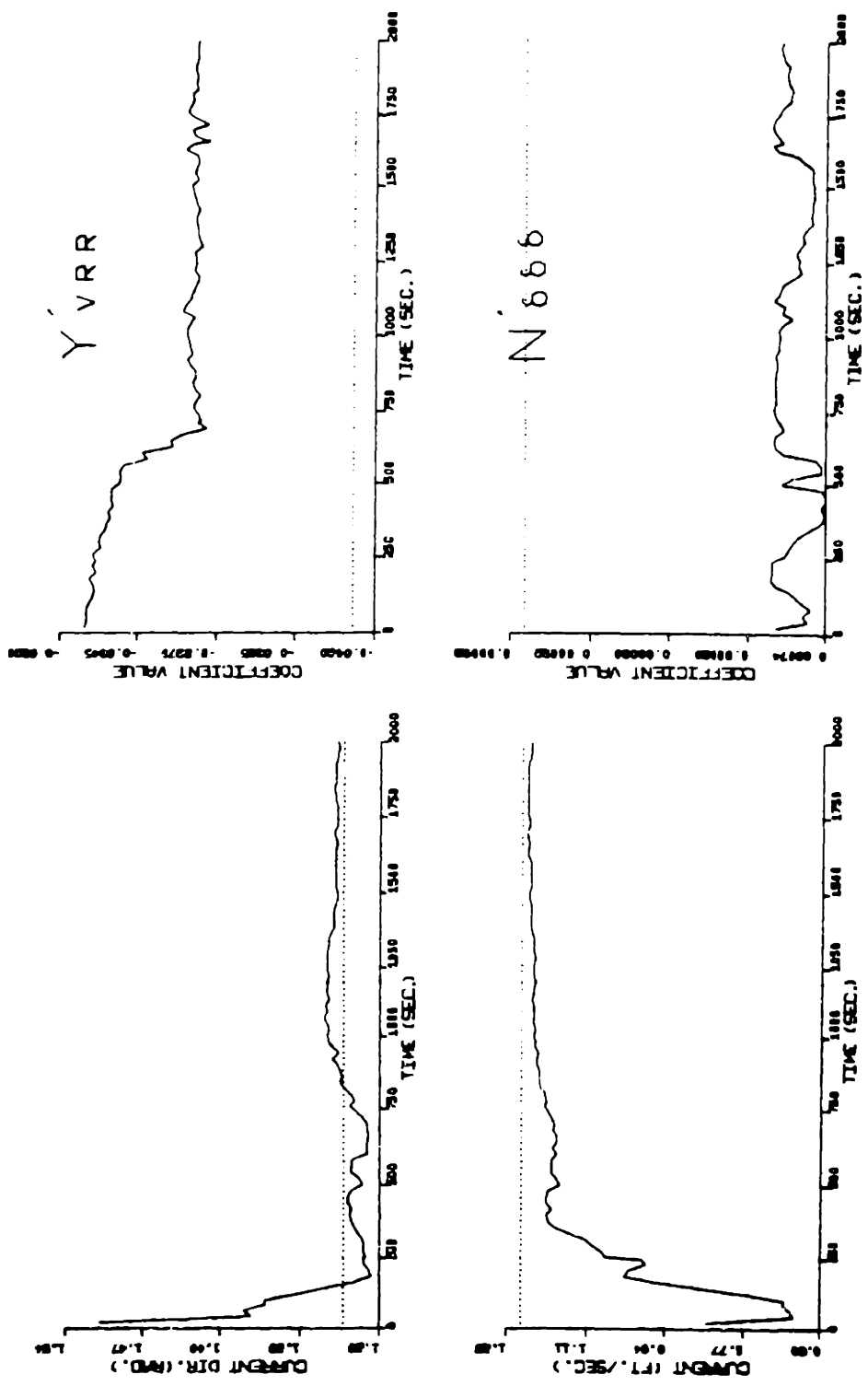
Figure 7.3.c Results of identification. Biased zigzag maneuvering data(simulated) is processed to estimate the nonlinear coefficients.

────── Estimation

...... True value

- 208 -

ooooo Measurement

———— Filtered state measurement
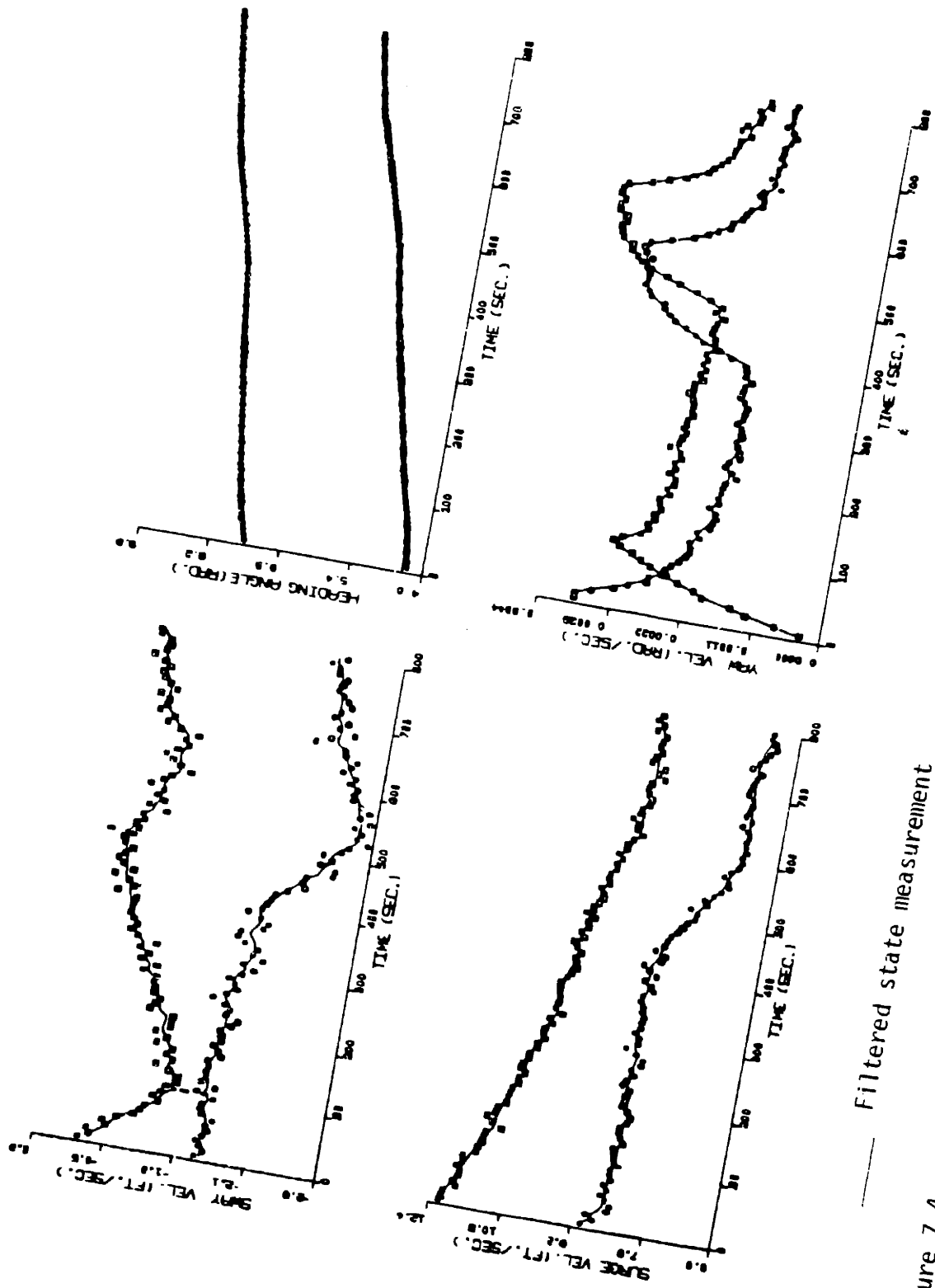
Figure 7.4.a Results of identification. The first portion and the second portion of the data file in Fig. 7.3.a, which are of 180° difference in heading, are parallelly processed to estimate the nonlinear coefficients.
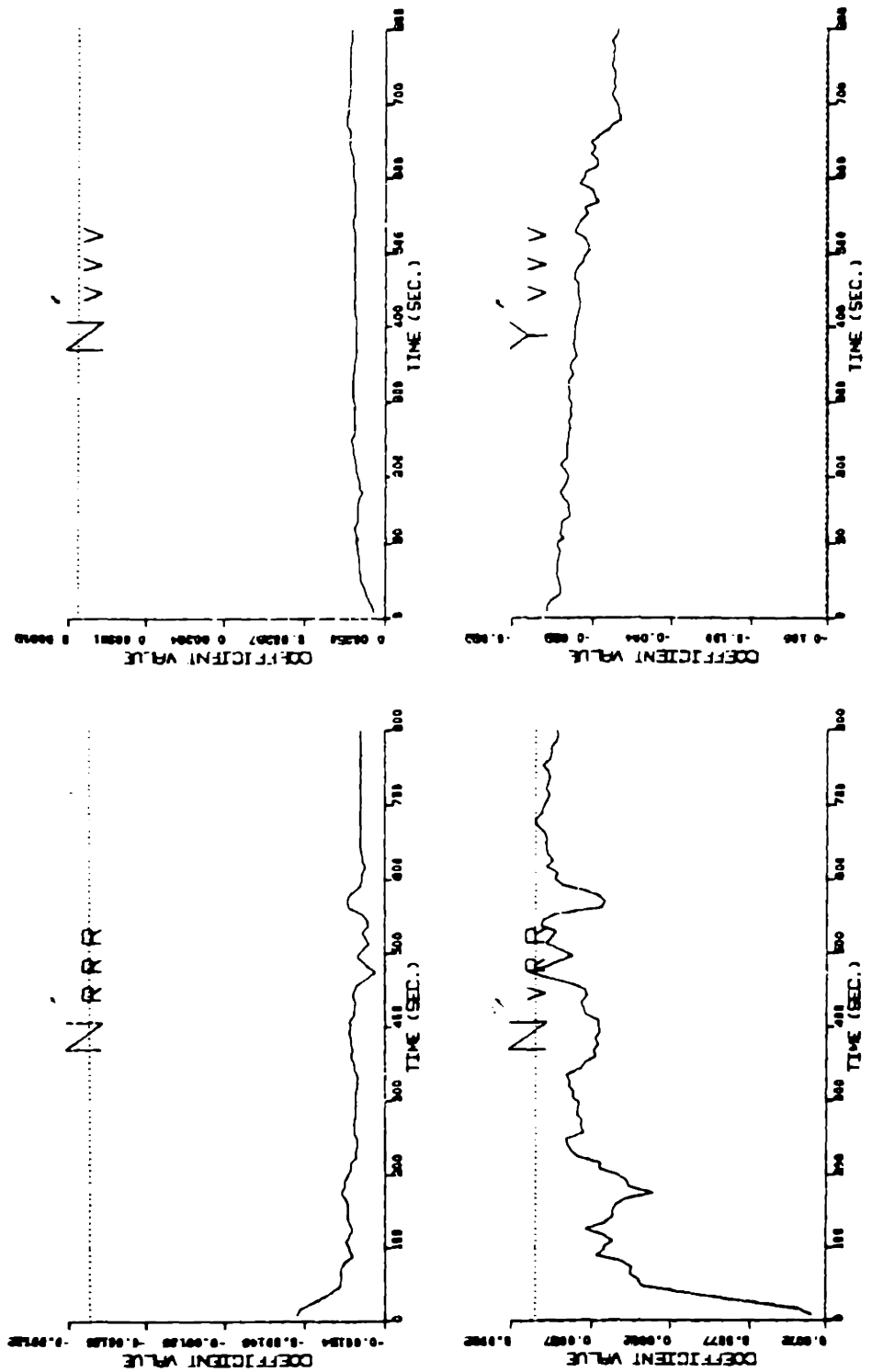
Figure 7.4.b Results of identification. The first portion and the second portion of the data file in Fig. 7.3.a, which are of 180° difference in heading, are parallelly processed to estimate the nonlinear coefficients.
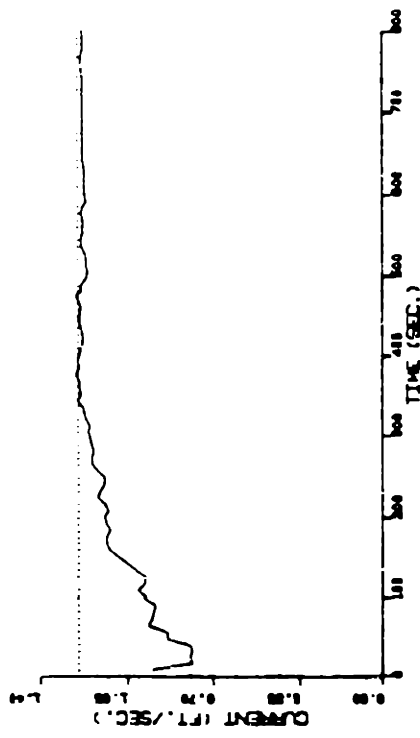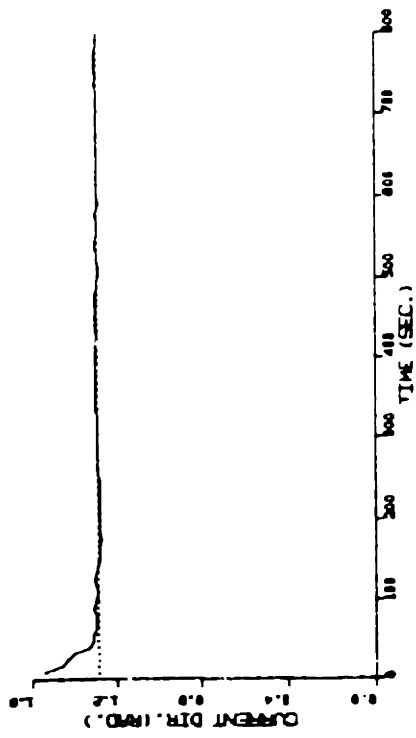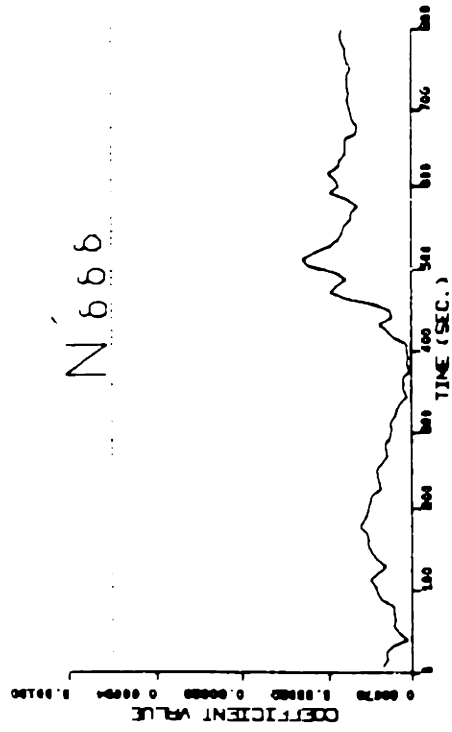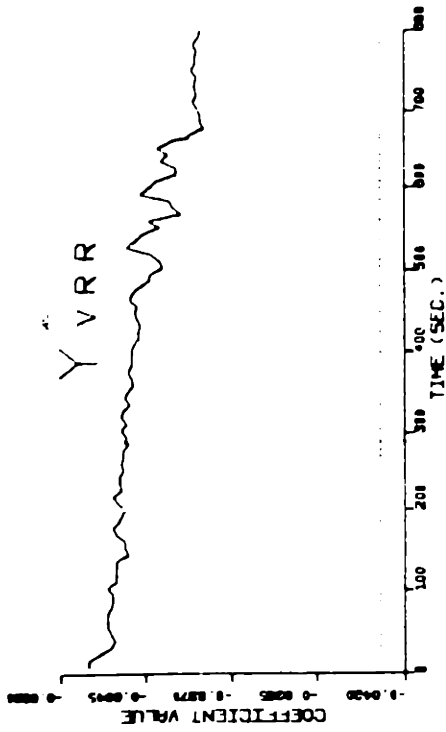
—————— Estimation   .... True value

Figure 7.4.c   Results of identification
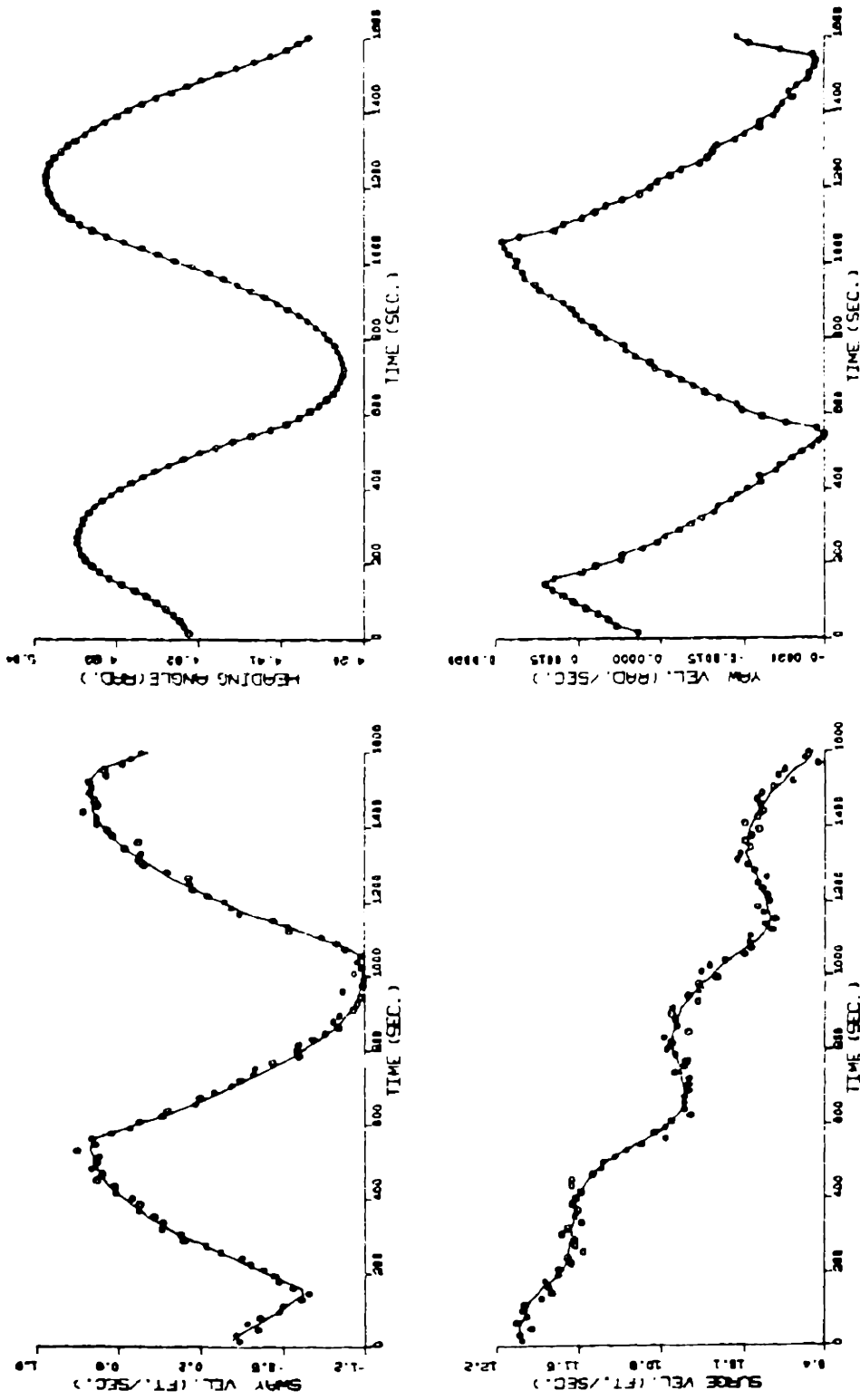
Figure 7.5.a Results of identification. Application of the "exaggerated over- and under-estimated initial guess" scheme to estimate the coefficients from simulated 10°/10° zigzag maneuvering data of ESSO OSAKA.

ーーーーーー Filtered state measurement　　ooooo Measurement
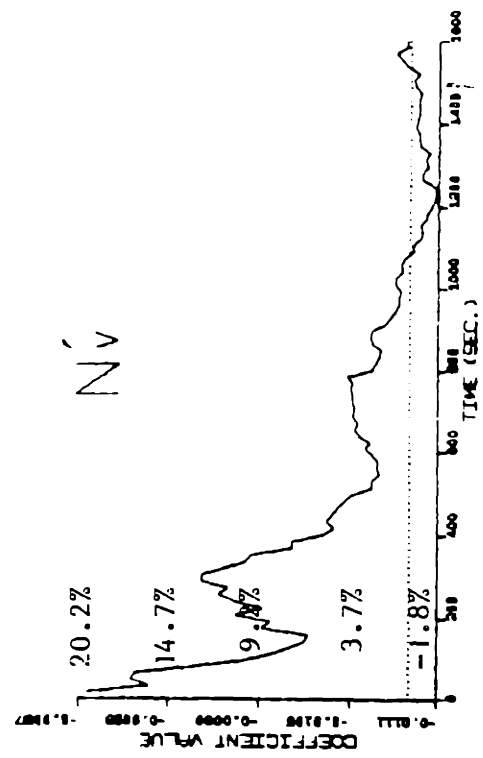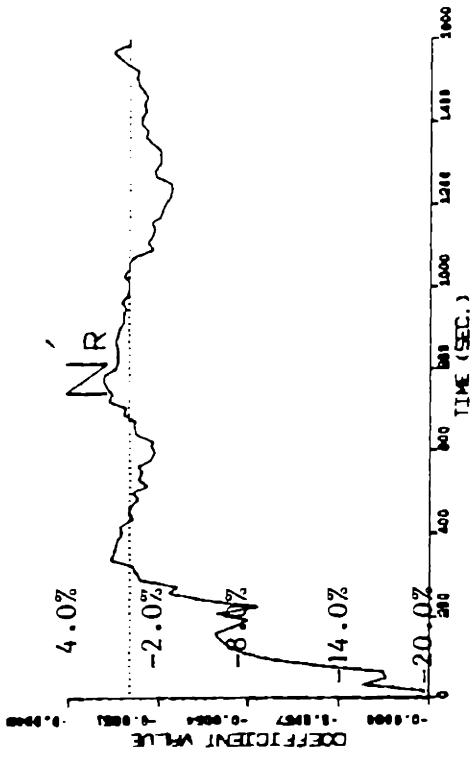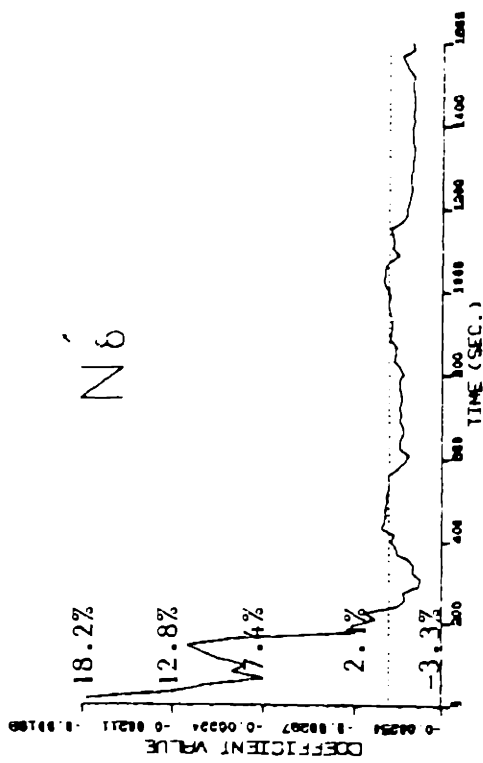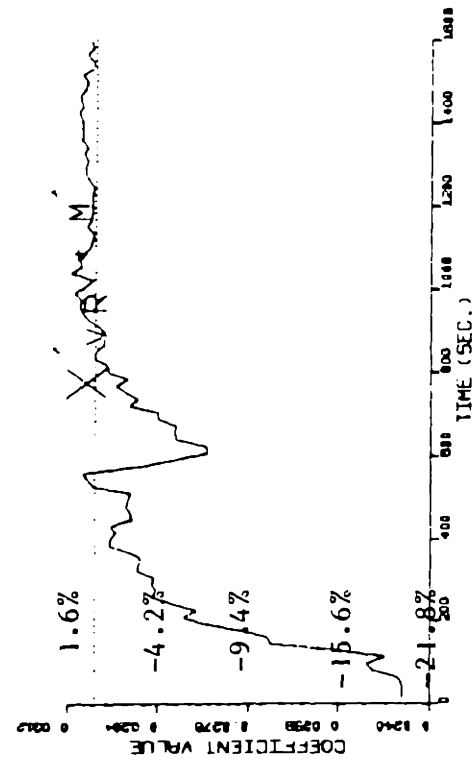
Figure 7.5.b Results of identification.
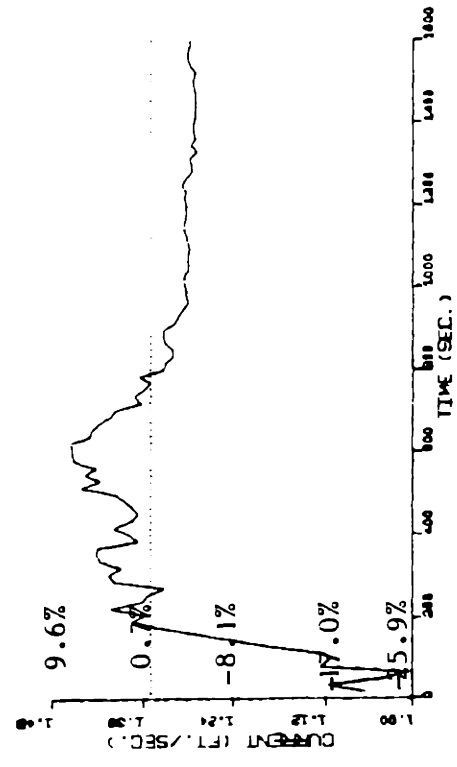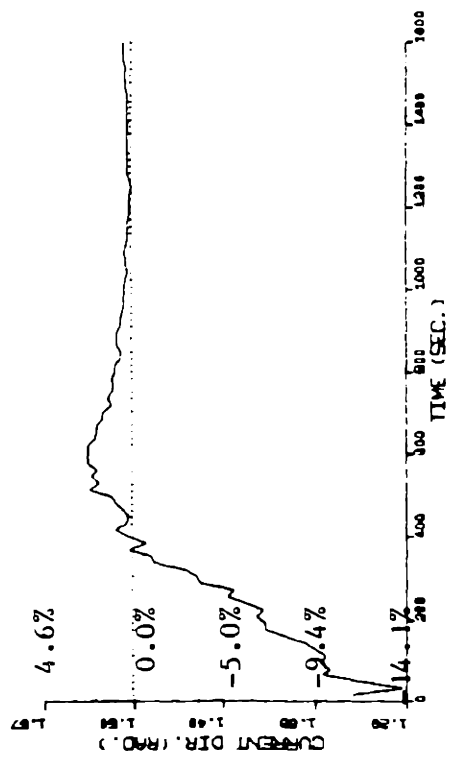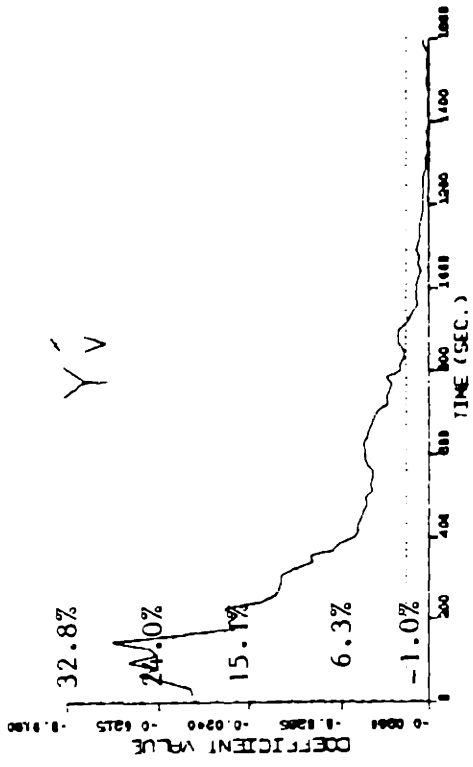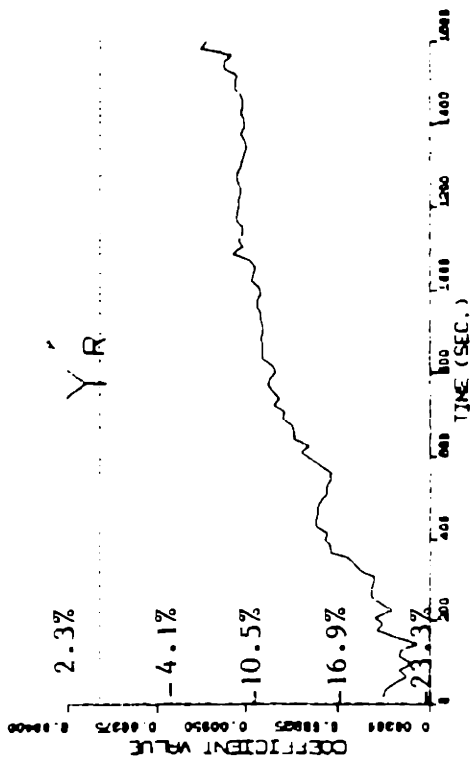
─────── Estimation   ...... True value

Figure 7.5.c   Results of identification

─── Estimation   ..... True value
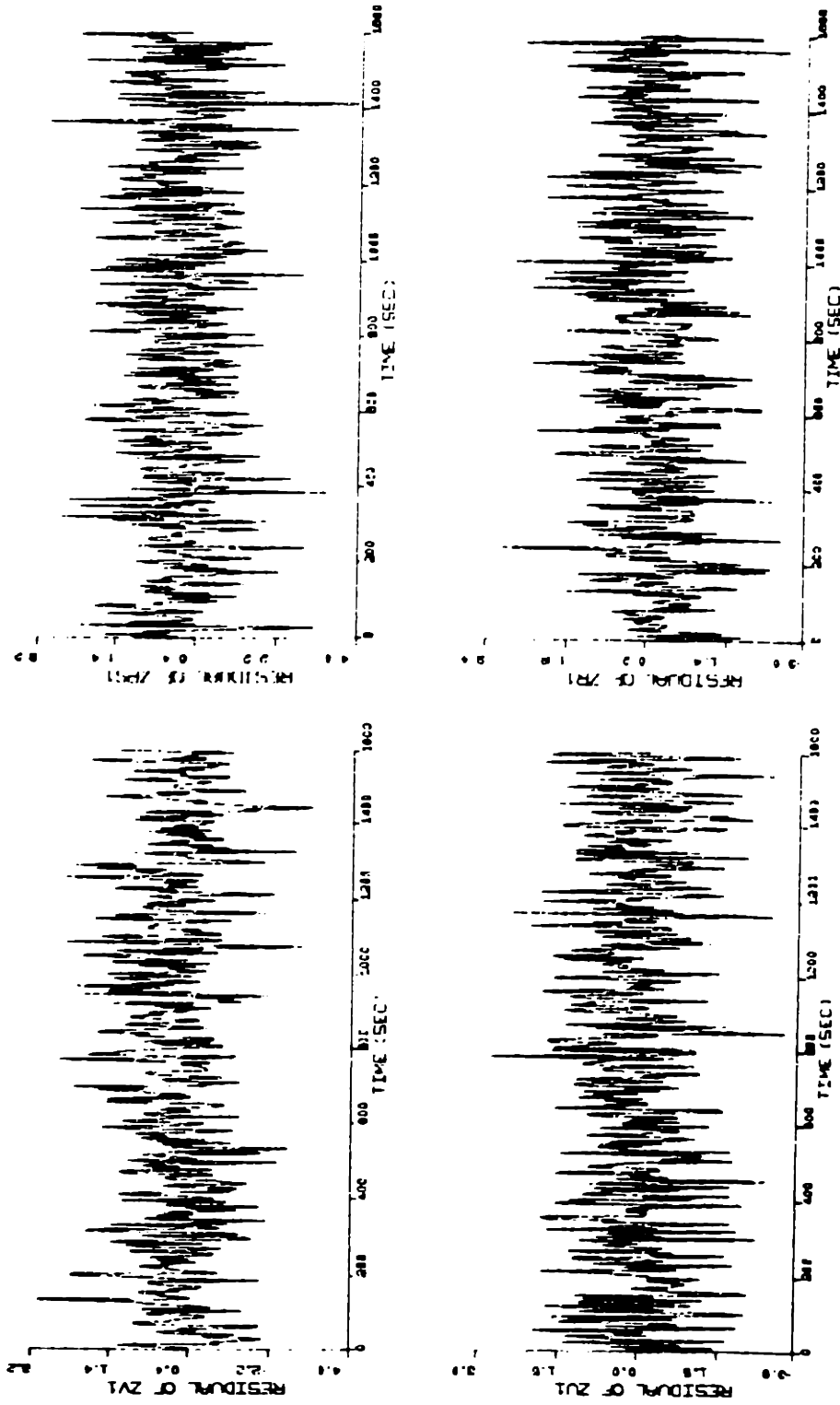
Figure 7.6.a Validity tests for the results of identification in Fig. 7.5.
Plots of normalized residuals.
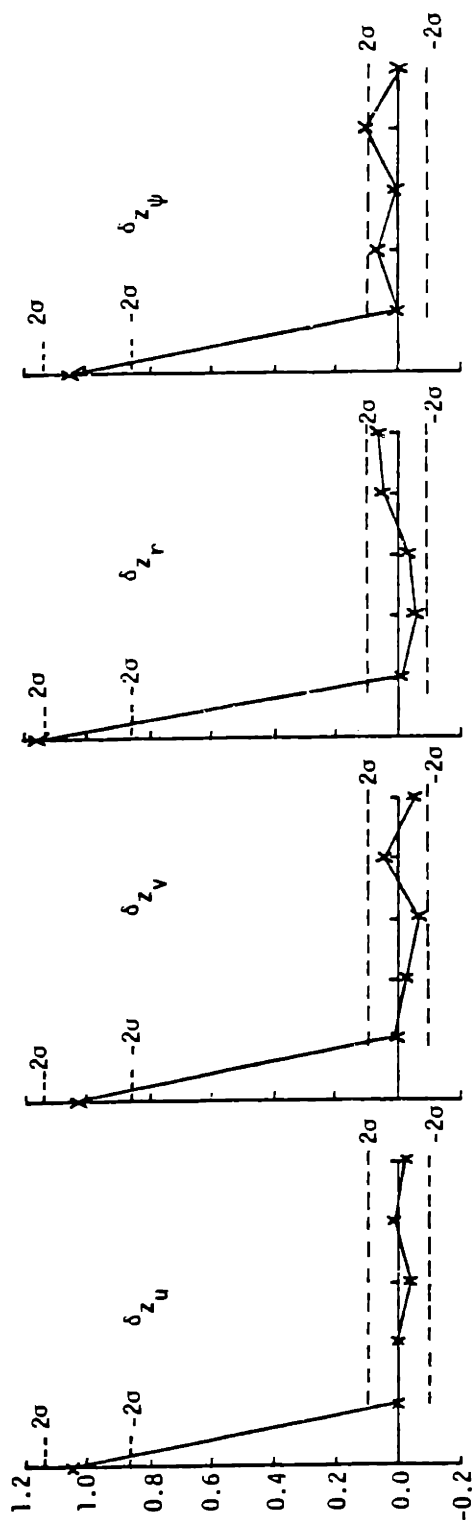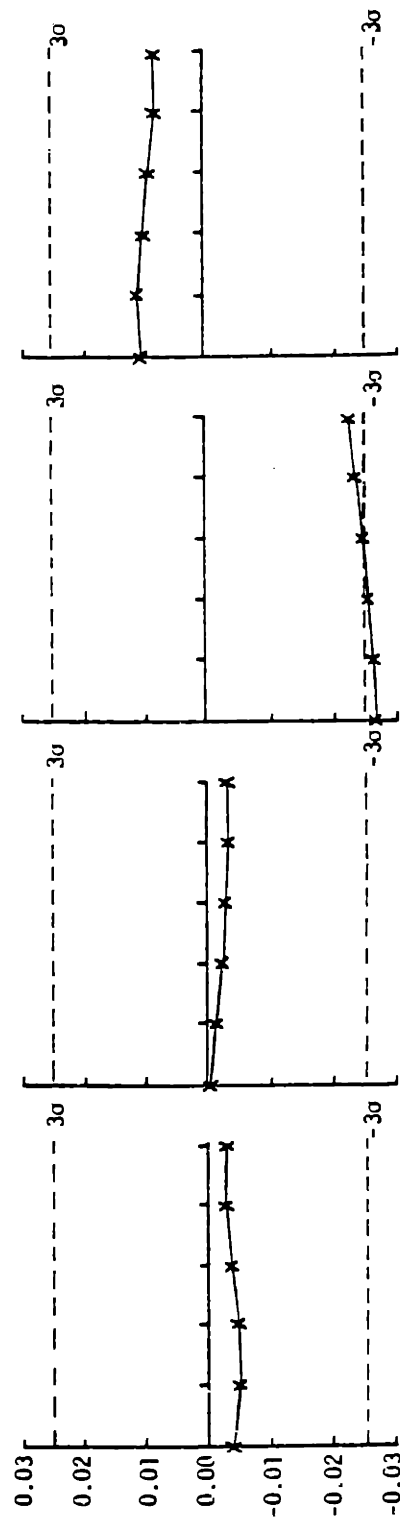
Sum of squared residuals=1706.3
If H₀ is true, E[sum of squared residuals]=1600.0, σ=56.57

Figure 7.6.b Validity tests for the results of identification in Fig. 7.5.
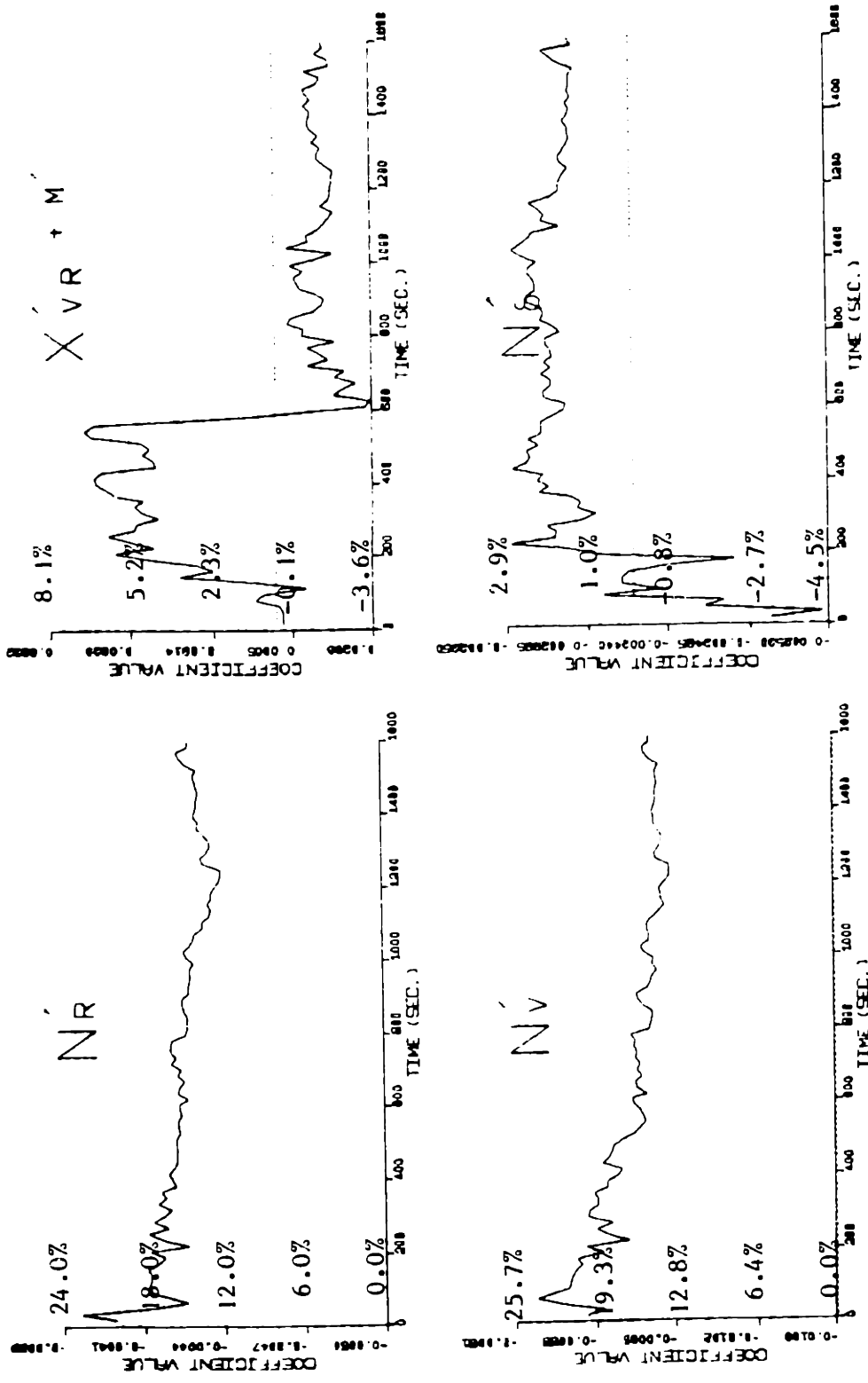
Figure 7.7.a Results of identification. The early occurance of simultaneous drift is obtained by providing a bad initial guess to the filter. The same simulated maneuvering data as in Fig. 7.5.a is processed here.
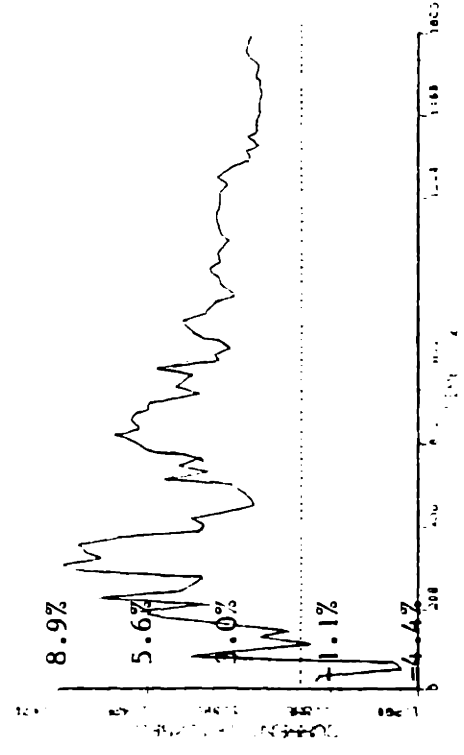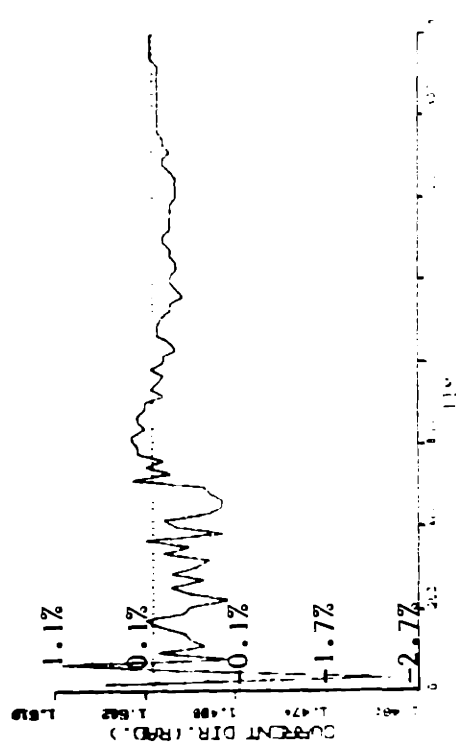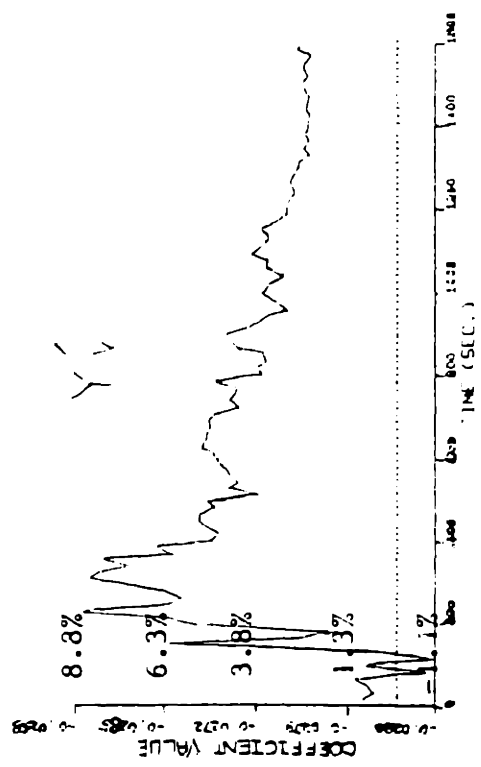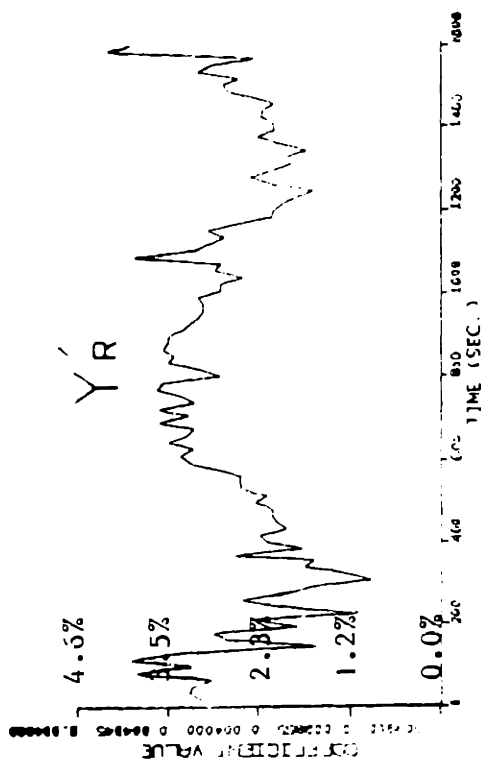
Figure 7.7.b   Results of identification

——————   Estimation

· · · · · ·   True value
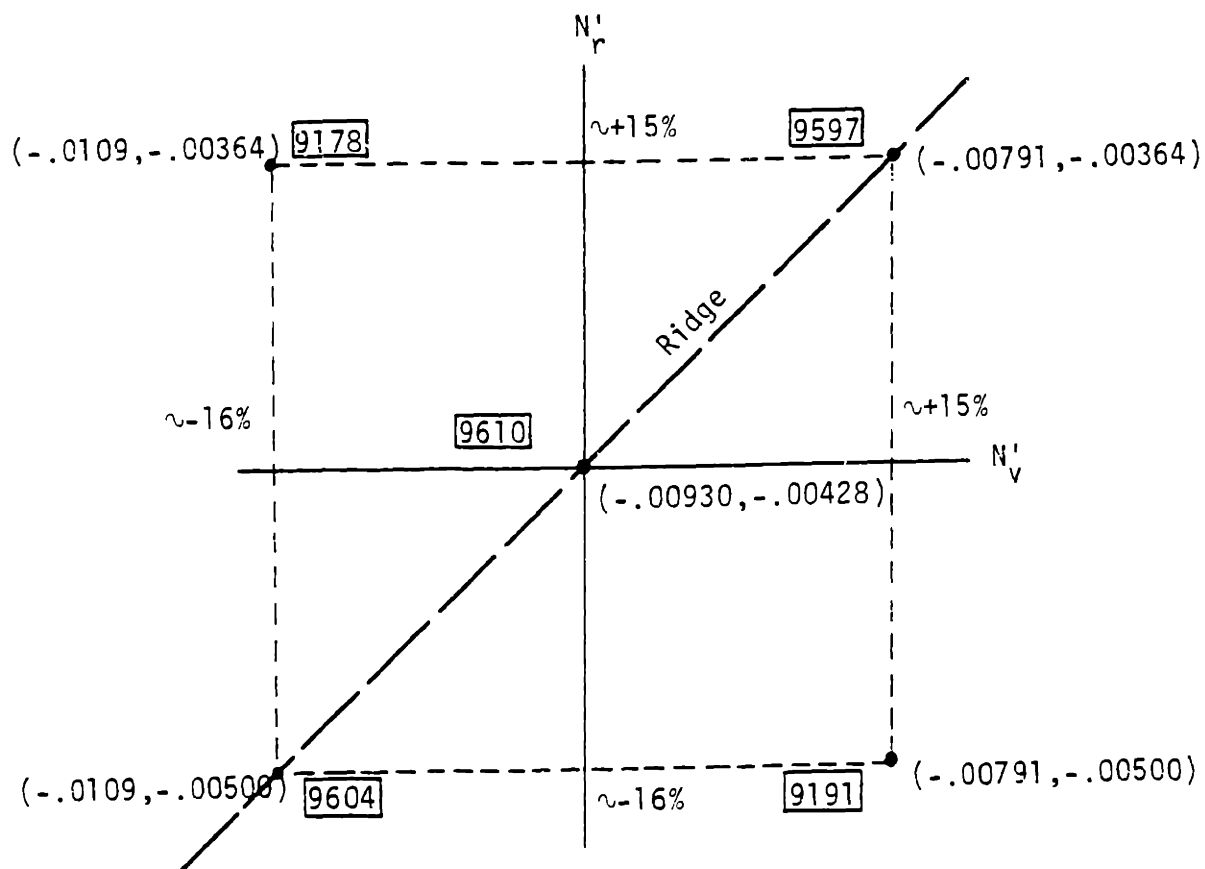
Figure 7.8 Ridge of log likelihood surface
(the number in the box is the log
likelihood at that point)
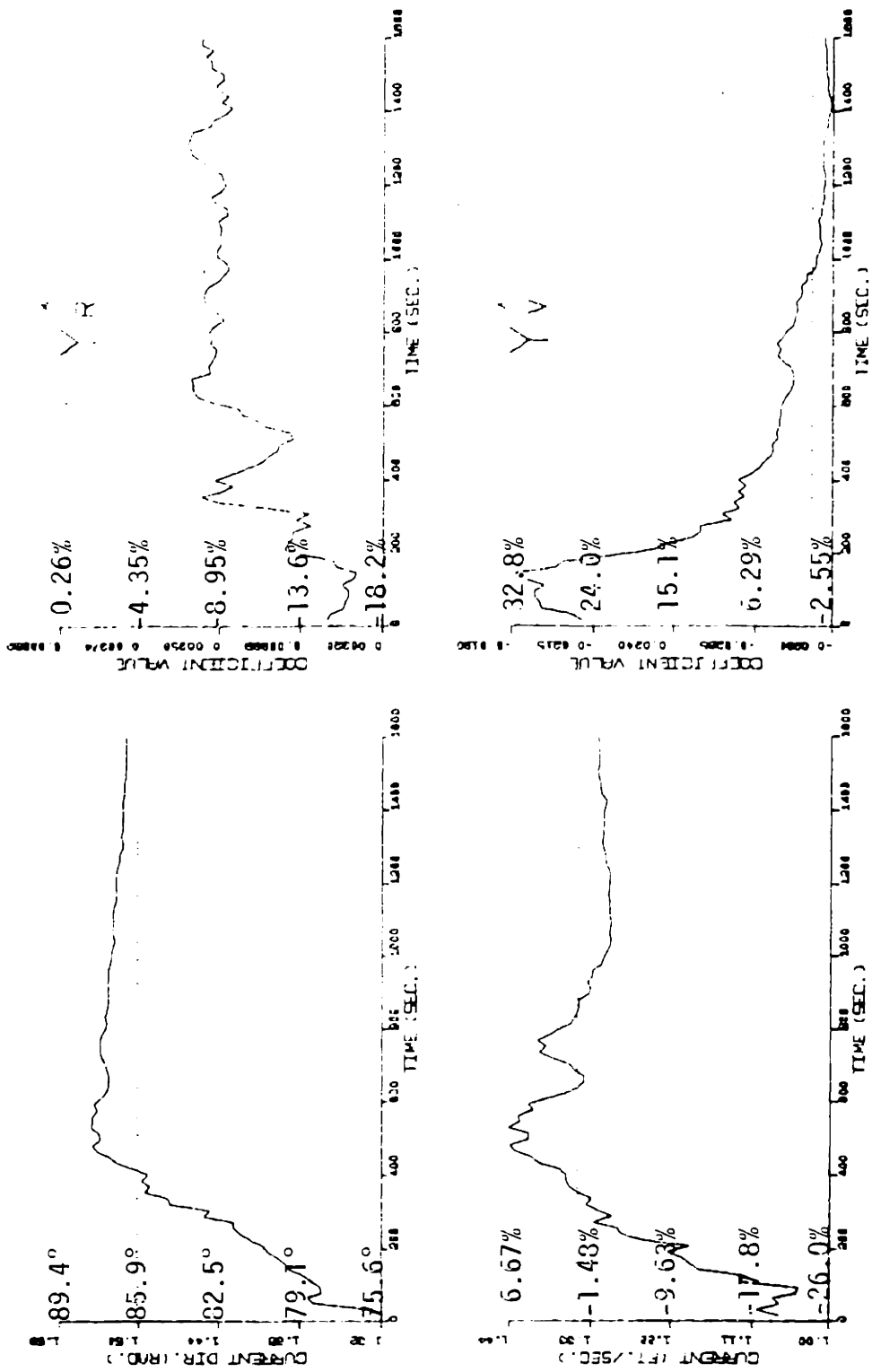
Figure 7.8-1.a   Results of identification.   Application of the "exaggerated over- and under-
estimated initial guesses" scheme to estimate the coefficients from the
simulated 10°/10° zigzag maneuvering data of ESSO OSAKA
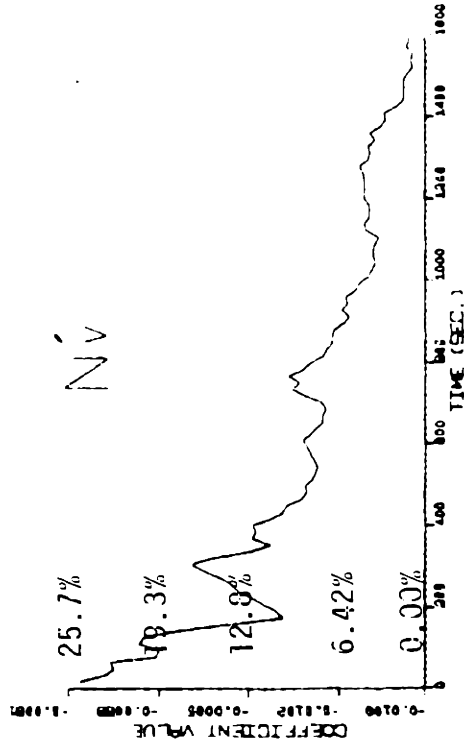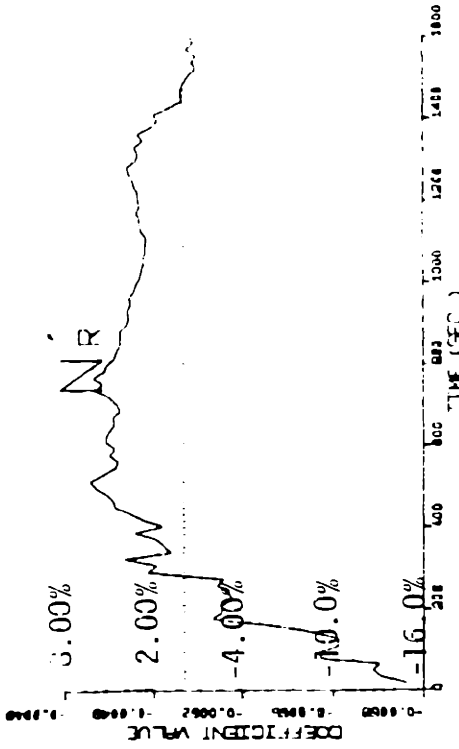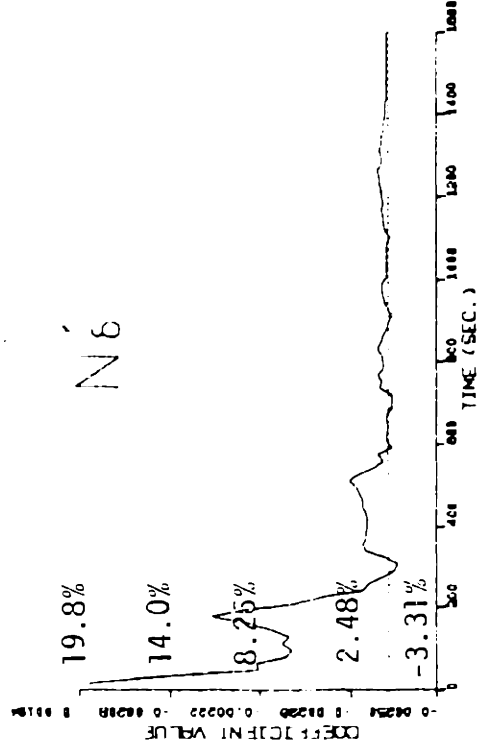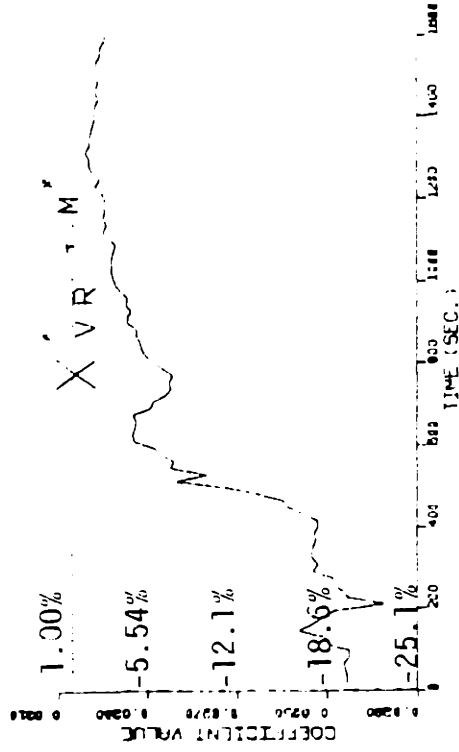
——— Estimation   ······· True value

Figure 7.8-1.b Results of identification

——— Estimation   ······· True value

- 221 -
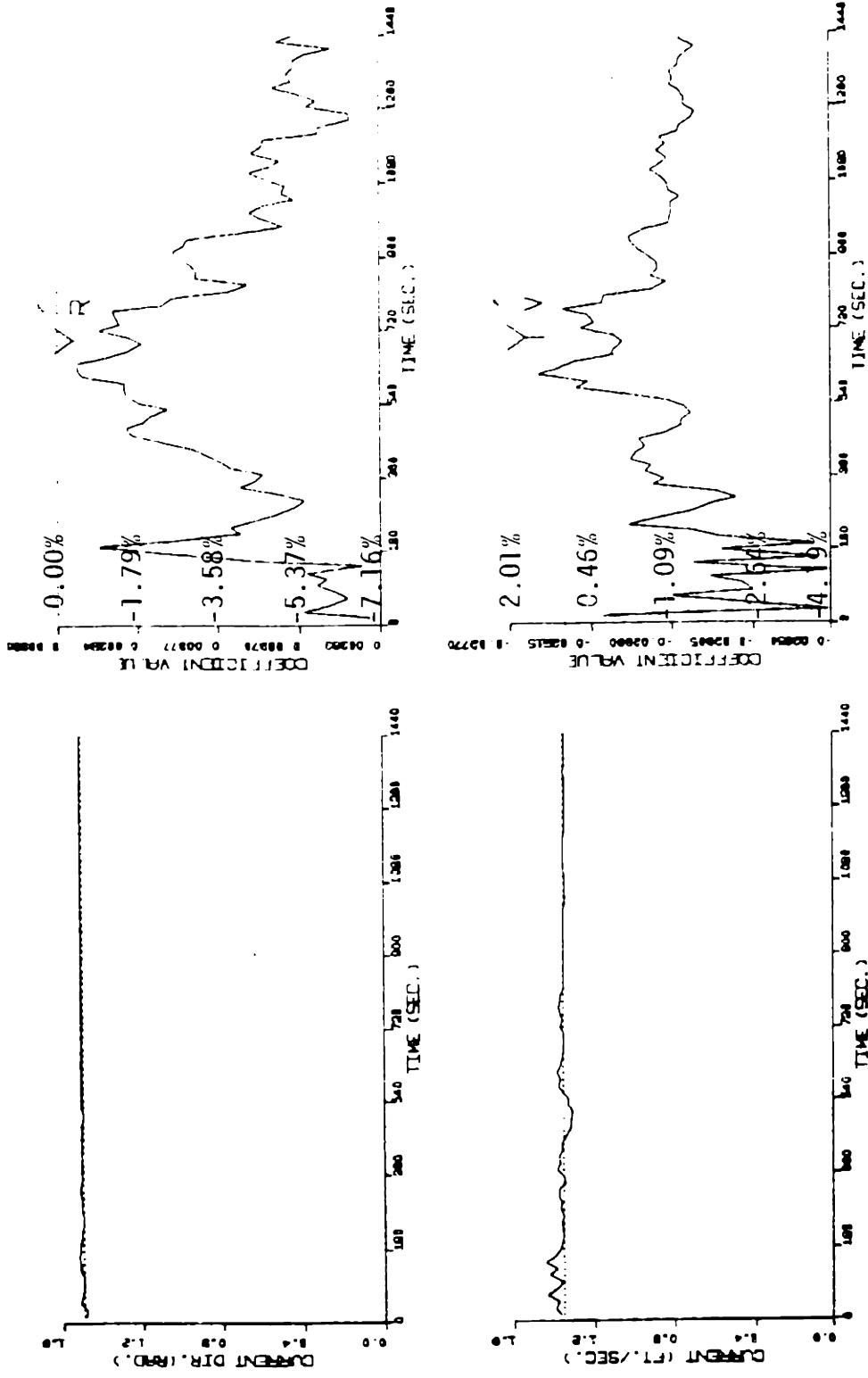
Figure 7.8-2.a Results of identification. Application of the "exaggerated over- and under-
estimated initial guesses" scheme and "parallel processing" scheme to esti-
mate the coefficients from the simulated 10°/10° zigzag maneuvering data
of ESSO OSAKA, second pass.

Estimation ——————   .... True value

- 222 -
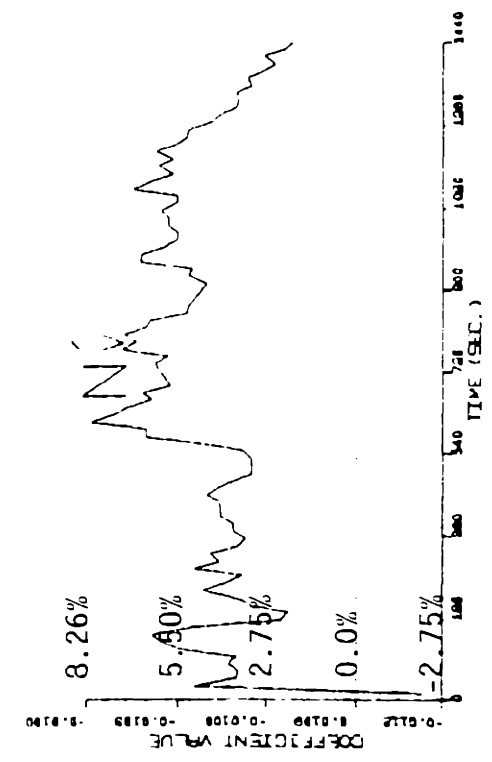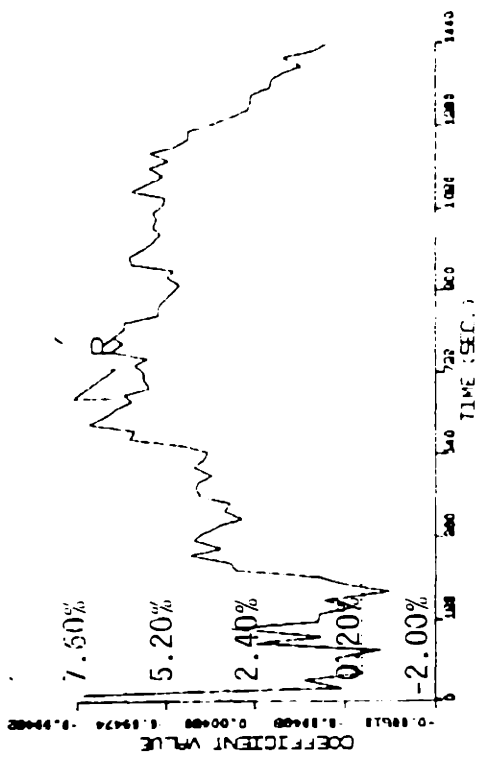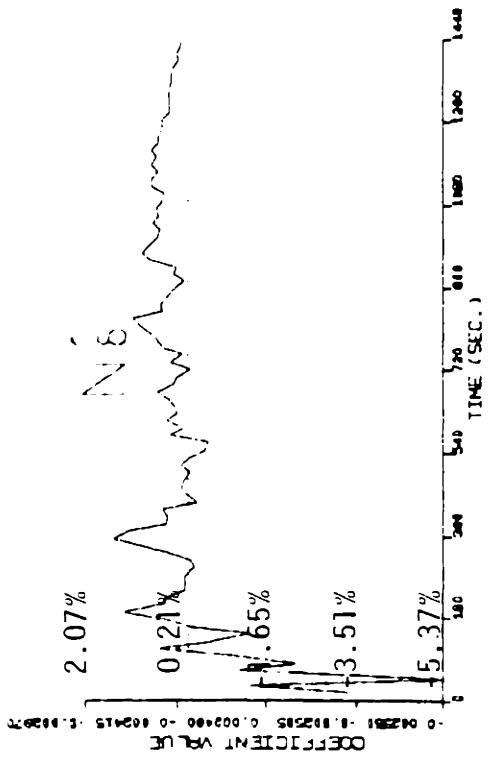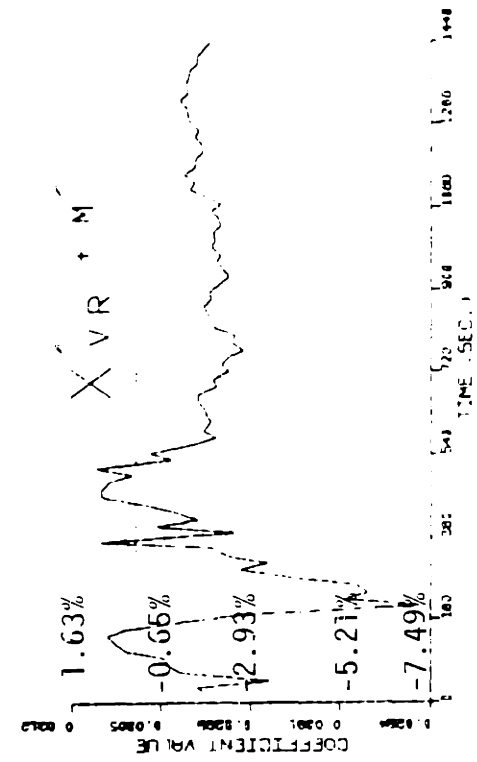
Figure 7.8-2.b   Results of identification
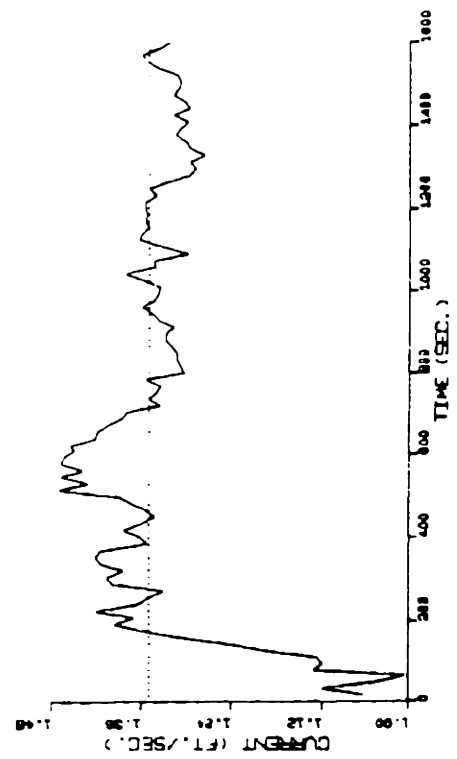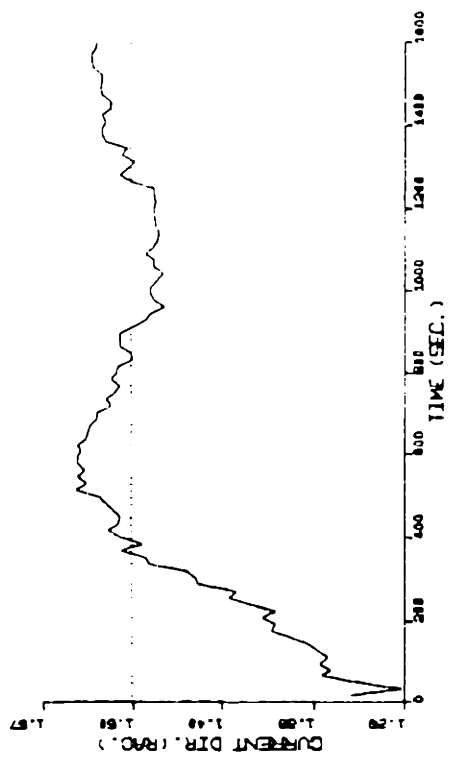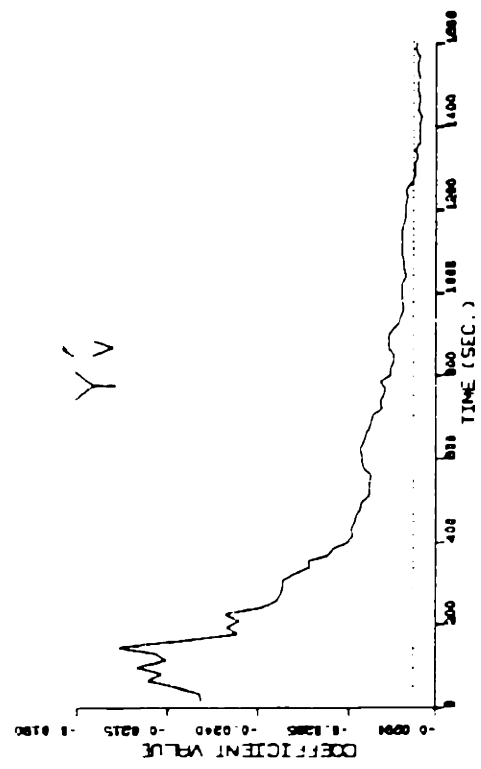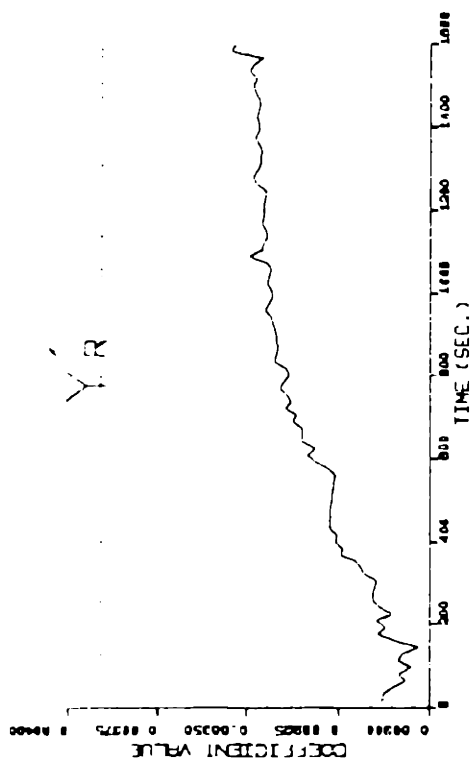
——————   Estimation   ....   True value

Figure 7.9.a   Results of identification. Non-zero process noise is assumed for the current magnitude u_c and the current direction α to track the variation of current.
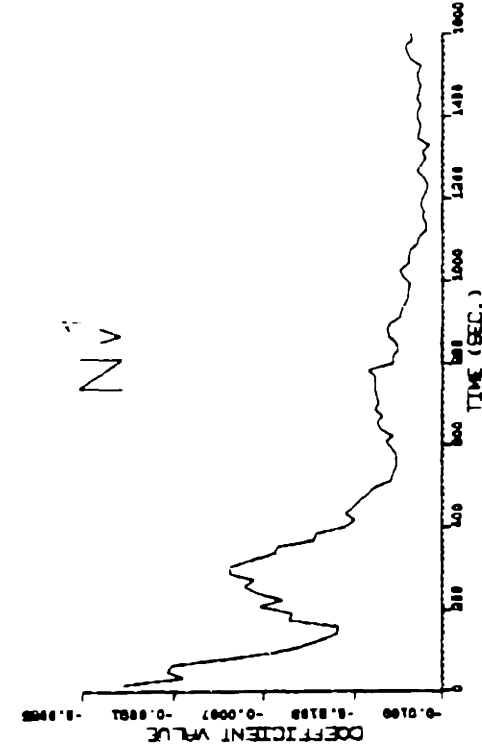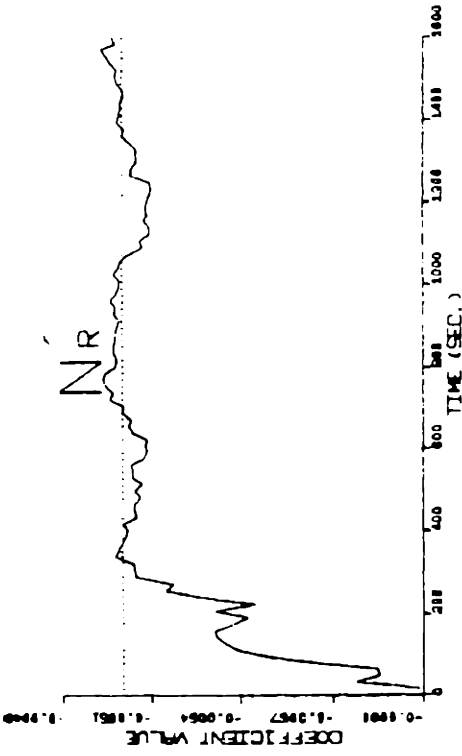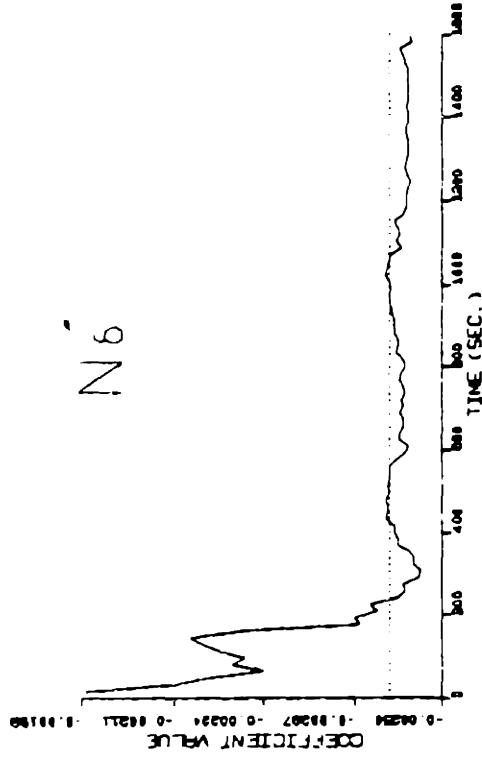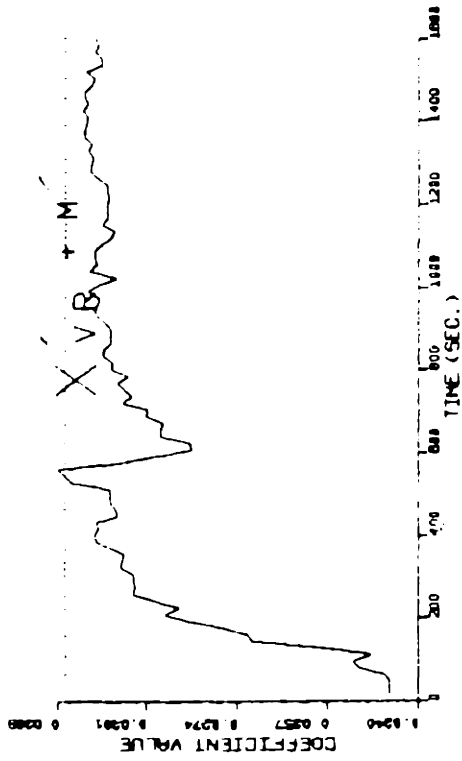
——— Estimation

······ True value

Figure 7.9.b Results of identification.

───── Estimation

...... True value
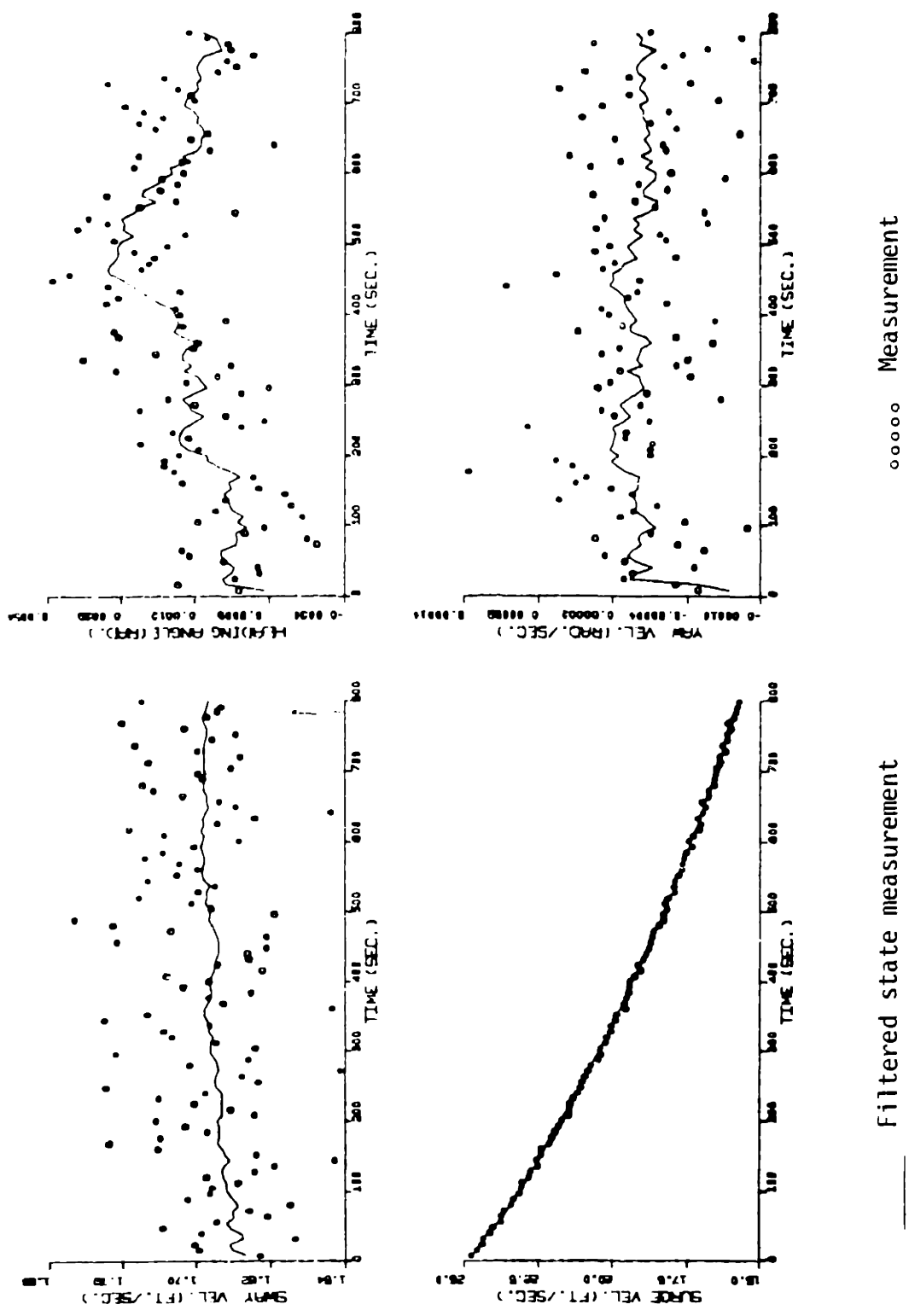
Figure 7.10.a Results of identification. The data of coasting maneuver(simulated) is
filtered to estimate the ship resistance coefficient. ψ=0°, α=90°.

ooooo   Measurement

_____   Filtered state measurement
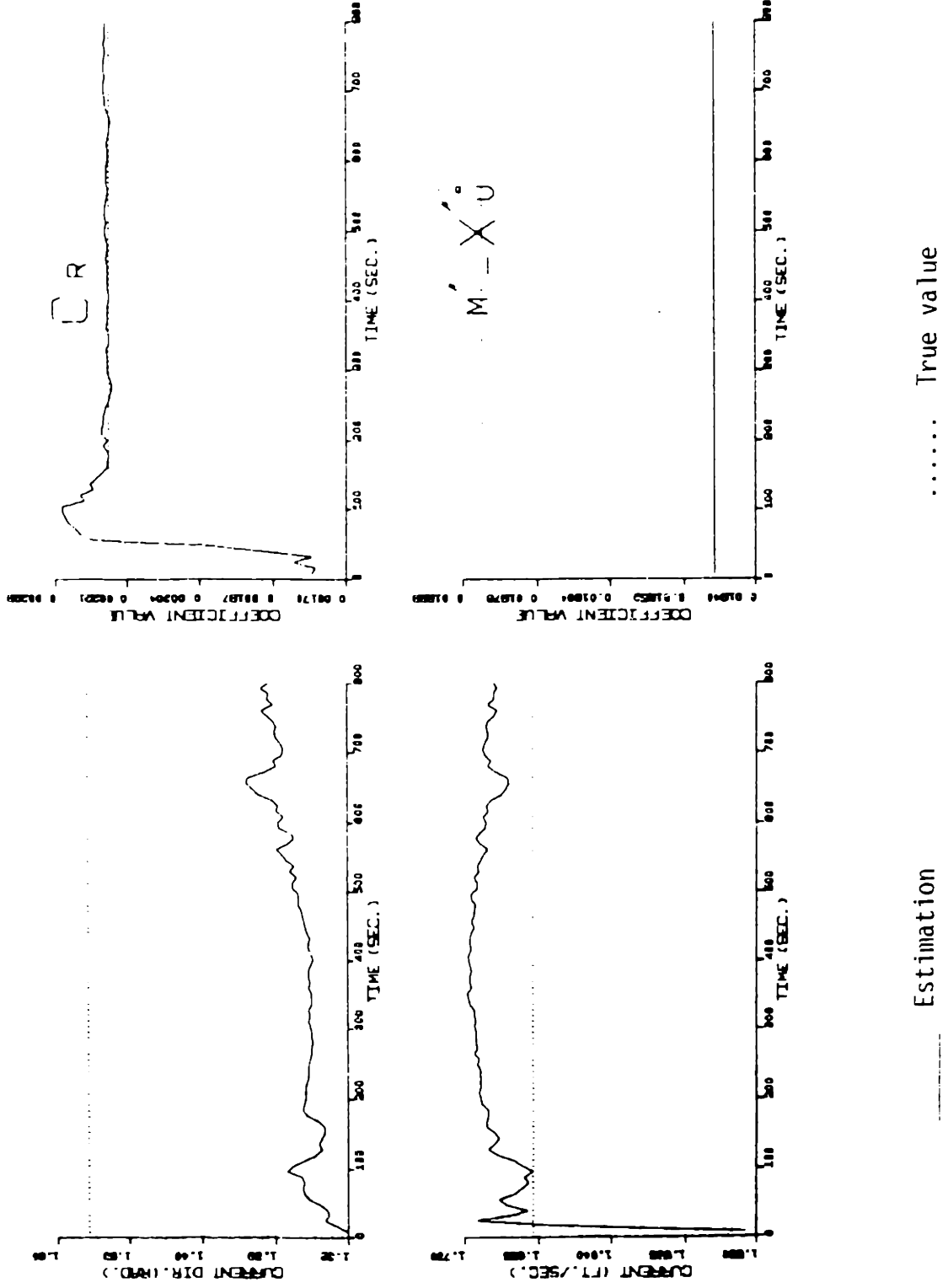
Figure 7.10.b   Results of identification. $m'-X'_u$ is fixed onto a value of 2% error.

_____   Estimation

....   True value
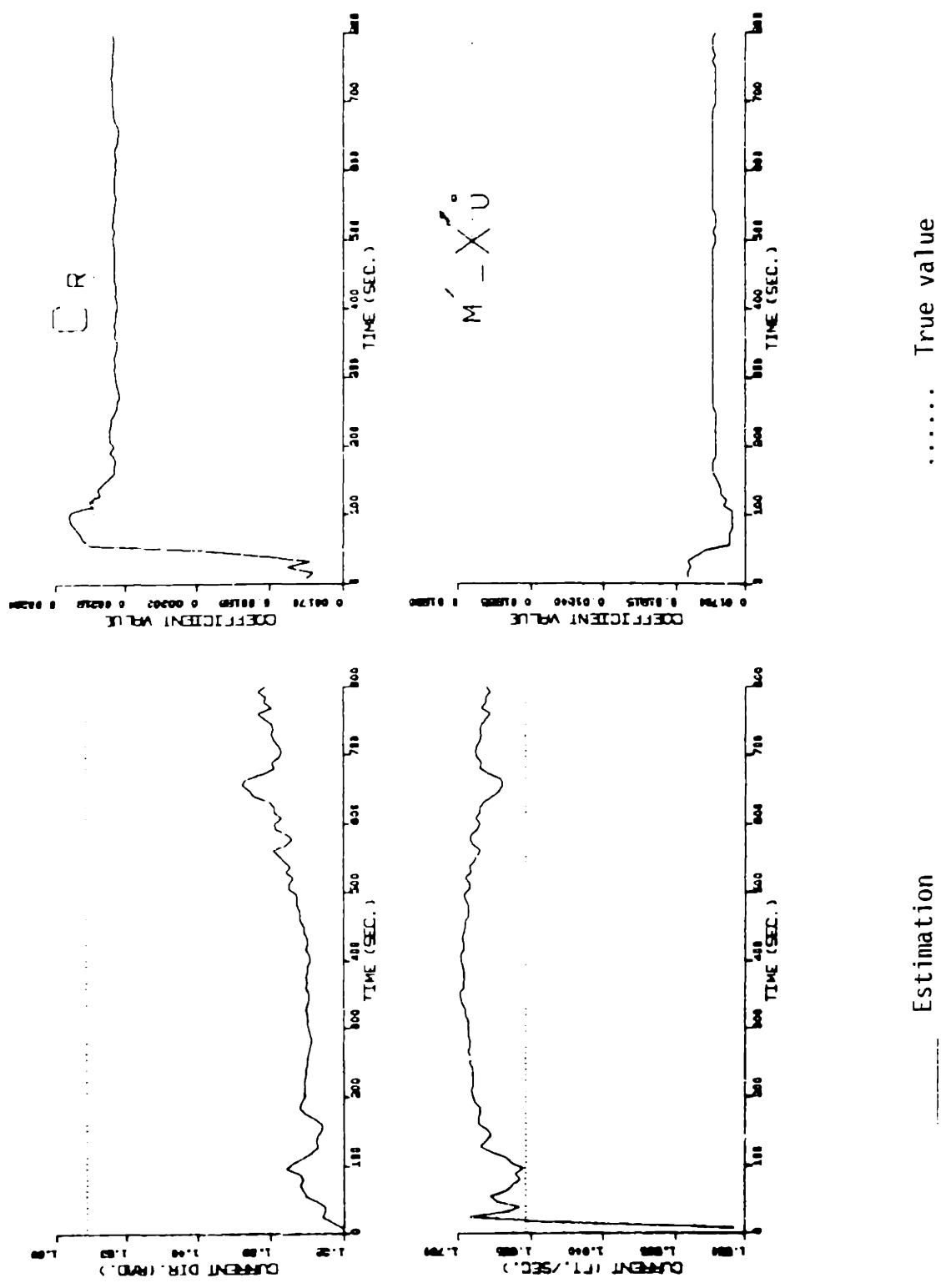
Figure 7.10.c   Results of identification. $m'-X_{\dot{u}}^{\cdot}$ is estimated together with C_R.
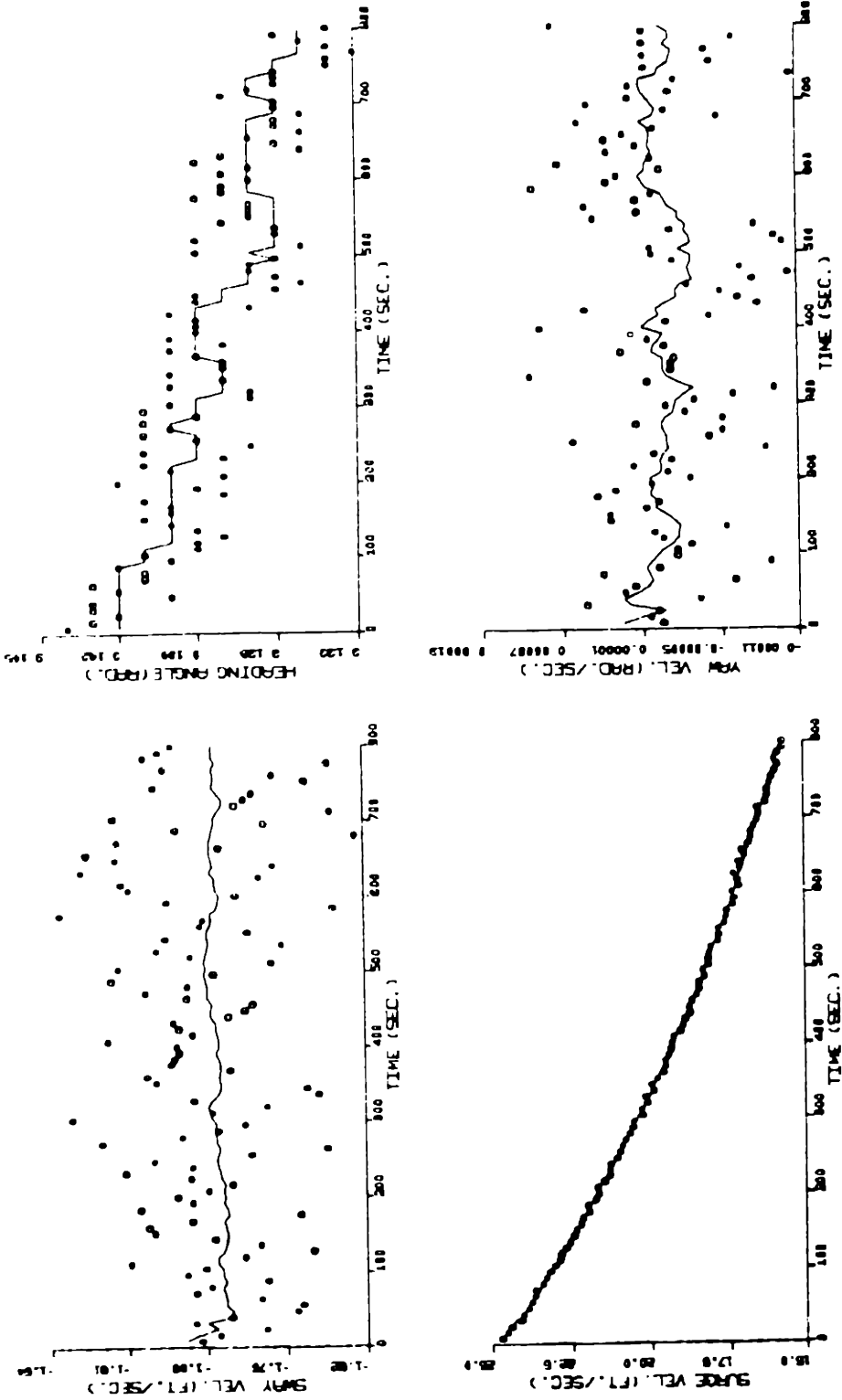
——————   Estimation

. . . .   True value

Figure 7.11.a   Results of identification.   The data of coasting maneuver(simulated) is
filtered to estimate the ship resistance coefficient. $\psi=180°$, $\alpha=90°$

ooooooo   Measurement

Filtered state measurement

- 229 -
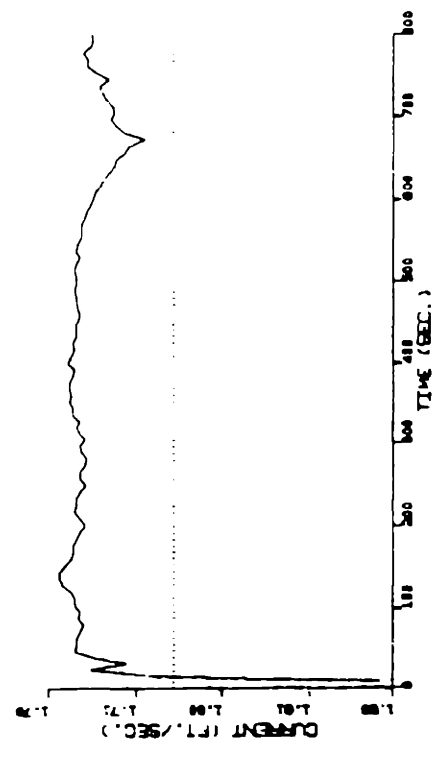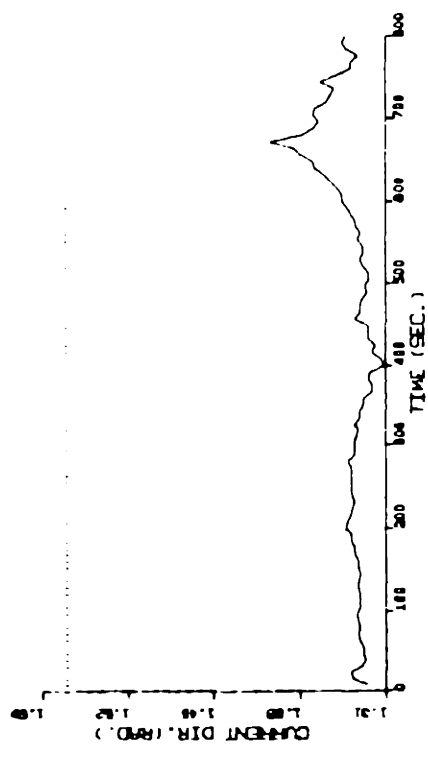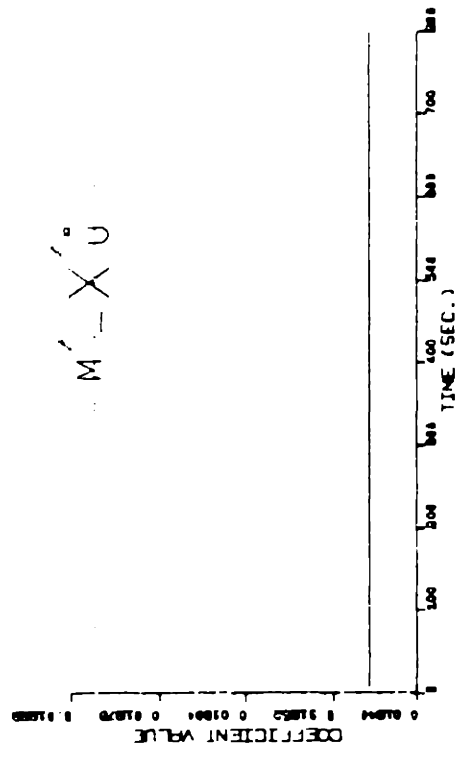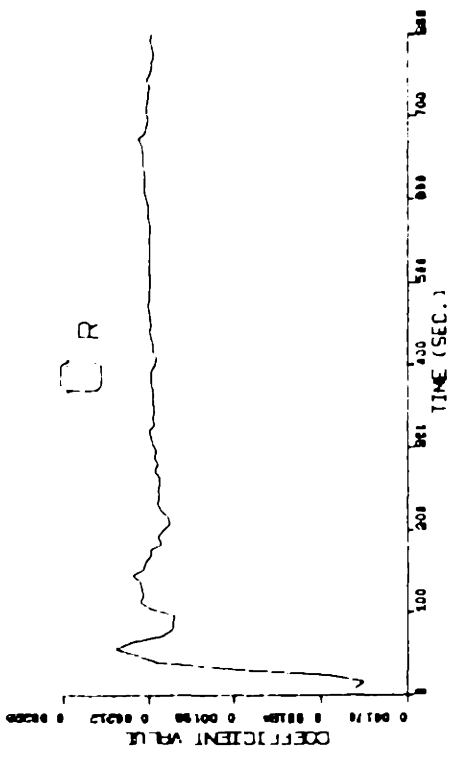
Figure 7.1i.b Results of identification. $m'-X'_u$ is fixed onto a value of 2% error.
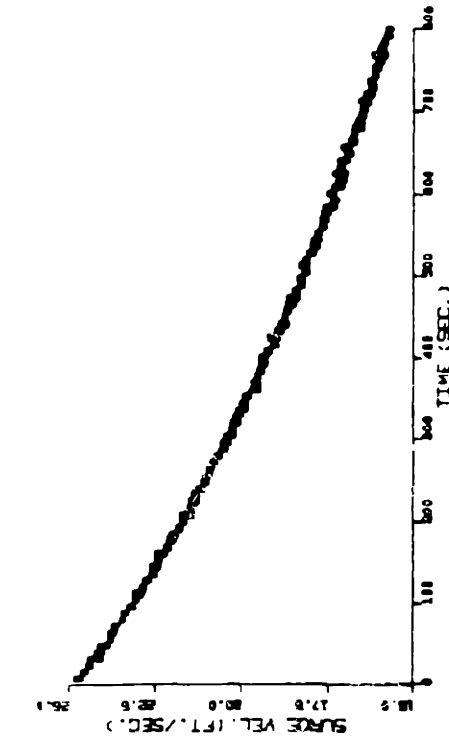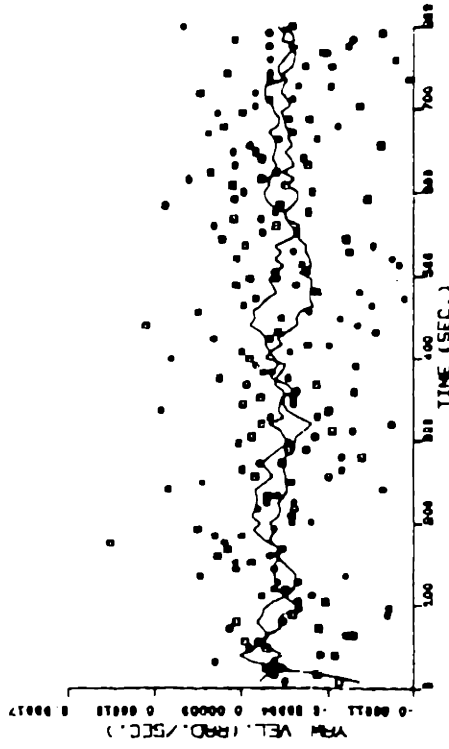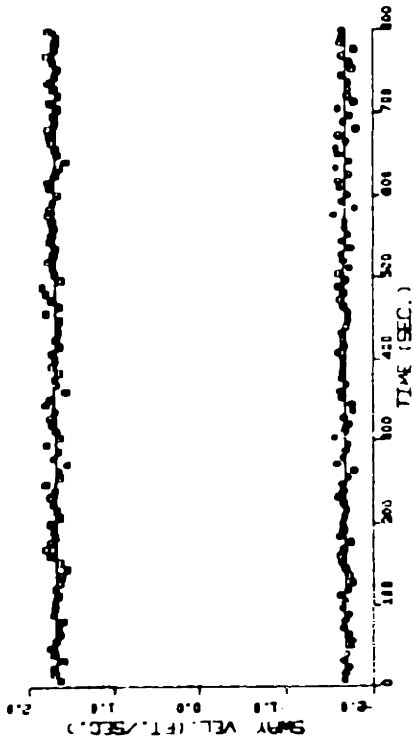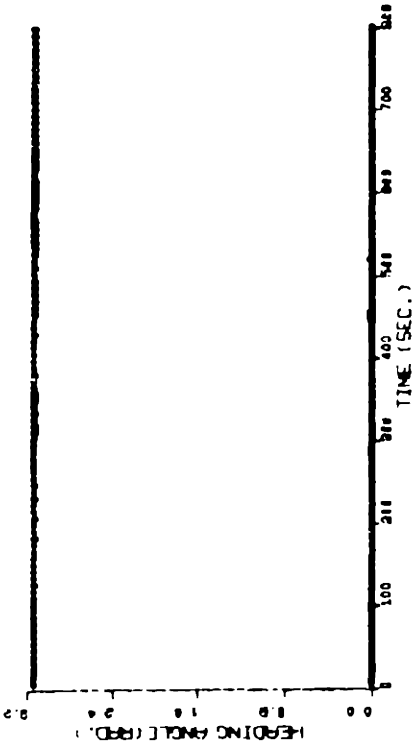
——— Estimation

······ True value

Figure 7.12.a   Results of identification. The data files of Figure 7.10.a and
Figure 7.11.a are parallelly processed to estimate the resistance
coefficient.
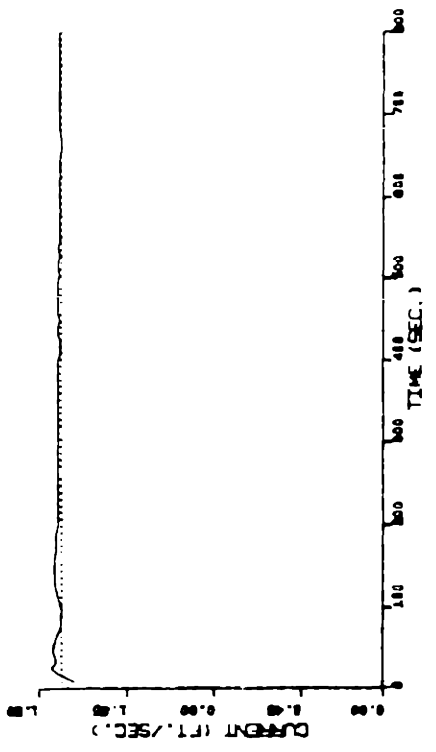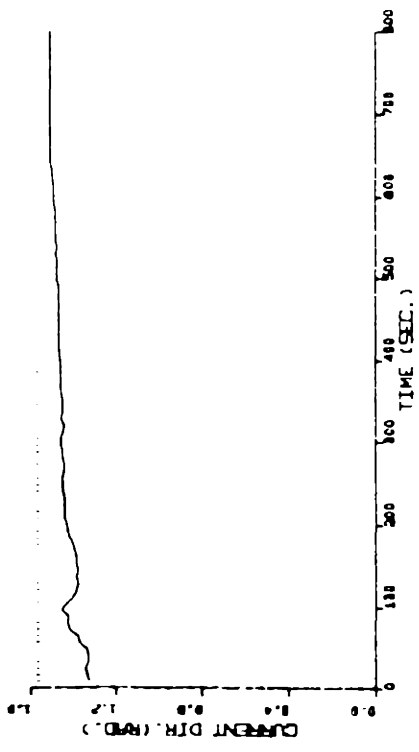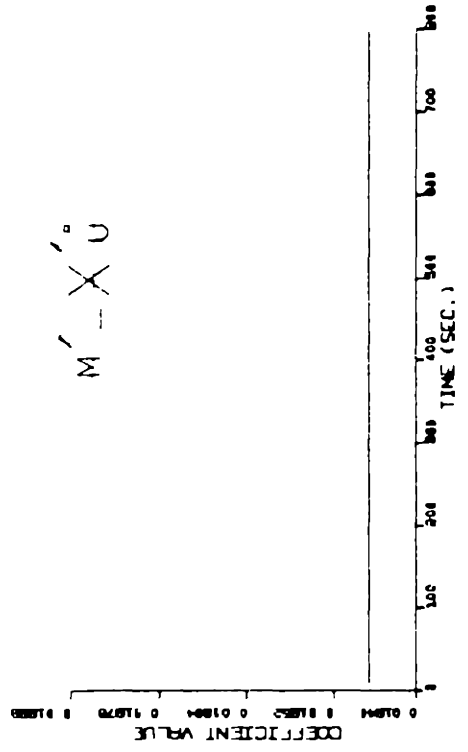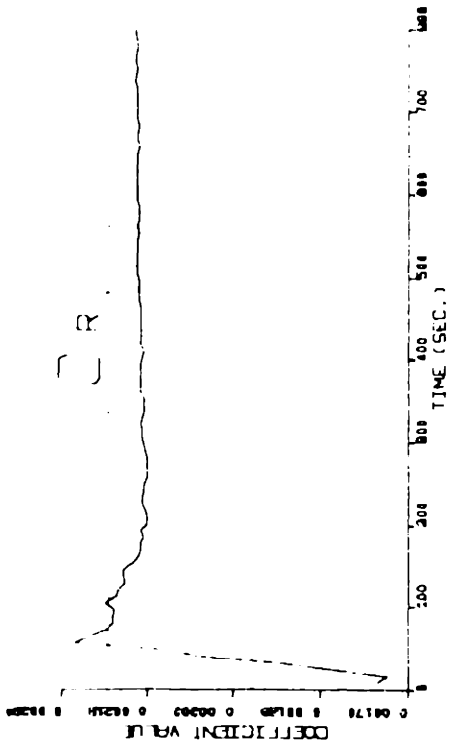
Figure 7.12.b Results of identification. $m' - X'_u$ is fixed onto a value of 2% error.
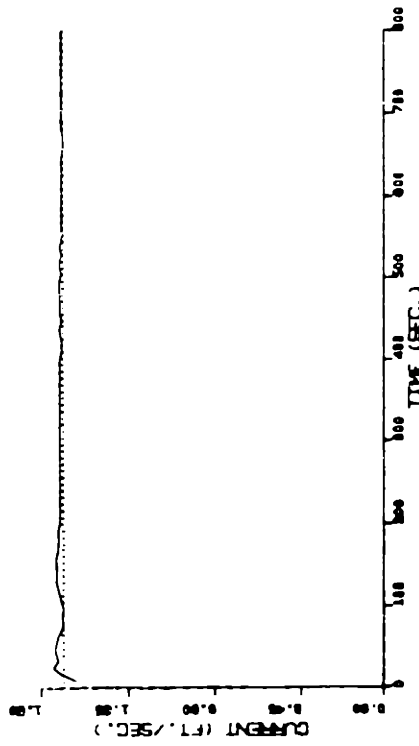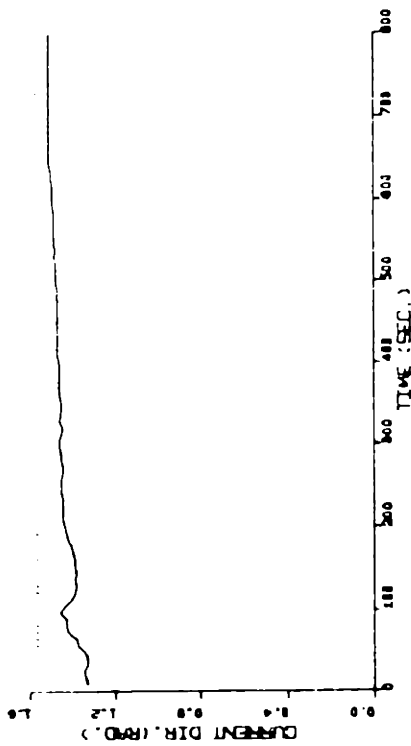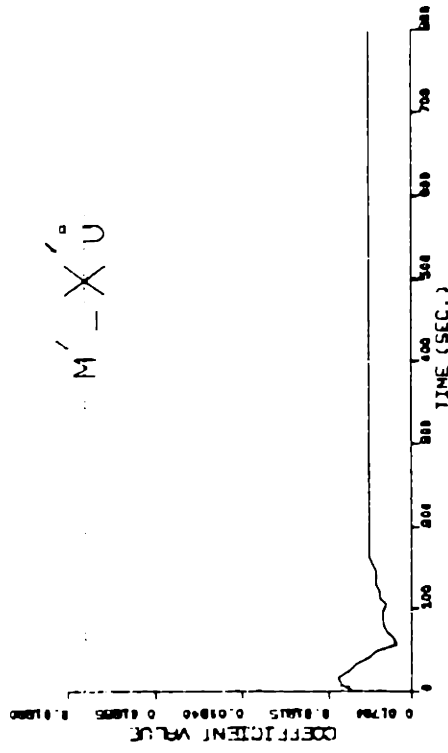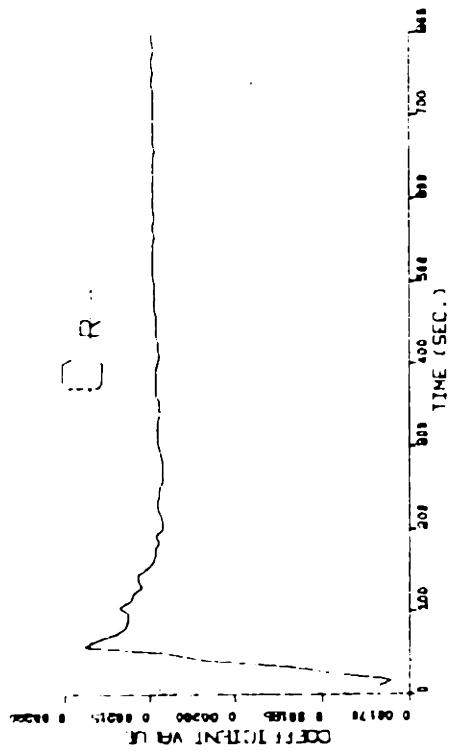
—————— Estimation

·········· True value

Figure 7.12.c   Results of identificaiton. $m'-X_u'$ is estimated together with C_R.

	TRUE VALUE	INITIAL GUESS & σ_i	ESTIMATED VALUE¶ & σ_f	ESTIMATED VALUE† & σ_f	ESTIMATED VALUE & σ_f(parallel)
u_c	1.689	1.351 ±0.20	1.713(1.40%) ±0.24E-1	1.735(2.72%) ±0.27E-1	1.689(-0.02%) ±0.48E-2
α	96.0°	75.0° ±5.0°	80.0°(-11.13%) ±3.82°	76.9°(-14.56%) ±3.79°	86.0°(-4.40%) ±0.10°
$m'-X_{\dot{u}}'$	0.01885	0.01847 ±0.0	0.01847(-2.02%) ±0.0	0.01847(-2.02%) ±0.0	0.01847(-2.02%) ±0.0
C_R	0.00256	0.01805 ±0.226E-3	0.02264(0.37%) ±0.294E-4	0.02117(-6.14%) ±0.269E-4	0.02200(-2.50%) ±0.863E-5

¶
u_0=24.8 ft/sec.
v_0=1.6889 ft/sec.
r_0=0.0 rad/sec.
ψ_0=0.0°

†
u_0=24.8 ft/sec.
v_0=-1.6889 ft/sec.
r_0=0.0 rad/sec.
ψ_0=180°

Table 7.3 Summary of resistance coefficient estimation with $m'-X_{\dot{u}}'$ fixed onto a value of 2% error. Current angle is 90°.
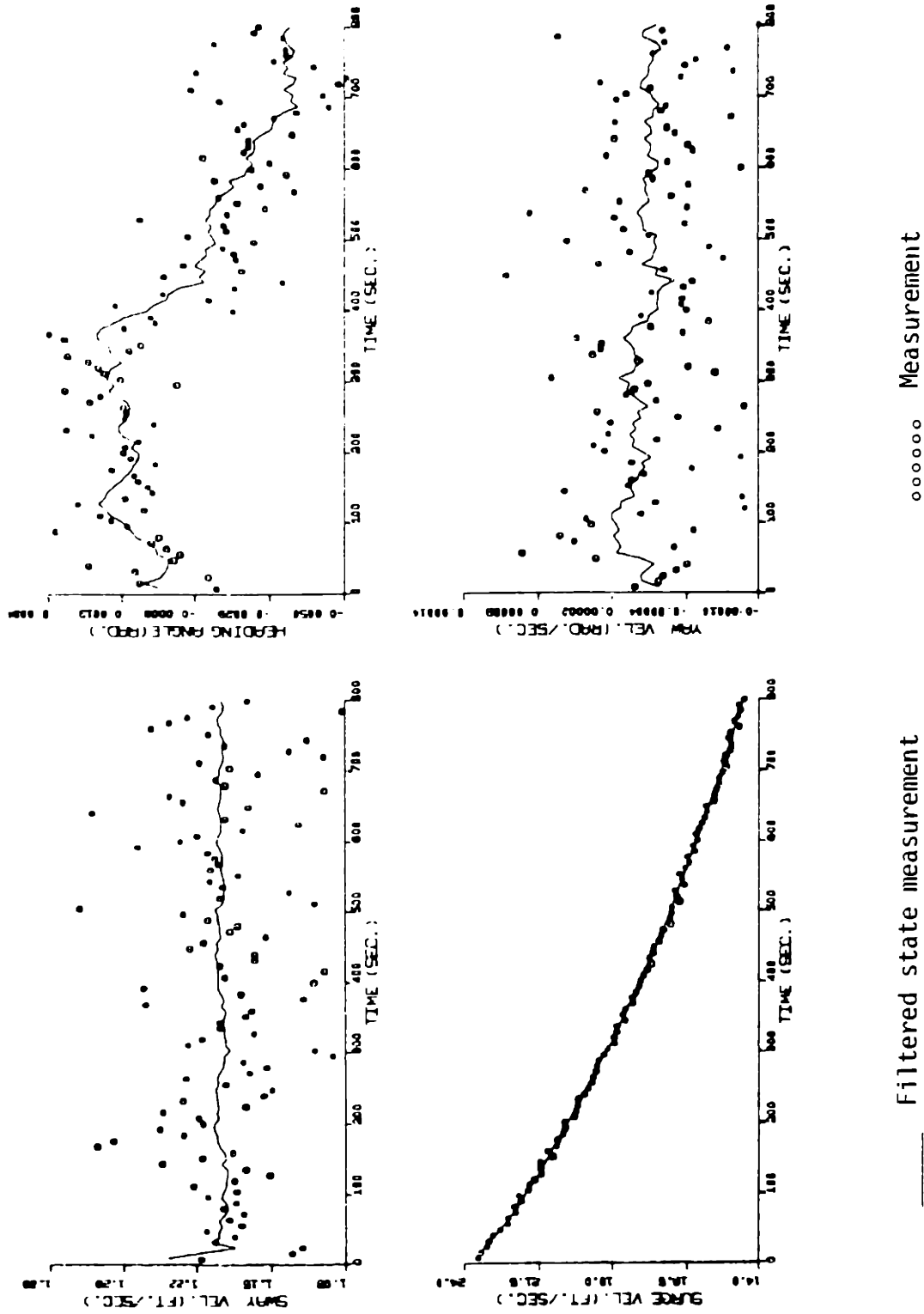
Figure 7.13.a   Results of identification.   The data of coasting maneuver(simulated) is filtered to estimate the ship resistance coefficient. $\psi = 0°$, $\alpha = 145°$.

oooooo   Measurement

——— Filtered state measurement
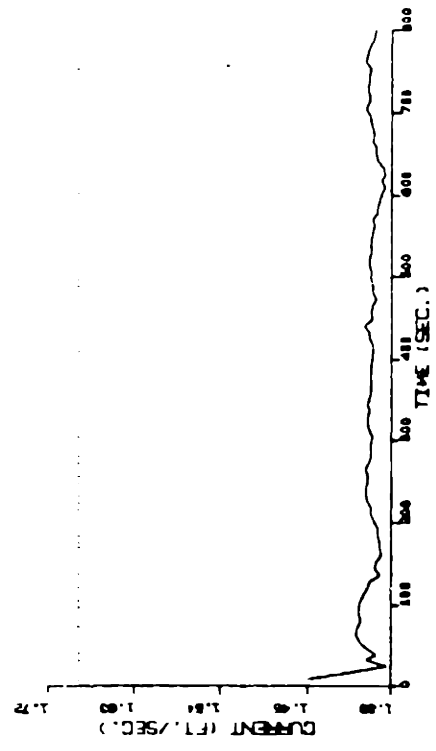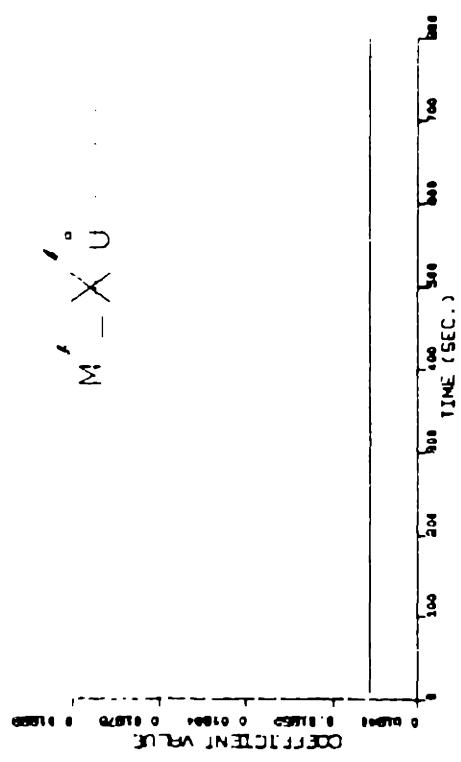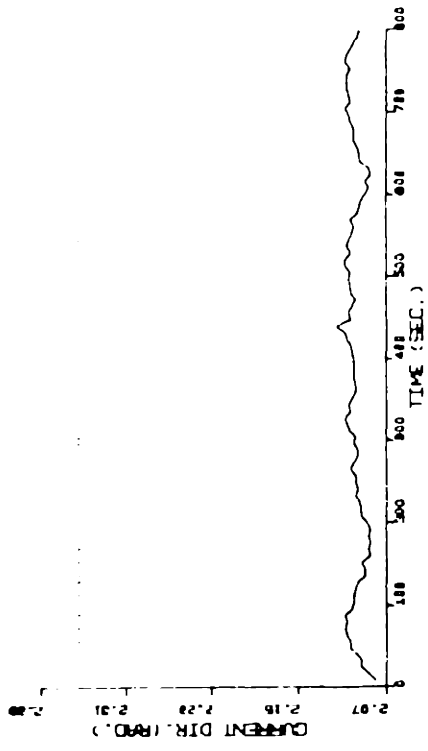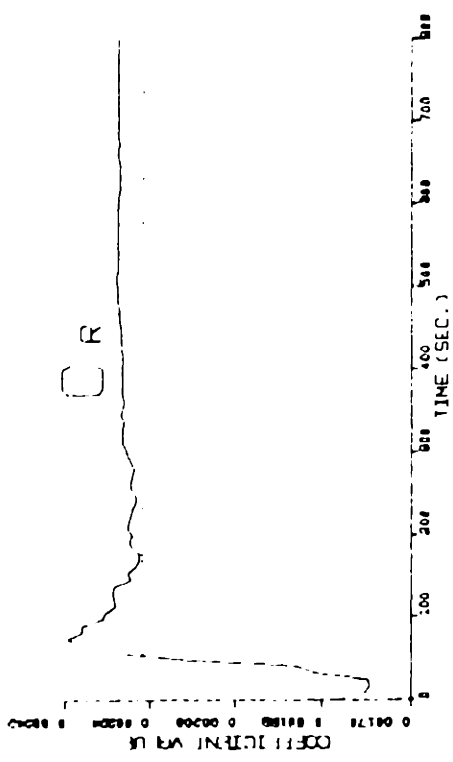
Figure 7.13.b Results of identification. $m'-X_u'$ is fixed onto a value of 2% error.

————— Estimation

······· True value
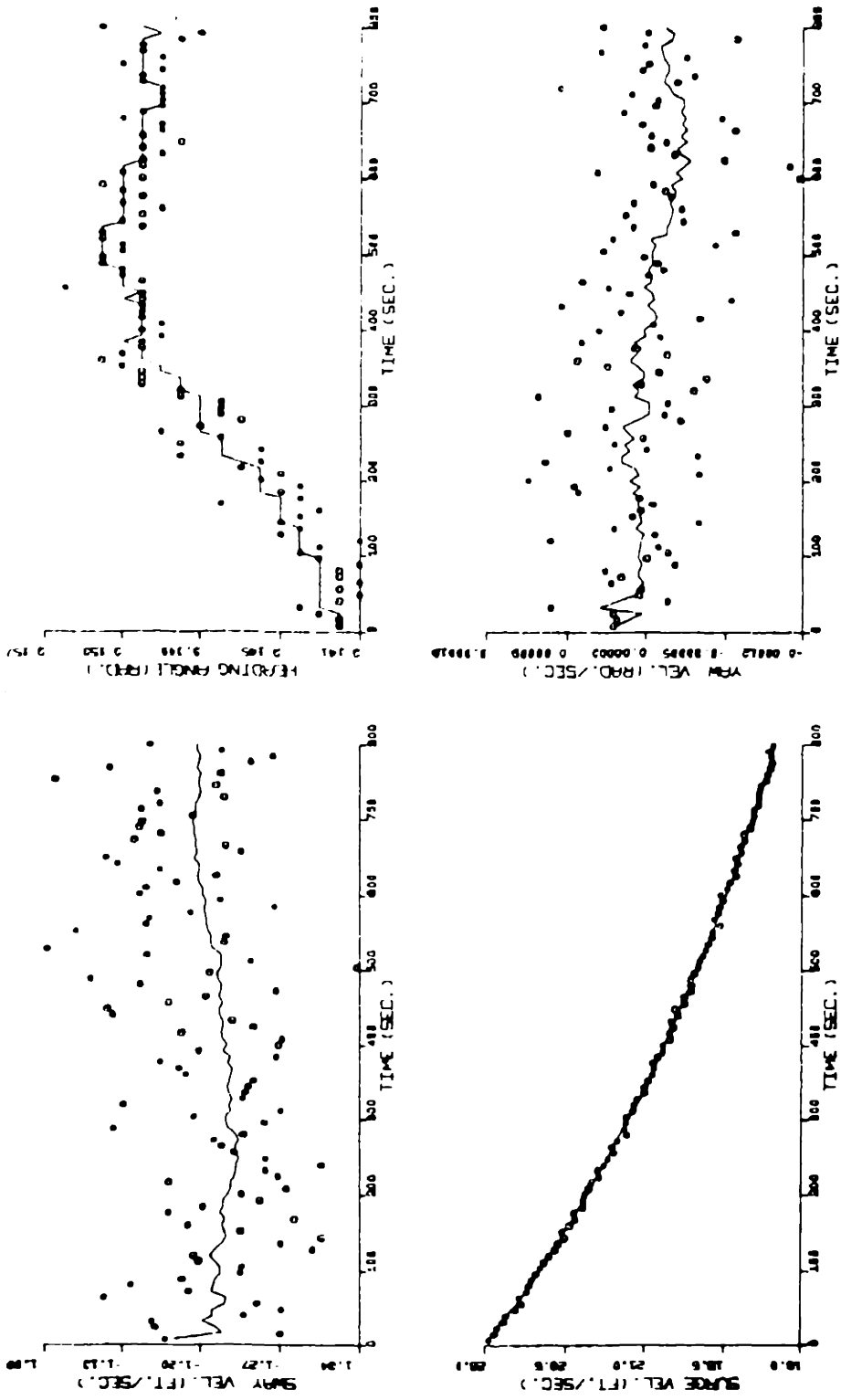
Figure 7.14.a Results of identification. The data of coasting maneuver(simulated) is filtered to estimate the ship resistance coefficient. $\psi=180°$, $\alpha=145°$.

- 237 -
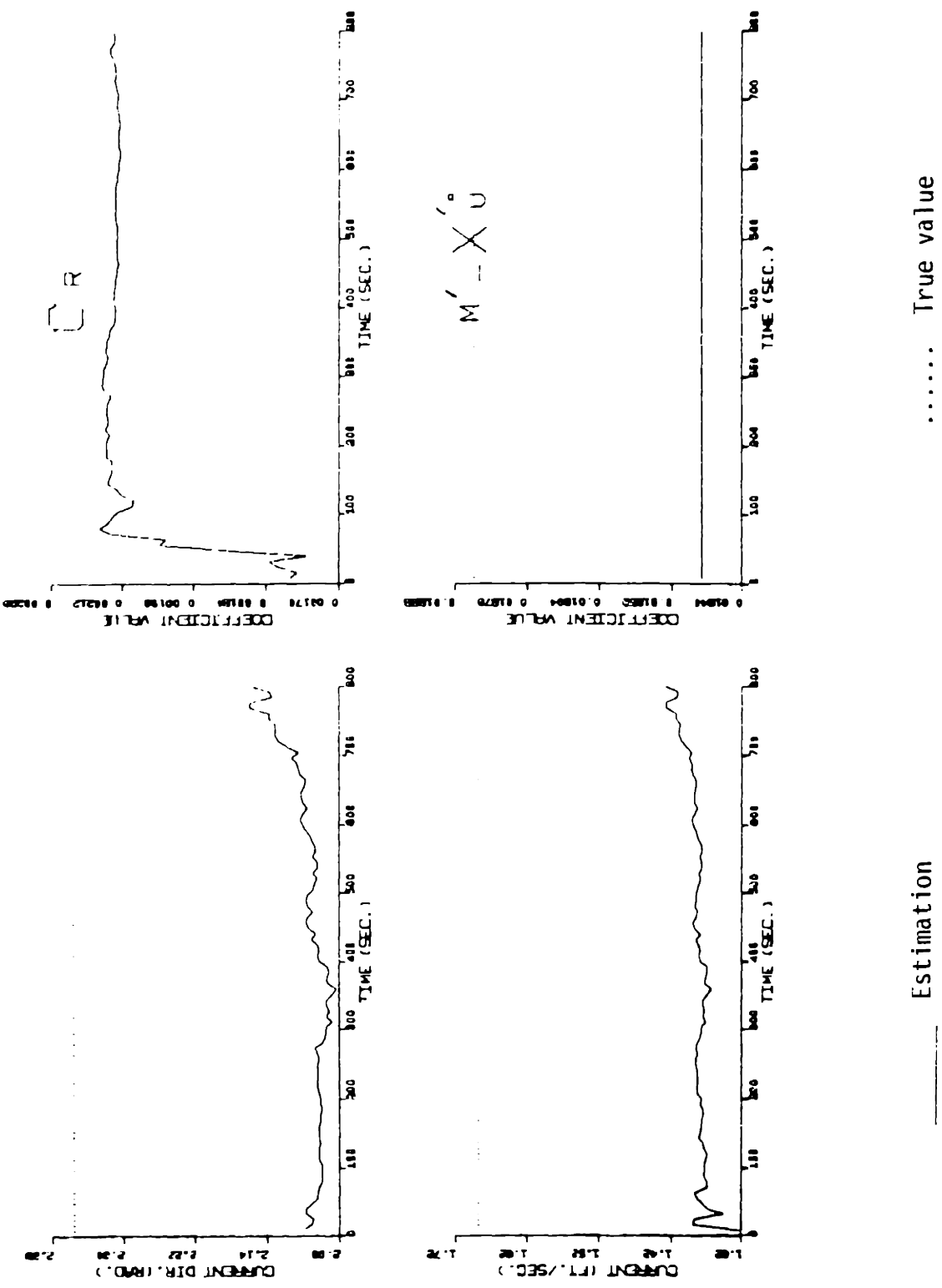
Figure 7.14.b Results of identification. $m' - X_u'$ is fixed onto a value of 2% error.
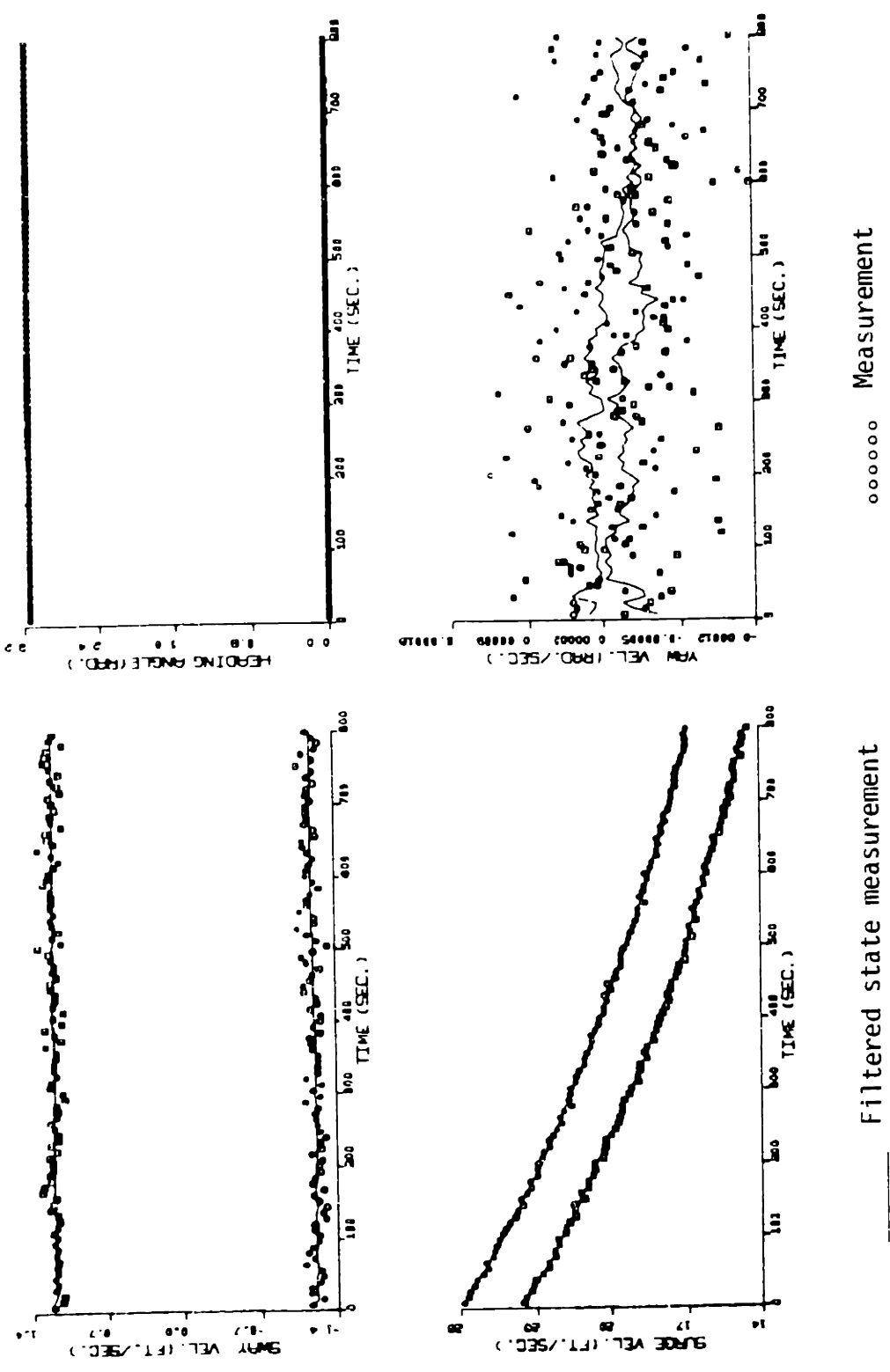
Figure 7.15.a   Results of identification.   The data files of Fig. 7.13.a and Fig. 7.14.a are parallelly processed to estimate the resistance coefficient.
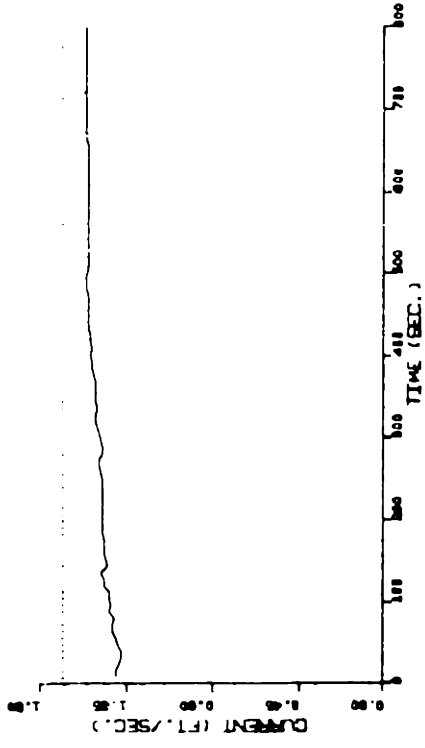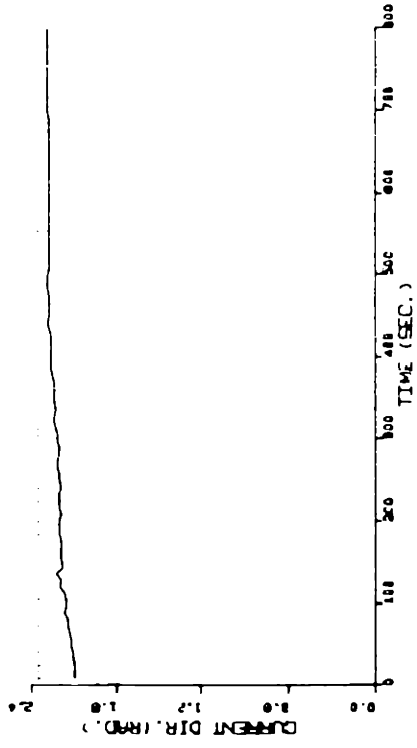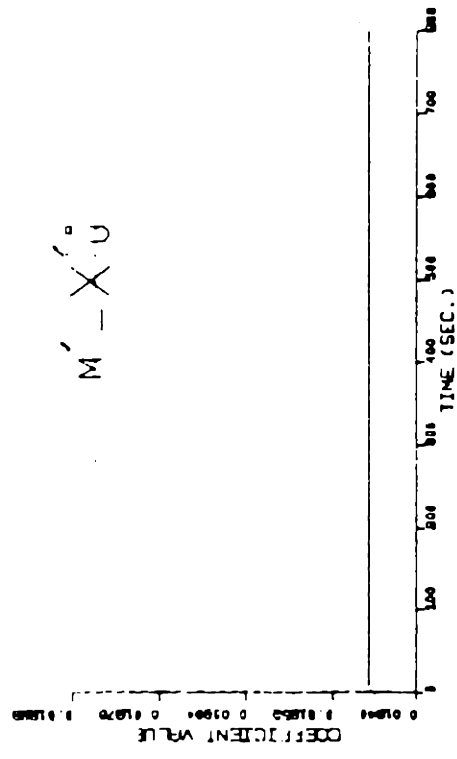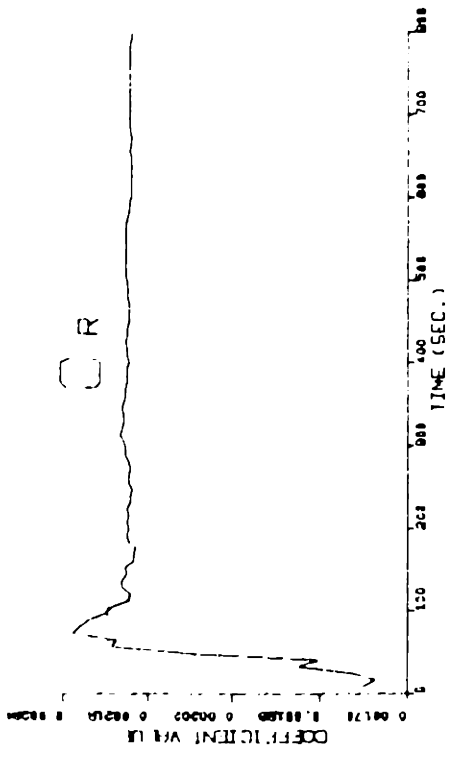
Figure 7.15.b Results of identification. m'-X'_u is fixed onto a value of 2% error.
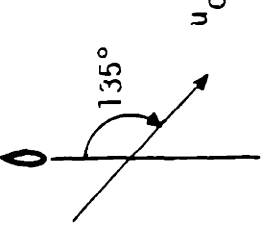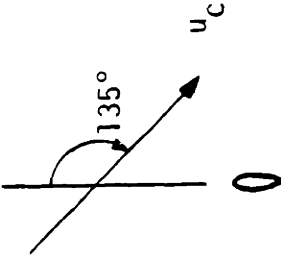
-------- True value

——— Estimation

	TRUE VALUE	INITIAL GUESS & σ_i	ESTIMATED VALUE¶ & σ_f	ESTIMATED VALUE† & σ_f	ESTIMATED VALUE & σ_f (parallel)
u_c	1.689	1.351 ±0.20	1.377(-18.45%) ±0.60E-1	1.429(-15.39%) ±0.51E-1	1.577(-7.79%) ±0.16E-1
α	135.0°	120.0° ±5.0°	120.0°(-11.14%) ±4.28°	123.6°(-8.41%) ±3.75°	130.4°(-3.41%) ±0.82°
$m'-X'_{\dot{u}}$	0.01885	0.01847 ±0.0	0.01847(-2.02%) ±0.0	0.01847(-2.02%) ±0.0	0.01847(-2.02%) ±0.0
C_R	0.002256	0.01805 ±0.226E-3	0.002309(2.33%) ±0.306E-4	0.002140(-5.13%) ±0.243E-4	0.002211(-2.01%) ±0.865E-5

¶
$u_0 = 23.606$ ft/sec.
$v_0 = 1.194$ ft/sec.
$r_0 = 0.0$ rad/sec.
$\psi_0 = 0.0°$

†
$u_0 = 25.994$ ft/sec.
$v_0 = -1.194$ ft/sec.
$r_0 = 0.0$ rad/sec.
$\psi_0 = 180.0°$

Table 7.4 Summary of resistance coefficient estimation with $m'-X'_{\dot{u}}$ fixed onto a value of 2% error. Current angle is 145°.
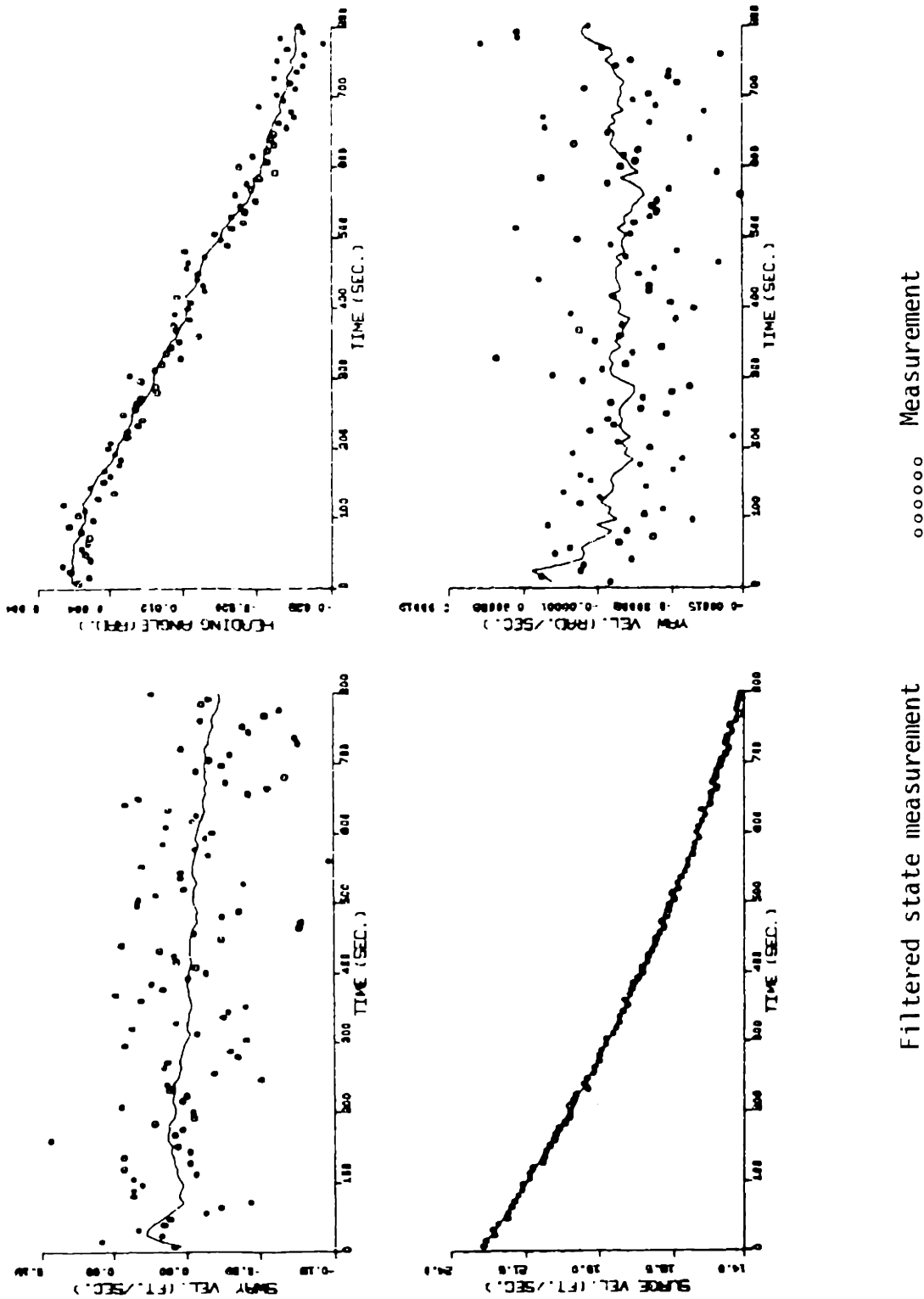
Figure 7.16.a   Results of identification. The data of coasting maneuver(simulated) is filtered to estimate the ship resistance coefficient. $\psi=0°$, $\alpha=180°$

oooooo   Measurement

———   Filtered state measurement
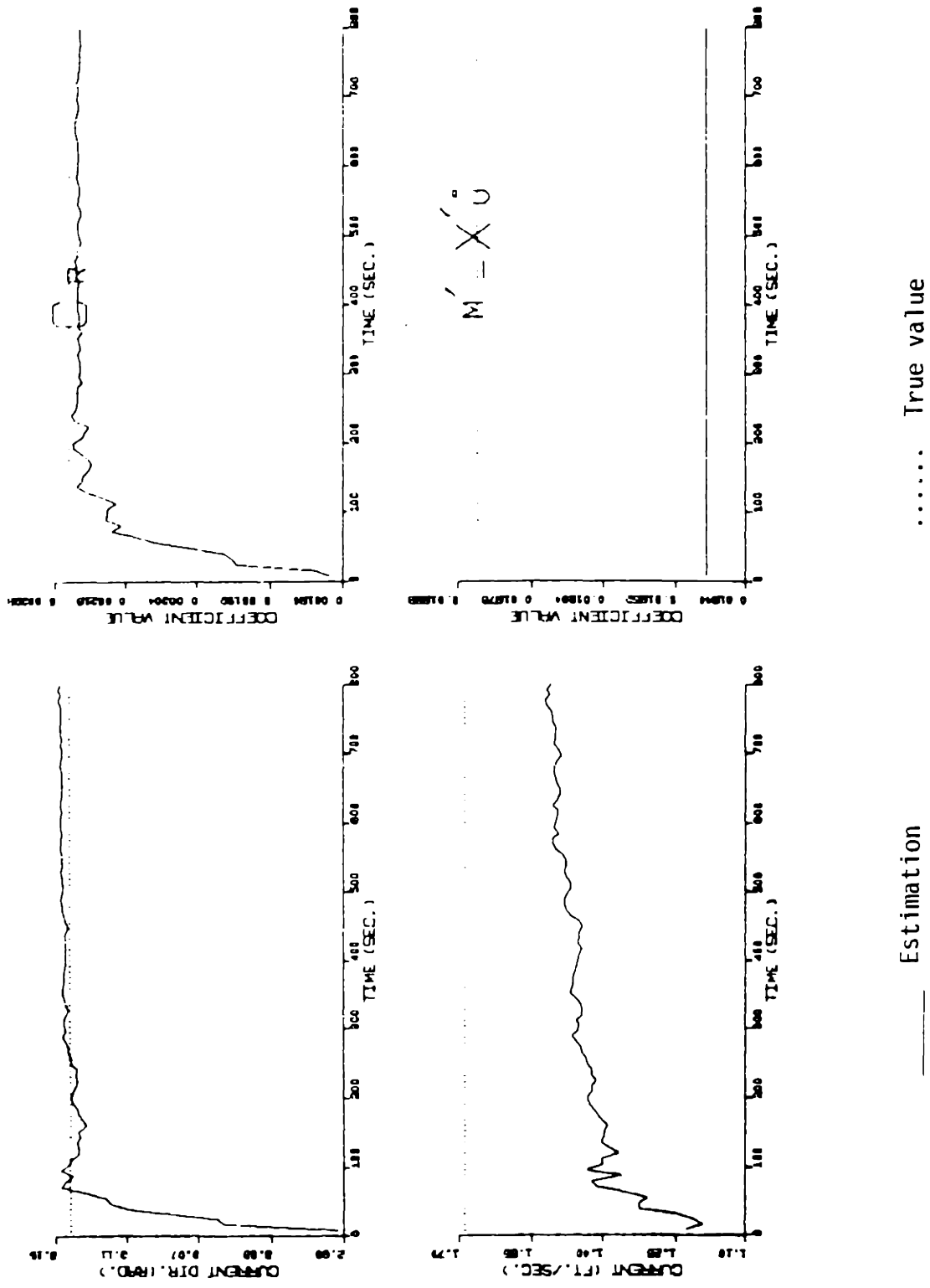
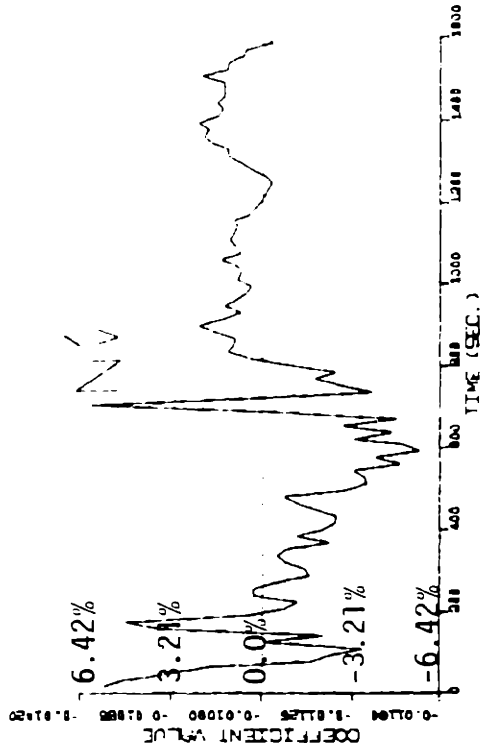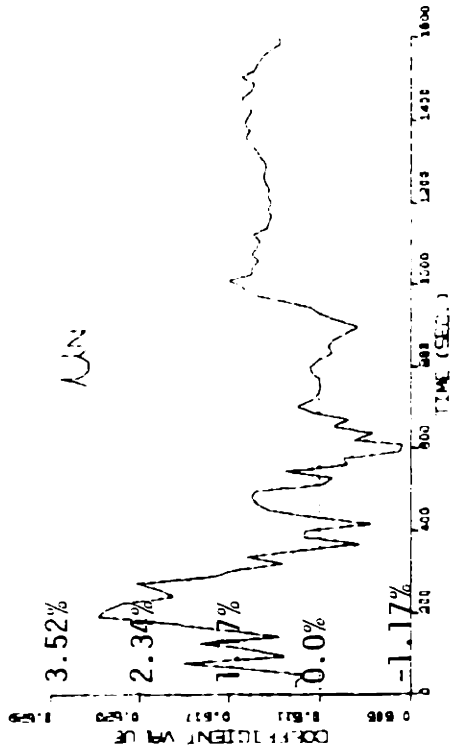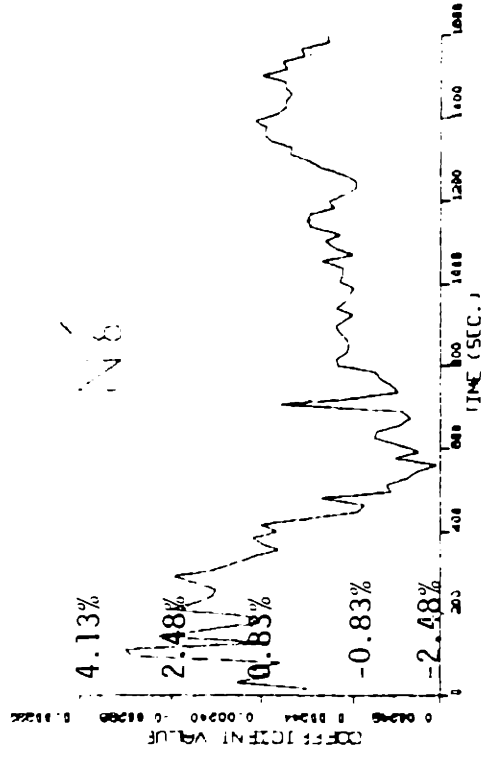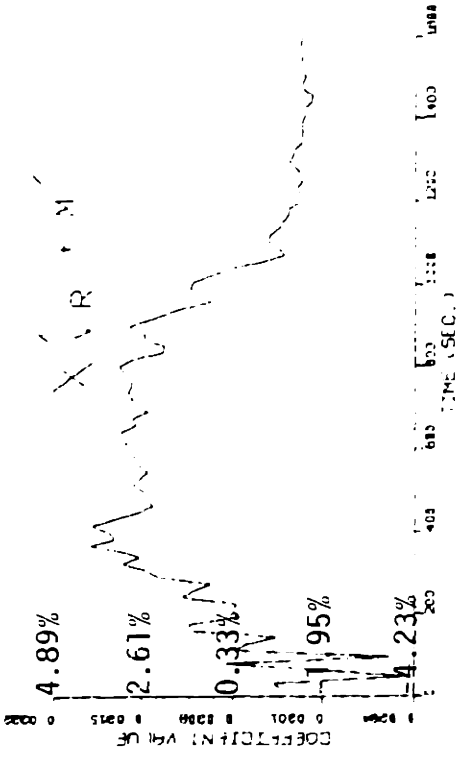Figure 7.16.b Results of identification. $m'-X_u'$ is fixed onto a value of 2% error.

$M' - X_u'$
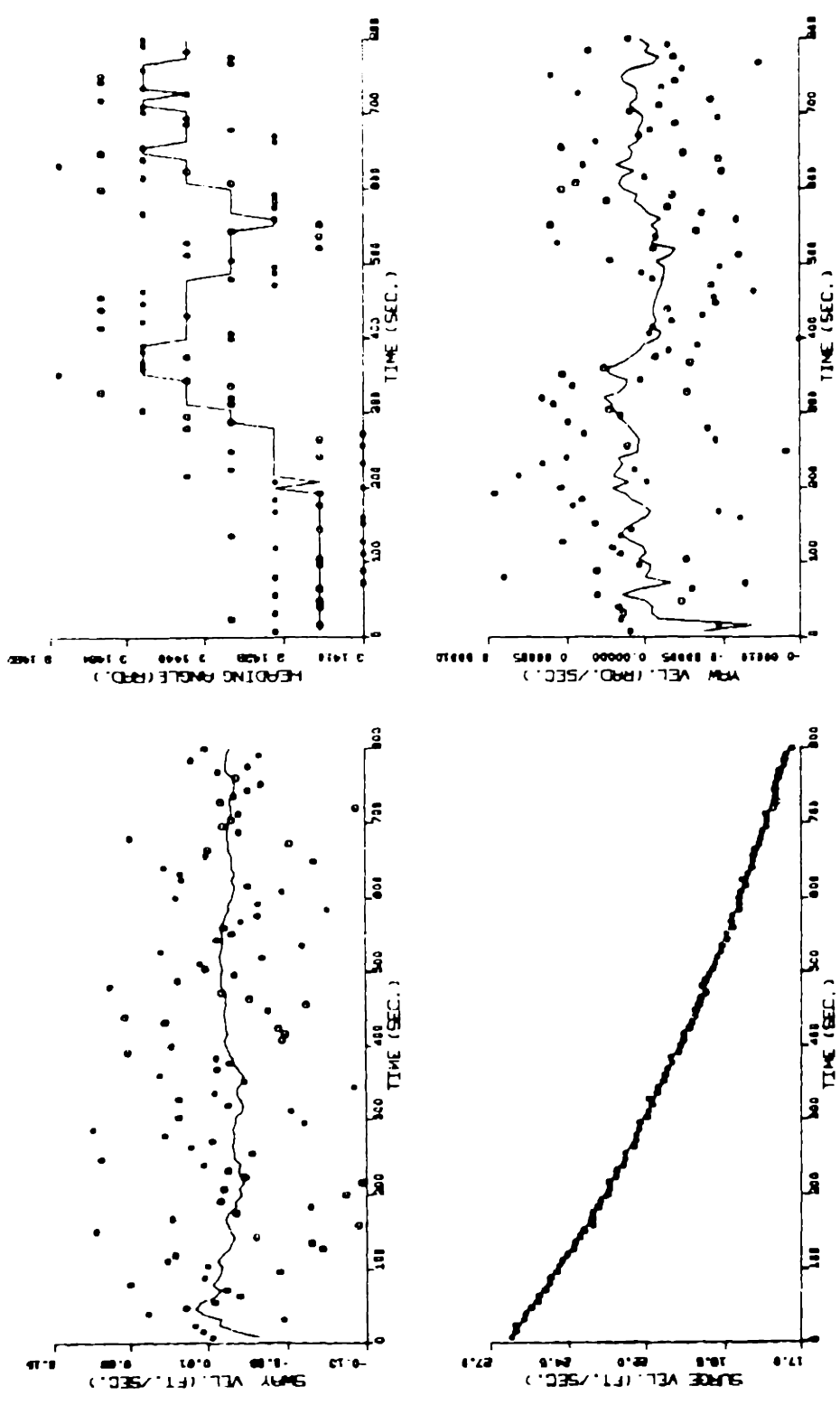
.... True value
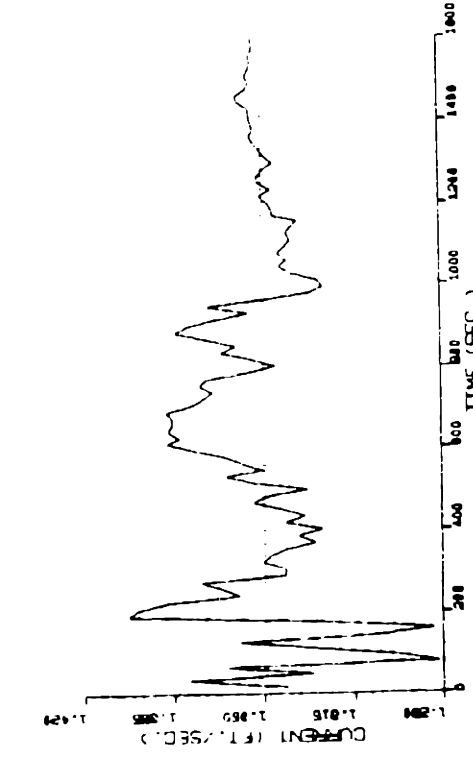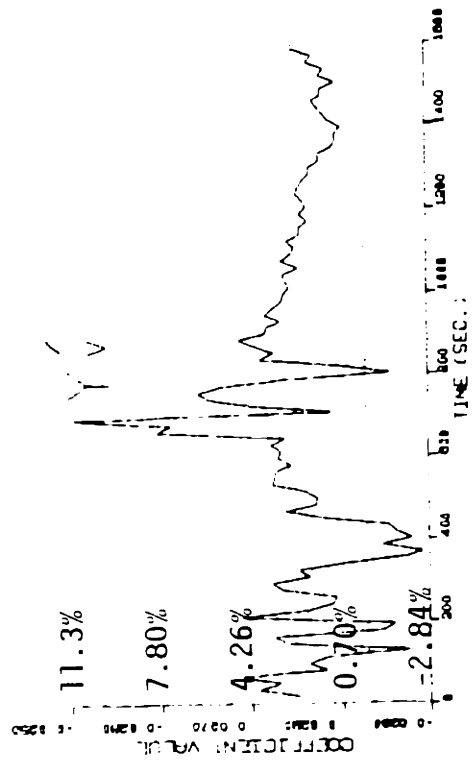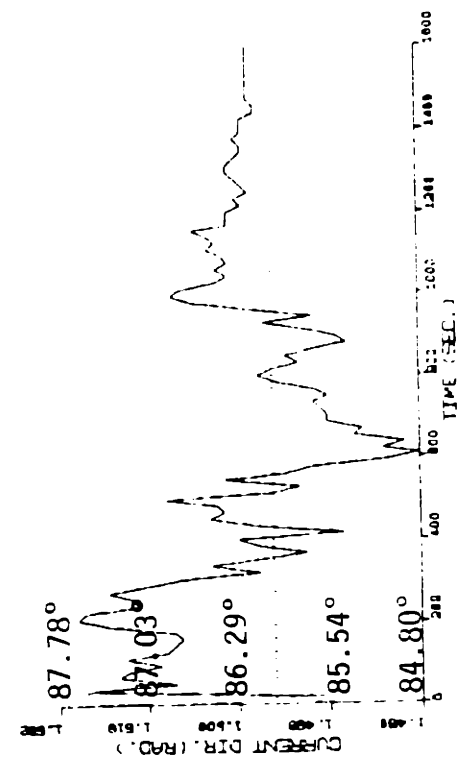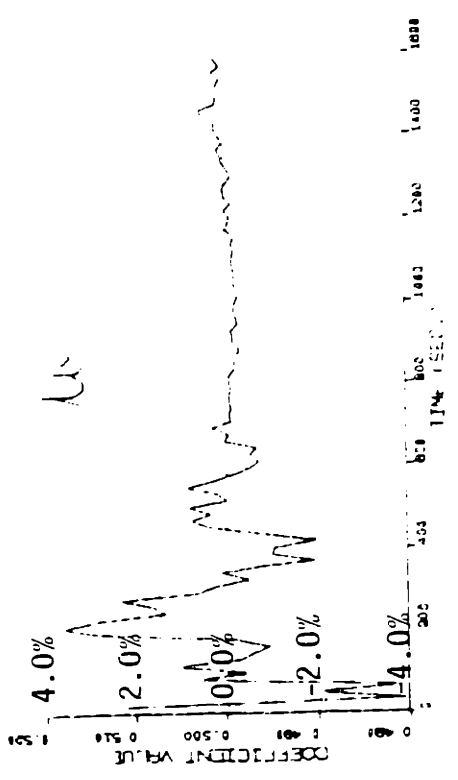
―――― Estimation

Figure 7.17.a Results of identification. The data of coasting maneuver(simulated) is filtered to estimate the ship resistance coefficient. ψ=180°, α=180°.
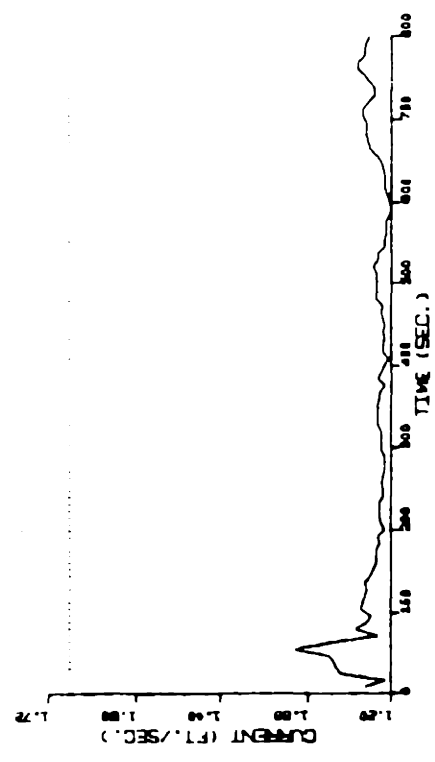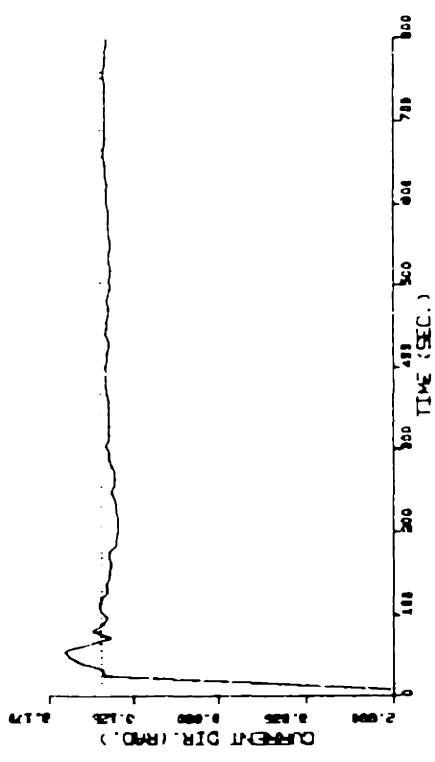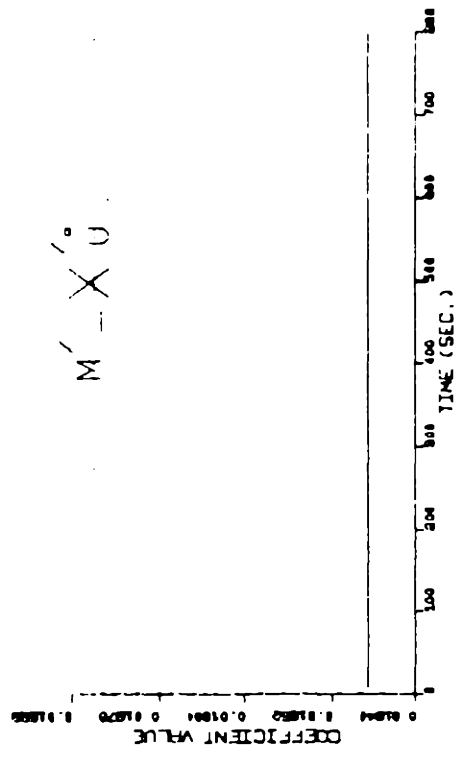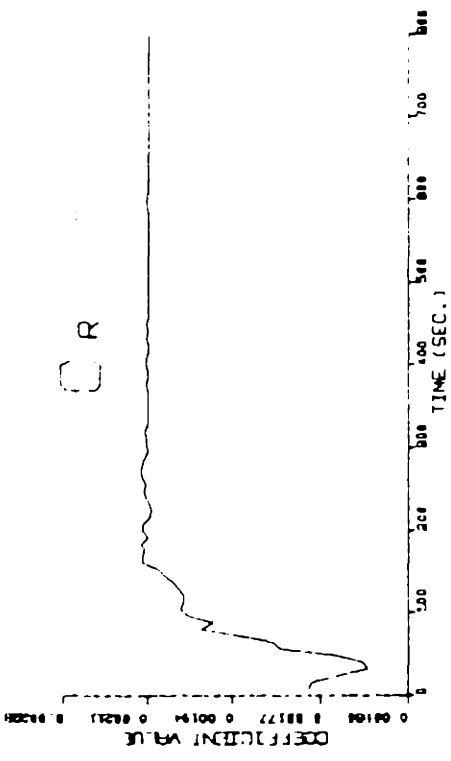
Figure 7.17.b Results of identification. $m' - X'_u$ is fixed onto a value of 2% error.

————— Estimation
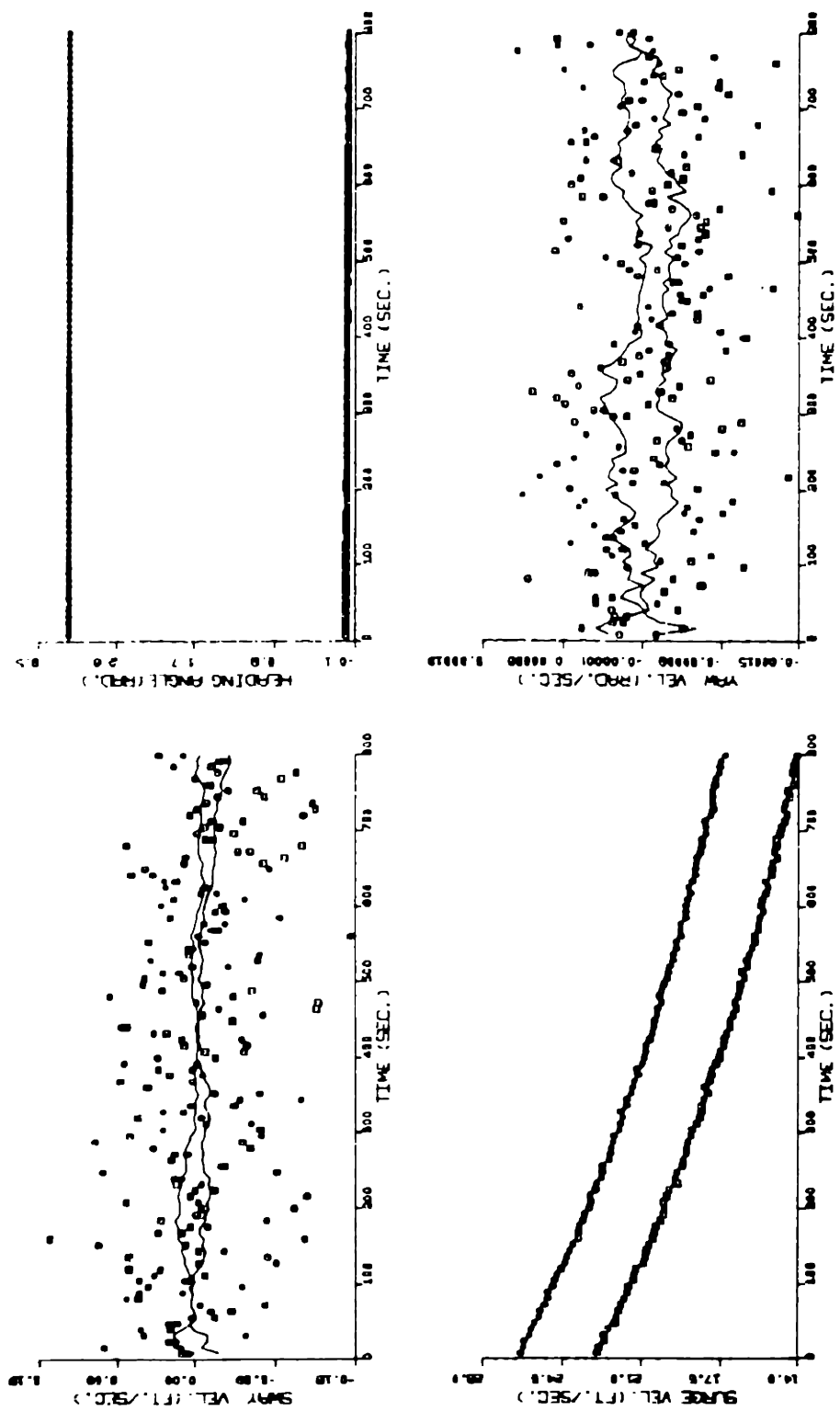
······· True value

Figure 7.18.a   Results of identification. The data files of Fig. 7.16.a and Fig. 7.17.a are parallelly processed to estimate the resistance coefficient.

ooooo   Measurement

―――――   Filtered state measurement
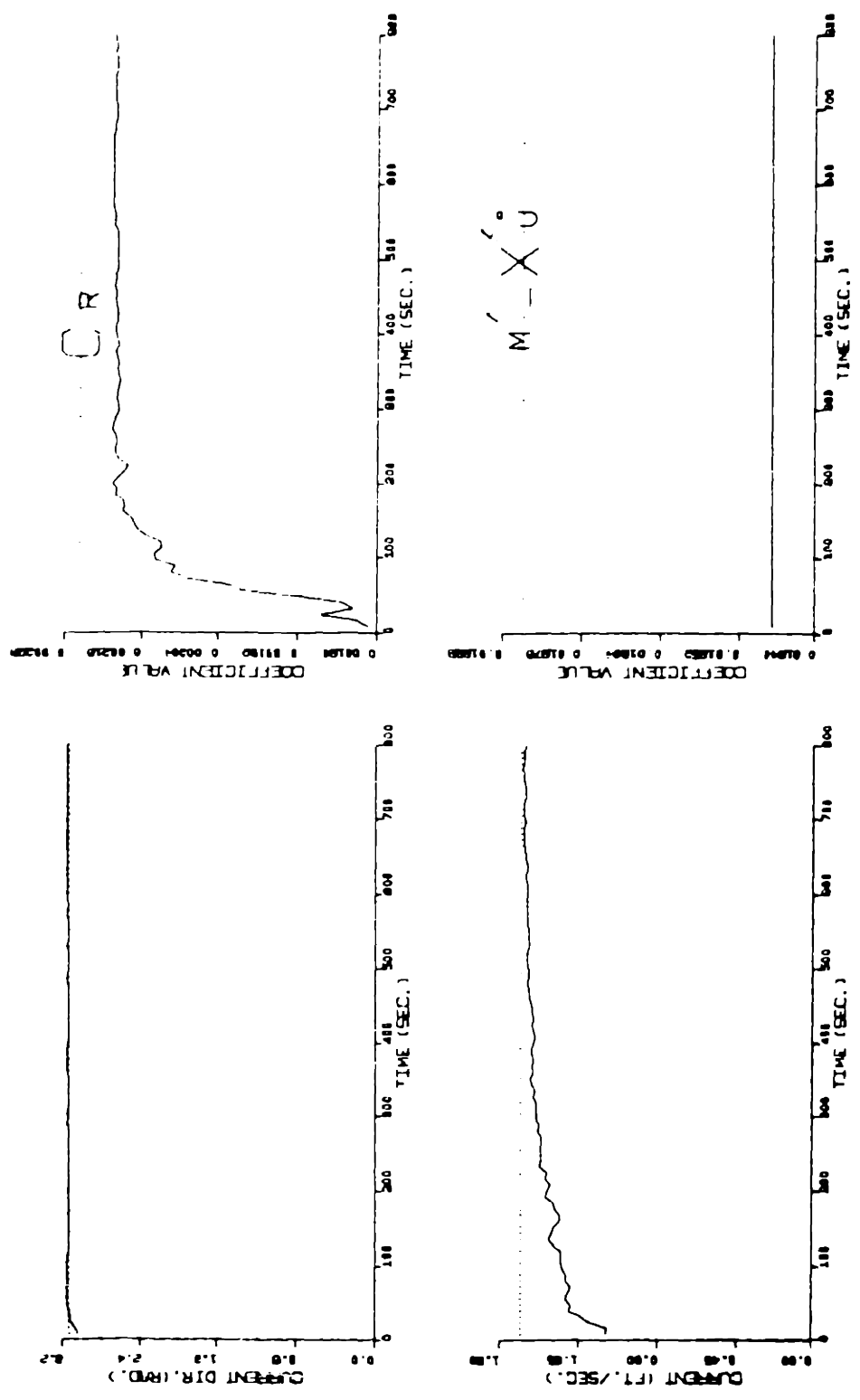
Figure 7.18.b Results of identification. $m'-X'_u$ is fixed onto a value of 2% error.
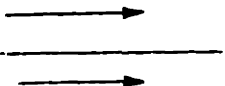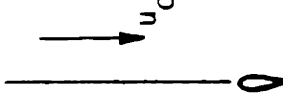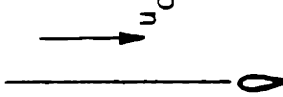
—————— Estimation

········ True value

	TRUE VALUE	INITIAL GUESS & σ_i	ESTIMATED VALUE¶ & σ_f	ESTIMATED VALUE† & σ_f	ESTIMATED VALUE & σ_f (parallel)
u_c	1.6889	1.351 ±0.20	1.509(-10.68%) ±0.108	1.235(-26.90%) ±0.135	1.657(-1.88%) ±0.37E-1
α	180.0°	165.0° ±5.0°	180.3°(0.18%) ±0.17°	179.8°(-0.11%) ±0.20°	180.0°(0.04%) ±0.11°
$m'-X'_u$	0.01885	0.01847 ±0.0	0.01847(-2.02%) ±0.0	0.01847(-2.02%) ±0.0	0.01847(-2.02%) ±0.0
C_R	0.002256	0.001805 ±0.226E-3	0.002239(-0.74%) ±0.271E-4	0.002109(-6.53%) ±0.296E-4	0.002202(-2.37%) ±0.864E-5

¶ u_0=23.111 ft/sec., v_0=0.0 ft/sec., r_0=0.0 rad/sec., ψ_0=0.0°

† u_0=26.489 ft/sec., v_0=0.0 ft/sec., r_0=0.0 rad/sec., ψ_0=0.0°

Table 7.5   Summary of resistance coefficient estimation with $m'-X'_u$ fixed onto a value of 2% error.   Current angle is 180°.
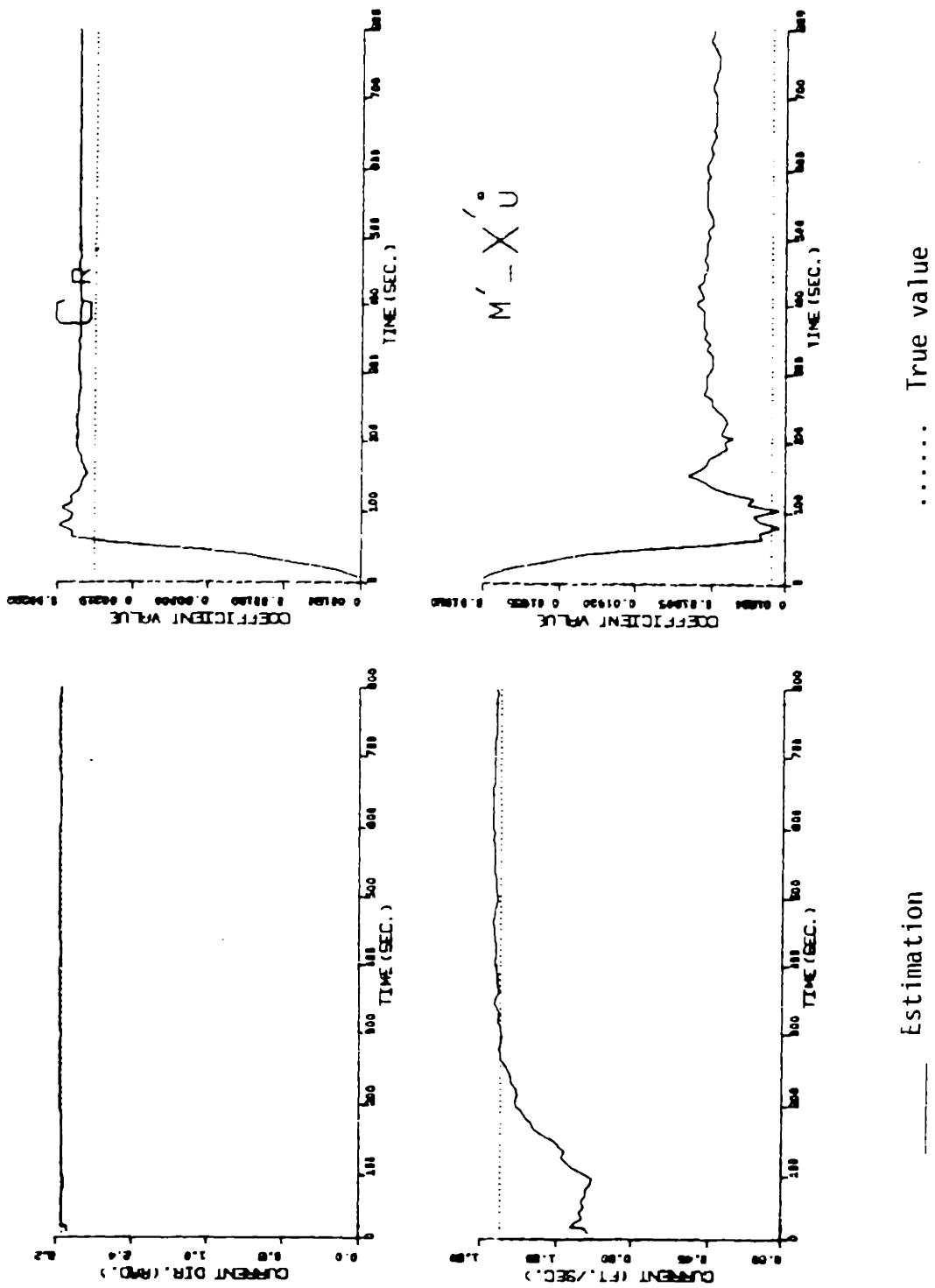
Figure 7.19   Results of identification.   The data of files of Fig. 7.16.a and
Fig. 7.17.a are parallelly processed to estimate the resistance
coefficient C_R together with $m'-X'_u$.
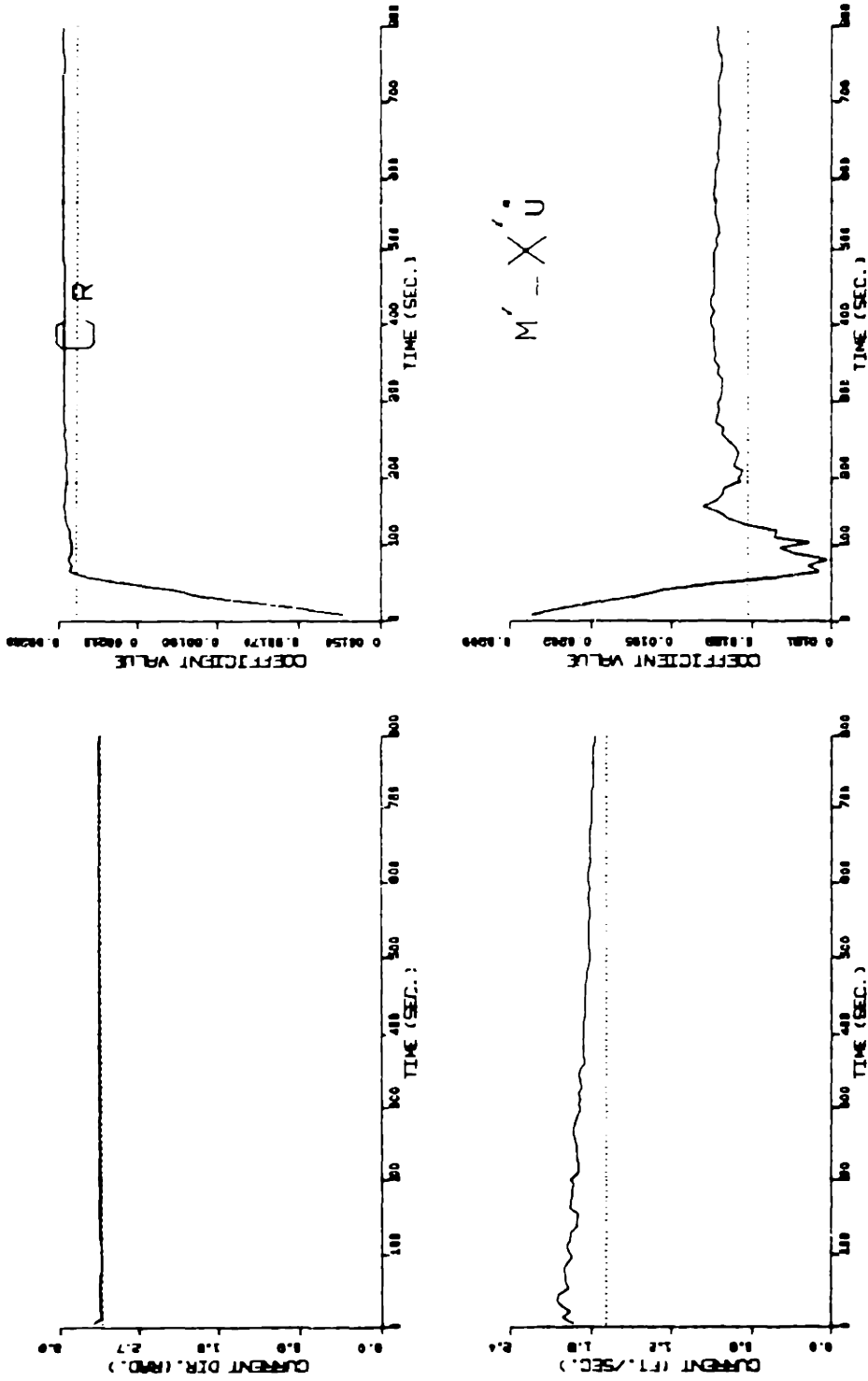
——— Estimation   ······· True value

Figure 7.20 Results of identification. The data of files of Fig. 7.16.a and Fig. 7.17.a
are parallelly processed to estimate the resistance coefficient C_R together
with $m'-X'_{\dot{u}}$.

——— Estimation   .... True value
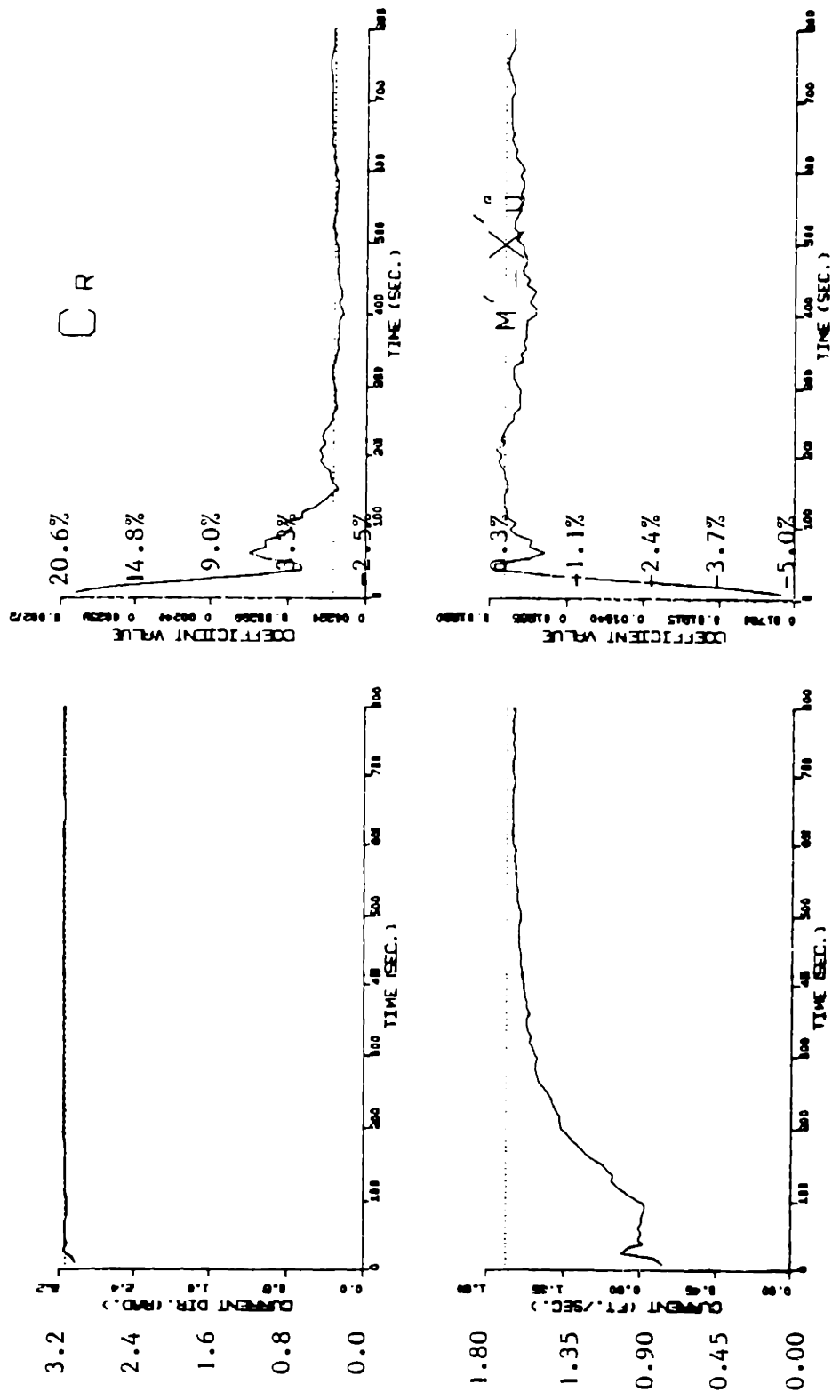
Figure 7.21 Results of identification. The data of files of Fig. 7.16.a and Fig. 7.17.a are parallelly processed to estimate the resistance coefficient C_R together with $m'-X_{\dot{u}}'$.
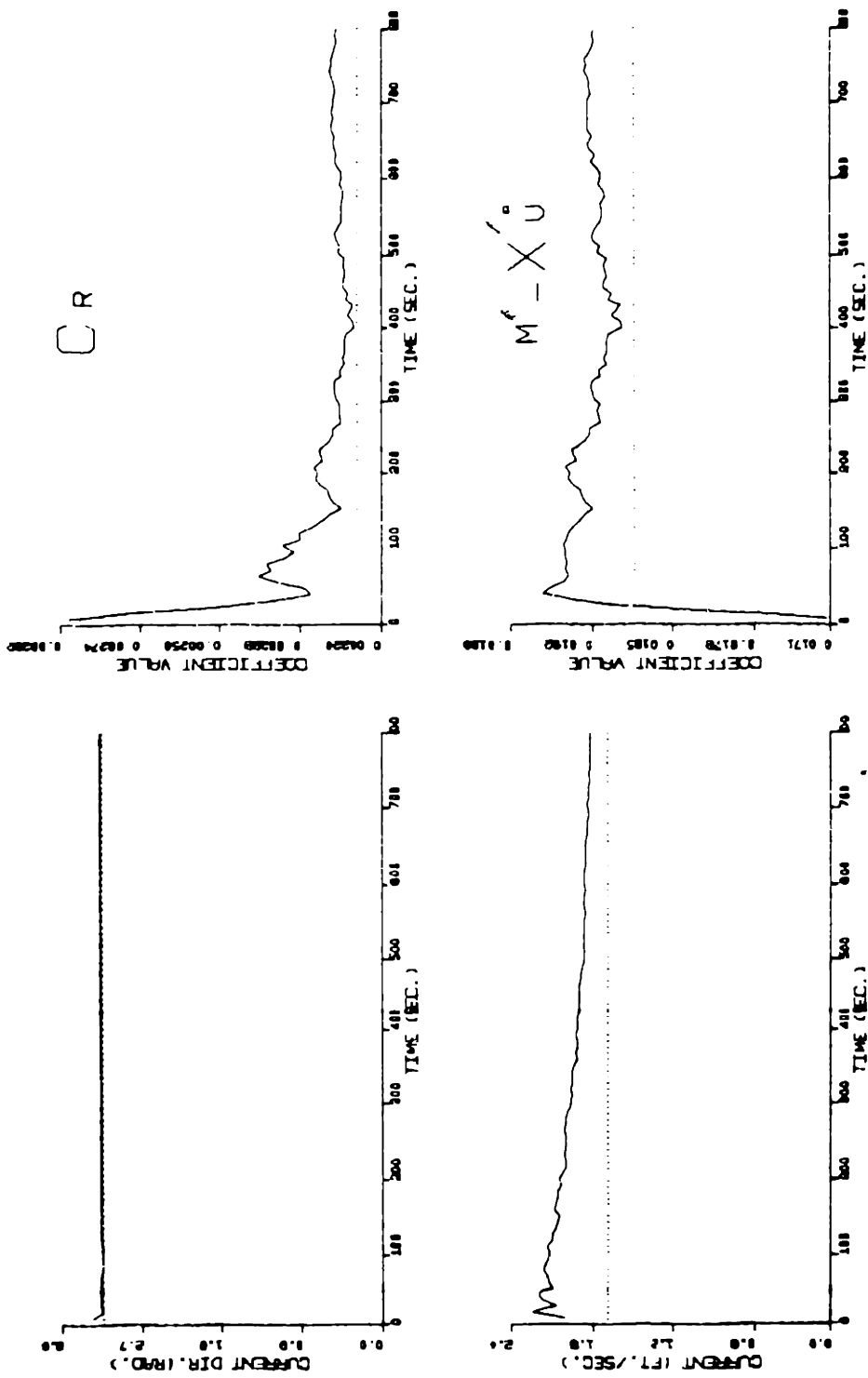
Figure 7.22 Results of identification. The data of files of Fig. 7.16.a and Fig. 7.17.a
are parallelly processed to estimate the resistance coefficient C_R together
with $m'-X'_{\dot{u}}$.

	TRUE VALUE	ESTIMATION OF FIGURE 7.19	ESTIMATION OF FIGURE 7.20	ESTIMATION OF FIGURE 7.21	ESTIMATION OF FIGURE 7.22
u_c	1.689	1.351(-20.0%)* ±0.20 ⋯ 1.707(1.04%)* ±0.375E-1	2.027(20.0%) ±0.20 ⋯ 1.776(5.13%) ±0.376E-1	1.182(-30.0%) ±0.30 ⋯ 1.641(2.84%) ±0.363E-1	2.196(30.0%) ±0.30 ⋯ 1.816(7.51%) ±0.360E-1
α	180.0°	165.0°(-15.0°) ±5.00 ⋯ 180.0°(0.02%) ±0.103E0	195.0°(+15.0°) ±5.00 ⋯ 180.0°(0.00%) ±0.890E-1	160.0°(-20.0°) ±7.00 ⋯ 180.1°(0.03%) ±0.113E0	200.0°(+20.0°) ±7.00 ⋯ 180.0°(0.01%) ±0.845E-1
$m'-X'_u$	0.01885	0.01980(5.0%) ±0.94E-3 ⋯ 0.01905(1.08%) ±0.827E-3	0.02074(10.0%) ±0.189E-2 ⋯ 0.01911(1.38%) ±0.146E-3	0.01791(-5.0%) ±0.94E-3 ⋯ 0.01882(0.17%) ±0.822E-3	0.01697(-10.0%) ±0.189E-2 ⋯ 0.01918(1.77%) ±0.145E-3
C_R	0.002256	0.001805(-20.0%) ±0.226E-3 ⋯ 0.002283(1.21%) ±0.989E-4	0.001579(-30.0%) ±0.338E-3 ⋯ 0.002291(1.55%) ±0.175E-3	0.002707(20.0%) ±0.226E-3 ⋯ 0.002256(0.00%) ±0.997E-4	0.002933(30.6%) ±0.338E-3 ⋯ 0.002300(1.96%) ±0.175E-3

* Initial guess is shown above the dash line and the estimated values are listed below.

Table 7.6 Summary of estimation from different initial guess. C_R and $m'-X'_u$ are simultaneously estimated for $\alpha=180°$ by parallel processing scheme.
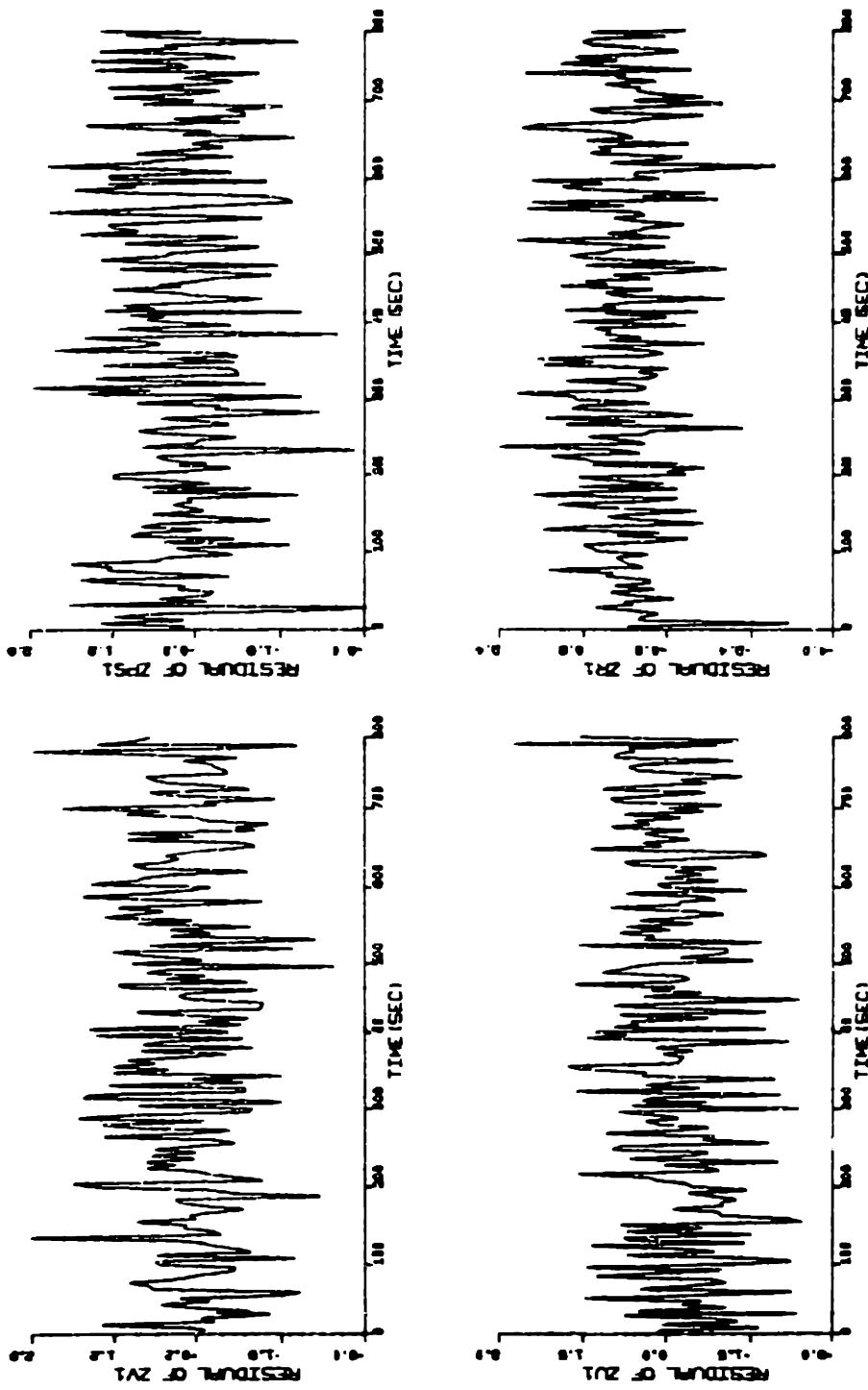
Figure 7.23.a   Validity tests for the results of identification in Figure 7.21.
Plots of normalized residuals for the first file.
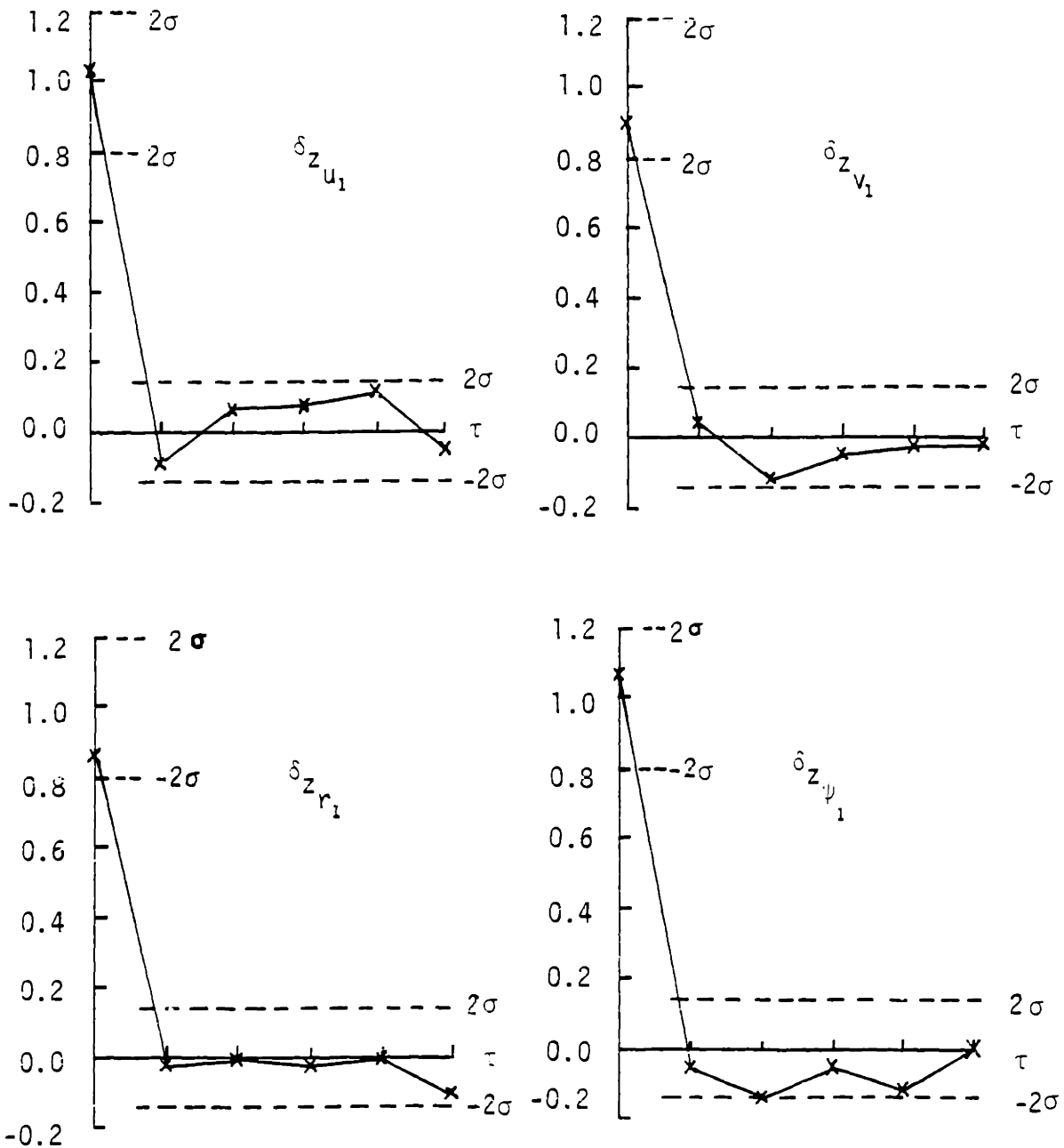
Auto-Correlation of Residuals

Sum of squared residuals = 1635.33
If H_0 is true, E[Sum of squared residuals]= 1600.00 σ=56.57

Figure 7.23.b   Validity tests for the results of identification in
Figure 7.21.   Auto-correlation of the normalized
residuals for the first file.

Table 7.7   Results of identification.   Application of the "parameter
             transformation" scheme to estimate the coefficients from
             the same simulated maneuvering data in Fig. 7.5.a.

NP = 37   MODEL VALUE = 0.13500D+01

STARTING VALUE = 0.10500D+01 + OR - 0.20000D+00
FILTERED VALUE = 0.13537D+01 + OR - 0.10942D-01
IDENTIFIED WITHIN 0.27% OF THE MODEL VALUE

NP = 38   MODEL VALUE = 0.86000D+02

STARTING VALUE = 0.76000D+02 + OR - 0.40000D+01
FILTERED VALUE = 0.86148D+02 + OR - 0.41266D+00
IDENTIFIED WITHIN 0.17% OF THE MODEL VALUE

NP = 6   MODEL VALUE = -0.28280D-01

STARTING VALUE = -0.23520D-01 + OR - 0.56000D-02
FILTERED VALUE = -0.27592D-01 + OR - 0.12952D-02
IDENTIFIED WITHIN -2.41% OF THE MODEL VALUE

NP = 7   MODEL VALUE = 0.50000D+00

STARTING VALUE = 0.33000D+00 + OR - 0.50000D-01
FILTERED VALUE = 0.49203D+00 + OR - 0.56753D-02
IDENTIFIED WITHIN -0.24% OF THE MODEL VALUE

NP = 12   MODEL VALUE = -0.10960D-01

STARTING VALUE = -0.67900D-02 + OR - 0.22000D-02
FILTERED VALUE = -0.10338D-01 + OR - 0.69410D-03
IDENTIFIED WITHIN 1.75% OF THE MODEL VALUE

NP = 13   MODEL VALUE = 0.51100D+00

STARTING VALUE = 0.58000D+00 + OR - 0.54000D-01
FILTERED VALUE = 0.51548D+00 + OR - 0.60300D-01
IDENTIFIED WITHIN 0.88% OF THE MODEL VALUE

NP = 14   MODEL VALUE = -0.24290D-02

STARTING VALUE = -0.12400D-02 + OR - 0.24200D-03
FILTERED VALUE = -0.24094D-02 + OR - 0.51114D-04
IDENTIFIED WITHIN -0.65% OF THE MODEL VALUE

NP = 21   MODEL VALUE = 0.30700D-01

STARTING VALUE = 0.24560D-01 + OR - 0.30700D-02
FILTERED VALUE = 0.30214D-01 + OR - 0.41387D-03
IDENTIFIED WITHIN -1.58% OF THE MODEL VALUE

Table 7.7   Continued
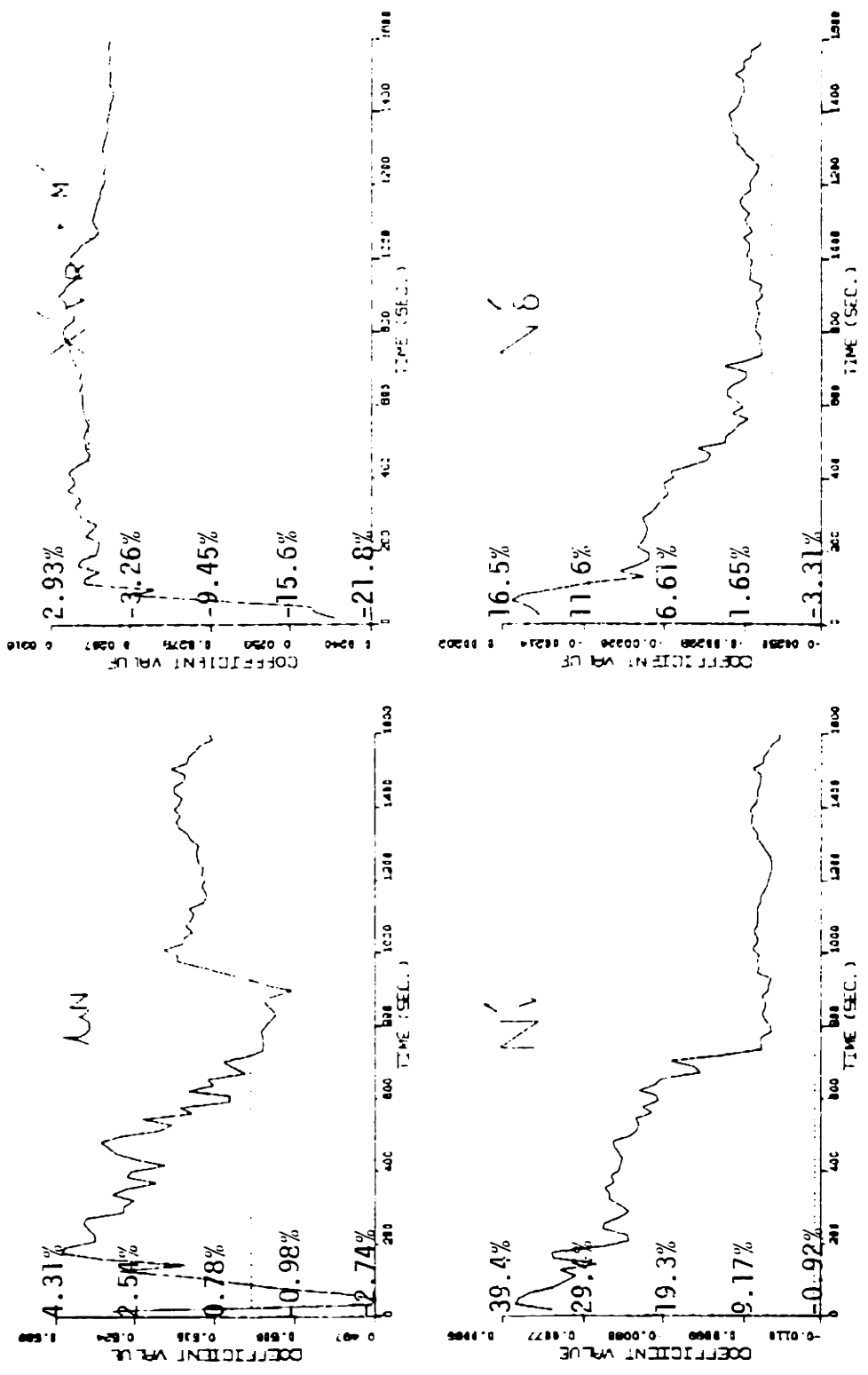
Figure 7.24.a   Results of identification. Application of the "parameter transformation"
scheme to estimate   the coefficients from the same simulated maneuvering
data in Figure 7.5.a.
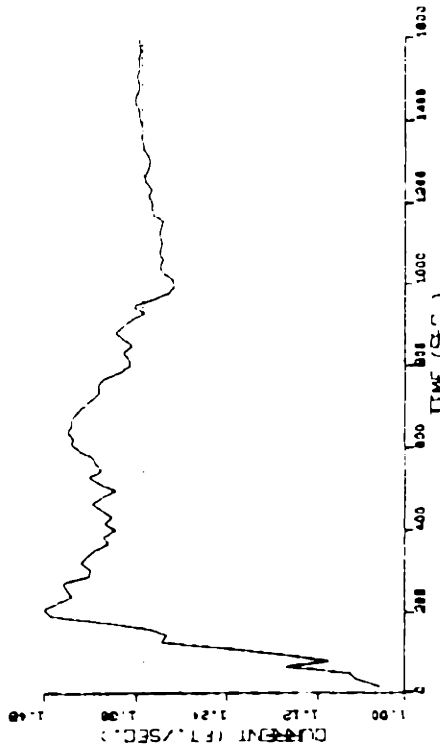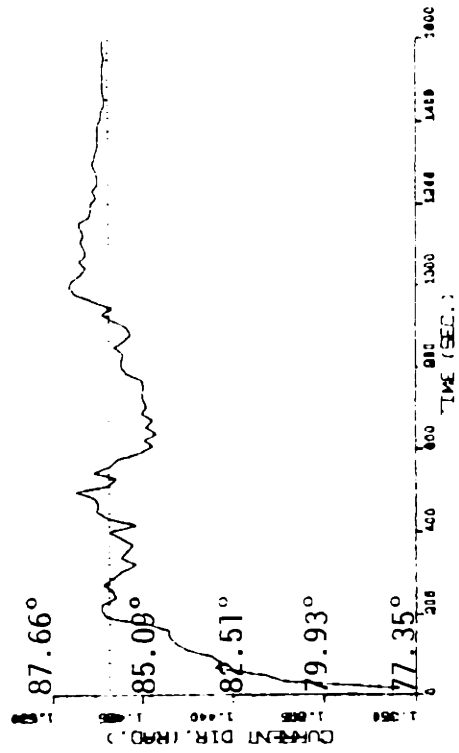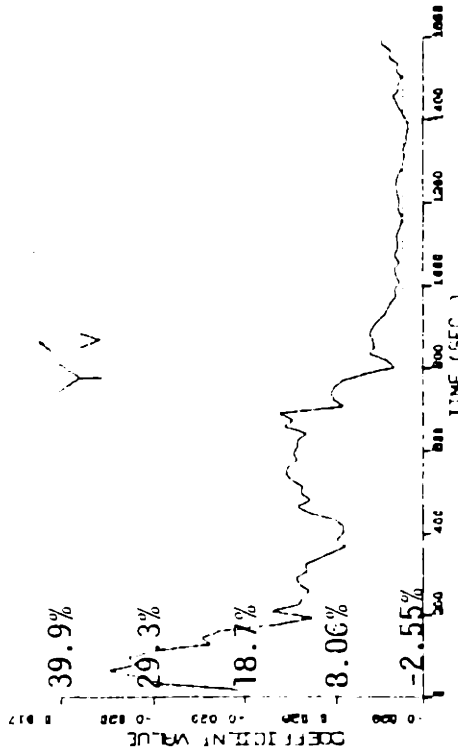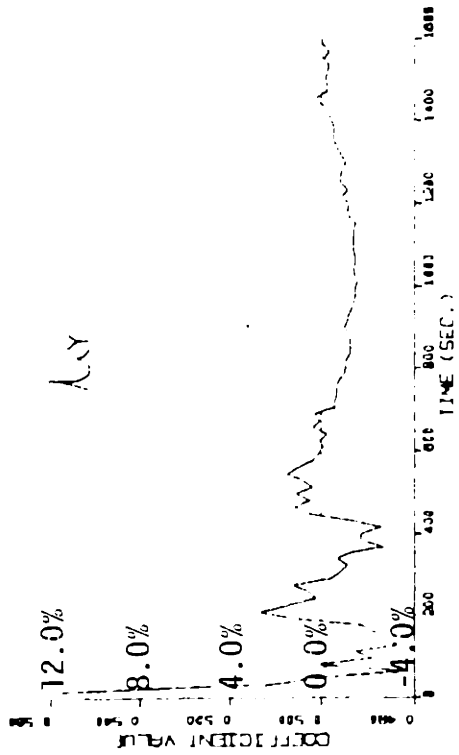
Figure 7.24.b Results of identification.

——— Estimation   ······· True value

NP = 12   MODEL VALUE =   -0.10990D+01

STARTING VALUE =   -0.10990D-01 + OR -   0.20000D-02

FILTERED VALUE =   -0.10931D-01 + OR -   0.6501D-03

IDENTIFIED WITHIN   0.29% OF THE MODEL VALUE

NP = 13   MODEL VALUE =   0.51100D+00

STARTING VALUE =   0.51500D+00 + OR -   0.5200D-01

FILTERED VALUE =   0.51374D+00 + OR -   0.61074D-02

IDENTIFIED WITHIN   0.54% OF THE MODEL VALUE

NP = 14   MODEL VALUE =   -0.24200D-02

STARTING VALUE =   -0.24000D-02 + OR -   0.24200D-03

FILTERED VALUE =   -0.24285D-02 + OR -   0.47565D-04

IDENTIFIED WITHIN   0.35% OF THE MODEL VALUE

NP = 21   MODEL VALUE =   0.30740D-01

STARTING VALUE =   0.30210D-01 + OR -   0.30740D-01

FILTERED VALUE =   0.30278D-01 + OR -   0.40417D-03

IDENTIFIED WITHIN   -1.30% OF THE MODEL VALUE

NP = 39   MODEL VALUE =   0.13500D+01

STARTING VALUE =   0.13540D+01 + OR -   0.20000D+00

FILTERED VALUE =   0.13532D+01 + OR -   0.10190D-01

IDENTIFIED WITHIN   0.22% OF THE MODEL VALUE

NP = 30   MODEL VALUE =   0.86000D+02

STARTING VALUE =   0.86100D+02 + OR -   0.40000D+01

FILTERED VALUE =   0.86175D+02 + OR -   0.39489D+00

IDENTIFIED WITHIN   0.21% OF THE MODEL VALUE

NP = 6   MODEL VALUE =   -0.20280D-01

STARTING VALUE =   -0.27600D-01 + OR -   0.56000D-02

FILTERED VALUE =   -0.27351D-01 + OR -   0.12619D-02

IDENTIFIED WITHIN   0.35% OF THE MODEL VALUE

NP = 7   MODEL VALUE =   0.50000D+00

STARTING VALUE =   0.50000D+00 + OR -   0.50000D-01

FILTERED VALUE =   0.50108D+00 + OR -   0.50202D-02

IDENTIFIED WITHIN   0.22% OF THE MODEL VALUE

Table 7.8 Results of identification. Second pass of the parameter estimation of
Figure 7.24.a and 7.24.b.

Figure 7.25.a Results of identification. Second pass of the parameter estimation of Figure 7.24.a and 7.24.b.

Figure 7.25.b Results of identification

_____ Estimation   .... True value
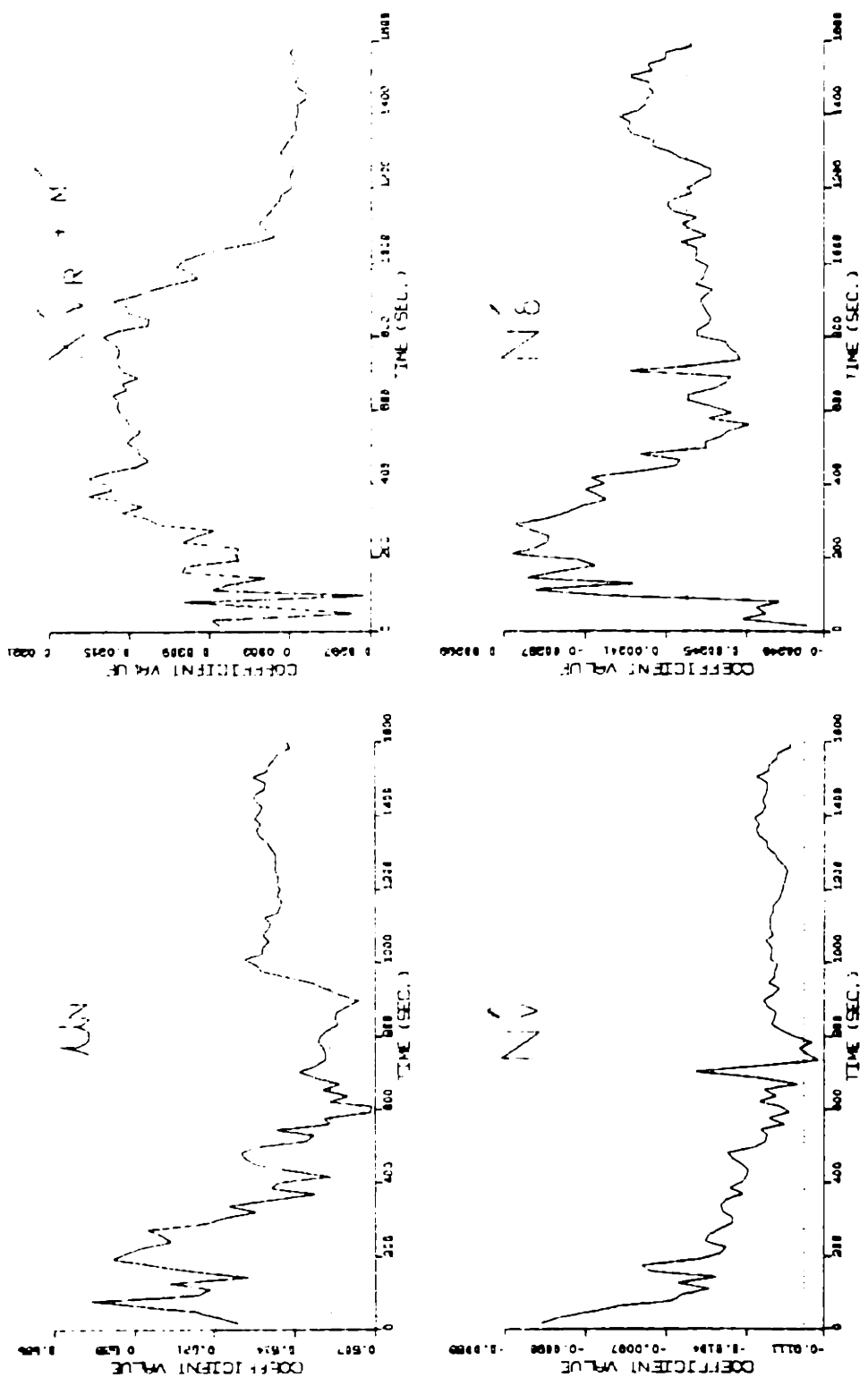
Figure 7.26.a Results of identification. Application of the "parameter transformation" scheme to estimate the coefficients from the same simulated maneuvering data as in Figure 7.5.a. Initial guesses of the parameters correspond to those in Figure 7.7.a and 7.7.b.
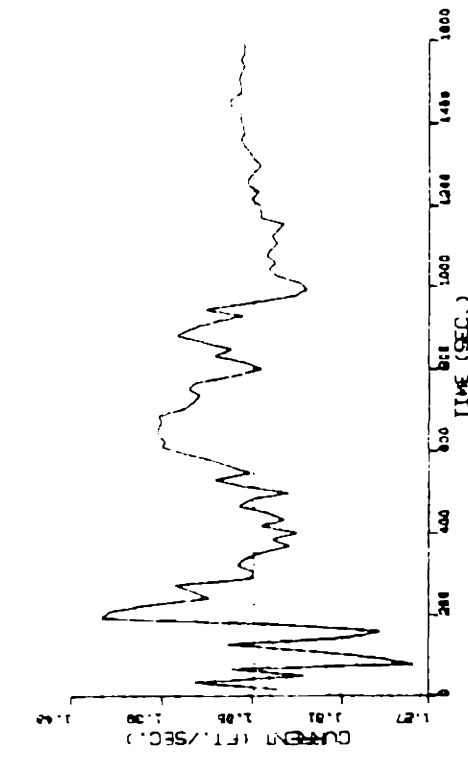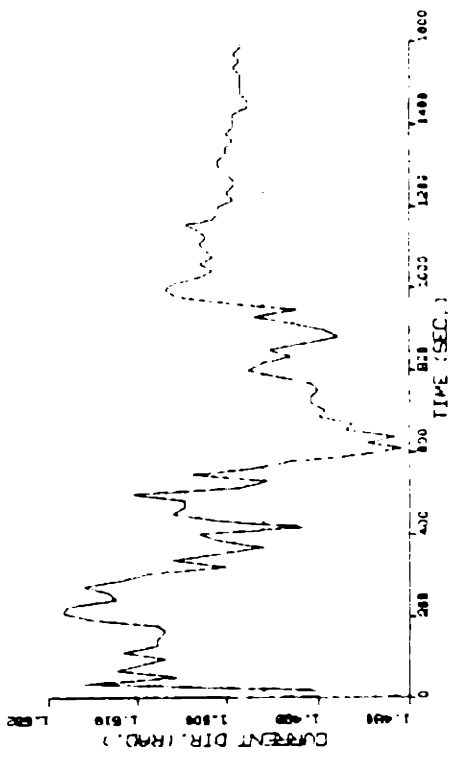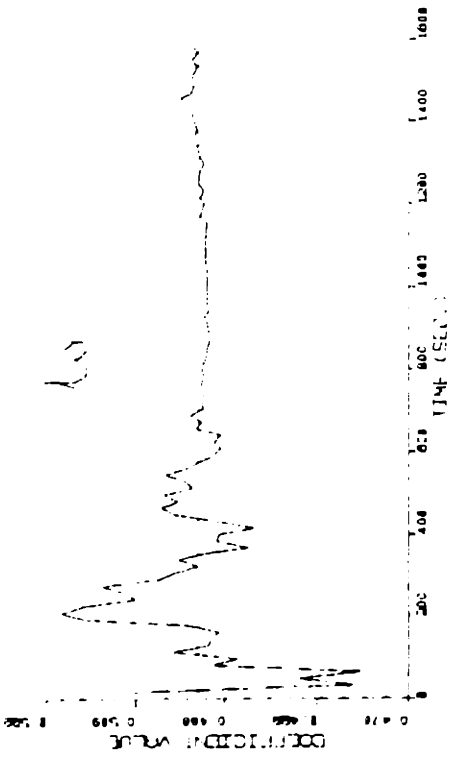
.... True value

——— Estimation

Figure 7.26.b Results of identification

———— Estimation   ⋯⋯⋯ True value

Figure 7.27.a   Results of identification. Estimation of N_0' by parallelly processing the sea trial 10°/10° zigzag maneuvering data and the 20°/20° zigzag maneuvering data.

——————   Estimation

· · · · · · ·   Model testing value or initial guess

.... Model testing value or initial guess

―――― Estimation

Figure 7.27.b Results of identification
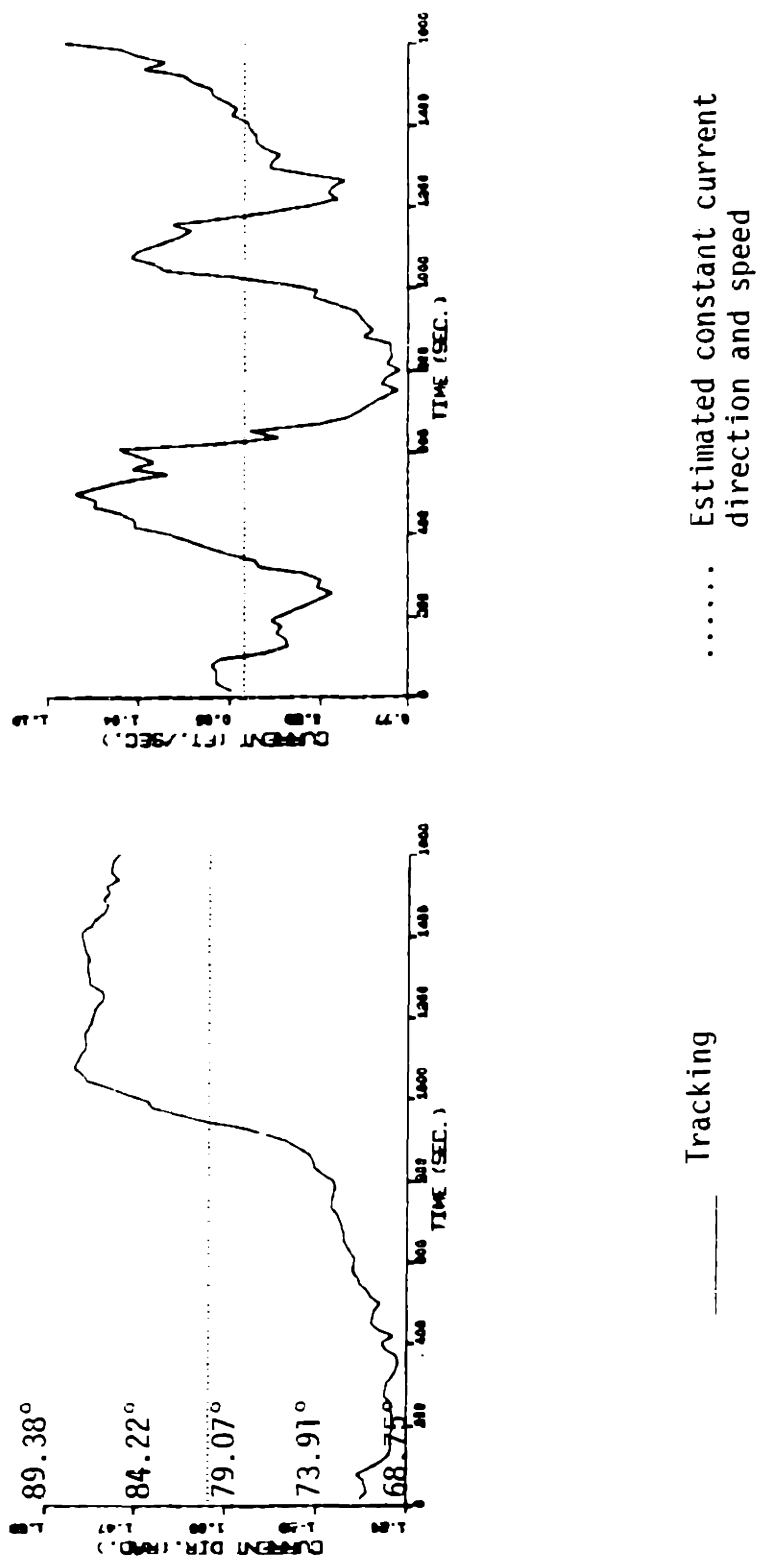
Figure 7.28 Tracking the variation of current in the 10°/10° zigzag sea trial maneuvering data of ESSO OSAKA.

——————— Tracking

.... Estimated constant current direction and speed
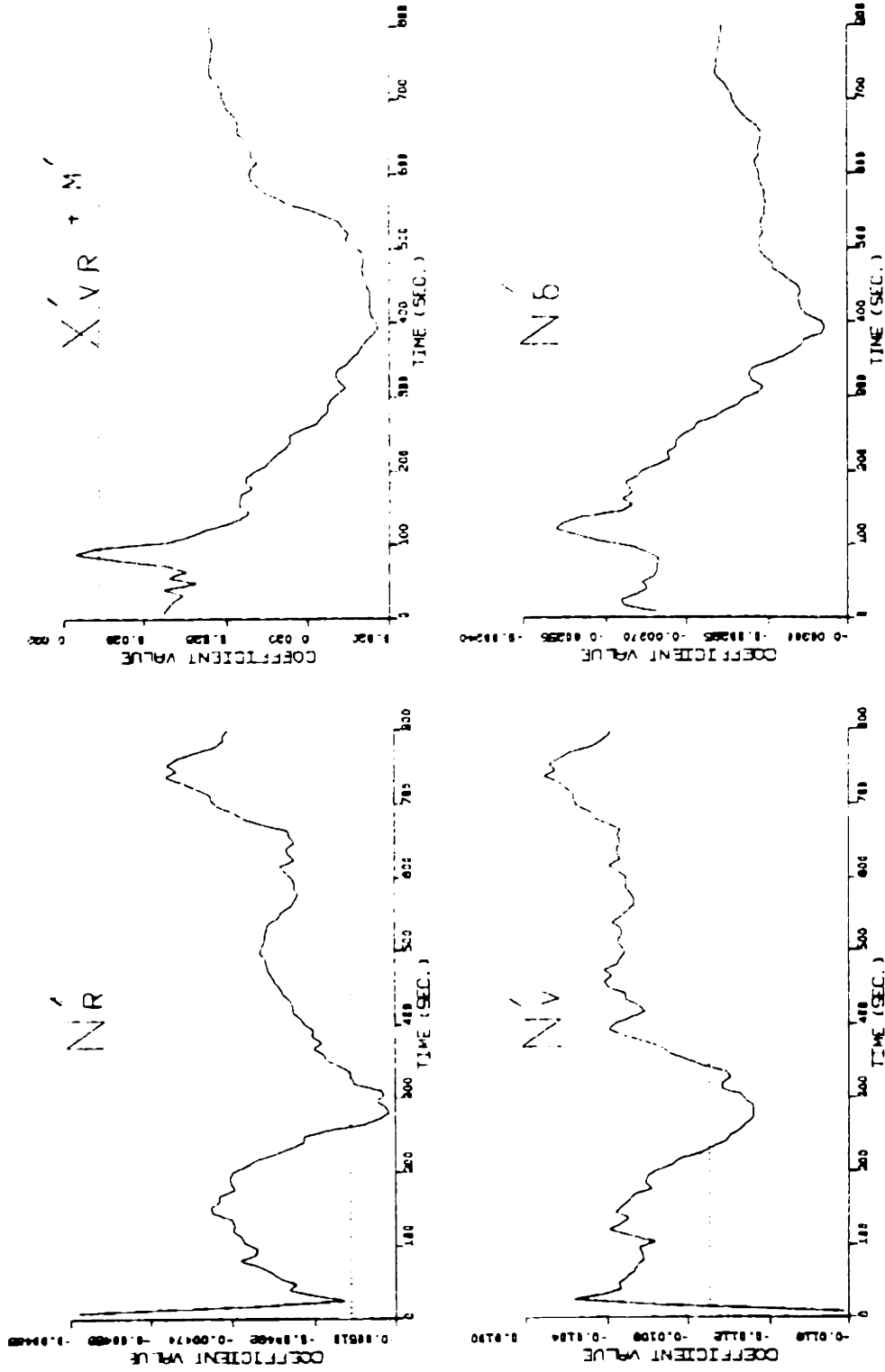
Figure 7.29.a Results of identification. Major linear coefficients of ESSO OSAKA are estimated by processing the 10°/10° zigzag sea trial maneuvering data.

Figure 7.29.b Results of identification.
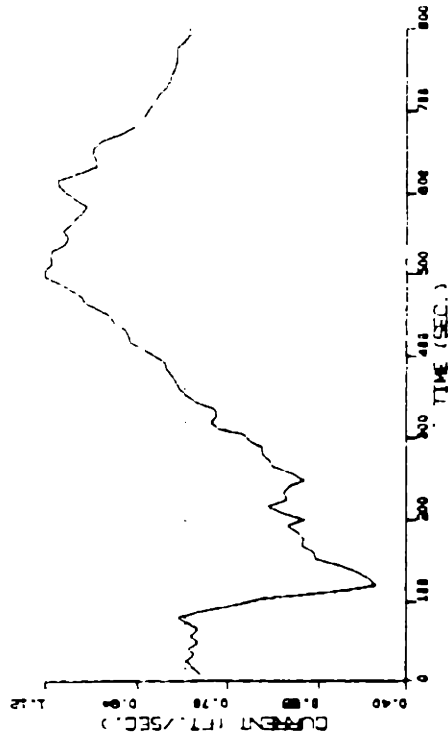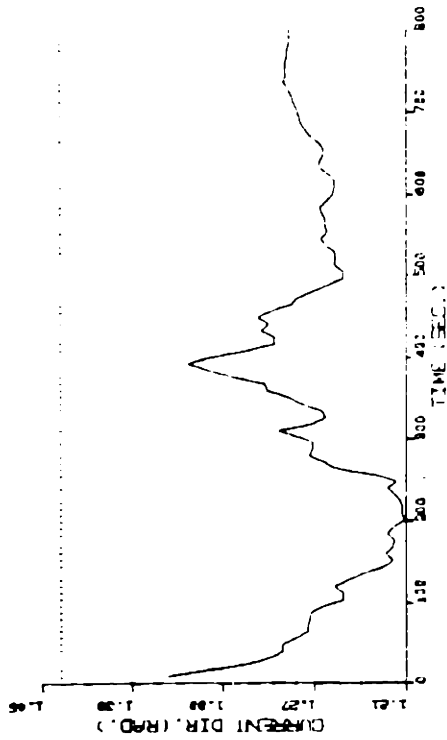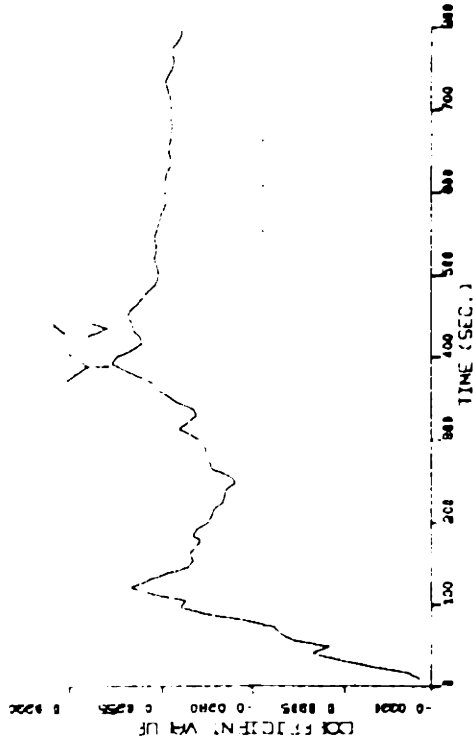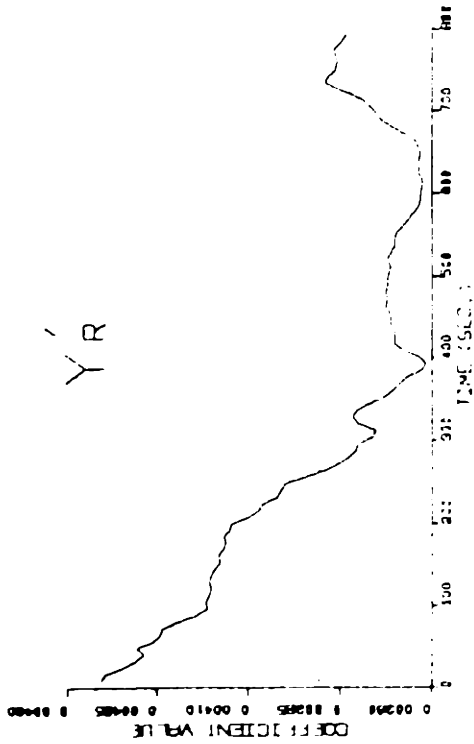
Estimation

...... Model testing value or initial guess

Figure 7.30.a Results of identification. Nonlinear coefficients of ESSO OSAKA are estimated by processing the 35° rudder turning sea trial maneuvering data.

Figure 7.30.b Results of identification
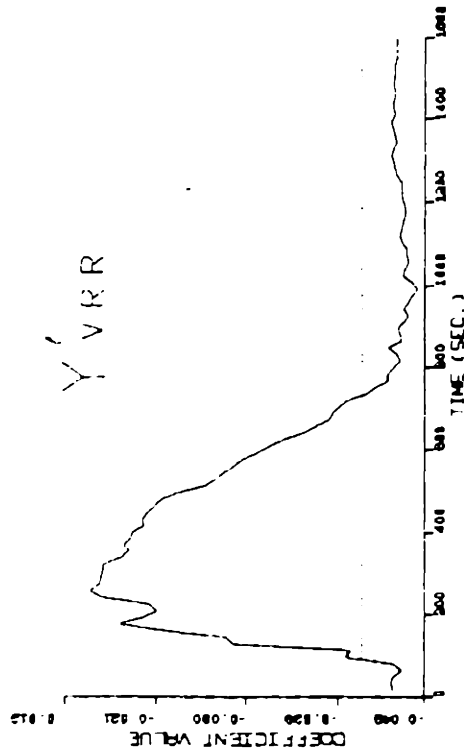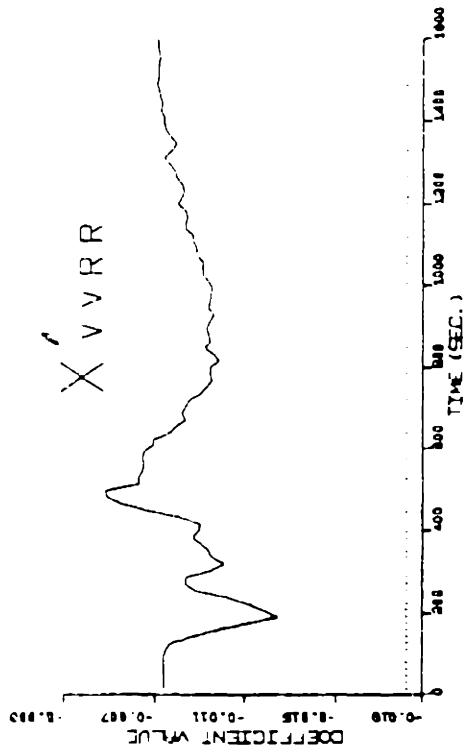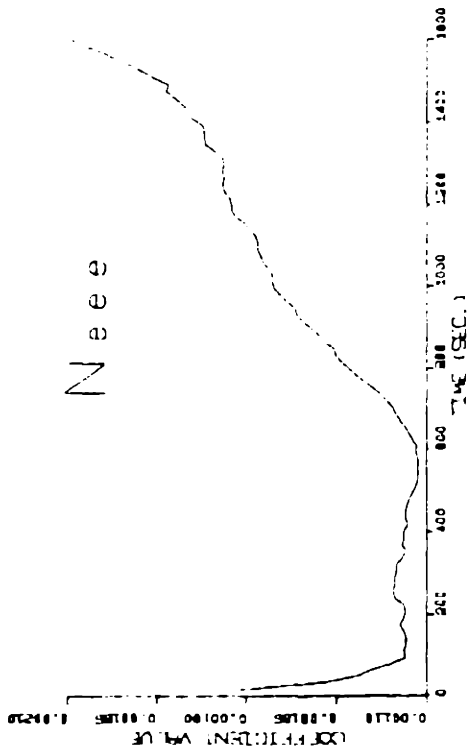
——— Estimation

······· Model testing value
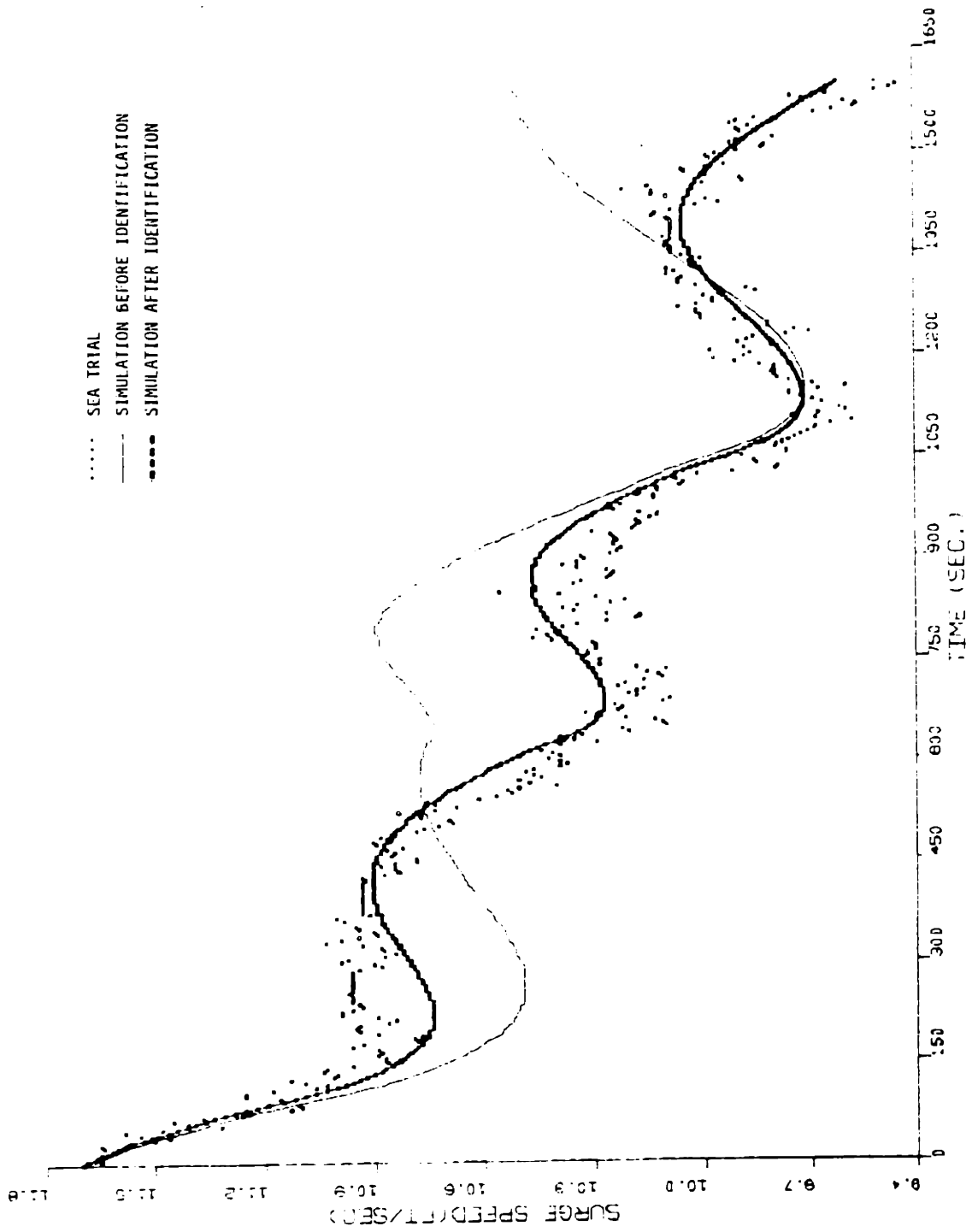
Figure 7.31.a Improvement on the surge speed simulation of 10°/10° zigzag maneuver for ESSO OSAKA after the identification
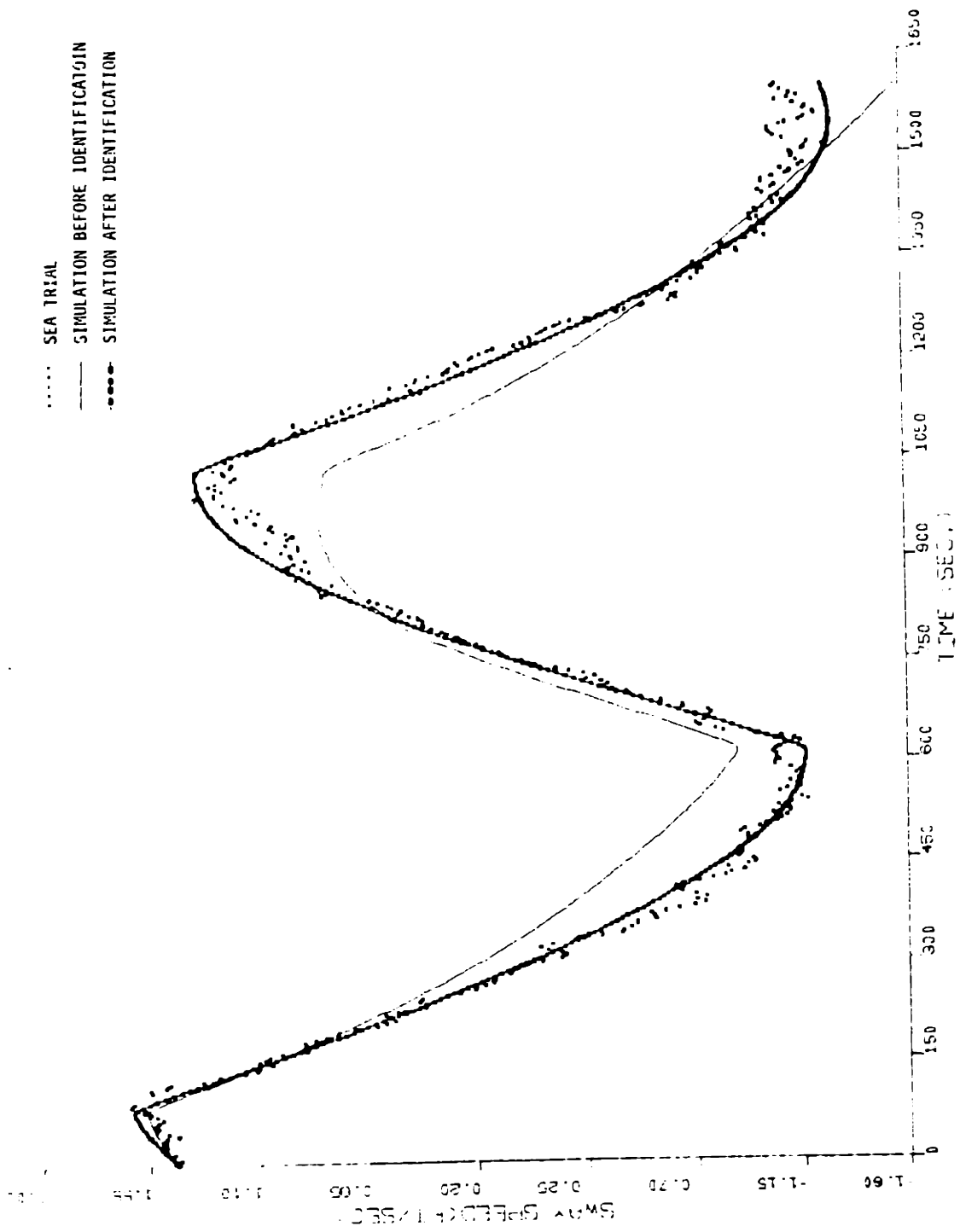
Figure 7.31.b Improvement on the sway speed simulation of 10°/10° zigzag maneuver for ESSO OSAKA after the identification
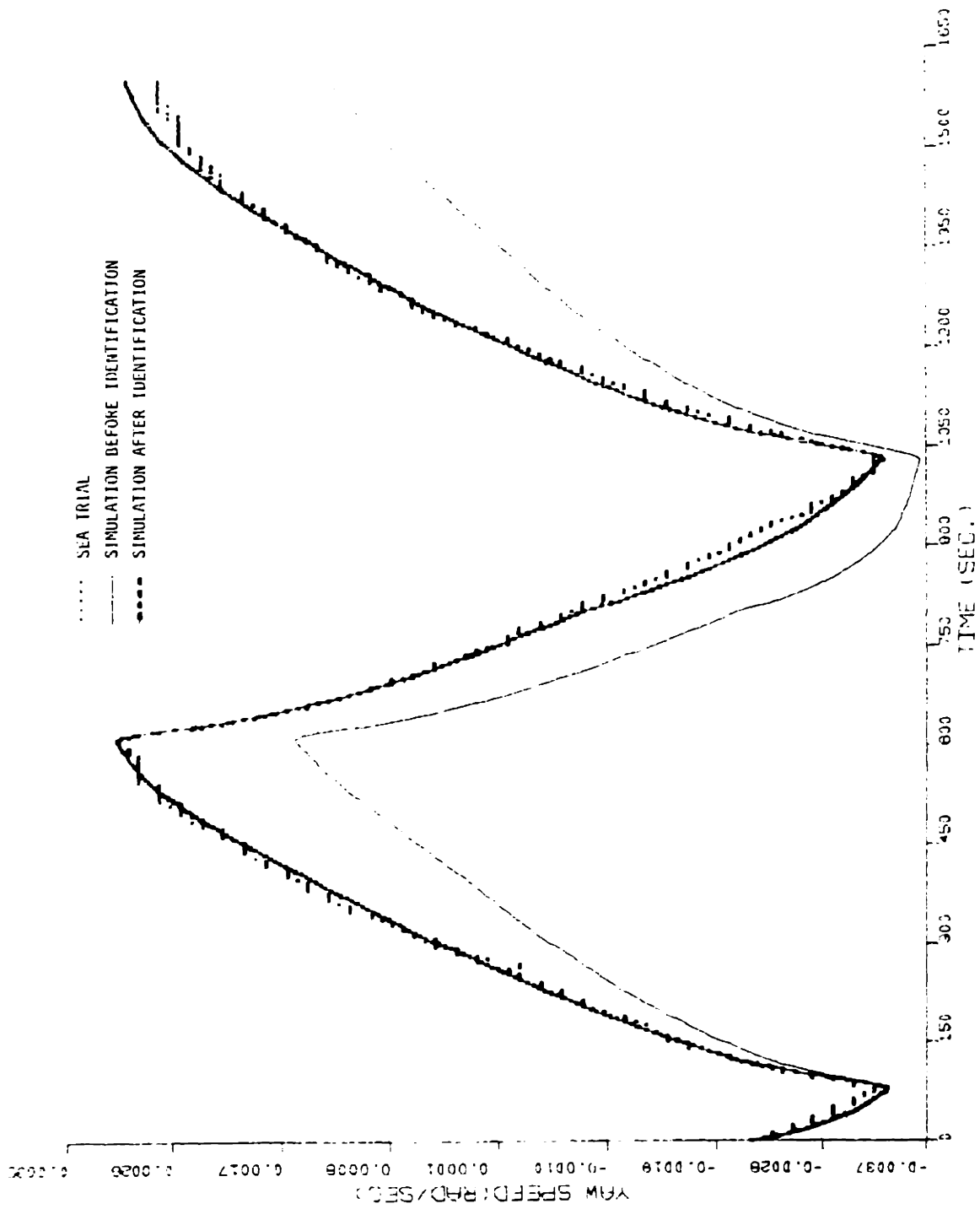
Figure 7.31.c Improvement on the yaw speed simulation of 10°/10° zigzag maneuver for ESSO OSAKA after the identification.
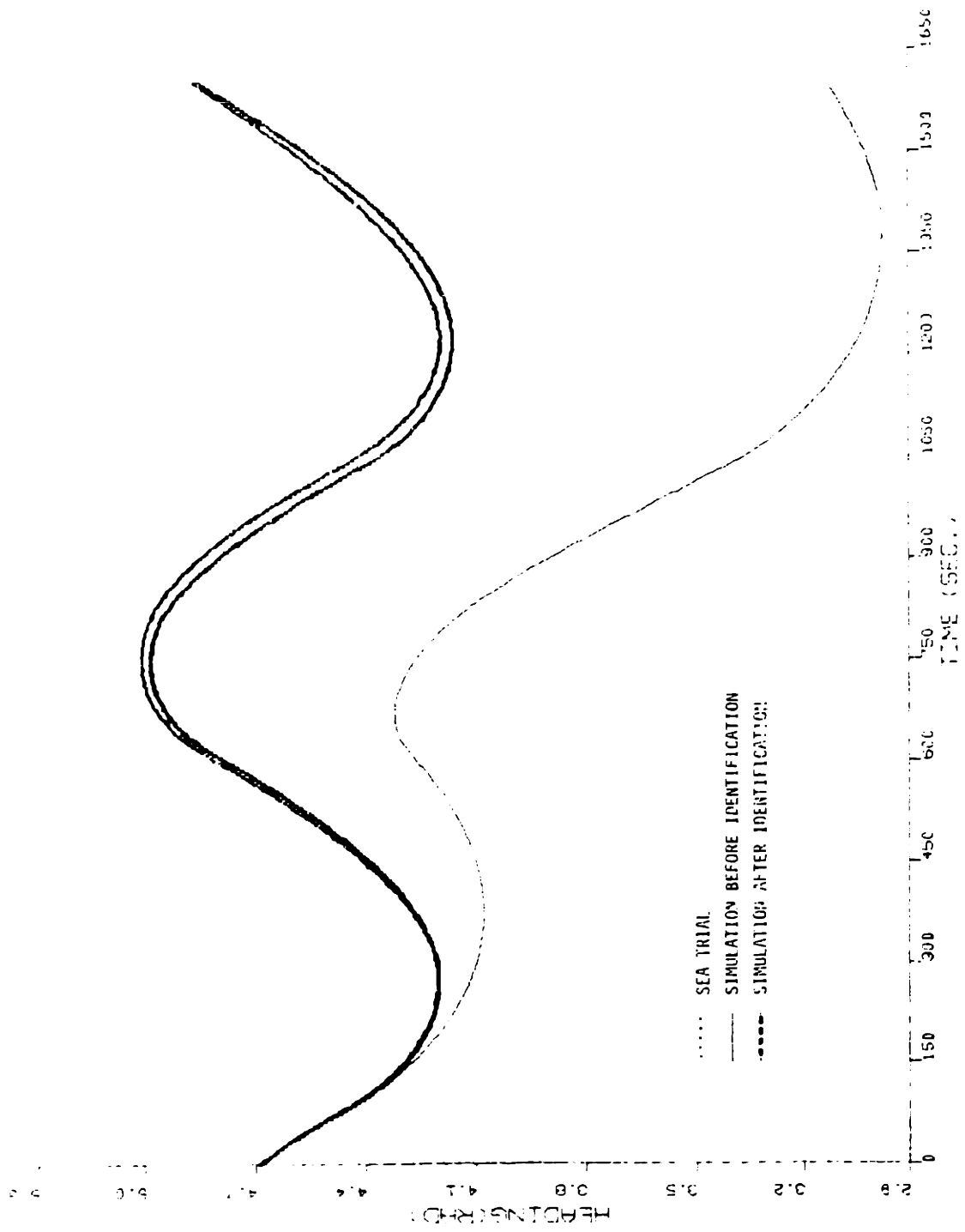
Figure 7.31.d Improvement on the heading simulation of 10°/10° zigzag maneuver for ESSO OSAKA after the identification.
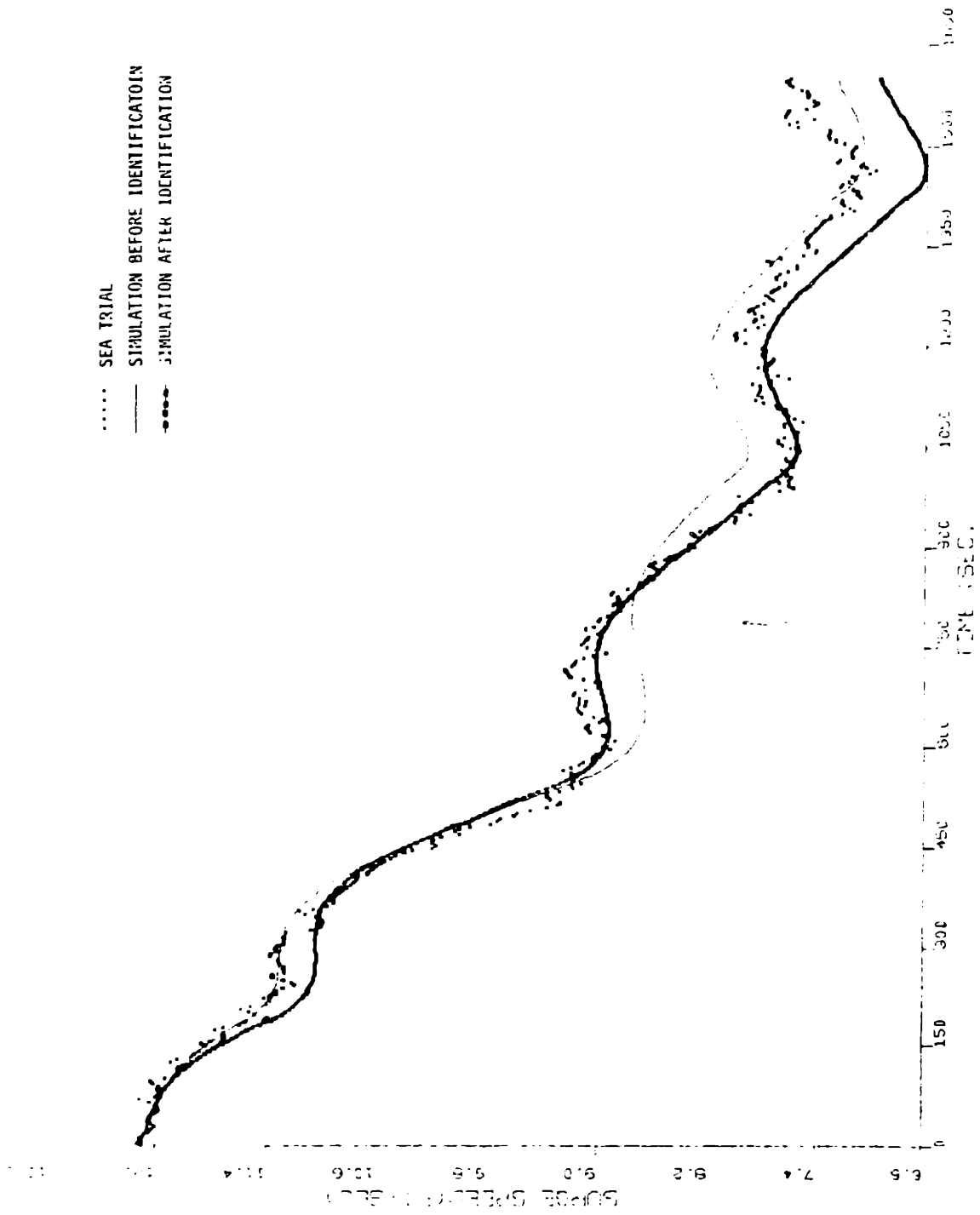
Figure 7.32.a Improvement on the surge speed simulation of 20°/20° zigzag maneuver for ESSO OSAKA after the identification.

- 276 -
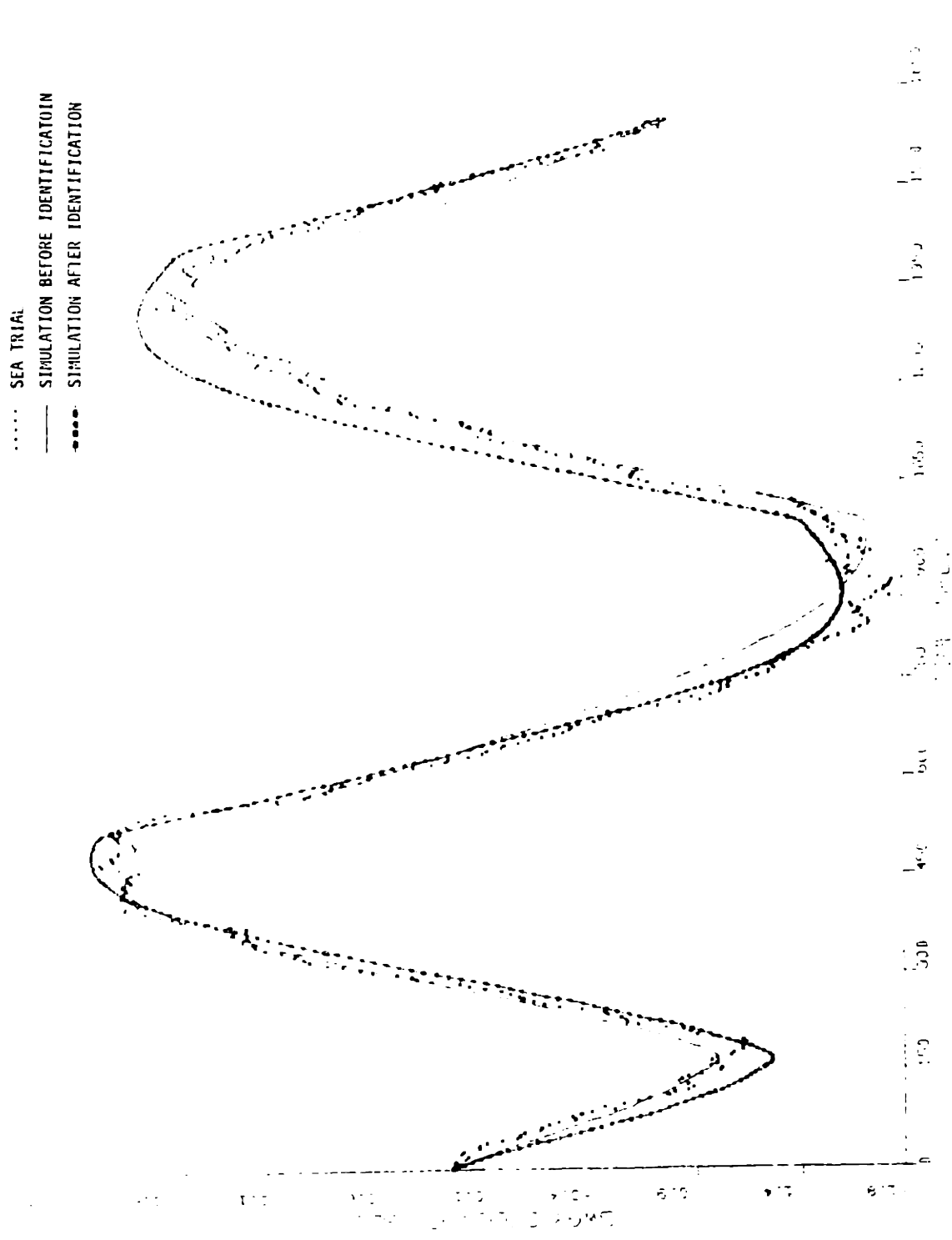
Figure 7.32.b Improvement on the sway speed simulation of 20°/20° zigzag maneuver for ESSO OSAKA after the identification.
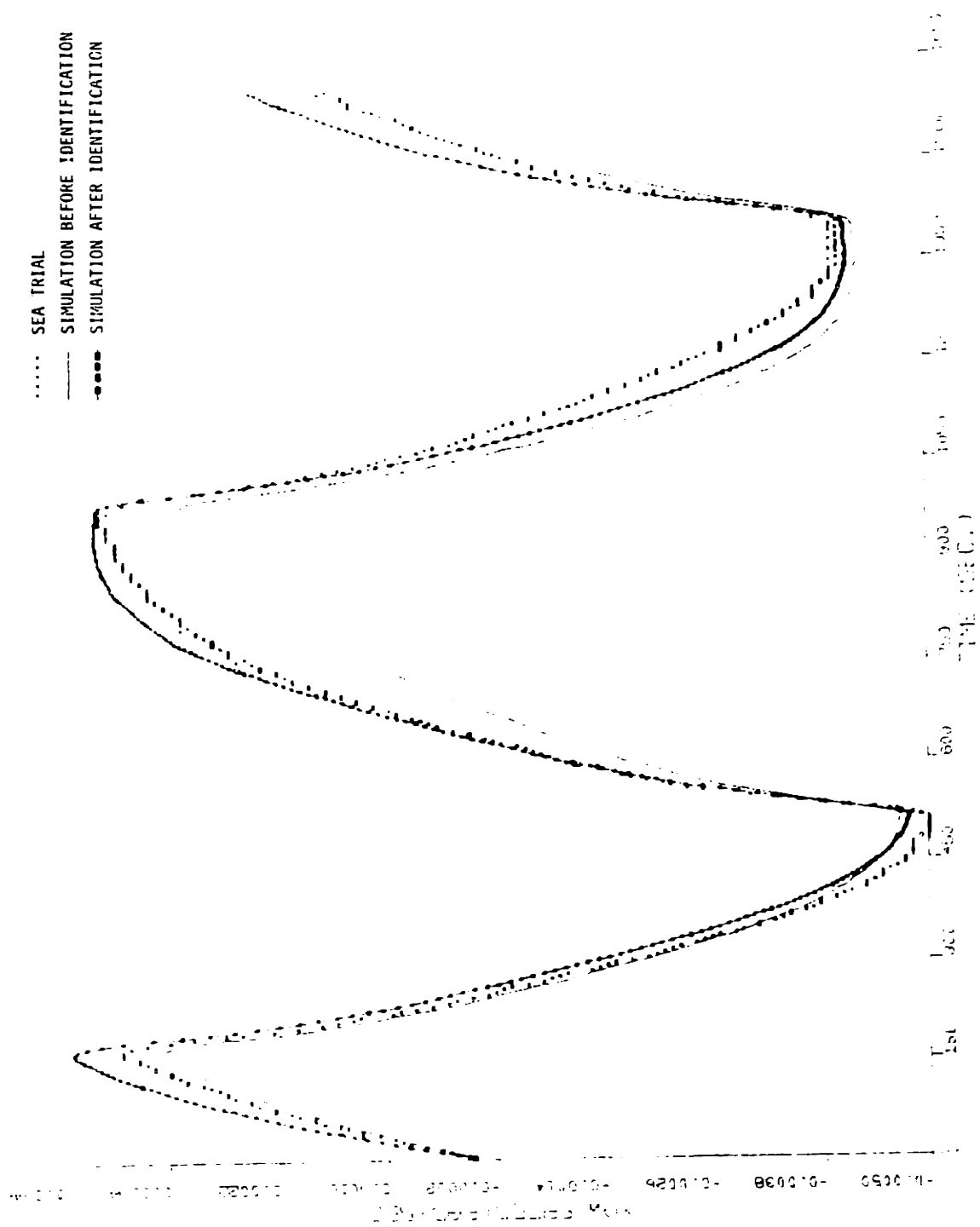
Figure 7.32.c   Improvement on the yaw speed simulation of 20°/20° zigzag maneuver for ESSO OSAKA after the identification.

Figure 7.32.d   Improvement on the heading simulation of 20°/20° zigzag maneuvre. for
ESSO OSAKA after the identification.

SEA TRIAL
SIMULATION BEFORE IDENTIFICATION
SIMULATION AFTER IDENTIFICATION
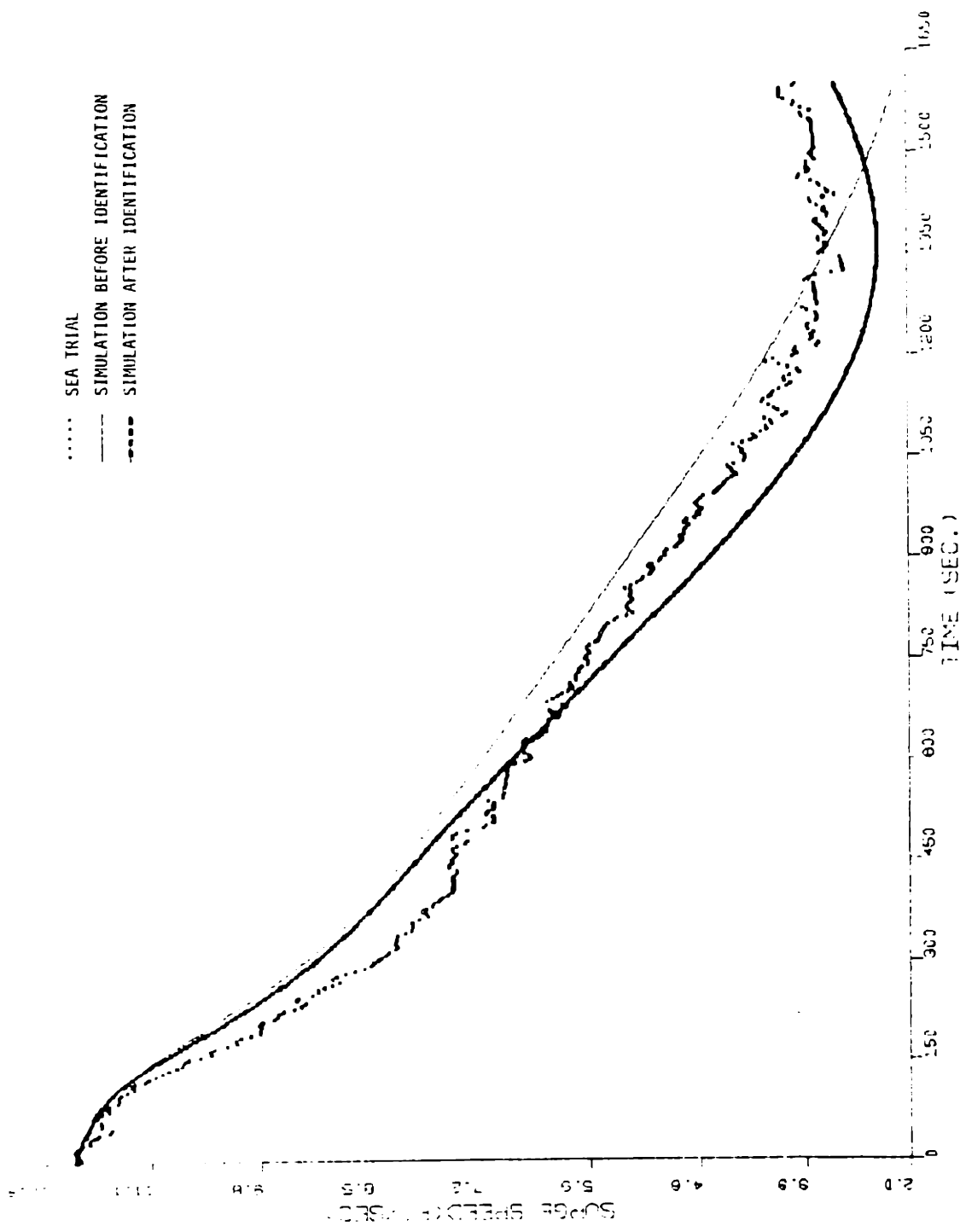
Figure 7.33.a Improvement on the surge speed simulation of 35° rudder turning maneuver for ESSO OSAKA after the identification.
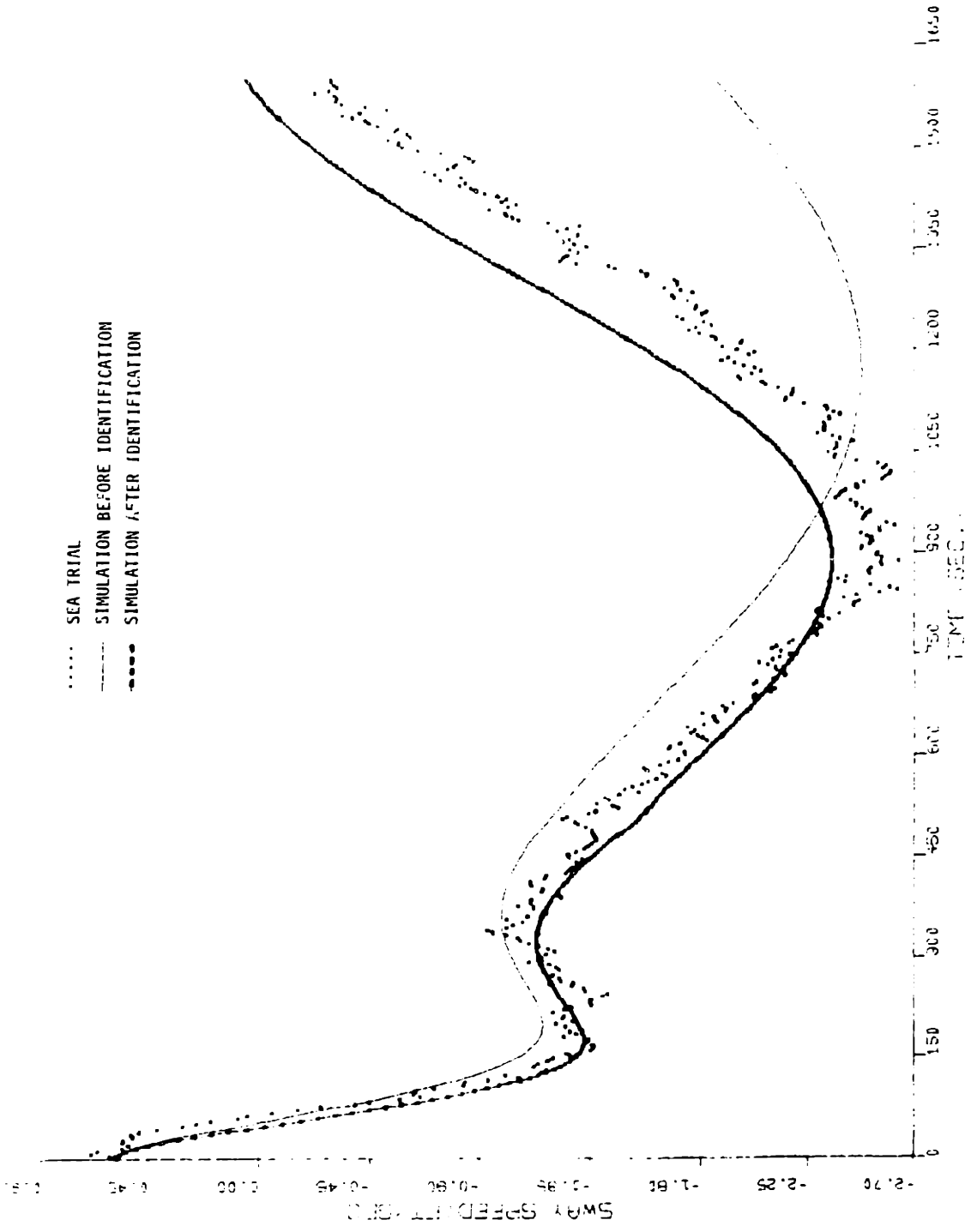
Figure 7.33.b Improvement on the sway speed simulation of 35° rudder turning maneuver for ESSO OSAKA after the identification.
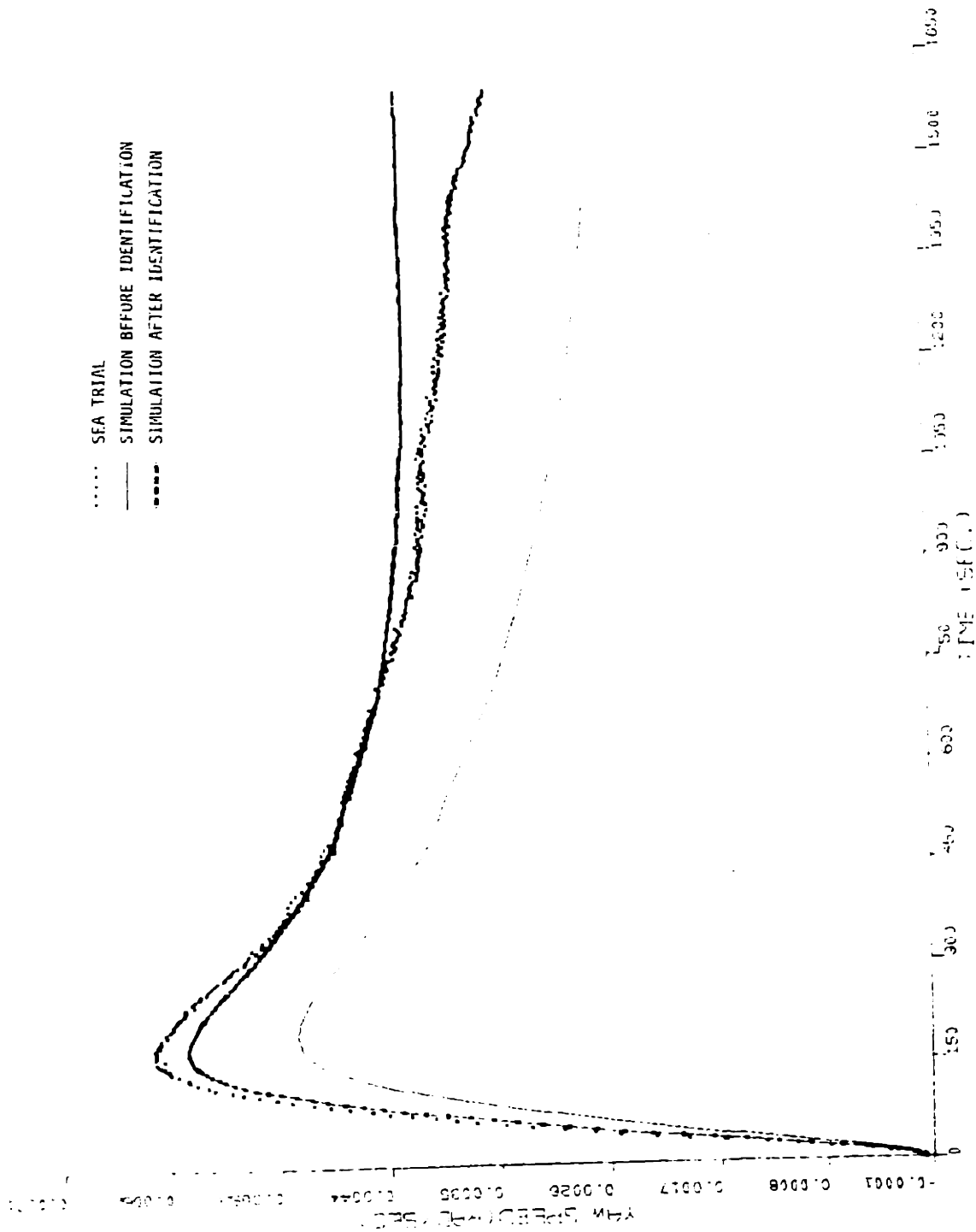
Figure 7.33.c Improvement on the yaw speed simulation of 35° rudder turning maneuver for ESSO OSAKA after the identification.
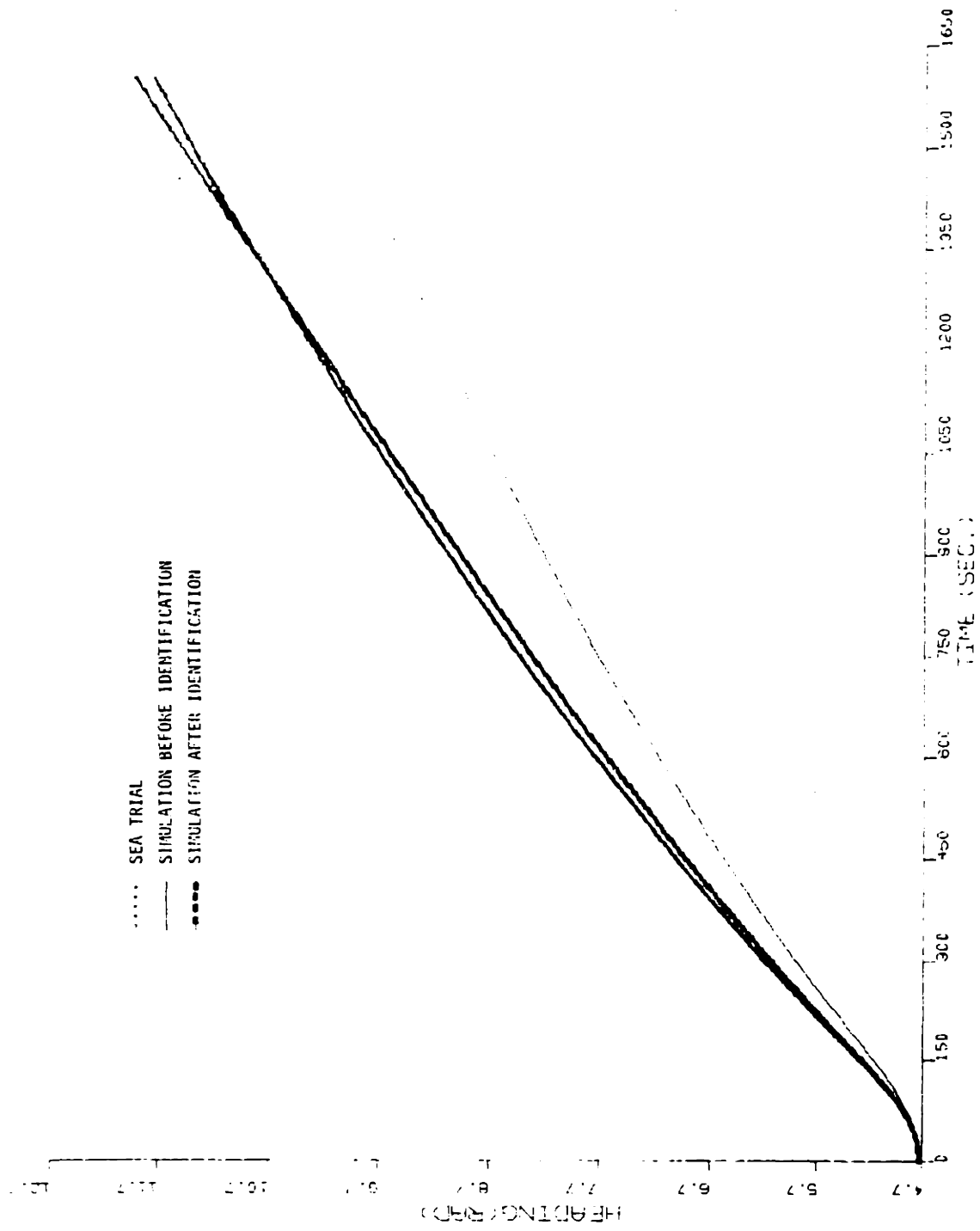
Figure 7.33.d Improvement on the heading simulation of 35° rudder turning maneuver for ESSO OSAKA after the identification.

8. CONCLUSIONS AND RECOMMENDATIONS

8.1 Conclusions

1. Based on the experience of processing the sea trial data, the conventional model of ship maneuvering was modified to give a better modelling:

a. Instead of the ship speed, the averaged flow velocity over rudder was employed as the dimensional parameter for the rudder induced forces and moments.

b. $X_u \Delta u + X_{uu} (\Delta u)^2 + X_{uuu} (\Delta u)^3$ was replaced by $n_1 u^2 + n_2 un + n_3 n^2 - \frac{\rho}{2} C_R u^2 S$ to be independent of the equilibrium point about which the Taylor series was expanded.

c. The effect of unequilibrium propeller loading on the hydrodynamic coefficient was modelled by a more "natural" expression instead of a series expansion.

d. The ship forward speed u was replaced by the propeller induced velocity at propeller, i.e., $0.5u_{A\infty}$ as the velocity parameter for the unbalanced force Y_0' and moment N_0' due to the odd number of propeller, such that the model could meet the extreme case of locked propeller, windmilling propeller and starting acceleration.

e. A simplified representation of nonlinear forces and moments arising from the cross coupling of v, r and δ was used to replace the lengthy Taylor expansions of the nonlinear forces and moments involving rudder deflections.

f. Since a small error in $X_{vr}' + m'$ could induce a significant effect on

surge speed, X'_{vvrr} was introduced for better modelling.

After these modifications, the model is not only physically more realistic but also more concise in form.

2. The simultaneous drift of hydrodynamic coefficients, when EKF was utilized for parameter estimation, was found caused by the cancellation of the coefficients' contributions to the hydrodynamic forces and moments. This cancellation effect is an intrinsic nature of the dynamics of ship maneuvering motion, and no maneuver is discriminated. The slender body theory was applied to show this nature.

3. Theoretically, "parallel processing" helps the EKF to obtain a better estimation of coefficient. When this technique was applied to improve the simultaneous drift, it only delayed the occurance of simultaneous drift, because of the cancellation effect exists for all the maneuvers.

4. When simulated data was processed, the true value of coefficients and the estimated coefficient values of simultaneous drift gave almost the same log likelihood. Therefore, the estimated coefficient values of simultaneous drift was mathematically acceptable, although they might not be feasible in the physical sense.

5. For SAEKF, "exaggerated over- and under-estimated initial guesses" together with the application of parallel processing, with multiple passes if it is necessary, is a practical scheme to overcome the problem of identifiability during the parameter estimation. It worked on the simulated data, but no rigorous proof was developed to confirm its validity.

6. The ship resistance coefficient C_R could be estimated very accu-

rately by utilizing both the "parallel processing" technique and the "exaggerated over- and under-estimated initial guesses" scheme. The study showed that when ship travelled parallelly to the current, the estimation was most accurate.

7. "parameter transformation" is a formal way to eliminate the simultaneous drift of coefficients being estimated. This technique has been successful when simulated data was tested.

8. Since the sway speed is about 180° out of phase with the yaw speed, the v and r cross correlated nonlinear coefficients can compensate each other to give the same nonlinear effect. Therefore, to estimate all the nonlinear coefficient will be in vain. In this work, a set of non-linear coefficient was chosen to be estimated to give an equivalent non-effect of the true system.

9. The current magnitude and the current direction were estimated very accurately in processing the simulated data. Since the current variation is significant in some portion of the sea trial data, it can degrade the estimation of hydrodynamic coefficients' values.

10. The current variation in sea trial data was tracked by treating the current magnitude and direction as random process after the hydrodynamic coefficients' values were estimated satisfactorily.

11. The sensitivity analysis was studied in order to help the parameterization for parameter estimation. Since each coefficient plays different role, not only in different maneuvers but also for different ships, the reuslt of sensitivity analysis is only valid to ESSO OSAKA.

12. SAEKF has been quite successful in dealing with both the simulated data and the sea trial data. Its special feature of estimation time history has helped us to improve the mathematical model of ship dynamics. Therefore, SAEKF is an eligible method for the identification of ship system.

8.2 Recommendations

1. Since the identified system for ESSO OSAKA gives a very accurate simulation of sea trial 10°/10° zigzag maneuver. The simulation of 35° rudder turning circle, although satisfactory, is less accurate. The modelling of nonlinear effect still needs some improvement to make the model even better.

2. In this work, the log likelihood was calculated to show that the coefficients' value in simultaneous drift gave the same optimality as the true coefficient value in processing the simulated data. In the future, the maximum likelihood method can be used to double check the result from the state augmented extended Kalman filtering.

3. Since for modern ships, the dual axis Doppler sonar and heading gyro are common installations, u, v and ψ are the readily available information for the purpose of system identification. Therefore, it would be very interesting to see whether the ship system can be identified by using only the measurement of u, v and ψ. If it is successful, the advantage is not only on the easy access to the necessary information for the identification of ship system(possibily from ships of opportunity), but also on the saving of computational effort for solving the Riccati

equation(one order less).

4. Because the current varaition has a significant effect on the estimation of hydrodynamic coefficient value. Accurate measurements on the current information is indispensible. In addition, the effect of current variation should be accounted for properly in the mathematical model for the ship motion simulation.

8.3 Summary

In summary, this thesis accomplished the following work:

1. The phemomena of simultaneous drift during the estimation of hydrodynamic coefficients' value was explained.

2. An effective way was developed to overcome the problem of identifiability due to the cancellation effect.

3. The mathematical model was modified interactively with the processing of sea trial data. Various hydrodynamic phenomena were analyzed in order to determine the form of the model and the magnitude of the coefficient.

4. The sensitivity of the ship motion response to the variation of each coefficient in different maneuvers was studied and a procedure was developed to estimate the coefficients systematically.

5. The necessary technique was developed and applied for the estimation of ship resistance coefficient.

REFERENCES

Abkowitz, M. A., 1969, <u>Stability and Motion Control of Ocean Vehicles</u> The MIT Press, Cambridge, Mass.

Ankudinov, V. and Miller, E., 1977, "Predicted Maneuvering Characteristics of the Tanker "ESSO OSAKA" in Deep and Shallow Water", Hydronautics, Inc. Technical Report 7778-1.

Åstrom, K. J. and Källstrom, C. G., 1976, "Identification of Ship Steering Dynamics". <u>Automatica</u>, Vol. 12, pp. 9-22.

Åstrom, K. J. and Källstrom, C. G., 1973, "Application of System Identification Techniques to the Determination of Ship Dynamics" Proceedings 3rd IFAC Symposium on Identification and System Parameter Estimation, The Hague, The Netherlands.

Brinati, H. L., 1973, "System Identification Applied to Maneuvering Trials" M.I.T. Engineer Thesis, Department of Ocean Engineering

Burcher, R. K., 1971, "Developments in Ship Maneuverability", TRINA, London.

Bystrom, L. and Källstrom, C. G., 1978, "System Identification of Linear and Non-linear Ship Steering Dynamics", Proceedings 5th Ship Control System Symposium, Washington, D.C.

Chen, H. H., 1969, "Some Aspects of Ship Maneuverability", <u>Journal of Ship Research</u>, Vol. 12, pp. 111-128.

Crane, C. L., 1979, "Maneuvering Trials of the 278,000 DWT ESSO OSAKA in Shallow and Deep Waters", Exxon International Company, Tanker Department - Research and Development, Report No. EII.4TM.79

Dand, I. W., 1976, "Hydrodynamic Aspects of Shallow Water Collisions", RINA Spring Meeting, April 8.

Eda, Haruzo and Crane, L. C., Jr., 1965, "Steering Characteristics of Ships in Calm Water and Waves", Trans. SNAME, vol. 73.

Eykhoff, P., 1974, System Identification, Wiley, London.

Fujino, M., Takashina, J., Yamamoto, S., 1974, "On the Three-Dimensional Correction Factors for the Added Mass and the Added Mass Moment of Inertia Related to Maneuverability in Shallow Water", Journal Society Naval Architects, vol. 135, Japan.

Fujino, M. 1976, "Maneuverability in Restricted Waters: State of the Art" Department of Naval Architecture and Marine Engineering, The University of Michigan, Report No. 184.

Gelb, A., ed., 1974, Applied Optimal Estimation , The M.I.T. Press, Cambridge, MA.

Gill, A. D., 1975, "The Identification of Maneuvering Equations from Ship Trials Results", TRINA.

Gill, A. D. 1975, "The Requirements of Data Acquisition from a Ship Tracking Test", Proceedings of the 14th ITTC, pp. 609.

Goodman, A. Gertler, M. and Kohl, R., 1977, "Experimental Techniques and Methods of Analysis Used at Hydronautics for Surface-Ship Maneuvering Predictions", Eleventh Symposium on Naval Hydrodynamics.

Gertler, Morton and Kohl, 1974, "Resistance, Propulsion and Maneuverability Characteristics of MARAD Systematic Series for Large Full-Form Merchant Ships", Hydronautics, Inc. Technical Report 7370-1.

Grauge, D., 1976, Identification of Systems , Krieger Publishing Co., Inc.

Hayes, M. N., 1971, "Parameters Identification of Nonlinear Stochastic Systems Applied to Ocean Vehicle Dynamics", M.I.T., Ph.D. Thesis, Department of Ocean Engineering.

Hooft, J. P., 1973, "Maneuvering Large Ships in Shallow Water - I ", Journal of Navigation, vol. 26. pp. 189 - 201.

Hooft, J. P., 1973, "Maneuvering Large Ships in Shallow Water - II", Journal of Navigation, vol. 26, pp. 211 - 319.

Kaplan, P., et. al., 1972, "The Application of System Identification to the Dynamics at Naval Craft", 9th Symposium on Naval Hydrodynamics.

Lee, C. K., 1964, Optimal Estimation, Identification, and Control, M.I.T. Press.

Loukakis, T. A. and Sclavounos, P. D., 1978, "On the Semi-Coupled Nature of the Rolling Motion of a Ship", International Shipbuilding Progress.

Lundblad, J. G., 1974, "Application of the Extended Kalman Filtering Technique to Ship Maneuvering Analysis", M.I.T. Master Thesis, Department of Ocean Engineering.

Mandel, P., 1967, "Ship Maneuvering and Control", In Principles of Naval Architecture, ed. J. P. Comstock, pp. 463 - 606, New York: Society of Naval Architects and Marine Engineers.

Morris, R. L., 1978, "Low Order Model Identification for a Drum-Type Power Plant", M.I.T. Engineer Thesis, Department of Electrical Engineering and Computer Science.

Motora, S., 1972, "Maneuverability, State of the Art", Fourtieth Anniversary Symposium of the Netherlands Ship Model Basin, pp. 136 - 169.

Newman, J. N., 1966, "Some Hydrodynamic Aspects of Ship Maneuverability" 6th Symposium of Naval Hydrodynamics, Washington, D.C., pp. 203 - 237.

Newman, J. N., 1969, "Lateral Motion of a Slender Body Between Two Parallel Walls", J. Fluid Mechanics vol. 39, part 1, pp. 97-115.

Newman, J. N., 1977, Marine Hydrodynamics, Cambridge, MA.: The MIT Press.

Nomoto, K., 1975, "A Handy Method of Maneuverability Prediction from Free Model Testing", Proceedings of the 14th ITTC.

Norrbin, N. H., Astrom, K. J., Bystrom, L. and Kallstrom, C. G., 1977, "Further Studies of Parameter Identification of Linear and Non-Linear Ship Steering Dynamics", Report 1920-6, Swedish State Shipbuilding Experiment Tank, Gothenburg, Sweden.

Ogawa, A. and Kasai, H., 1978, "On the Mathematical Model of Maneuvering Motion of Ships", International Shipbuilding Progress, vol. 25, pp. 306 - 319.

Peterson, D. W. , 1975, "Hypothesis, Estimation and Validation of Dynamic Social Model - Energy Demand Modelling", M.I.T. Ph.D. Thesis, Department of Electrical Engineering.

Rawson, K. J. and Tupper, E. C., 1968, Basic Ship Theory , London: Longmans.

Sandman, B. E. and Kelly, J. G., 1974, "System Identification: Application to Underwater Vehicle Dynamics", J. Hydrodynautics, vol. 8, no. 3, pp. 94 - 99.

Schweppe, F. C., 1973, Uncertain Dynamic Systems, Prentice Hall, Inc.

Scragg, C. A., 1979, "Memory Effects in Deepwater Maneuvering", Journal of Ship Research, vol. 22, no. 3, pp. 175 - 187.

Strom-Tejsen, J. and Chislett, M. S., 1966,"A Model Testing Technique and Method of Analysis for the Prediction of Steering and Maneuvering Qualities of Surface Vessels", Sixth Symposium on Naval Hydrodynamics pp. 317 - 381, Washington, D.C.: Government Printing Office.

Szeto, F. F., 1977, "System Identification from Ship Maneuvers in Currents", M.I.T. Ocean Engineer Thesis, Department of Ocean Engineering.

Tsakanas, S., Kim, C. H., Eda, H. and Jacobs, W. R., 1977, "Lateral Stability Derivatives of a Ship in Shallow Water", Davidson Laboratory Report SIT-DL-1905.

Van Leeuwen, G., 1972, "Prediction of Ship Maneuverability", Netherlands Ship Research Center, TNO, Report No. 1583.

APPENDIX A

A Summary of

Continuous(system)-Discrete(measurement) Extended Kalman Filter

System Model $\quad\quad \underline{\dot{x}}(t)=\underline{f}(\underline{x}(t),\underline{u}(t),t)+\underline{w}(t)$

$n=1,2,\ldots\ldots$

Measurement Model $\quad \underline{z}(n)=\underline{h}(\underline{x}(t_n),n)+\underline{v}(n)$

Initial Conditions $\quad \underline{x}(0) \sim N(\underline{\hat{x}}(0),\underline{P}(0))$

Assumptions $\quad\quad \underline{w}(t) \sim N(\underline{0},\underline{Q}(t))$ $\qquad\qquad$ white

$\quad\quad\quad\quad\quad\quad \underline{v}(n) \sim N(\underline{0},\underline{R}(t))$ $\qquad\qquad$ white

$\quad\quad\quad\quad\quad\quad E\{\underline{w}(t)\underline{v}(n)^T\}=\underline{0}$ $\qquad$ for all t and all n

$\quad\quad\quad\quad\quad\quad E\{\underline{w}(t)\underline{x}(t)^T\}=\underline{0}$

$\quad\quad\quad\quad\quad\quad E\{\underline{v}(n)\underline{x}^T(t)\}=\underline{0}$

State Estimate
Propagation $\quad\quad \underline{\hat{\dot{x}}}(t)=\underline{f}(\underline{x}(t),\underline{u}(t),t)$

Error Covariance
Propagation $\quad\quad \underline{\dot{P}}(t)=\underline{F}(\underline{\hat{x}}(t),\underline{u}(t),t)\underline{P}(t)+\underline{P}(t)\underline{F}(\underline{\hat{x}}(t),\underline{u}(t),t)+\underline{Q}(t)$

Predicted State $\quad\quad \underline{\hat{x}}(n|n-1)=\underline{\hat{x}}(n-1|n-1)+\int_{t_{n-1}}^{t_n}\underline{\hat{\dot{x}}}(t)dt$

Predicted
Measurement $\quad\quad \underline{\hat{z}}(n|n-1)=\underline{h}(\underline{\hat{x}}(n|n-1))$

Residuals $\quad\quad\quad \underline{\delta}_z(n|n-1)=\underline{z}(n)-\underline{\hat{z}}(n|n-1)$

Predicted State
Covariance $\quad\quad \underline{P}(n|n-1)=\underline{P}(n-1|n-1)+\int_{t_{n-1}}^{t_n}\underline{\dot{P}}(t)dt$

Predicted measure-
ment Covariance $\quad \underline{\Sigma}(n|n-1)=\underline{H}(n)\underline{P}(n|n-1)\underline{H}^T(n)+\underline{R}(n)$

Normalized Predicted Measurement Residuals

$$\tilde{\underline{\delta}}_z(n|n-1) = \sqrt{\underline{\Sigma}_z^{-1}} \, \underline{\delta}_z(n|n-1)$$

Updated State Estimate

$$\hat{\underline{x}}(n|n) = \hat{\underline{x}}(n|n-1) + \underline{K}(n)\underline{\delta}_z(n|n-1)$$

Updated State Covariance

$$\underline{P}(n|n) = [\underline{I} - \underline{K}(n)\underline{H}(n)]\underline{P}(n|n-1)$$

$$= [\underline{I} - \underline{K}(n)\underline{H}(n)]\underline{P}(n|n-1)[\underline{I} - \underline{K}(n)\underline{H}(n)]^T$$

$$+ \underline{K}(n)\underline{R}(n)\underline{K}^T(n)$$

Gain Matrix

$$\underline{K}(n) = \underline{P}(n|n-1)\underline{H}^T(n)[\underline{H}(n)\underline{P}(n|n-1)\underline{H}^T(n) + \underline{R}(n)]^{-1}$$

Definitions

$$\underline{F}(\hat{\underline{x}}(t),t) = \left. \frac{\partial \underline{f}(\underline{x}(t),\underline{u}(t),t)}{\partial \underline{x}(t)} \right|_{\underline{x}(t)=\hat{\underline{x}}(t)}$$

$$\underline{H}(\hat{\underline{x}}(n|n-1)) = \left. \frac{\partial \underline{h}(\underline{x}(t_n),n)}{\partial \underline{x}(t_n)} \right|_{\underline{x}(t_n)=\hat{\underline{x}}(n|n-1)}$$

$N(\underline{m},\underline{c})$ represents a random vector of normal distribution, with mean $\underline{m}$ and covariance $\underline{c}$

APPENDIX B

Model Testing Values of Hydrodynamic Coefficients for ESSO OSAKA

LP	COEFFICIENT	DIMENSIONAL FACTOR	$H/T=\infty$	$H/T=1.5$	$H/T=1.2$
1	$m'-X'_{\dot{u}}$	$0.5\rho L^3$			
2	n'_1	$0.5\rho L^2$			
3	Y'_{rrr}	$0.5\rho L^5 U^{-1}$	$-0.5190d-2$	$-0.5200d-2$	$-0.5200d-2$
4	$m'-Y'_{\dot{v}}$	$0.5\rho L^3$	$0.3520d-1$	$0.3400d-1$	$0.4000d-1$
5	$m'x'_G-Y'_{\dot{r}}$	$0.5\rho L^4$	$0.5720d-3$	$0.5720d-3$	$0.5720d-3$
6	Y'_v	$0.5\rho L^2 U$	$-0.2828d-1$	$-0.2338d-1$	$-0.4021d-1$
7	Y'_r	$0.5\rho L^3 U$	$0.3910d-2$	$0.6660d-2$	$0.7760d-2$
8	Y'_δ	$0.5\rho L^2 c^2$	$0.5080d-2$	$0.5080d-2$	$0.5080d-2$
9	Y'_0	$0.5\rho L^2 (0.5u_{A\infty})^2$	$0.1900d-5$	$0.1900d-5$	$0.1900d-5$
10	$m'x'_G-N'_{\dot{v}}$	$0.5\rho L^4$	$0.5720d-3$	$0.5720d-3$	$0.5720d-3$
11	$I'_z-N'_{\dot{r}}$	$0.5\rho L^5$	$0.2220d-2$	$0.2240d-2$	$0.2400d-2$
12	N'_v	$0.5\rho L^3 U$	$-0.1090d-1$	$-0.9210d-2$	$-0.1335d-1$
13	N'_r	$0.5\rho L^4 U$	$-0.5000d-2$	$-0.4290d-2$	$-0.4650d-2$
14	N'_δ	$0.5\rho L^3 c^2$	$-0.2420d-2$	$-0.2420d-2$	$-0.2420d-2$
15	N'_{vrr}	$0.5\rho L^5 U^{-1}$	$0.9050d-2$	$-0.1936d-1$	$-0.2843d-1$
16	n'_2	$0.5\rho L^3$			
17	n'_3	$0.5\rho L^4$			
18	X'_{vv}	$0.5\rho L^2$	$-0.6000d-2$	$-0.6850d-2$	$-0.1180d-1$
19	$X'_{rr}+m'x'_G$	$0.5\rho L^4$	$0.5720d-2$	$0.5720d-2$	$0.5720d-2$
20	$X'_{\delta\delta}$	$0.5\rho L^2 c^2$	$-0.2490d-2$		
21	$X'_{vr}+m'$	$0.5\rho L^3$	$0.3070d-1$	$0.3404d-1$	$0.4005d-1$
22	$X'_{v\delta}$	$0.5\rho L^2 c$			
23	N'_{rrr}	$0.5\rho L^6 U^{-1}$	$-0.1240d-2$	$-0.1000d-3$	$-0.1000d-3$
24	N'_0	$0.5\rho L^3 (0.5u_{A\infty})^2$	$-0.2250d-5$		
25	Y'_{vvv}	$0.5\rho L^2 U^{-1}$	$-0.1058d-0$	$-0.9950d-1$	$-0.1890d-0$
26	$Y'_{\delta\delta\delta}$	$0.5\rho L^2 c^2$	$-0.1850d-2$	$-0.1850d-2$	$-0.1850d-2$
27	Y'_{rvv}	$0.5\rho L^3 U^{-1}$	$-0.1153d-1$	$-0.9440d-2$	$-0.4040d-3$
28	$Y'_{\delta vv}$	$0.5\rho L^2$			
29	$Y'_{v\delta\delta}$	$0.5\rho L^2 U$			
30	N'_{vvv}	$0.5\rho L^3 U^{-1}$	$0.3160d-2$	$0.7060d-2$	$0.1165d-1$
31	$N'_{\delta\delta\delta}$	$0.5\rho L^3 c^2$	$0.9700d-3$	$0.9700d-3$	$0.9700d-3$
32	N'_{rvv}	$0.5\rho L^4 U^{-1}$	$-0.1182d-1$	$-0.1742d-1$	$-0.7180d-1$
33	$N'_{\delta vv}$	$0.5\rho L^3$			
34	$N'_{v\delta\delta}$	$0.5\rho L^3 U$			
35	Y'_{vrr}	$0.5\rho L^4 U^{-1}$	$-0.4126d-1$	$-0.7046d-1$	$-0.1273d-0$
36	C'_R	$0.5\rho S u^2$			

- 295 -

APPENDIX C

ESSO OSAKA's Motion Responses to the Variation

of Hydrodynamic Coefficient Values

±LP is defined in Table C.5
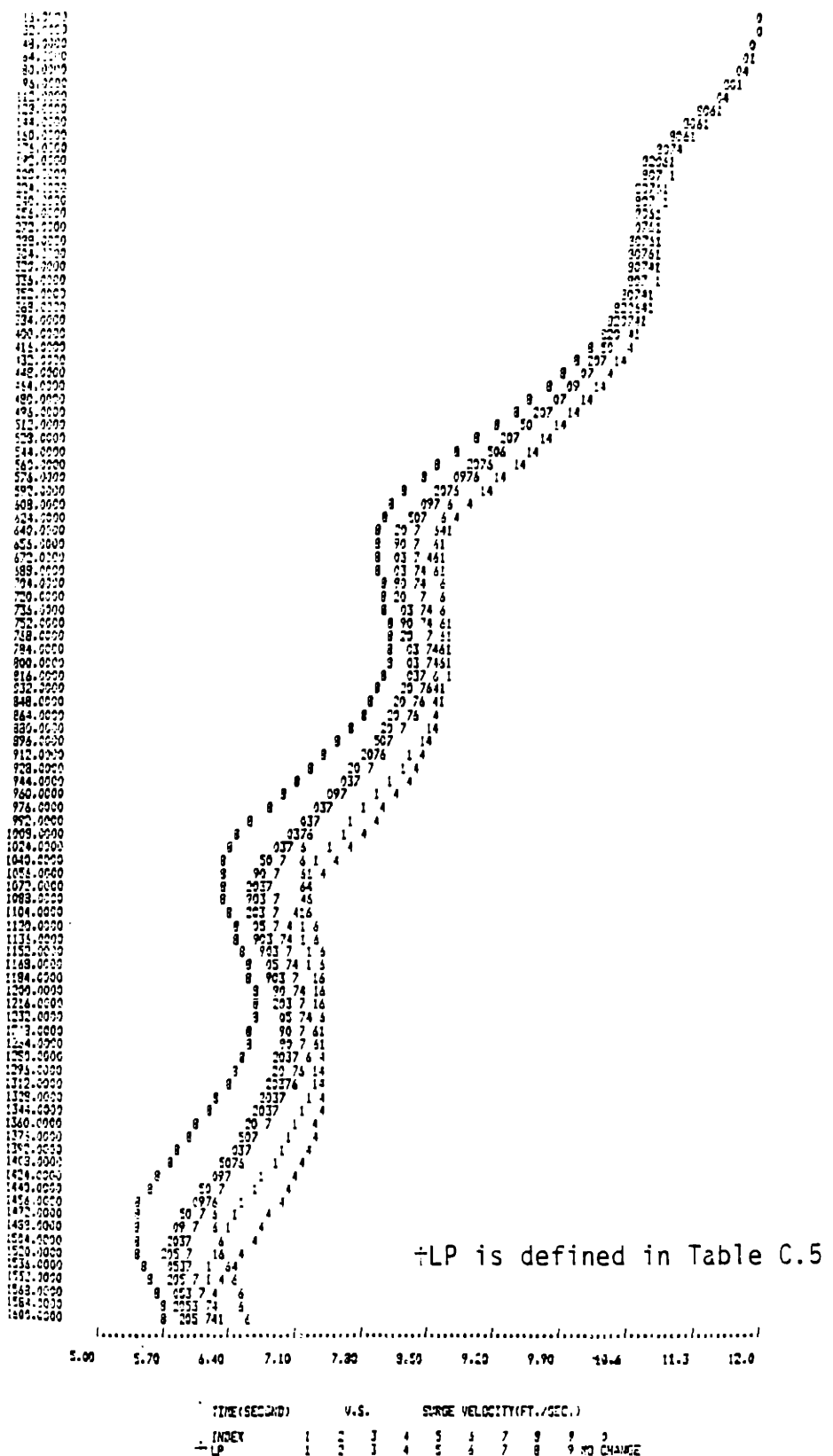
Figure C.1 Perturbed surge speed, corresponding to the variation of each coefficient, during a 20°/20° zigzag maneuver of ESSO OSAKA.
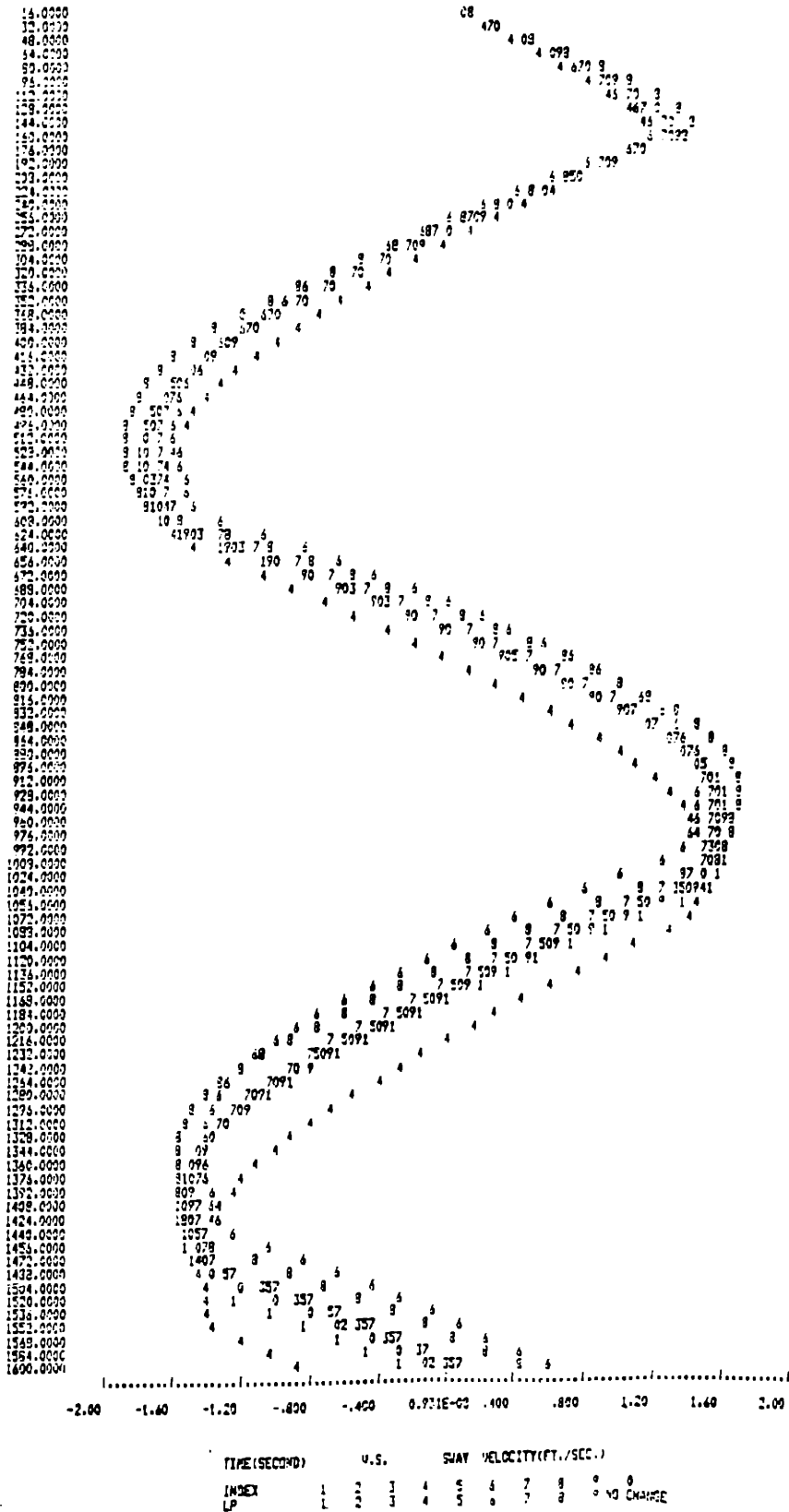
Figure C.2 Perturbed sway speed, corresponding to the variation of each coefficient, during a 20°/20° zigzag maneuver of ESSO OSAKA.
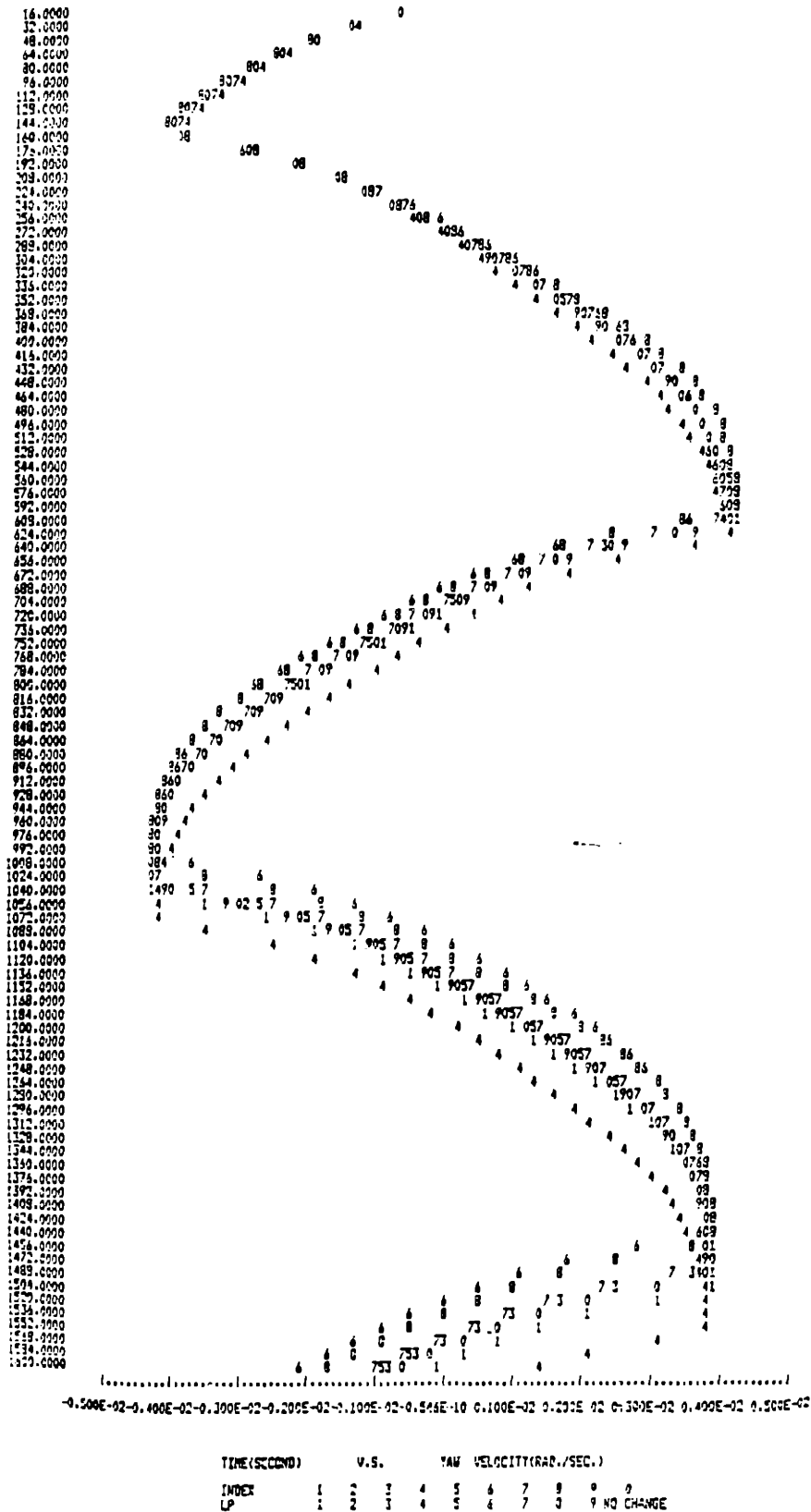
Figure C.3   Perturbed yaw speed, corresponding to the variation of each
coefficient, during a 20°/20° zigzag maneuver of ESSO OSAKA.
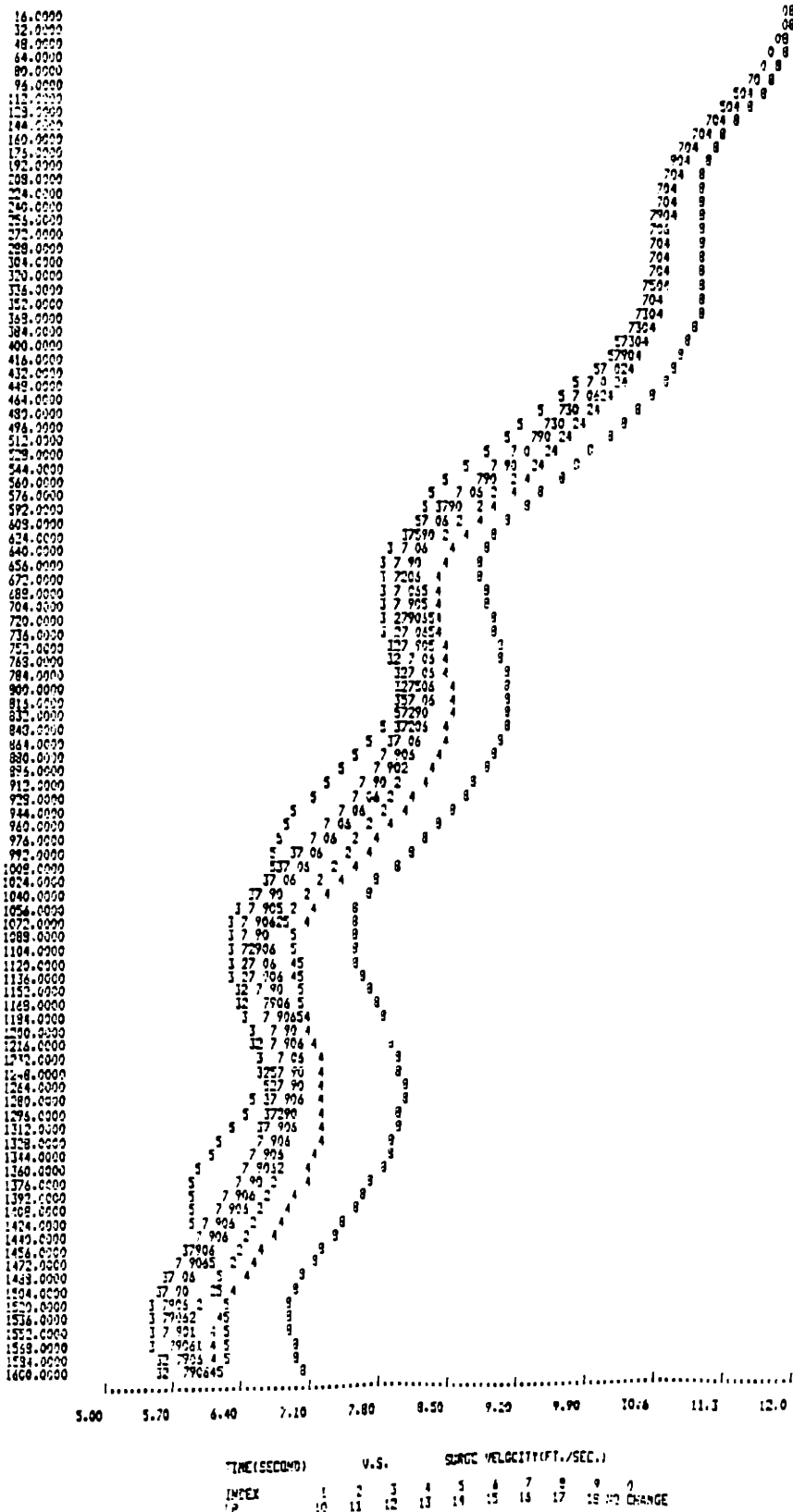
Figure C.4 Perturbed surge speed, corresponding to the variation of each
coefficient, during a 20°/20° zigzag maneuver of ESSO OSAKA.
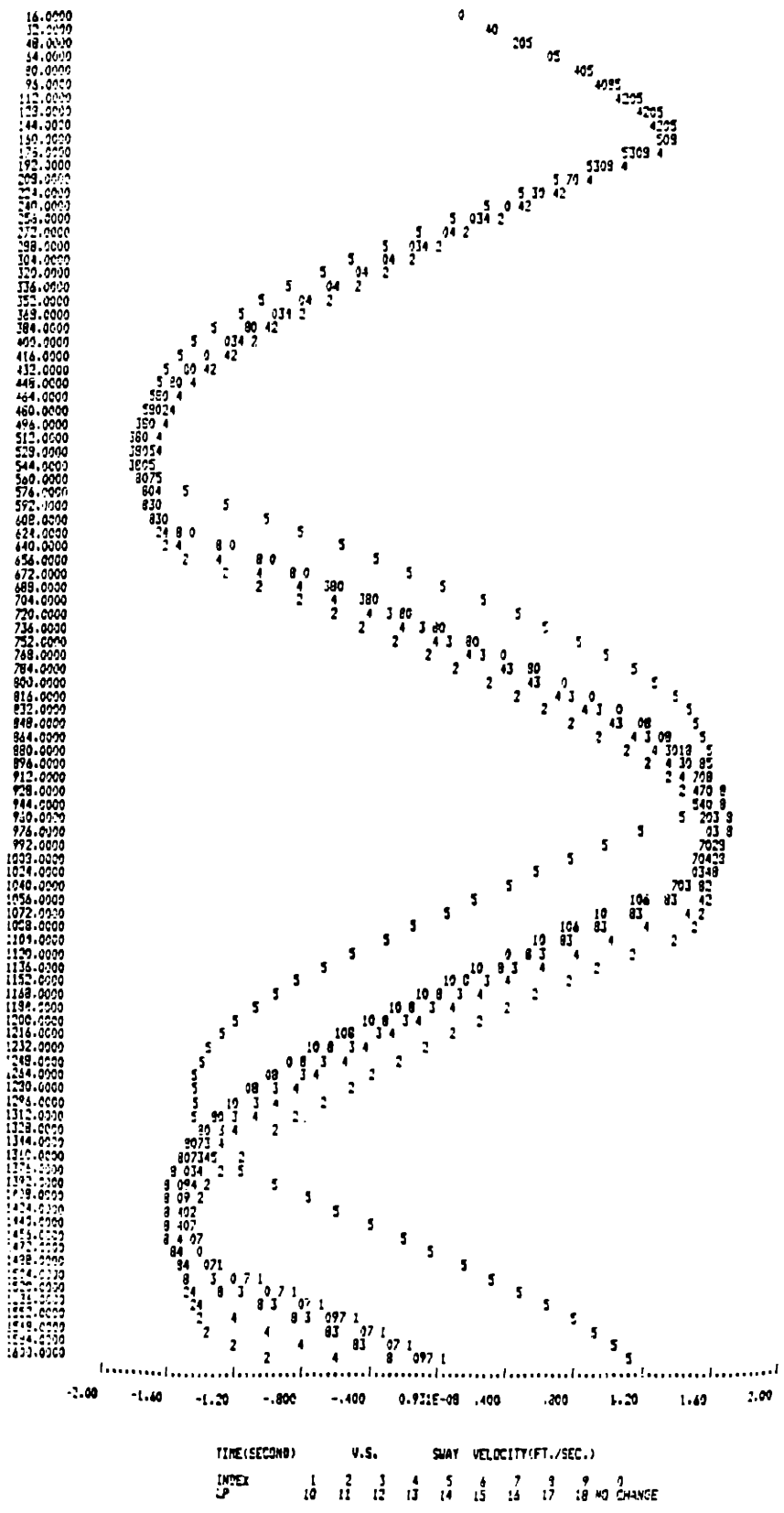
Figure C.5 Perturbed sway speed, corresponding to the variation of each coefficient, during a 20°/20° zigzag maneuver of ESSO OSAKA.
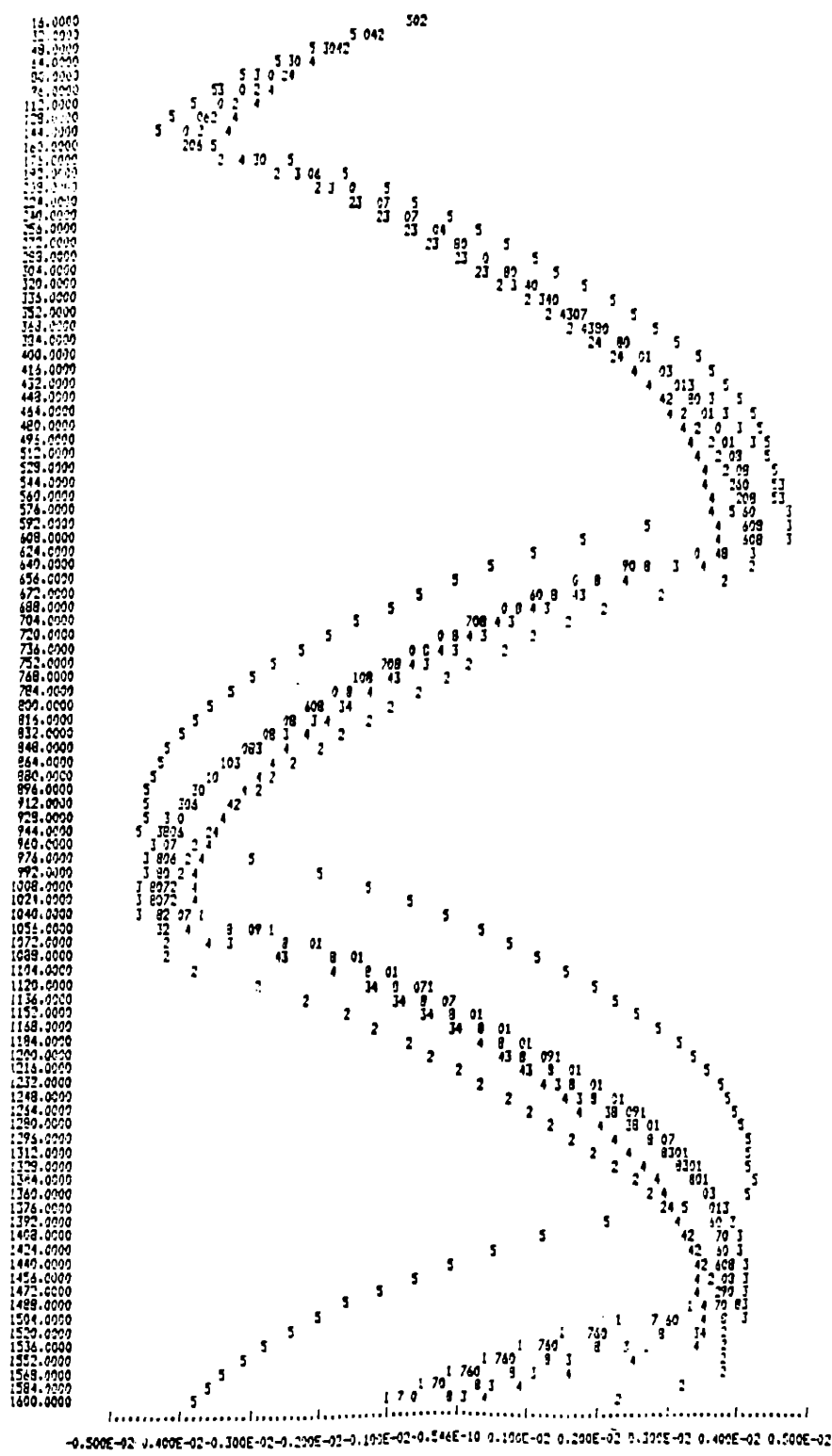
Figure C.6 Perturbed yaw speed, corresponding to the variation of each coefficient, during a 20°/20° zigzag maneuver of ESSO OSAKA.

- 303 -
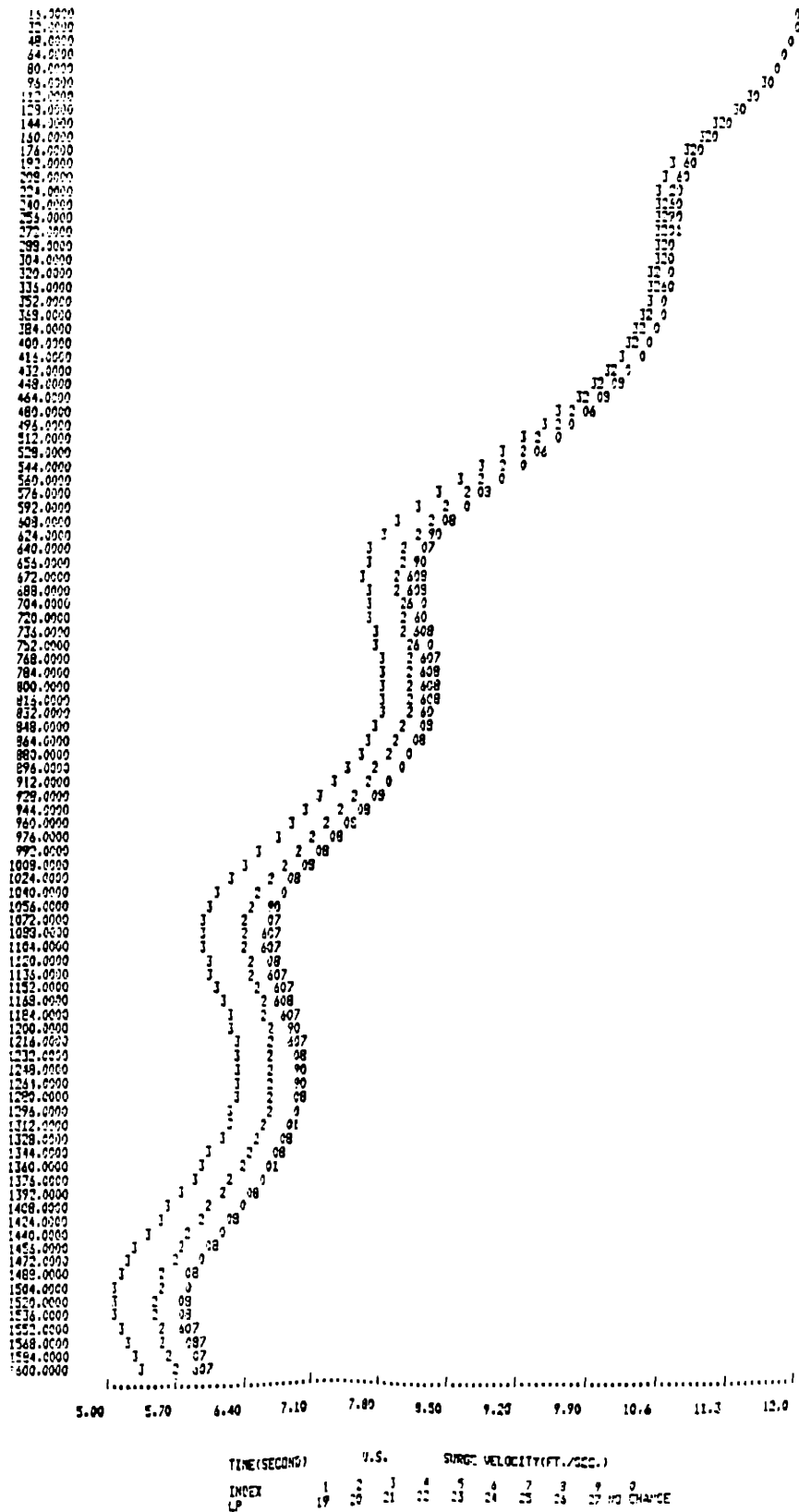
Figure C.7 Perturbed surge speed, corresponding to the variation of each
coefficient, during a 20°/20° zigzag maneuver of ESSO OSAKA.
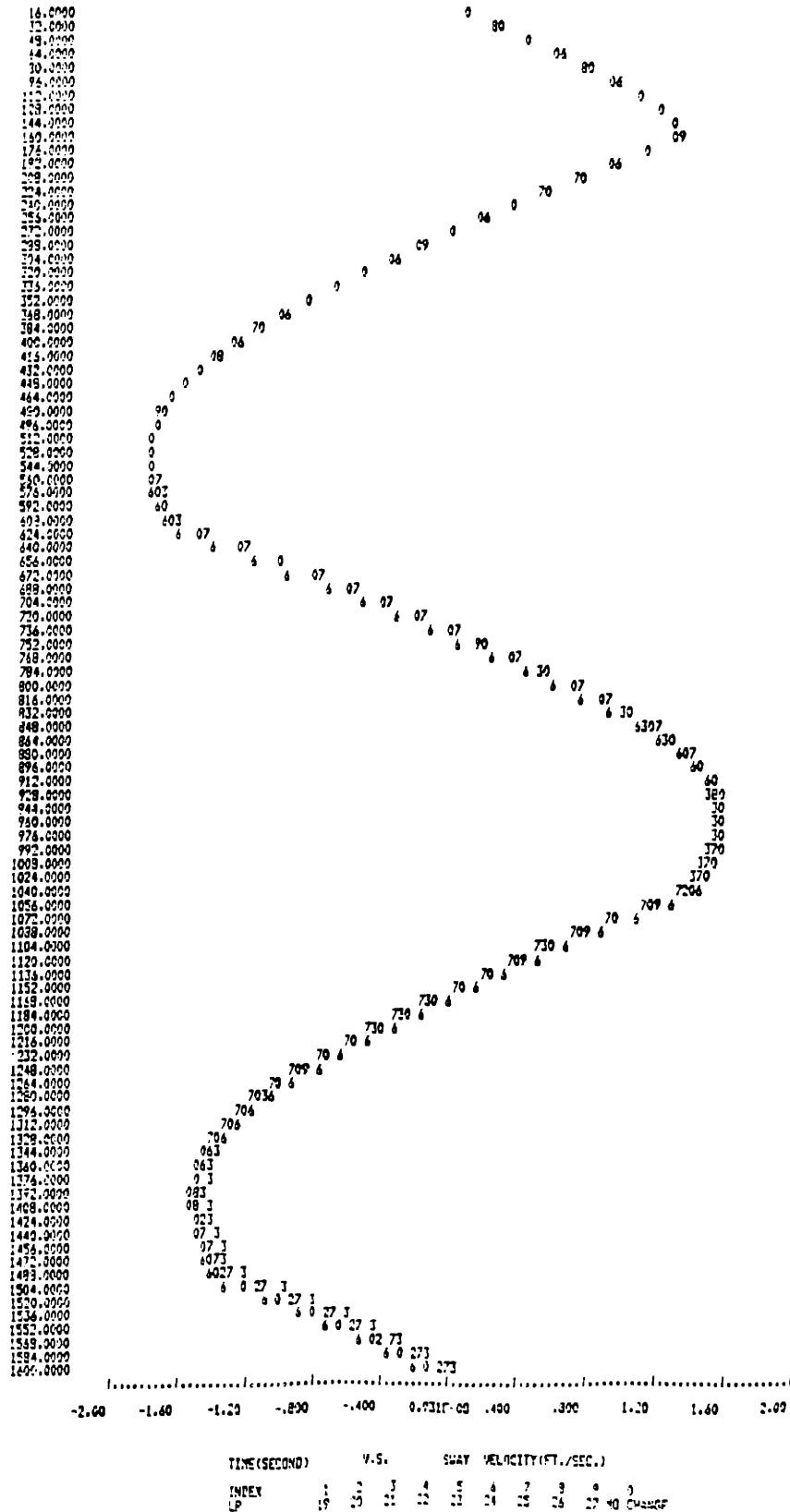
Figure C.8   Perturbed sway speed, corresponding to the variation of each coefficient, during a 20°/20° zigzag maneuver of ESSO OSAKA.
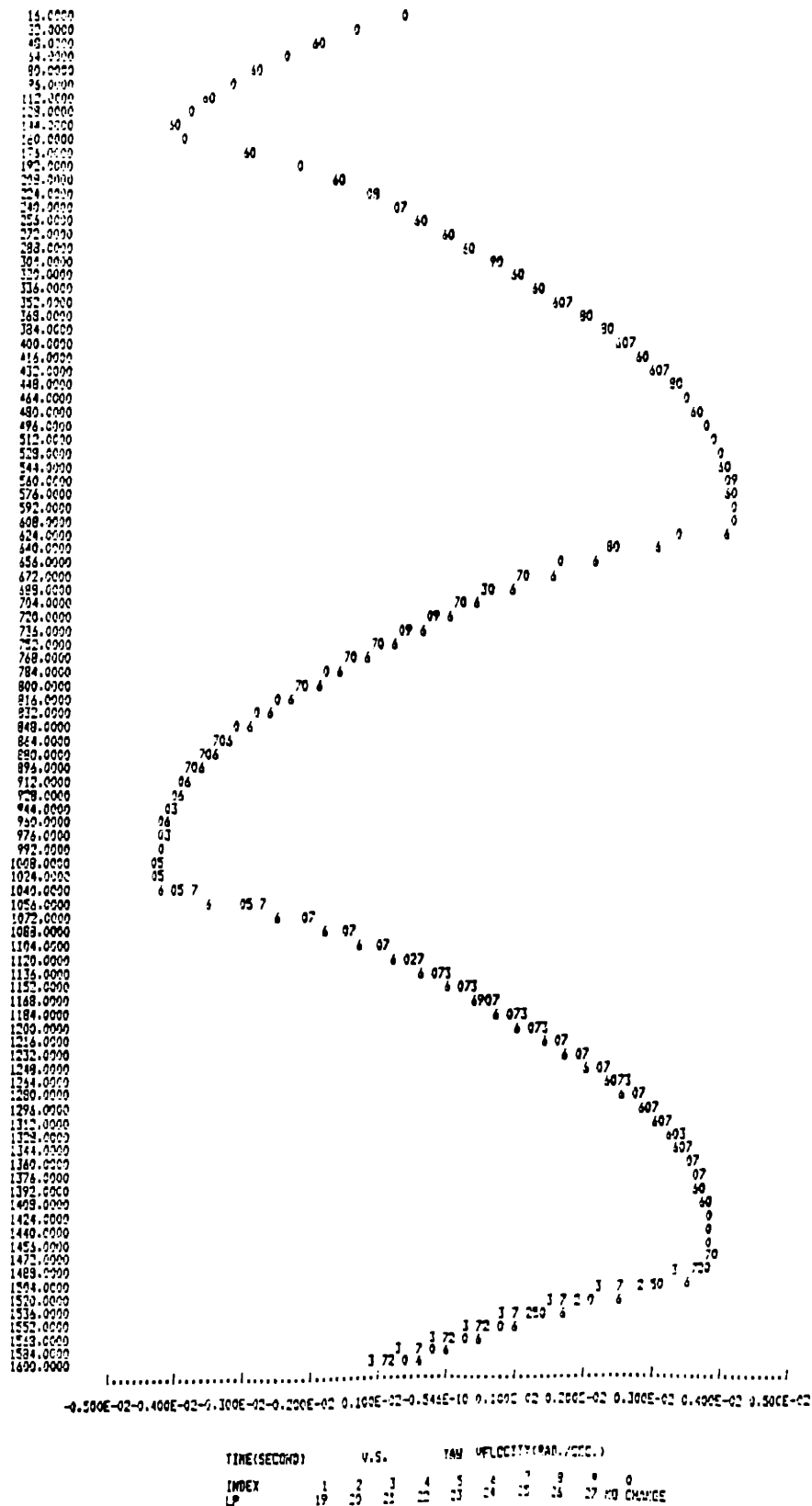
Figure C.9 Perturbed yaw speed, corresponding to the variation of each coefficient, during a 20°/20° zigzag maneuver of ESSO OSAKA.
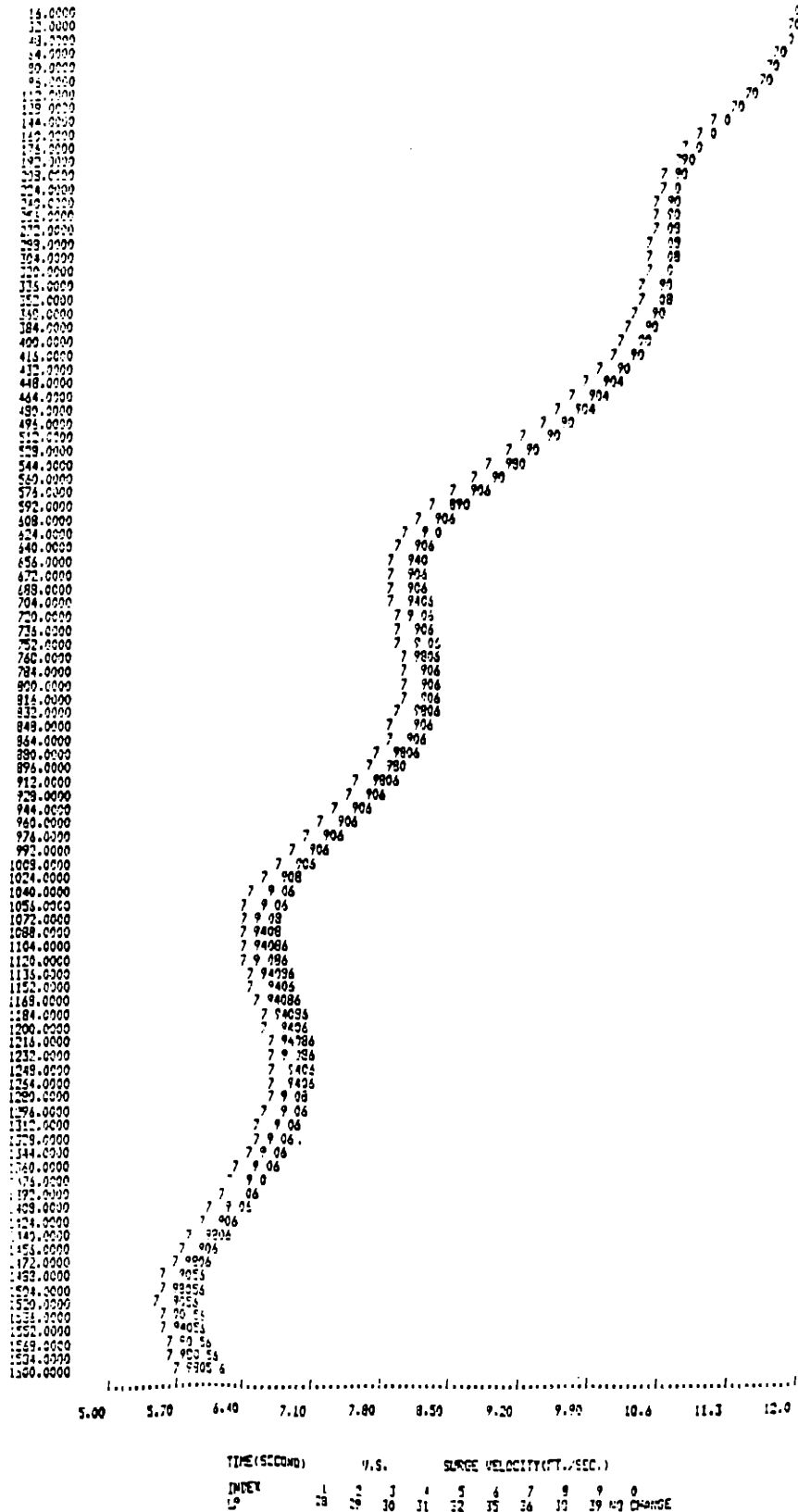
Figure C.10 Perturbed surge speed, corresponding to the variation of each coefficient, during a 20°/20° zigzag maneuver of ESSO OSAKA.
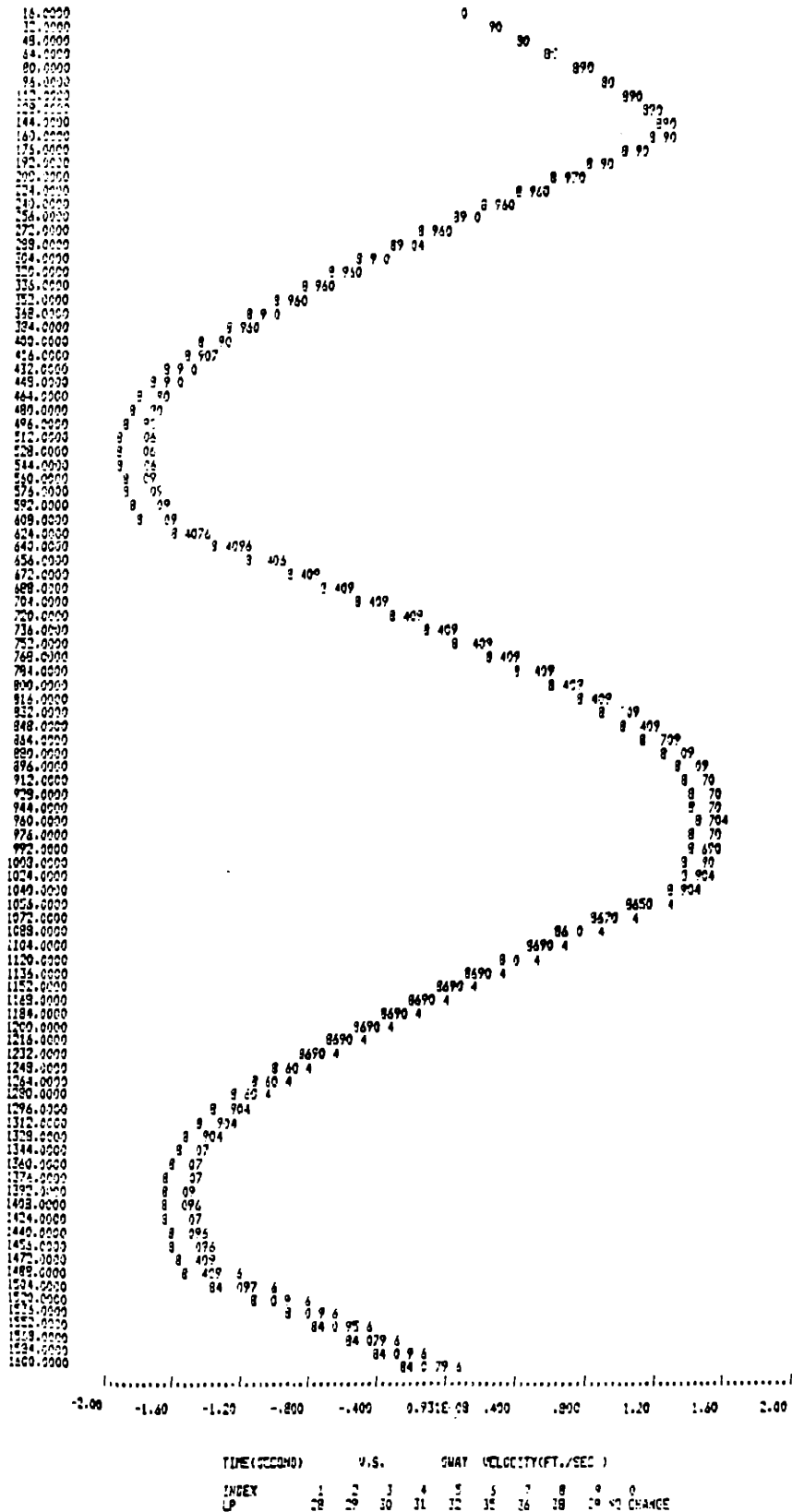
Figure C.11 Perturbed sway speed, corresponding to the variation of each coefficient, during a 20°/20° zigzag maneuver of ESSO OSAKA.
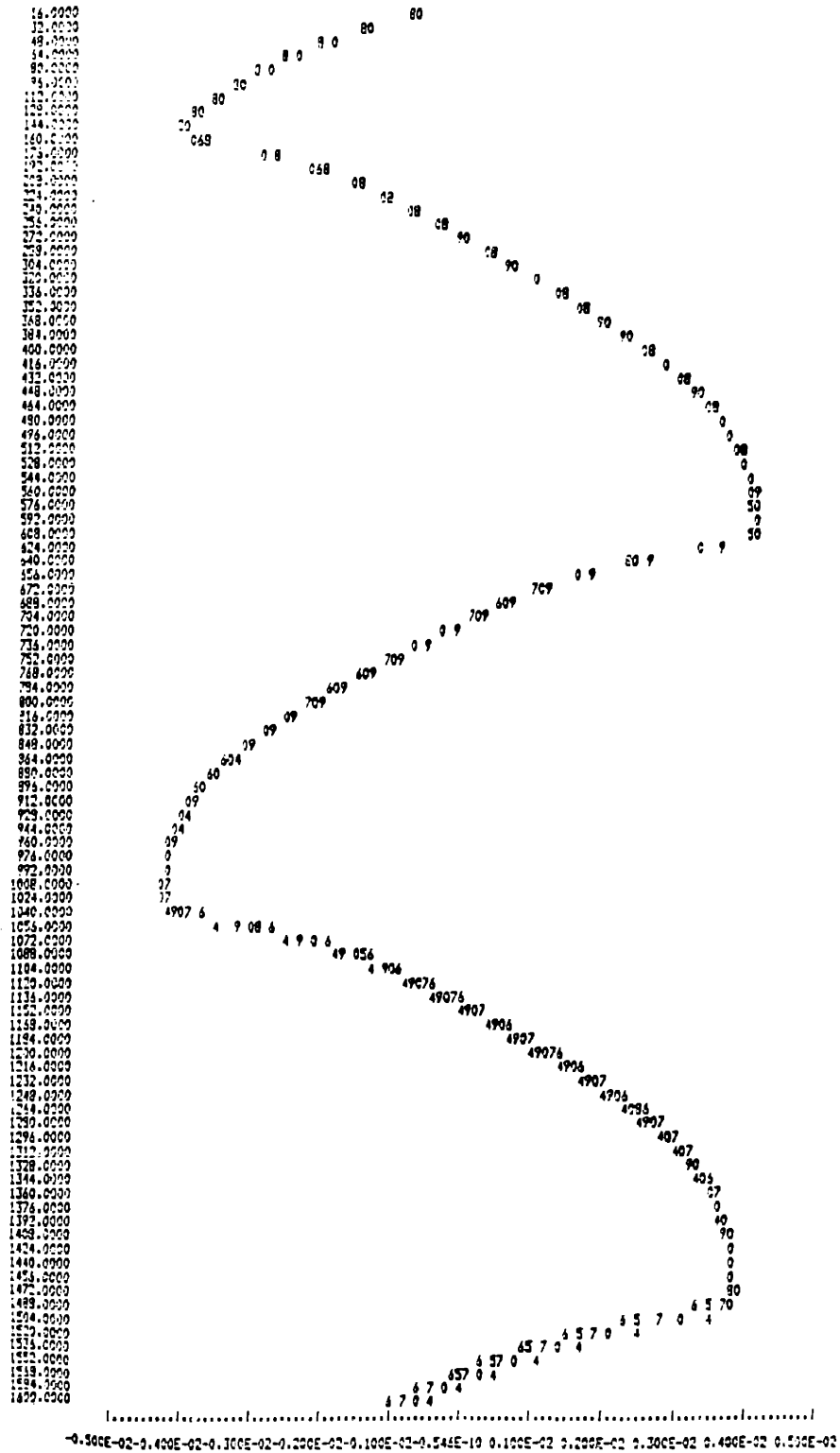
Figure C.12 Perturbed yaw speed, corresponding to the variation of each coefficient, during a 20°/20° zigzag maneuver of ESSO OSAKA.

- 309 -

†The code LP for each coefficient is
defined in Table C.5

Table C.1.a Maximum differences in u,
v and r between the per-
turbed and the original
simulation of a 5°/5°
zigzag maneuver.

Table C.1.b Individual relative sensitivity
of u, v and r and the overall
sensitivity of 5°/5° zigzag
maneuver to the variance of
coefficients.

†The code LP for each coefficient is defined in Table C.5

Table C.2.a Maximum differences in u, v and r between the perturbed and the original simulation of a 10°/10° zigzag maneuver.

Table C.2.b Individual relative sensitivity of u, v and r and the overall sensitivity of 10°/10° zigzag maneuver to the variance of coefficients.

†The code LP for each coefficient is
defined in Table C.5

Table C.3.a   Maximum differences in u, v
and r between the perturbed
and the original simulation
of a 20°/20° zigzag maneuver.

Table C.3.b   Individual relative sensitivity of
u, v and r and the overall sensi-
tivity of 20°/20° zigzag maneuver
to the variance of coefficients.

†The code LP for each coefficient is
defined in Table C.5

Table C.4.a   Maximum differences in u, v
and r between the perturbed
and the original simulation
of a biased zigzag maneuver.

Table C.4.b   Individual relative sensitivity of
u,v and r and the overall sensi-
tivity of biased zigzag maneuver
to the variance of coefficients.

LP	COEFFICIENT	LP	COEFFICIENT
1	$m'-X'_{\dot{u}}$	20	$X'_{\delta\delta}$
2	n'_1	21	$X'_{vr}+m'$
3	Y'_{rrr}	22	$X'_{v\delta}$
4	$m'-Y'_{\dot{v}}$	23	N'_{rrr}
5	$m'x'_G-Y'_{\dot{r}}$	24	N'_0
6	Y'_v	25	Y'_{vvv}
7	Y'_r	26	$Y'_{\delta\delta\delta}$
8	Y'_δ	27	Y'_{rvv}
9	Y'_0	28	$Y'_{\delta vv}$
10	$m'x'_G-N'_{\dot{v}}$	29	$Y'_{v\delta\delta}$
11	$I'_z-N'_{\dot{r}}$	30	N'_{vvv}
12	N'_v	31	$N'_{\delta\delta\delta}$
13	N'_r	32	N'_{rvv}
14	N'_δ	33	$N'_{\delta vv}$
15	N'_{vrr}	34	$N'_{v\delta\delta}$
16	n'_2	35	Y'_{vrr}
17	n'_3	36	C'_R
18	X'_{vv}	38	α
19	$X'_{rr}+m'x'_G$	39	u_c

Table C.5 Label explanation in Table C.1 to C.4

Calculation of the Pivot Position by Using
the Time History $Y'_v v'$, $(Y'_r - m'u')$, $N'_v v'$ and $(N'_r - m'x')r'$

In the study of Leeuwen and Journee[1972], the time histories of sway forces $Y'_v v'$, $(Y'_r - m'u')r'$ and yaw moments $N'_v v'$, $(N'_r - m'_G x')r'$ are plotted in Fig. 5.5 for a simulated turning motion of BRITISH BOMBARDIAR. It is possible to evaluate the instantaneous pivot position during the maneuver by using this information.

To represent the incomplete cancellation, let the difference between the nondimensionalized forces $Y'_v v'$ and $-(Y'_r - m'u')r'$ be ε_Y, and the difference between the nondimensionalized moments $N'_v v'$ and $-(N'_r - m'x')r'$ be ε_N, thus

$$Y'_v v' + (Y'_r - m'u')r' = \varepsilon_Y \tag{D.1}$$

$$N'_v v' + (N'_r - m'x'_G)r' = \varepsilon_N \tag{D.2}$$

Solve for v' and r', it follows that

$$v' = \frac{\varepsilon_Y(N'_r - m'x'_G) - \varepsilon_N(Y'_r - m'u')}{Y'_v(N'_r - m'x'_G) - N'_v(Y'_r - m'u')} \tag{D.3}$$

$$r' = \frac{Y'_v \varepsilon_N - N'_v \varepsilon_Y}{Y'_v(N'_r - m'x'_G) - N'_v(Y'_r - m'u')} \tag{D.4}$$

According to the definition of pivot position,

$$v(x_p) + r \cdot x_p = 0 \tag{D.5}$$

Therefore, the nondimensionalized position of pivot point, x_p', has the following espression:

$$x_p' = \frac{v'}{r'}$$

$$= \frac{\varepsilon_Y(N_r'-m'x_G')-\varepsilon_N(Y_r'-m'u')}{Y_v'\varepsilon_N-N_v'\varepsilon_Y} \qquad (D.6)$$